Molecular programming for the ultra-sensitive detection of biomarkers involved in neurodegenerative diseases

Antoine Masurier

PSL UNIVERSITÉ PARIS

THÈSE DE DOCTORAT
DE L'UNIVERSITÉ PSL

Préparée à l'ESPCI Paris

Molecular programming for the ultra-sensitive detection of biomarkers involved in neurodegenerative diseases

Programmation moléculaire pour la détection ultrasensible de biomarqueurs impliqués dans les maladies neurodégénératives

Soutenue par

Antoine Masurier

Le 07/10/2021

École doctorale n°563

Médicament, Toxicologie, Chimie, Imagerie

Spécialité

Interface chimie-biologie

Composition du jury :

Nadia Cherradi Directrice de recherche INSERM, CEA Grenoble	*Examinatrice et présidente du jury*
Frédéric Ducongé Directeur de recherche CEA, CEA Paris-Saclay	*Rapporteur*
Didier Gasparutto Directeur de recherche CEA, CEA Grenoble	*Rapporteur*
Stéphanie Descroix Directrice de recherche CNRS, Institut Curie	*Examinatrice*
Alexis Vlandas Chargé de recherche CNRS, IEMN	*Examinateur*
Yannick Rondelez Directeur de recherche CNRS, ESPCI Paris	*Directeur de thèse*

Confidentielle jusqu'au 07/10/2022

ESPCI PARIS | PSL

Acknowledgments

Je souhaite tout d'abord commencer par remercier Yannick Rondelez et Guillaume Gines pour m'avoir fait confiance pour ce projet de thèse, m'avoir permis de travailler dans d'excellentes conditions et de m'avoir encadré et guidé tout au long de ce projet.

Je voudrais ensuite remercier mes rapporteurs, Frédéric Ducongé et Didier Gasparutto, pour avoir accepté cette charge exigeante, pour leur relecture attentive et leurs avis d'expert sur ce travail. Je remercie également mes examinateurs, Stéphanie Descroix, Nadia Cherradi et Alexis Vlandas pour leur étude de ce manuscrit et les discussions enrichissantes qui en ont découlées.

Je tiens à remercier tous les membres du laboratoire Gulliver, en particulier Oliver Dauchot pour m'avoir accueilli dans son laboratoire.

Je souhaite remercier l'équipe SPM avec laquelle j'ai collaboré durant ces 3 années. Thomas, Roberta, Anne-Sophie, Rémi, Adèle, Vincent, Thibault, Rocío, Vasily, Taro, Margarida, Coline, Mats et Anis, merci pour votre soutien !

Je remercie également les membres du laboratoire Gulliver avec lesquels j'ai interagis au jour le jour lors des repas, des sorties entre membres du laboratoire, etc. Martina, Martyna, Vincent, Pierre, Paul, Charles, Jeremy, Haggai, Juliane, Claire, Samuel, … merci pour tous ces moments que j'ai partagés avec vous.

Je voudrais exprimer toute ma gratitude aux membres de l'IEMN avec lesquels j'ai eu l'occasion de collaborer : Alexis Vlandas, Yannick Coffinier, Gurpreet Kaur et Thomas Jet.

Je voudrais remercier les personnes de l'University of Applied Sciences of Kaiserslautern avec lesquels j'ai collaboré : Karl-Herbert Schäfer, Anne Christmann, Vivek Pachauri, Sven Ingebrandt et Marcel Tintelott.

Je souhaite remercier les membres du laboratoire de biochimie de l'ESPCI avec lesquels j'ai eu l'occasion de collaborer : Andrew Griffiths, Satyam Banerjee, Pablo Ibanez et Gaël Blivet.

Je voudrais remercier les membres du Laboratoire Jean Perrin pour les discussions très enrichissantes que j'ai eu avec eux : André Estevez-Torres, Jean-Christophe Galas, Anis Senoussi et Marc Van Der Hofstadt Serrano.

Je voudrais remercier Valérie Taly et Anthony Genot pour les échanges enrichissants que j'ai eus avec eux tout au long de cette thèse.

Je voudrais remercier les membres de mon comité de suivi, Michel Minier, Mathilde Reyssat et André Estevez-Torres, pour les discussions très enrichissantes qui en ont découlées.

Merci à l'ANR pour son soutien financier pour la réalisation de cette thèse.

Je souhaite remercier mes amis pour le soutien moral durant ces trois années.

Enfin, je tiens à remercier ma famille, en particulier Régine et Jean-Pierre, mes par-

ents, ainsi que Alexandre, mon frère, pour leur soutien moral et matériel durant toutes mes années d'études supérieures.

Contents

List of Figures

List of Tables

List of abbreviations

3G	third generation
3WJ	three way junction
A30P	early symptomatic synuclein
Ab	antibody
ACTH	adrenocorticotropic hormone
AD	Alzheimer's disease
AGO	argonaute
ALISA	aptamer-linked Immobilized Sorbent Assay
AP	alkaline phosphatase
ARNm	ARN messagers
At	amplification time
aT	autocatalytic template
BSA	bovine serum albumin
Bst LF	Bst large fragment
BW	binding and washing buffer
cDNA	complementary DNA
Cq	quantitative cycle
CSF	cerebrospinal fluid
cT	conversion template
DNA	deoxyribonucleic acid
ds	double stranded
EIA	enzyme immunoassay
ELASA	enzyme-linked apta-sorbent assays
ELISA	enzyme-linked immunosorbent assay
ELISPOT	enzyme-linked immunospot
ELONA	enzyme-linked oligonucleotide assay
EXPAR	exponential amplification reaction
Fab	antigen-binding fragments
GDNF	glial cell line-derived neurotrophic factor
hCG	human chorionic gonadotropin
HPLC	high-performance liquid chromatography
HRP	horseradish peroxidase
HS	helper strand
IC 3D	integrated comprehensive droplet digital detection
INFg	interferon γ

ISFET	ion-sensitive field-effect transistors
Klenow	Klenow fragment (3'→5' exo-)
LAMP	loop-mediated isothermal amplification
LFA	lateral flow assay
LOD	limit of detection
miARN	microARN
miRNAs	microRNAs
mRNA	messenger RNA
NASBA	nucleic acid sequence-based amplification
Nb	number
NW	nanowire
PAGE	polyacrylamide gel electrophoresis
PD	Parkinson's disease
PDGF	platelet-derived growth factor
PEA	proximity extension assay
PEGDVS	poly(ethylene glycol) divinyl sulfone
PEN DNA Toolbox	polymerase exonuclease nickase dynamic network assembly toolbox
PLA	proximity ligation assay
PMMA	poly (methyl methacrylate)
pre-miRNA	precursor-miRNA
pri-miRNA	primary miRNA
PSA	prostate specific antigen
pT	pseudo template
PTO	phosphorothioate
PUMA	programmable ultrasensitive molecular amplifier
RCA	rolling circle amplification
RISC	RNA-induced silencing complex
RNA	ribonucleic acid
RNAi	RNA interference
rRNA	ribosomal ribonucleic acid
rT	reporter template
RT-qPCR	reverse transcription quantitative polymerase chain reaction
SB	storage buffer
scFv	single chain variable fragments
SDS	sodium dodecyl sulfate
SELEX	systematic evolution of ligands by exponential enrichment
SIMOA	single molecule array
SLP	stem-loop primer
SLTD	stem-loop template DNA
SOMAmer	slow off-rate Modified Aptamer
ss	single stranded
sT	self-activated template
TCEP	tris(2-carboxyethyl)phosphine
THA	thiolated hylaronic acid
tRNAs	transfer RNAs

TSA	total seq A
TSB	total seq B
TT-LAMP	target-triggered version of LAMP
UASK	university of applied sciences Kaiserslautern
UMI	unique molecular identifier
UTR	untranslated region
Vent	Vent(exo-)
WS	warm start

Introduction

I.1 Neurodegenerative diseases

With increasing life expectancy, the prevalence of neurodegenerative diseases, such as Parkinson's disease (PD) or Alzheimer's disease (AD), is expected to increase. For example, AD is foreseen to affect 1 in 85 people worldwide by 2050 [1]. However, according to Jack et al., analysis of cerebrospinal fluid (CSF), obtained via lumbar puncture, is the most suitable way of obtaining relevant biological samples for early detection [2]. This fairly intrusive technique cannot be performed routinely. Noteworthy, current AD biomarkers are either linked to amyloid-β plaques or to tau-related neurodegeneration. A tailored detection method must therefore be able to quantify particular target proteins. However, it has recently been shown that microRNAs (miRNAs) can also be used as biomarkers for AD [3]. We therefore decided to focus on the co-detection of these two classes of biomarkers: proteins and miRNAs.

We will first describe the interest and challenges of protein and miRNA detection. Then, we will present the classical detection methods used for protein detection, followed by those used for miRNA detection and finally we will see how some nucleic acid detection methods have been adapted for protein detection.

I.2 Interest and challenges in protein detection

Natural proteins result from the translation of genetic information provided by a messenger RNA (mRNA), which is interpreted by the ribosome into a polypeptide [4]. As there are twenty different type of amino acids in a protein and only four different nucleotides in mRNA, there is no one-to-one correspondence between nucleic acid sequences and amino acid chains [5]. The rules used for the conversion are known as the genetic code: the nucleotides are red in succession in groups of three, called codon. Each codon corresponds either to an amino acid or a stop codon, which stops the translation. The translation of mRNA relies on the use of adaptor molecules known as transfer RNAs (tRNAs): they recognize and bind to a specific codon and its corresponding amino acid.

The ribosome is constituted of two subunits, which are separated when they are not synthetizing proteins. They assemble on an mRNA molecule to start the synthesis of a protein. The mRNA is pulled through the ribosome and the mRNA is translated into an amino acid sequence as the tRNAs add individual amino acid in the sequential order to the polypeptide chain (figure I.1.a.). The amino acids are added by the formation of an amide bond between the carboxyl group at the end of a growing polypeptide chain and a free amino group of the incoming amino acid. Therefore, the protein is synthesized from N-terminus to

C-terminus. When the ribosome encounters a stop codon, the translation is aborted and its two subunits are released.

During and at the end of its production, a protein folds and acquires its secondary and tertiary structures (figure I.1.b.). Proteins can then be modified by a variety of post translational modifications, such as glycosylation, phosphorylation, acetylation and methylation (figure I.1.c.).

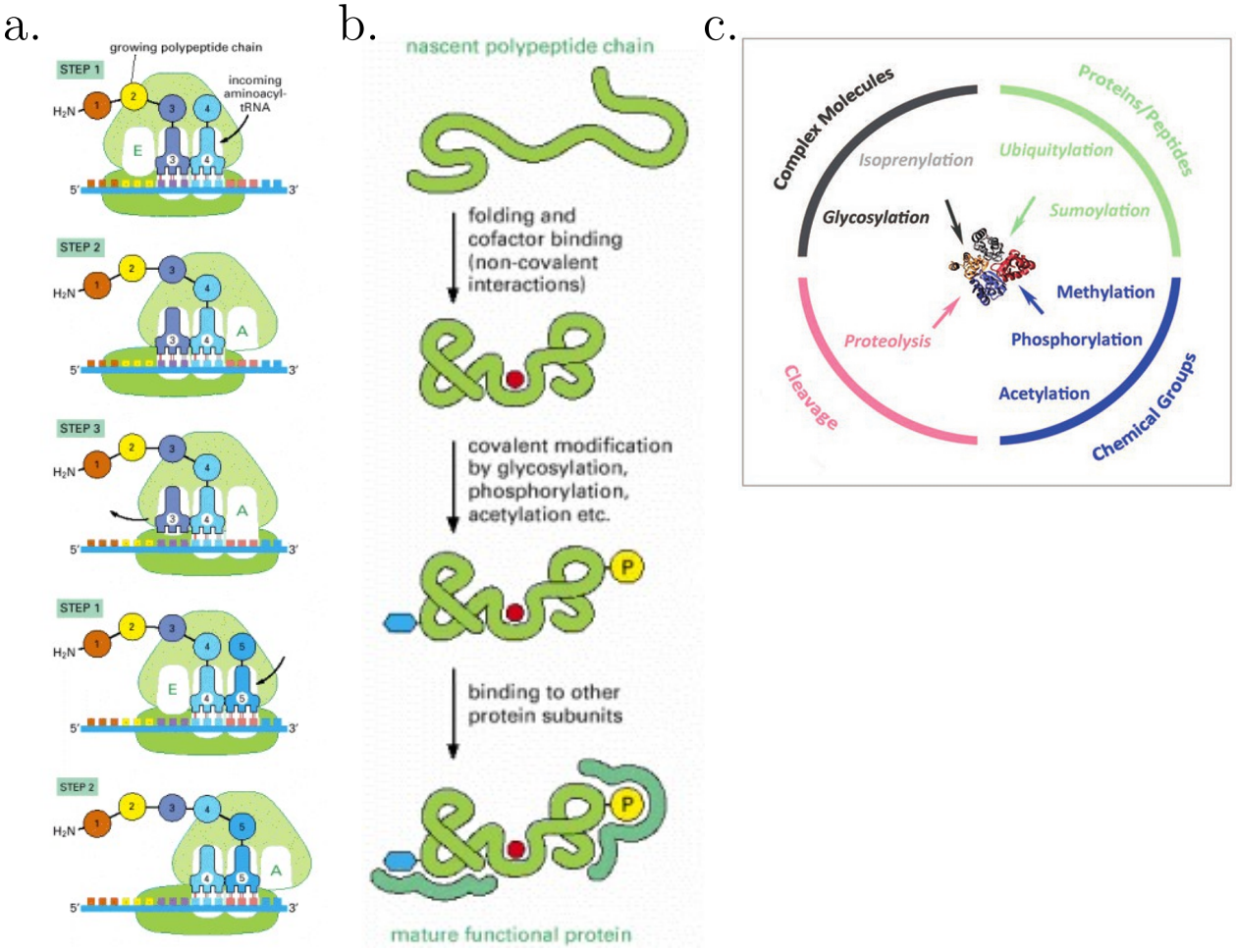

Figure I.1: **Protein translation. a.** Translation of a mRNA molecule. The three-step cycle is repeated multiple times during protein synthesis. An aminoacyl-tRNA binds to the A-site of the ribosome, bringing an amino acid selected by base paring between its anticodon and the next codon on the mRNA (step 1). An amide bond is formed in step 2, adding one amino acid to the C-terminus of the polypeptide chain at each cycle. The mRNA shifts a distance of three nucleotides (it is red in the 5' to 3' sens) in step 3, discarding a processed tRNA and thus returning to the step 1 situation. **b.** After translation, the newly synthesized protein fold into its three-dimensional conformation induced by non covalent bonds. The protein eventually undergoes covalent post translationnal modification. The protein may also binds to other protein subunits if applicable. **c.** Mains categories of possible post translationnal modifications. Image and information extracted from [5] and [6].

I.2.1 Challenges in protein detection

Proteins play an important role in biological processes. Indeed, proteins are involved in replicating genomic information, transcribing mRNA, regulating gene expression, catalyzing metabolic reactions, signaling and transporting molecules [7]. Therefore, protein dysregulation is involved in many diseases including neurodegenerative diseases [8], cancer [9] or diabetes [10]. These dysregulations can be caused by protein misfolding [11] or mutated proteins [12] for example. It is thus necessary to detect specific proteins for the diagnosis of certain diseases. It has been estimated than the human genome contains approximately 20 000 protein-coding genes [13] [14]. Due to aternative mRNA splicing, post-translational modifications, and proteolytic cleavage, a single gene can encode up to 50 different protein species [15]. Therefore, the human proteome encompasses at least 20 000 proteins but is estimated to be tens of thousands of proteins.

Thus, detecting sensitively and specifically a protein in a biological sample is challenging. As one cell can contain between one and more than 100 000 copies of a single protein [16], the dynamic range of the detection method ideally needs to cover 6 orders of magnitude. The detection method may also need to distinguish between very similar proteins, for example to discriminate an irregular phosphorylation pattern [17]. Finally, simultaneous detection of several proteins can be required to obtain a characteristic protein signature of a disease or an infection [18].

I.3 Interest and challenges in miRNA detection

MiRNAs are a class of short RNAs (21-25 nucleotides) involved in the post-transcriptional regulation of approximately 60% of human genes [19]. First discovered in 1993 in *Caenorhabditis elegans* [20], the associated regulatory process was described in 1998 by Andrew Fire and Craig Mello [21]. They were awarded the 2006 Nobel Prize in Medicine and Physiology for their work on this process, called RNA interference (RNAi). Thousands of miRNAs have since been discovered [22].

The main pathway for miRNA biogenesis is called the canonical pathway (figure I.2) [23]. The RNA polymerase II initiates the biogenesis of miRNAs by transcribing miRNA genes into primary miRNAs (pri-miRNAs), which are approximately 1 kb long [24]. The pri-miRNA undergoes a maturation step by RNase III Drosha and cofactor DGCR8, called microprocessor complex [25], is cleaved and released as precursor-miRNA (pre-miRNA), a 65 base long RNA hairpin. The pre-miRNA is exported from the nucleus to the cytoplasm where RNase III endonuclease Dicer cleaves the pre-miRNA into a small RNAs duplex. This duplex is loaded on an Argonaute (AGO) protein [26], forming the RNA-induced silencing complex (RISC). An helicase then unwinds the RNA duplex and only one RNA strand remains in the complex, producing the mature RISC.

Two mains mechanisms are involved in RNAi (figure I.3). Firstly, the miRNA can completely hybridize inside the coding region of a mRNA, leading to its cleavage by the AGO protein and thus represses mRNA translation. Secondly, the 5' extremity of the miRNA can hybridize to the 3' untranslated region (UTR) of a targeted mRNA thanks to a region known as the miRNA "seed". Factors inhibiting mRNA translation are recruited by the RISC proteins, inhibiting mRNA translation.

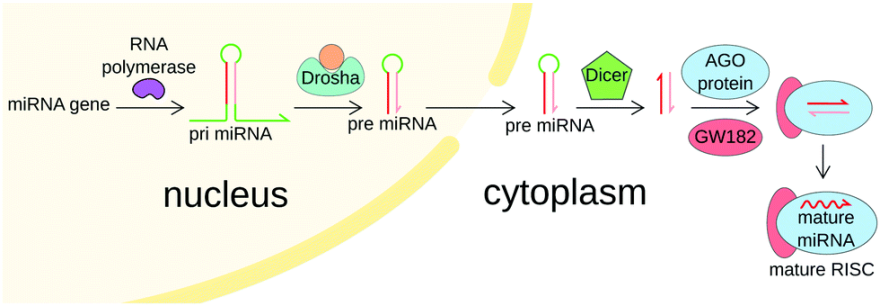

Figure I.2: **Simplified miRNA biogenesis pathway.** The miRNA gene is transcribed into pri-miRNA by RNA polymerase II. The pri-miRNA is cleaved near the hairpin loop by the Drosha and is then exported from the nucleus to the cytoplasm where it is cleaved in a RNA duplex by Dicer. This duplex is loaded on an Argonaute protein, forming the RISC, and is then unwinded by a helicase. Only one RNA strands remains in the complex, forming the mature RISC. Image and information extracted from [27].

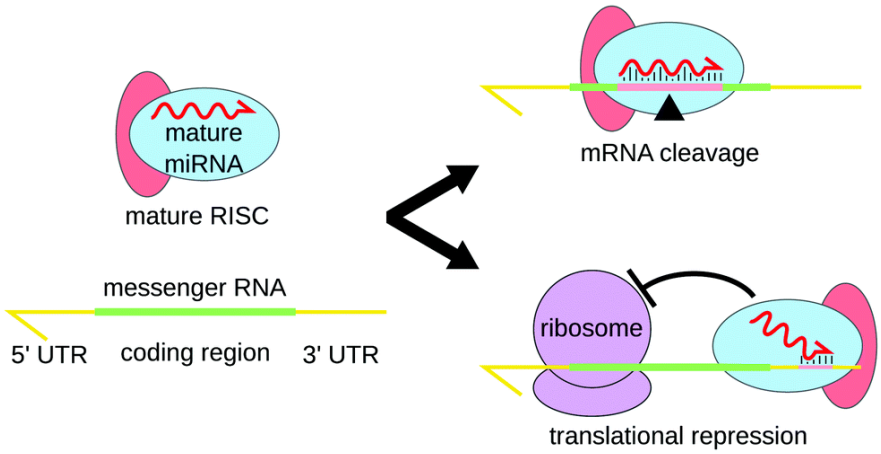

Figure I.3: **The two main miRNA-induced pathways for post-transcriptional regulation.** miRNA can completely hybridize to the targeted mRNA, leading to its cleavage by the RISC complex. Alternatively, the "seed" region of the miRNA can partially hybridize to one of the UTR of the mRNA, triggering the recruitment of translation inhibiting factors and/or promoting mRNA deadenylation. Image and information extracted from [27].

I.3.1 Challenges in miRNA detection

miRNA dysregulation is involved in several diseases, such as neurodegenerative diseases [28] [29] [30] [31], cancers [32] or diabetes [33]. These dysregulations can be caused, for example, by gene deletions, amplifications or mutations [34] as well as defect of the biogenesis machinery [35], among others.

Although miRNAs are attractive biomarkers, their detection presents several challenges. Indeed, miRNAs are short and sometimes very similar nucleic acids sequences. For example, the Let7a family contains 9 miRNAs which differ from each other from 1 to 5 bases [36]. To specifically differentiate these miRNAs, it is therefore necessary to be able to discriminate sequences with only 1 base mismatch.

miRNAs represent 0.01% of the total RNA mass [37]. Furthermore, in blood plasma their concentration goes from a few copies to hundred of thousands per microliter of sample, corresponding to concentrations comprised from femtomolar to picomolar [38]. Thus, a dynamic range covering at least 4 orders of magnitude [39] is required for miRNA detection.

Moreover, both healthy and diseased patients produce miRNAs. The information is contained in small variations in miRNA concentrations, which requires sensitive detection methods. More recently, studies suggested that detecting miRNA signatures provides more information than detection of a single miRNA [40].

I.4 Basics of protein detection and quantification

In this section are exposed the main methods used for protein detection and quantification. In most cases, a protein detection assay is composed of three major components: an affinity reagent, a signal transducer, and a detector [7] [41]. The affinity reagent specifically binds to the protein of interest. This binding is converted in a measurable signal by the signal transducer. Finally, the detector converts the measurable signal into a readout.

I.4.1 Affinity reagents

A compound that binds specific substances is called an affinity reagent. We will present the main classes of protein affinity reagents in this section. Several parameters are critical to choose an adapted affinity reagent, including affinity, specificity, cost, stability and reproducibility. Moreover, the affinity reagent might need to be adsorbed or attached to a surface [42] and need to interact with the signal transducer, either directly or via an intermediate molecule. Ideally, it should not interfere with the interaction between affinity reagent and the target protein. Antibodies and aptamers are the the most common affinity reagents used in protein detection.

I.4.1.1 Antibodies

Antibodies are a key component of the immune system. Their production is a response to the presence of foreign molecules or organisms. They are known to bind to a target molecule named antigen. An antibody binds to an epitope, which is a structure on the antigen [43]. Antibodies are composed of four polypeptides: two heavy chains (∼55 kD) and two light chains (∼25 kD) which are held together by disulfide and noncovalent bonds. The resulting molecular complex forms a Y-shaped molecule of ∼160 kD. (figure I.4). Light and heavy chains variable domains form the antigen binding domain, referred to as the Fab.

The diversity of antibodies is ensured by a recombination mechanism allowing, for example, a human being to produce up to 10^{12} antibodies, each with a different binding site [5]. Antibody production generally takes place in a living organism by affinity maturation [45]. As most antigens present numerous epitopes, several lymphocytes recognize them, are activated to proliferate and differentiate into plasma cells, thus resulting in a polyclonal antibody production [46]. However, a single B lymphocyte clone produces a monoclonal antibody. In 1975, Köhler and Milstein fused splenic B cells with myeloma cells, resulting

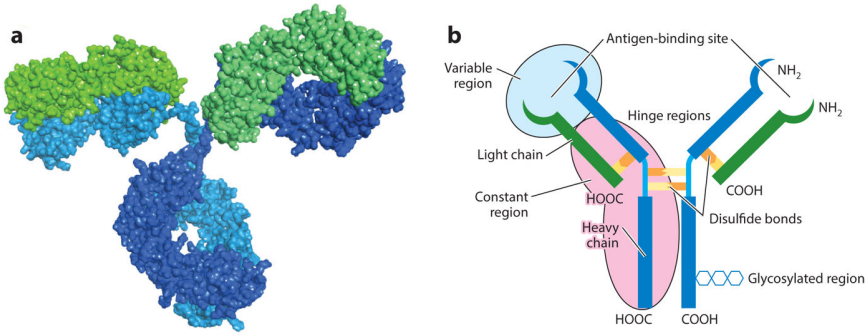

Figure I.4: **IgG structure. a.** Antibody X-Ray crystal structure. Heavy chains are colored in blue/turquoise while the light chains are colored in green. **b.** Scheme of an antibody. Image and information extracted from [44]

in immortal hybridomas, each producing a unique monoclonal antibody [47]. They were awarded a part of the 1984 Nobel Prize in Physiology or Medicine [48] for their work.

Monoclonal antibodies have the advantage of being homogeneous and provide a monospecificity useful to evaluate changes in molecular conformation or phosphorylation states, for example. Once the desired hybridoma is obtained, monoclonal antibodies can be produced easily and reproducibly. On the other hand, polyclonal antibodies are heterogeneous and recognize several epitopes of an antigen, they are thus more robust to small changes on various epitopes. However, polyclonal antibodies produced for the same antigen using different animals will vary among animals, raising issues of reproducibility from batch to batch.

The antigen-antibody interactions have low K_d values (i.e. high affinity). After maturation, K_d in picomolar to nanomolar ranges are typically reached [49] [50]. Antibodies have a high specificity, even though cross reactivity is still possible [51] [52].

I.4.1.2 Aptamers

Aptamers are small three-dimensional structures of oligonucleotides selected to bind to a target of interest with high affinity and specificity [53]. First discovered in 1990 [54] [55], aptamers are mainly generated and selected by the systematic evolution of ligands by exponential enrichment (SELEX) process. During a SELEX, a library of nucleic acid sequences is generated, introduced to the target molecule and sequences binding to the target molecule are separated from the unbound sequences. The bound sequences are collected and amplified by PCR. They can then be used for subsequent rounds of enrichment. Multiple rounds, typically between 8 and 15, are performed, until reaching a sequence with a sufficient affinity [56]. The identified sequence can then be reproducibly produced by chemical synthesis at low cost, have a high stability and a high specificity with dissociation constants in the femtomlar to nanomolar range [57]. Aptamers can be introduced into protein assay as a substitution to antibodies. Moreover, they can be easily modified with molecules and functional groups. [58]. However, aptamers suffer several drawbacks, such as quick degradation in biological samples, especially for RNA aptamers, or the need for a purified protein to realize the selection [59].

I.4.1.3 Other affinity reagents

In 1993, it was discovered that camelids, such as camel and lamas, produce antibodies that lack the light chain [60]. A similar discovery was realized in 1995 on sharks [61]. Those single domain antibodies are known as VHH or nanobodies and have K_ds in the picomolar to nanomolar range [62]

More recently, antibody fragments have been used. They can be class into three categories: antigen-binding fragments (Fab), single chain variable fragments (scFv) and "third generation" (3G) [63].

Lectins, proteins with two or more carbohydrate binding sites [64], are also used as affinity reagent to detect glycoproteins [65] [66].

Antibody mimetics are molecules that bind to a specific antigen in a similar fashion to antibodies. However, they are not related to antibodies [44] [67].

Oligonucleotide bearing chemically modified deoxyuridine residues that are uniformly functionalized at the 5-position are called Slow Off-rate Modified Aptamer (SOMAmer) [68]. These modifications introduce hydrophobic interactions leading to novel secondary and tertiary structural motifs. SOMAmer can achieve high affinity for specific proteins, with dissociation constants in picomolar to nanomolar levels [69].

Among others, protein ligands [70] or molecularly imprinted polymers [71] can also be used.

I.4.2 Enzyme-linked immunosorbent assay

In 1960, Yalow measured human plasma insulin with a competitive immunoassay using radioactive labels [72]. He used antibodies that preferentially bind to human insulin rather than crystalline beef insulin-I^{131}. Then, the concentration of antibody-bound insulin-I^{131} and free insulin-I^{131} was measured by paper chromato-electrophoresis, providing the concentration of human insulin. Miles then developed and used radioactive labelled antibodies instead of labelled antigens [73]. For safety reasons, it was necessary to replace the radioactive components [74]. In 1971, two different groups developed an enzyme-based immunoassay. Engvall and Perlmann introduced the Enzyme-Linked Immunosorbent Assay (ELISA) and quantitatively measured IgG in rabbit serum using alkaline phosphatase [75]. In the same year, van Weemen and Schuurs developed the enzyme immunoassay (EIA) to quantify human chorionic gonadotropin (hCG) concentrations in urine with horseradish peroxidase [76].

ELISA is now the commonly gold standard for protein detection. Different types of ELISA tests have been developed, respectively direct ELISA, indirect ELISA, sandwich ELISA and competitive ELISA [77]. Three enzymes are commonly used: horseradish peroxidase (HRP), alkaline phosphatase (AP), and β-galactosidase. Several substrates are available for these enzymes, generating products that can be detected by colorimetric, fluorescent, chemiluminescent and electrochemical readouts [7]. A protein standard range is realized for each ELISA assay to comparatively quantify each protein sample.

In all the ELISA types describe in the following, a washing step is performed between each step. In a direct ELISA, the antigen to be detected is adsorbed on a surface and tagged with a specific enzyme-conjugated antibody (figure I.5.a.). However, finding a detection antibody that can be labelled for each antigen is time consuming and expensive. Indirect

ELISA allows to target different antigens with several unmodified primary antibodies from one species. All of the primary antibodies can then be labelled with the same enzyme-conjugated secondary antibody (figure I.5.b.). In a sandwich ELISA, a capture antibody is physisorbed on the plate, the sample containing the antigen added, followed by the enzyme-labelled detection antibody. The sandwich assay is more time consuming but allows to work with non purified samples, contrary to direct and indirect ELISA (figure I.5.c.). In an indirect ELISA, the detection antibody is incubated with the sample containing antigen and then added to an antigen coated plate. The free detection antibodies bind to the antigens coated on the plate and can then be detected by an enzyme labelled secondary antibody (figure I.5.d.). Competitive ELISA inverts the signal compared to the other ELISA methods: the higher the amount of antigen, the lower the signal [78]. A competitive ELISA is less sensitive than a sandwich ELISA but it is quicker, more flexible and has good reproducibility.

ELISA methods typically span 4 orders of magnitude with a LOD in the picomolar range [79] [80]. ELISA tests are time consuming but are user-friendly and very sensitive and specific compared to other methods such as western blot. Therefore, they are widely used.

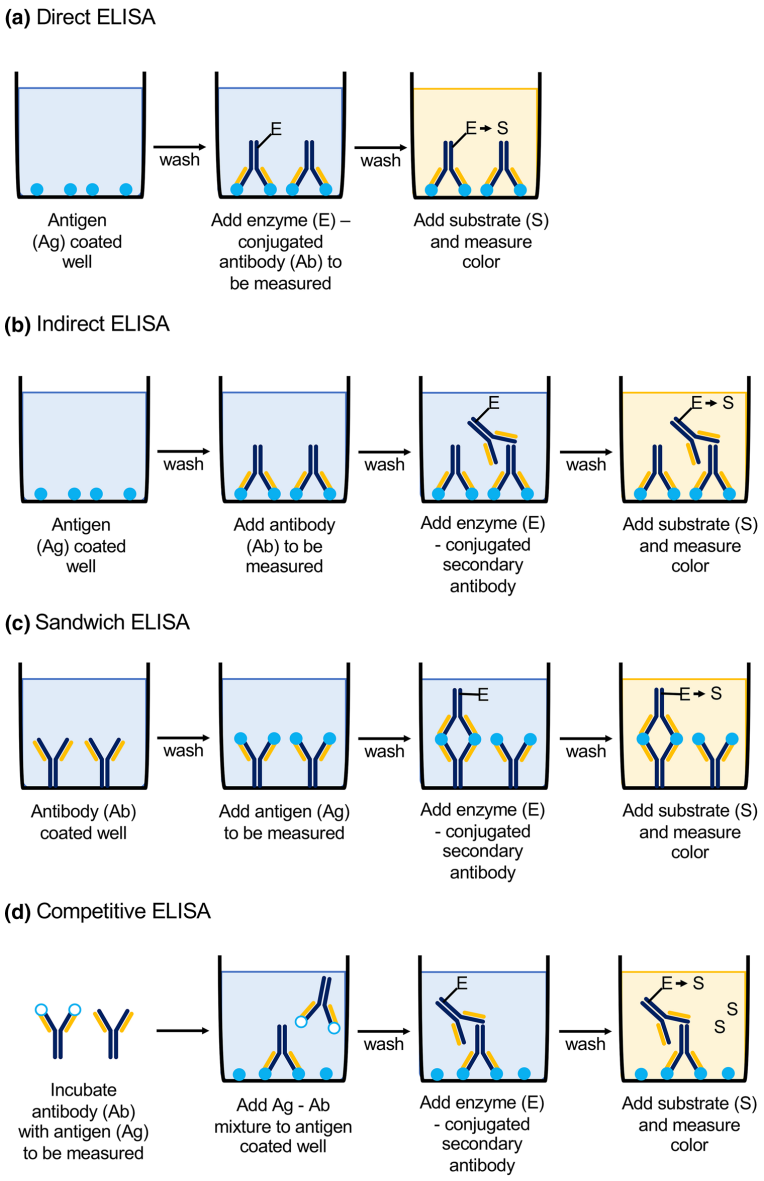

Figure I.5: **Schematic representation of different types of ELISA. a.** Direct ELISA. The antigen contained in the sample is coated on a surface and is detected using an enzyme labelled detection antibody. **b.** Indirect ELISA. The antigen contained in the sample is coated on a surface, a detection antibody is firstly added, followed by an enzyme labelled secondary antibody. **c.** Sandwich ELISA. The surface is coated with a capture antibody, the sample containing the antigen is added, followed by an enzyme labelled detection antibody. **d.** Competitive ELISA. The surface is coated with the antigen. Simultaneously, the detection antibody is incubated with the sample containing the antigen : due to the high detection antibody concentration, only a part of the detection antibodies will bind to the antigen. This mixture is then added to the previously coated plate. The free antibodies will bind to the antigen coated on the surface. An enzyme labelled secondary antibody is added, allowing to quantify the antibodies that were not bound to a sample antigen, thus leading to the concentration of antigen in the sample. Image and information extracted from [77].

I.4.3 Enzyme-linked apta-sorbent assays

A modification of the ELISA has been realized, where antibodies are replaced by aptamers. This approach is called enzyme-linked apta-sorbent sssays (ELASA) [81], aptamer-linked immobilized sorbent assay (ALISA) [82] or enzyme-linked oligonucleotide zssay (ELONA) [83]. As for ELISA, four main types of ELASA are used: standard assay, indirect assay, sandwich assay and competitive assay [57], three of them are represented in figure I.6. Recently, the detection of ochratoxin A was carried out via ELASA, achieving a a LOD of 2.1 pM and a dynamic range spanning over 7 orders of magnitude [84]. In the same study, an ELISA test was realized, showing the same LOD and a dynamic range spanning over 6 orders of magnitude. We can reasonably assume that the selected aptamers had a higher affinity for the target than the selected antibodies. However, those results are very similar.

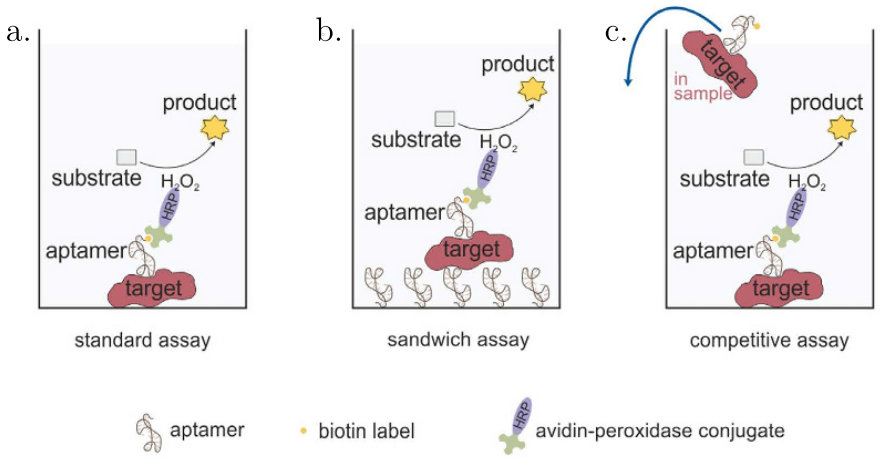

Figure I.6: **Schematic representation of different types of ELASA. a.** Direct ELASA. The target contained in the sample is coated on a surface and is detected using an enzyme labelled aptamer. **b.** Sandwich ELASA. The surface is coated with a capture aptamer, the sample containing the target is added followed by an enzyme labelled detection aptamer. **c.** Competitive ELASA. The surface is coated with the target. Simultaneously, the detection aptamer is incubated with the sample containing the target : due to the high detection aptamer concentration, only a part of the detection aptamer will bind to the target. This mixture is then added to the previously coated plate. The free aptamers will bind to the target coated on the surface. An enzyme labelled secondary aptamer is added, allowing to quantify the aptamers that were not bound to a sample target, thus leading to the concentration of target in the sample. Image and information extracted from [83].

I.4.4 Enzyme-linked immunospot

The enzyme-linked immunospot (ELISPOT) has been developed in order to detect secreted antibodies by live cells in vitro [85]. The antigen is coated on a plate, cells introduced, incubated and removed. Then, an HRP-secondary antibody is added as well as a substrate producing a colored precipitate. The assay was later adapted for the detection of secreted proteins (other than antibodies), following the same principle as a sandwich ELISA: the plate

is coated with a protein specific capture antibody, cells are added, incubated and removed. Finally, an enzyme-labelled detection antibody is added, producing a colored precipitate [86]. ELISPOT are easy to realize on many samples at the same time. They are for example used to assess human immune responses to vaccines. A detection limit of 25 interferon-γ-producing T cells per million in peripheral blood mononuclear cells has been reported [87].

I.4.5 Western blot

The Western blot technique has been introduced independently by three different groups and is used to identify specific proteins [88] [89] [90]. The sample is separated by sodium dodecyl sulfate (SDS)–polyacrylamide gel electrophoresis (PAGE), transferred to an adsorbent membrane, blotted with a labelled antibody and finally analyzed [91] (figure I.7). Western blot separates proteins by their molecular weight, thus providing more information than an ELISA test. However, Western blot requires more skills and more time than ELISA methods but no complex equipment. Western Blot is currently used for the detection of protein-protein interactions, of post-translational modification or for antibody development [92].

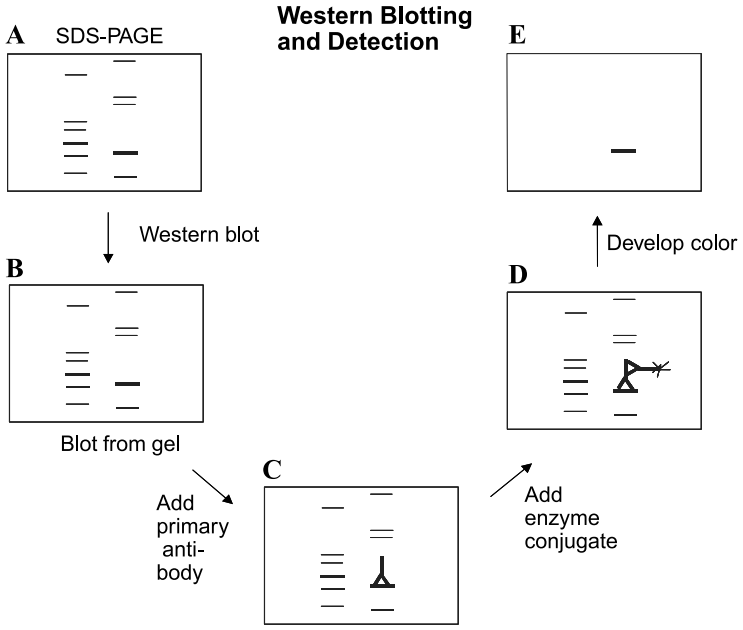

Figure I.7: **Western blot principle.** (A) The sample is separated by SDS–PAGE. (B) The gel is transferred to an adsorbent membrane. (C) Primary antibody binding to a specific protein. (D) Labelled secondary antibody binding to primary antibody. (E) Color development of specific band. Image and information extracted from [91].

I.4.6 Protein microarrays

Protein microarrays enable multiplexed protein detection by spatially separating the protein specific receptors that are immobilized on a planar surface. Their fabrication habitually use either contact printing or piezoelectric deposition methods [93]. Protein microarrays

can be divided in two classes. The first one is based on sandwich immunoassay (figure I.8.a.). Briefly, the targeted protein binds to capture antibodies coated on the microarray surface and is then detected with a labelled detection antibody, leading to the detection of femtomolar levels of proteins [94] [95]. Multiplexing is achieved by immobilizing different specific capture antibodies at different positions in space. The second type of microarray is known as reverse phase array (figure I.8.b.). The sample is deposited on the surface of the microarray, the proteins bind to the surface and the protein of interest is detected with a specific antibody. Either the specific antibody is labelled or a labelled secondary antibody is added, leading to the detection of nanomolar levels of proteins [96]. A fluorescent, chemiluminescent, electrochemiluminescent or colorimetric signal is usually obtained [7]. It should be noted that this technology also exists for the detection of miRNA [97].

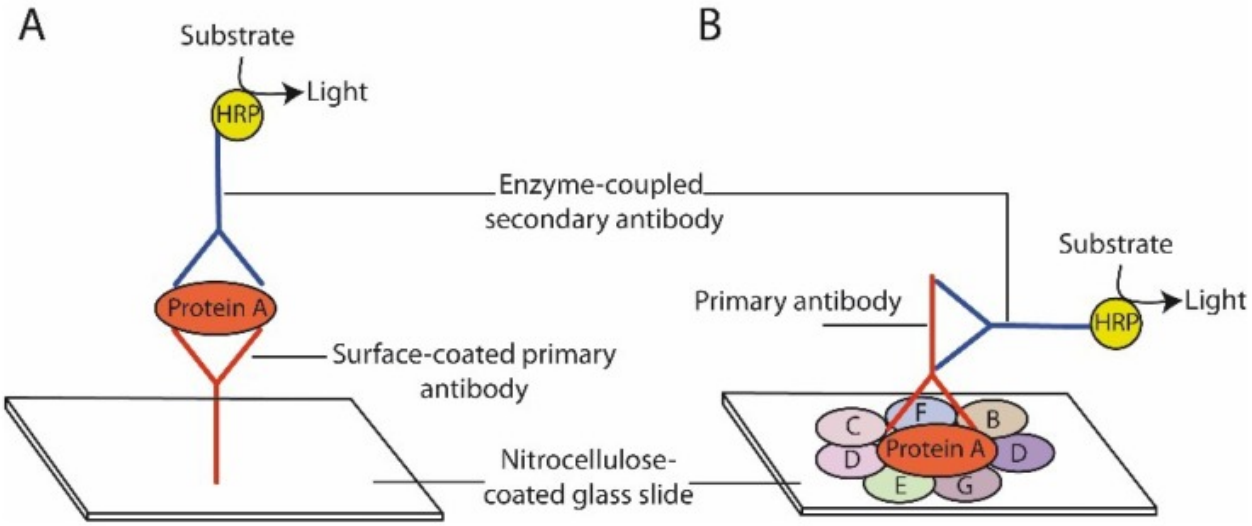

Figure I.8: **Microarrays principle. a.** Schematic representation of immunoassay based microarray. A capture antibody coated on a surface binds to the targeted protein. An enzyme labelled detection antibody is then added, converting a substrate into a detectable signal. **b.** Schematic representation of reverse phase protein array. The sample is deposited on the surface of the microarray, proteins bind to the surface and the protein of interest is detected with a specific antibody. Image and information extracted from [98].

I.4.7 Single-molecule arrays

The single molecule array (SIMOA) is a suspension array commercialized by Quanterix corporation. It relies on digital ELISA using antibody-coated capture particles (see section I.5.6.1 for explanation on digital detection). An excess of particles is incubated in presence of a sample containing the targeted protein. According to Poisson statistics, either zero, one or a few target molecules bind to each particle. Biotinylated detection antibody and a streptavidin-enzyme, such as streptavidin-ß-galactosidase, are then added. The particles are isolated in an array of femtoliter-sized compartments designed to contain at most one particle. A fluorogenic substrate is added and the wells are sealed. A fluorescent signal will be generated in the wells containing an immunocomplex. Due to the small volume of the wells,

this results in a high enough fluorescent product concentration to be detected by fluorescent imaging. This allows the detection of protein at the single molecule level. The detection of prostate specific antigen (PSA) down to 250 aM over 4 orders of magnitude was achieved [99]. This approach has then been multiplexed for the detection of six different cytokines [100] using dye-encoded particles.

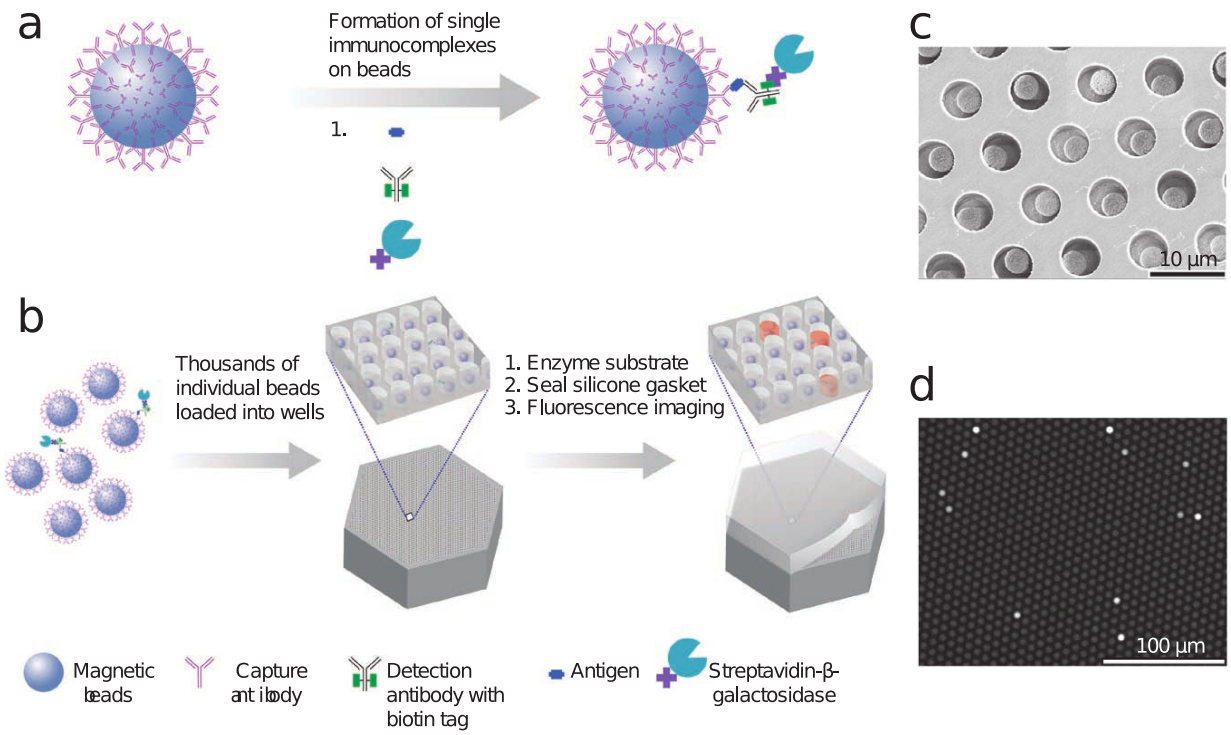

Figure I.9: **SIMOA principle. a.** Capture antibody coated particles are used to capture the targeted protein. **b.** Particles, with or without an enzyme labelled immunocomplex, are loaded into femtoliter-sized array with a fluorescent substrate. Wells are sealed and imaged. **c.** Scanning electron micrograph of bead containing femtoliter-volume well array. **d.** Fluorescence images of a femtoliter-sized array after fluorescent signal generation. Image and information extracted from [101].

I.4.8 Lateral flow assay

A lateral flow assay (LFA) is based on sample movement across a membrane via capillary force [102]. A LFA is composed of four parts: a sample pad, a conjugate pad, a reaction membrane and an absorption pad (figure I.10). The sample is deposited on the sample pad and is drawn by capillary action to the conjugate pad where the targeted protein binds to specific antibodies conjugated to colored fluorescent particles. The mixture migrates to the reaction membrane where affinity reagents are immobilized in lines. The presence of the targeted protein results in the formation of an immunocomplex on the test line, while secondary antibodies present on the control line allow to indicate a proper liquid flow. A colored or fluorescent readout is obtained, its intensity is correlated to the target protein

concentration. The excess reagents are absorbed by the absorption pad. FLA are carried out in a few minutes, making it a method of choice for medical diagnosis. The immunoassay LFA is the most common. For example, hCG detection via LFA is the core technology for pregnancy test [103]. Aptamer based LFA are also available, with typical LODs in the nanomolar range [104].

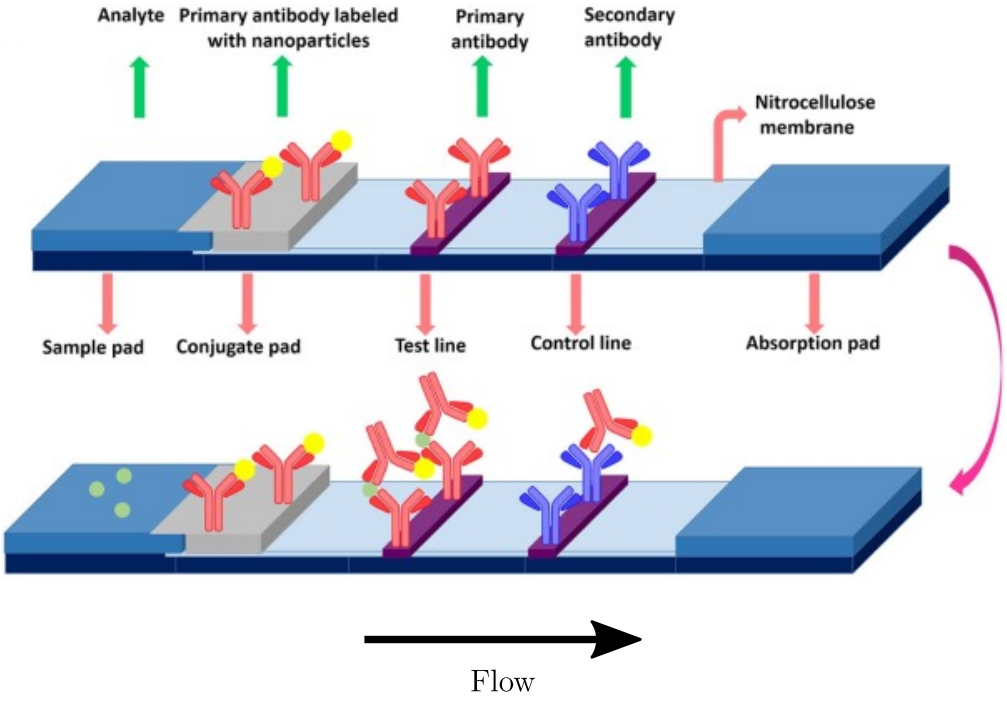

Figure I.10: **FLA principle.** The sample is added on the sample pad and migrates to the conjugation pad where antibodies conjugated to a label are stationed. Targeted protein binds to the labelled antibodies and, as the mixture moves to the test line, binds to immobilized capture antibodies. On the control band are immobilized antibodies that capture the labelled antibodies to check that the test is working properly. Excess reagents are absorbed by the absorption pad. Targeted protein concentration is correlated to the signal intensity of the band. Image and information extracted from [102] and [7]

I.5 Exponential nucleic acid amplification based methods and applications to miRNA

The detection of miRNAs, present in the femtomolar range, requires a high sensitivity and specificity. The vast majority of miRNA detection techniques rely on methods that amplify the target sequence or an intermediate sequence. Although many nucleic acid amplification methods exist, only a few have been adapted to the detection of short sequences such as miRNAs. In this section, we present the exponential nucleic acid amplification methods used for miRNA detection. For a more complete overview of nucleic acid amplification methods used for miRNA detection, we refer the reader to a review of our group [105].

I.5.1 RT-qPCR

Reverse transcription quantitative polymerase chain reaction (RT-qPCR) was first developed for long DNA quantification [106] and has then been adapted for long RNA quantification [107]. Adaptations have been realized for miRNA quantification.

Of all the existing miRNA detection methods, RT-qPCR is definitely the gold-standard. This is due to several advantages such as sensitivity, specificity, small sample size and cost efficiency [108]. RT-qPCR allows the detection of miRNA down to femtomolar concentrations, with a dynamic range covering 8 orders of magnitude [109].

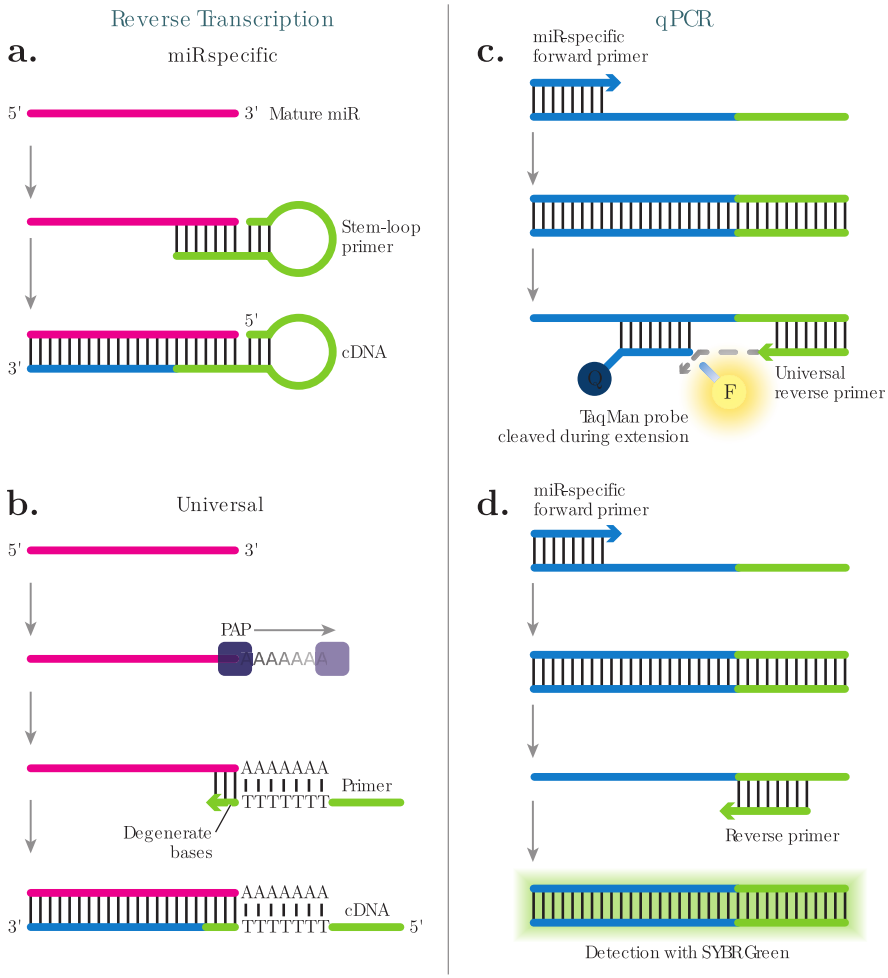

Figure I.11: **Two steps RT-qPCR.** During the reverse transcription step, the miRNA is reverse transcribed into cDNA using either a stem-loop primer (a) or universal polyA tail primer (b). A PCR is carried out, leading to the exponential amplification of the cDNA. The reaction is monitored by real-time fluorescence using either a specific molecular beacon (c), hydrolyzed during the polymerase primer extension thus releasing a fluorophore, or a dsDNA intercalating fluorescent dye (d). Image and information extracted from [110].

RT-qPCR comprises two steps: a first step of reverse transcription where a reverse transcriptase synthesises a complementary DNA (cDNA) from the targeted miRNA and a DNA primer (figures I.11.a and b.). During the reverse transcription step, either a target spe-

cific stem-loop primer partially complementary to the targeted miRNA or a universal polyA tail primer are used. The step-loop primers are used for specific targeting of a miRNA while the polyA tail primer is used to convert all miRNAs into cDNAs [110]. Then, the cDNA is amplified by a polymerase and a set of specific primers during a PCR step. The amplification is monitored in real time either by using a specific fluorescent probe (e.g hydrolysis of profluorescent probes) (figure I.11.c.) or by using a nonspecific DNA intercalating dye (e.g. EvaGreen) (figure I.11.d.). The number of cycles necessary to cross a fluorescence threshold is called quantitative cycle (Cq) and is determined for a sample. By comparison with a range of standard samples, it is possible to quantify the targeted miRNA in the sample.

Androvic et al. introduced a method named two-tailed RT-qPCR [111]. The primers are composed of two hemiprobes complementary to two distinct parts of the target miRNA, linked together by a hairpin structure. This design increases the specificity of the method.

I.5.2 Loop-mediated isothermal amplification

Loop-mediated isothermal amplification (LAMP) was originally developed for DNA amplification with a single polymerase and a set of four primers (two inner and two outer primers) [112]. LAMP is composed of an initiation step and an amplification step performed in a one-pot reaction. During the initiation step, the four primers generate a dumbbell structure in presence of the targeted DNA sequence and the DNA template. This dumbbell structure is then used for a continuous DNA amplification using isothermal strand displacement.

LAMP has been adapted to miRNA detection by Li et al., using the targeted miRNA as a one of the two outer primers to generate the dumbbell structure [113]. However, this design requires a relatively long ssDNA template (around 200 bases), containing 6 pre-defined sequences (figure I.12). This renders the method quite complex and not user-friendly.

In an attempt to optimize this method, other research group have proposed optimized designs. Sun et al. proposed a target-triggered version of LAMP (TT-LAMP) in which the reaction is initiated by two rationally designed sequences [114]. In presence of the targeted miRNA, the stem-loop template DNA (SLTD) and the stem-loop primer (SLP) produce the dumbell structure initiating the LAMP. The authors report a LOD of 100 attoM for let-7a as well as a specificity allowing to discriminate the let-7a from all the other miRNAs of the let-7 family. Tian et al. have coupled LAMP with padlock probe based rolling circle amplification [115]. The RCA is used to produce the stem-loop structure for LAMP initiation. They reached a LOD of 10 aM and successfully discriminated between different miRNAs of the let-7 family. More recently, Abdullah AL-maskri et al. introduced a novel reverse transcription-based LAMP strategy for miRNA detection which requires two stem-loop probes inspired by the dumbbell shaped amplicons and inner primers used in conventional LAMP reactions [116]. They reached a LOD of 10 fM for miR-152.

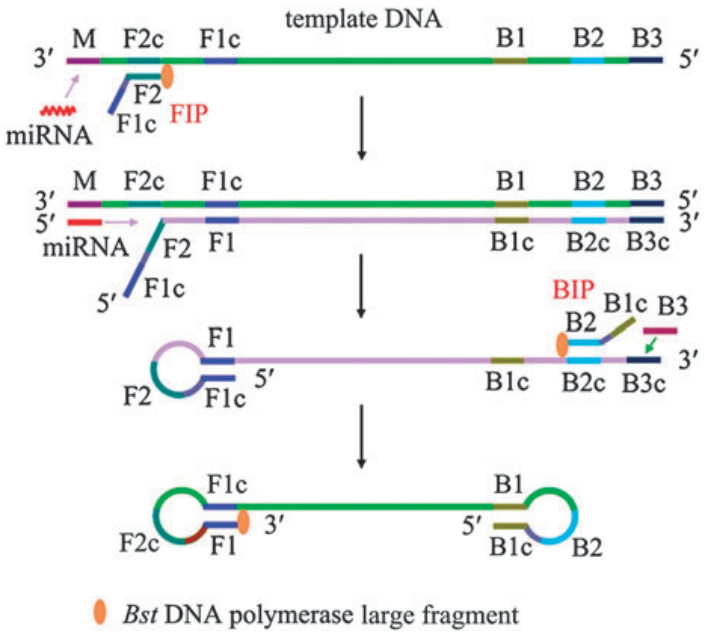

Figure I.12: **LAMP initiation principle.** The DNA template contains 6 sequences of interest: B3, B2, B1, F1c, F2c and M. The targeted miRNA is complementary to the M sequence. For the other sequences, the "c" note stands for "complementary", for example F1c is the F1 complementary sequence. A first set of inner and outer primers initiate single stranded (ss) DNA synthesis, generating a ssDNA molecule via strand displacement. A second set of inner and outer primers binds to this newly synthesized ssDNA molecule, leading to a stem loop structure. Alternative hybridization of inner primers to the loops of the structure generates inverted repeats of the target that are shaped like a cauliflower. Image and information extracted from [113] and [105].

I.5.3 Rolling circle amplification

Rolling circle amplification (RCA) is an amplification method which uses a circular single stranded template. It has first been introduced by Kool's group to synthesized RNAs by rolling transcription of DNA circular templates [117]. A short RNA or DNA primer hybridizes to a circular ss template and is then extended by a polymerase, leading to the production of a concatemer composed of repetitions of the complementary sequence of the circular template [118].

By introducing padlock probes, Jonstrup et al. adapted RCA for miRNA detection with an enhanced specificity [119]. The targeted miRNA anneals to the padlock probe which is circularized by a DNA ligase. However, due a northern blot readout, the sensitivity remained low. Improvements in specificity have then been implemented by using SplintR Ligase [120] or using dumbbell probes [121]. To improve the sensitivity of the method, different strategies have been proposed to reach an exponential amplification [118], including hyper-branched RCA [122], generating multiple circles from the RCA products [123] or primer generation using nicking enzymes [124].

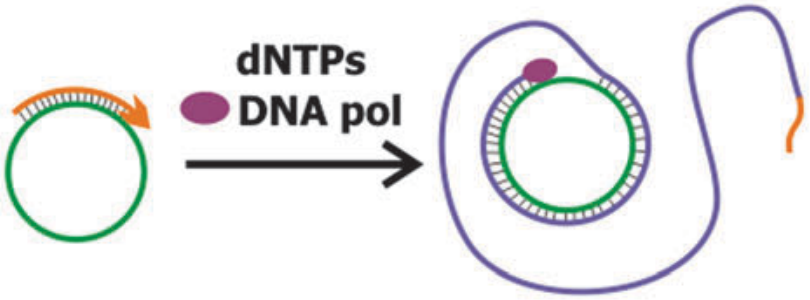

Figure I.13: **RCA principle.** A miRNA hybridizes on a circular single stranded template and is extended by a polymerase. By circling the template, the polymerase produces a DNA concatemer composed of repetitions of the complementary to the circular template. Amplification is monitored by hybridization of fluorescent probes complementary to the repeat sequence. Image and information extracted from [118] [27].

I.5.4 Exponential amplification reaction

EXponential Amplification Reaction (EXPAR) method was first introduced in 2003 by Van Ness et al. [125] [126]. In this approach, a DNA sequence is amplified using a DNA template, a polymerase and a nickase. However, this system suffers from unspecific amplification in absence of the targeted DNA strand [127]. Moreover, this unspecific amplification is correlated to the sequence of the DNA target [128]. In 2010, EXPAR has been used for the detection of Let7a, reaching a LOD of 10 fM with a dynamic range spanning over 10 orders of magnitude [129]. The amplification template contained two repeat sequences, respectively at its 3' terminus and at its 5' terminus, which were complementary to the targeted miRNA (figure I.14). However, no signicative difference was observed for the detection of let7a and let7e, highlighting a specificty issue. Several ameliorations have been proposed to enhance the design, such as adding a G-quadruplex DNAzyme into the reaction mechanism [130] to obtain a chemiluminescent signal or by changing the design to an asymmetric EXPAR based on a biotin/toehold featured template [131].

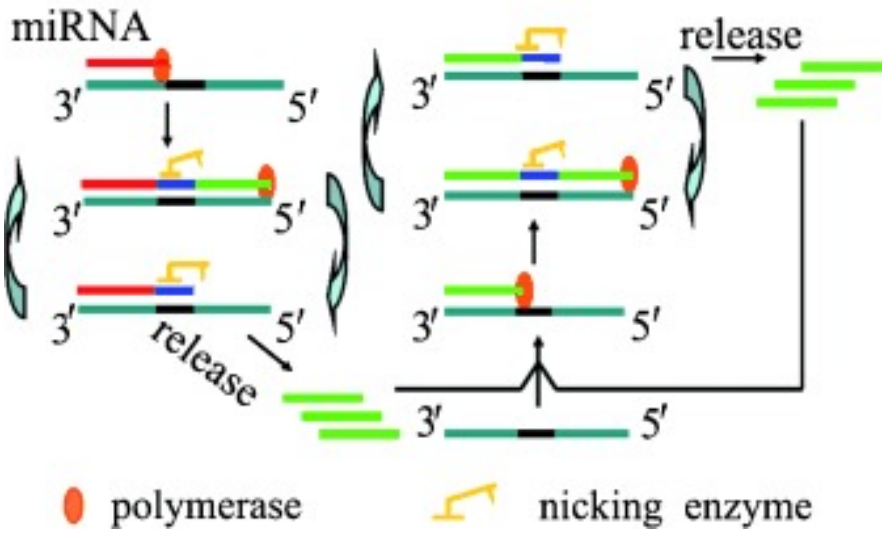

Figure I.14: **EXPAR principle.** The miRNA hybridizes to the 3' extremity of a template composed of two repeated sequences complementary to the miRNA and separated by the nicking recognition site of a nickase. The miRNA undergoes polymerisation and nicking cycles to generate DNA analogs of the miRNA. Those DNA analogs can then initiate polymerization and nicking cycles on other templates, resulting in an exponential amplification. Image and information extracted from [129].

I.5.5 Nucleic acid sequence-based amplification

Nucleic acid sequence-based amplification (NASBA) was designed to amplify ssRNA sequences [132] [133]. NASBA requires three enzymes: reverse transcriptase, RNase H, and DNA-dependent RNA polymerase [134]. A primer hybridizes to the targeted miRNA and a cDNA is produced by the reverse transcriptase (figure I.15). The RNAseH then hydrolizes the miRNA, another primer hybridizes to the previously produced cDNA and a dsDNA intermediate is formed. This dsDNA strands act as templates for T7 RNA polymerase, leading to an exponential amplification of the antisense miRNA complementary to the targeted miRNA.

NASBA is typically carried out at 41°C and 10^9-fold amplification in 2 hours. However, lack of reproducibility limits its potential application [135].

NASBA has been used for the multiplexed detection of 7 miRNAs and 7 mRNAs, using a microarray chip device [136]. First, a target specic RT step with a stem-loop primer was performed, converting all RNA targets into cDNAs. Then, a universal NASBA amplification reaction was carried out [105].

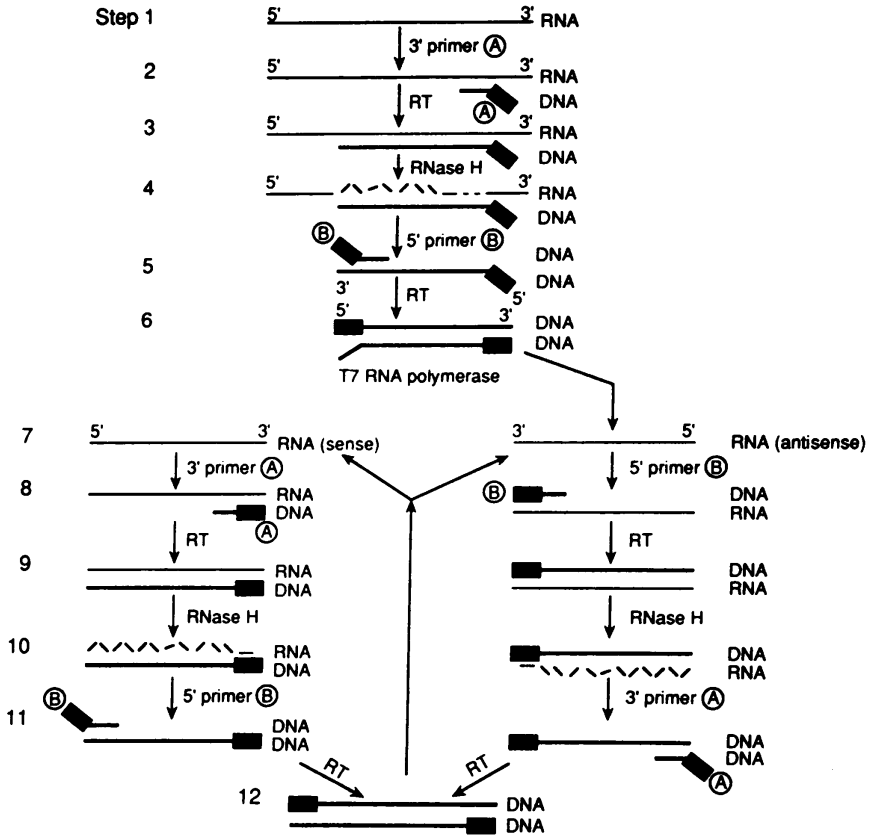

Figure I.15: **NASBA principle.** NASBA relies on three enzymes (reverse transcriptase, RNase H, and DNA-dependent RNA polymerase). A primer (primer A) hybridizes to the targeted ssRNA and is extended by the reverse transcriptase, producing a cDNA. The RNAseH then degrades the RNA sequence, primer B hybridizes to the previously produced cDNA and a dsDNA intermediate is formed. These DNA strands are then used as template to produce sense and antisense RNA strands, which can then be used to produce cDNA, resulting in an exponential amplification of the antisense RNA complementary to the target RNA. Image and information extracted from [134] [132].

I.5.6 Single molecule detection

I.5.6.1 Digital detection

Some of the previously described amplification chemistries have been adapted to a digital format. These are methods in which the target miRNA is partitioned into compartments following a poissonian distribution. Each compartment contains 0, 1 or a few miRNAs. After incubation, the percentage of positive compartments enables to compute the absolute miRNA concentration, The compartments are usually microdroplets [137] or microchambers [138]. RT-qPCR has been adapted to digital detection format in one [139] or two steps [140]. EXPAR has also been adapted to a digital format in droplets. This approach is called Integrated Comprehensive Droplet Digital Detection (IC 3D) [141]. A LOD of 10 copies per mL for synthetic miRNAs was reported.

I.5.6.2 Other techniques

There are other techniques that allow single molecule detection but do not rely on poissonian distribution of targets. After compartmentalization, the target concentration is obtained by counting the number of positive and negative compartments. For example, Hu et al. designed a method combining a padlock DNA ligation step with RCA. The RCA product assembled with fluorescent DNA probes to form nanoflower balls that were counted by flow cytometry [142]. Other techniques not based on nucleic acid amplification exist. We can mention the use of total internal reflection fluorescence [143]. We can also report the NanoString technology relying on a biotinylated microarray with a streptavidin capture probe and multiple detection probes binding to the miRNA forming a fluorescent barcode [27] [144].

I.6 Adaptation of nucleic acid amplification-based methods for protein detection

As seen previously, protein detection methods in solution have a sensitivity in the picomolar range. In contrast, exponential nucleic acid amplification methods can detect miRNAs down to the femtomolar range. Thus, the idea of coupling nucleic acid detection with an oligonucleotide labelled affinity reagent to detect proteins in a more sensitive manner has emerged. In this section, we will present the main protein detection methods based on a nucleic acid amplification approaches. These methods can be separated into two categories. Firstly, heterogeneous assays, based on the presence of a solid support, involving a capture step and washing steps. These methods allow the detection of analytes from crude or complex media thanks to the washing steps. Secondly, solution methods, in the absence of a solid phase. These have a simpler protocol, suitable for cases where there is no toxic effect or where heterogeneous detection is not possible, for example for secreted proteins.

I.6.1 Heterogeneous assays

I.6.1.1 Immuno-PCR

In 1992, Sano et al. introduced the immuno-PCR [145]. It is very similar to conventional ELISA but the enzyme labelled antibody has been replaced by a DNA-labelled antibody, which is then amplified by PCR. By doing so, a LOD of 2 fM was reached for the detection of bovine serum albumin (BSA), improving the sensitivity by 5 orders of magnitude compared to a conventional ELISA [146]. Three majors aspects of the protocol are essential for sensitivity, specificity and reproducibility: DNA-antibody linking, target immobilization and binding and assay readout [146]. In Sano's work, the DNA labelling of the antibody was achieved via the use of a chimeric protein. In order to apply this method to other proteins, Zhou et al. introduced a universal immuno-PCR protocol in which biotinylated antibody were used [147]. Streptavidin and biotinylated DNA label are then added consecutively, enabling a LOD of 9.6 fM for the detection of Ets1 protein, a transcription factor. As adding stepwise those last components is time consuming, covalent DNA labels were introduced [148], mapping the road for multiplexed immuno PCR where different DNA labels would be grafted on different specific antibodies. In the aim of increasing the number of oligonucleotides

carried per antibody, Niemeyer et al. used oligomers of self-assembled bis-biotinylated ds-DNA and strepatvidin, leading to linear nanostructures [149]. It was applied to rabbit IgG detection and immuno-PCR sensitivity was increased by a 10 fold factor. To improve target immobilization and binding and assay readout, detailed protocols have been published [150].

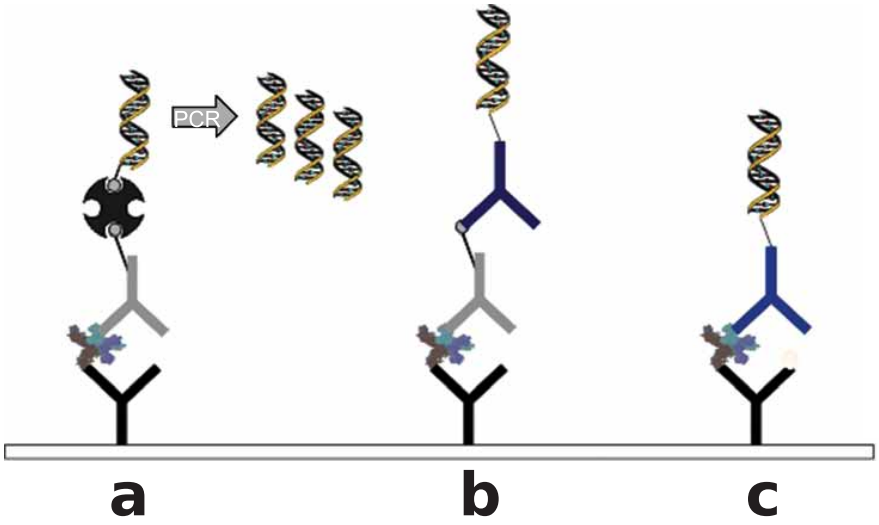

Figure I.16: **Immuno-PCR principle. a.** Sandwich immunoassay with a biotin labelled detection antibody. This antibody is then sequentially labelled with streptavidin and a biotinylated DNA oligonucleotide which is then quantify by PCR. **b.** Sandwich immunoassay with a biotin labelled detection antibody. A biotin speficic DNA labelled secondary antibody is then added, allowing quantification by PCR. **c.** Sandwich immunoassay with a DNA labelled detection antibody. Image and information extracted from [150].

I.6.1.2 Immuno-LAMP

The principle of immuno-LAMP has been exposed by Pourhassan-Moghaddam et al. in 2013 [151]. The principle is similar to immuno-PCR: the labelled DNA oligonucleotide present on the affinity reagent, such as antibody or aptamer, is instead amplified by LAMP (figure I.17). To the best of our knowledge, the first experimental implementation was carried out by Hua et al. one year after [152] for the detection of organophosphorus pesticides. They implemented a yes/no assay consisting of two steps: a competitive immunoreaction between the analyte and a phage-borne peptide followed by LAMP. They achieved a detection ranging from nanomolar to micromolar for 8 different organophosphorus pesticides. Quantification of biotynilated mucin 1 bound to streptavin-coated beads was achieved by coupling a mucin 1 specific aptamer with LAMP [153]. The dynamic range spanned over 7 orders of magnitude and a LOD of 1 aM was reached. The same group developed a DNA encapsulated liposome-LAMP amplification method for the quantification of P-glycoprotein [154]. Beads conjugated to capture antibodies were used to bind to the target protein and a DNA-liposome labelled detection antibodies staining was realized. Liposomes are used to engulf several DNA target that are then amplified by LAMP. They reached a LOD of 35 aM with a dynamic range spreading over 5 orders of magnitude. Liu et al. [155] used the same approach in wells with a

DNA liposome labelled secondary detection antibody to detect REG1A in urine. The LOD was 56 aM and the dynamic range spanned over 10 orders of magnitude.

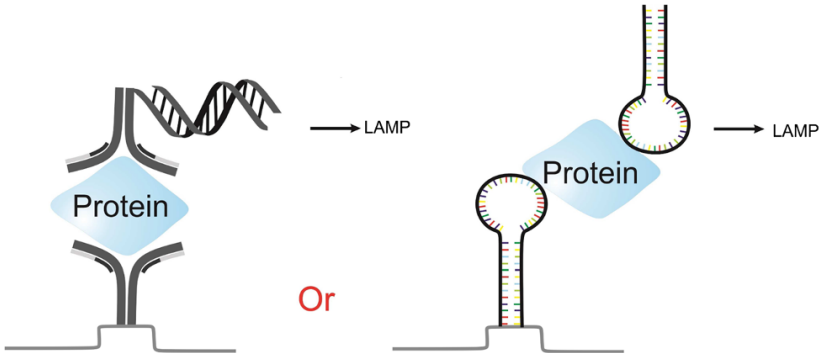

Figure I.17: **Immuno-LAMP principle.** Sandwich immunoassay with a DNA labelled detection antibody (left). Antibodies can be replaced by other affinity reagents such as aptamers (right). The DNA labelled affinity reagents are then quantified by LAMP. Image and information extracted from [151].

I.6.1.3 Immuno-RCA

Immuno-RCA was first reported by Schweitzer et al. [156]. The principle is similar to immuno-PCR: the labelled DNA oliognucleotide present on the antibody instead acts as a primer complementary to a circular template and is amplified by RCA (figure I.18). This led to an increase in sensitivity of 2–3 orders of magnitude over the conventional ELISA [80]. Morevoer, the RCA is isothermal and does not require thermal cycling, therefore not dissociating the antibody / antigen complexes and leading to a localized RCA around the complexes. This main advantage has led to the use of this method for micro-array based multiplexed protein detection [157]. It has been applied to multiple allergen-specific IgEs detection [158]. This method has also allowed to quantify simultaneously 75 cytokines with femtomolar sensitivity and a dynamic range spanning over three orders of magnitude [157]. Aptamers have been used to replace antibodies and achieved low pM detection limit for the detection of thrombin, this will be commented in section I.6.2.2.

I.6.1.4 Other immuno based exponential nucleic acid methods

A sandwich immunoassay coupled with EXPAR was developed for the detection of MUC1 [159] with a LOD of 1.63 pM and a dynamic range spanning over 4 orders of magnitude.

A sandwich immunoassay coupled with NASBA was carried out for the mulitplexed detection of adrenocorticotropic hormone (ACTH), synthetic peptide, and two common waterborne pathogens, Escherichia coli (E. coli) and rotavirus, in artificial samples [160]. The detection antibody has been labelled with a DNA tag instead of a RNA one because of the resistance of DNA to RNAse. A LOD of 0.1 fM was reached with a dynamic range spanning over 8 orders of magnitude.

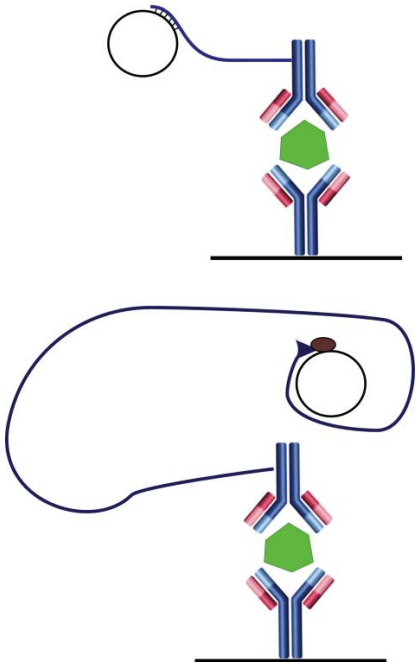

Figure I.18: **Immuno-RCA principle.** Sandwich immunoassay with a DNA labelled detection antibody. The DNA carried by the detection antibody is used as primer for RCA. Image and information extracted from [80].

I.6.2 Solution-based assays

In nucleic acid detection methods, the amplification is triggered by the presence of the target nucleic acid sequence. However, in the case of proteins, the amplification is triggered by the presence of the protein-specific oligonucleotide labelled affinity reagent. While in heterogeneous methods the washing steps allow to return to a condition of presence or not of the target oligonucleotide, it is not possible for solution based assays. Therefore, the amplification start mechanism must be adapted. Two approaches based on the use of a proximity effect for a pair of affinity reagents recognizing the same protein have been developed. The first one called proximity ligation assay (PLA) uses ligation and the second one called proximity extension assay (PEA) uses extension by a polymerase.

I.6.2.1 Proximity ligation assay

PLA was first introduced by Fredriksson et al. in 2002 [161]. Briefly, a matched pair of affinity reagents, typically antibodies [162] or nucleic acid aptamers [163], linked to specific oligonucleotides binds to the targeted protein, locally increasing the concentration of oligonucleotides. The oligonucleotides come in close proximity, hybridize together to a connector oligonucleotide, allowing a DNA ligation enzyme to join them. In the case of Fredriksson et al., the ligated DNA amplicon has then been detected by q-PCR, allowing detection of zeptomoles of platelet-derived growth factor (PDGF). Ke et al. cut the DNA amplicon with restriction enzymes, circularized it and quantified it with RCA [164]. They reached a LOD of 5 fM with a dynamic range over 5 orders of magnitudes for IL-6 detection. In comparison,

they reached a LOD of 9 fM with a dynamic range over 5 orders of magnitudes for q-PCR. The PLA assay has been multiplexed using different probes sequences and lengths, reaching a 24-plex assay [165]. However, DNA ligase can lose a part of its activity in complex biological samples such as human plasma, impairing assay performances.

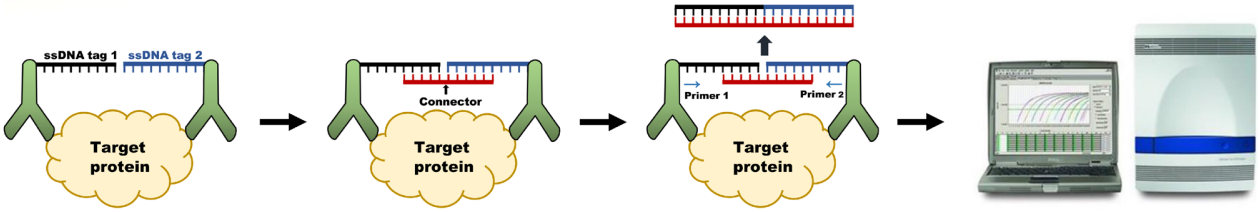

Figure I.19: **PLA principle.** Two oligonucleotide labelled affinity reagents bind to the targeted protein. The oligonucleotides come in close proximity and hybridize together to a connector oligonucleotide. A DNA ligase binds the two oligonucleotides together. The newly formed DNA amplicon can be detected by further analysis such as q-PCR. Image and information extracted from [162].

I.6.2.2 Proximity extension assay

In order to overcome the drawbacks of PLA, PEA has been introduced [166]. Similar to PLA, a matched pair of affinity reagents linked to specific oligonucleotides binds to the target protein, locally increasing the concentration of oligonucleotides. The oligonucleotides come in close proximity, hybridize to each other and one of them is extended by a polymerase, creating a DNA amplicon. This DNA amplicon can then be detected using nucleic acid detection methods. Lundberg et al. coupled it with q-PCR, reaching LOD of 48 fM and 9 fM for IL-8 and glial cell line-derived neurotrophic factor (GDNF) with a dynamic range spanning over four orders of magnitude [167]. Di Giusto achieved a low pM detection limit for thrombin detection via an aptamer based proximity extension-mediated RCA assay [168]. The PEA assay has been multiplexed using different probes sequences and lengths, for example Olink proposes different commercial 96-plex protein panels [169].

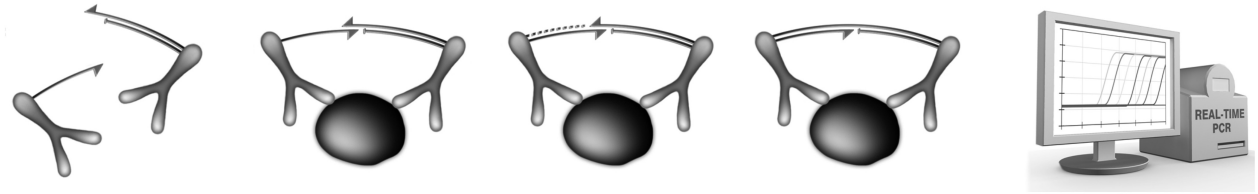

Figure I.20: **PEA principle.** Two oligonucleotide labelled affinity reagents bind to the targeted protein. The oligonucleotides come in close proximity and hybridize to each other. A DNA polymerase extends the oligonucleotide with the free 3' extremity. The newly formed DNA amplicon can be detected by further analysis such as q-PCR. Image and information extracted from [167].

I.7 Concluding remarks and objectives of the thesis

In this introduction, we presented the basic methods used for protein detection and the exponential nucleic acid amplification methods used for miRNA detection. These last are the most sensitive and it is thus tempting to adapt them for protein detection. However, this increase in sensitivity is possible at the cost of an increase in the complexity of the methods as well as skills required to perform these tests. It should be noted that these methods are often combined with each other. For example, simultaneous detection of several proteins has been achieved using antibody microarrays with RCA [170]. This allows to combine the different advantages of these methods.

The problem of specificity is challenging. Indeed, for proteins this specificity depends on the selectivity of the affinity reagent(s), which is not related to the detection method itself. Secondly, the link between these affinity reagents and the detection method can cause serious problems. For miRNAs it is sometimes necessary to be specific at the single nucleic acid level because of the high similarity between different miRNAs. Furthermore, to be used on biological samples, these methods must be robust to interfering components present in the different samples. For this aspect, heterogeneous methods including numerous washes, such as immunoassay based methods or suspension arrays have a clear advantage: although they are more time consuming, these washes allow to get rid of the toxic effects arising from biological samples.

Because common chemistry can be used for both miRNA and protein detection, it opens the door to both multiplexed and multimodal detection, meaning detection of multiple classes of biomarkers. Multimodal detection have been reported for cancer screening in liquid biopsy [171] [172] or for detection of PD-L1, a biomarker used to find patient eligible for immune checkpoint inhibitor therapy [173]. This approach only begins to be explored for neurodegenerative diseases. Indeed, as several miRNAs can regulate the expression of a gene, it is interesting to look at the expression of the corresponding protein, thus providing additional information. For example, miR-7, miR-153 and miR-203a-3p contain binding sites targeting the 3' UTR of the synuclein alpha gene and thus impact the synuclein alpha protein level involved in PD [174].

I.8 Aims of the thesis project

This thesis project is part of the collaborative ANR project MolPro2Biosens. The goal of MolPro2BioSens is to design a microfluidic device for the detection of multiple biomarkers in liquid biopsies, such as feces in order to diagnose Parkinson's or Alzheimer's disease. The device would integrate nucleic acid-based amplification chemistry, spatial multiplexing combined with an electronic readout. This project involves 4 research teams:

- The Enteric Nervous System Group from the University of Applied Sciences, Kaiserslautern, which is in charge of identifying the relevant biomarkers. They focused on miRNA and proteins that are relevant for neurogenerative diseases.

- Our team from ESPCI, Paris, in charge of developing a molecular-programming-based chemistry to detect these biomarkers at relevant concentrations.

- The Biomedical Signalling Group from the University of Applied Sciences, Aachen, in charge of designing silicon nanowires that will be grafted on the microfluidic device to perform the electronic readout.
- A team from the Institute of Electronics Microelectronics and Nanotechnology, Lille, in charge of the integration of the nanowire and the detection chemistry inside the microfluidic chip.

The aim of this thesis project is developed an amplification chemistry capable of detecting both miRNAs and proteins. The ultimate goal is to incorporate this chemistry in a multiplexed and multimodal microfluidic setup for the profiling of liquid biopsy biomarkers.

The first objective was to adapt the previous work of our team to detect miRNA involved in neurogenerative disease. Indeed, our group previously developed an exponential isothermal detection method suited for miRNA detection, called programmable universal molecular amplifier (PUMA). This method uses a noise-reducing molecular amplification network and is compatible with digital quantification using droplet microfluidics.

Once the detection of synthetic version of such miRNA achieved, we verified that we were able to detect two of them in total miRNA extracted from mouse striatum by introducing a capture step on particle. We then attempted to modify the capture step by cutting the conversion template in two parts: the introduction of a ligase allows, in the presence of the targeted miRNA, to reconstitute the conversion template. Finally, we tried to detect long nucleic acids with two different approaches: the first one based on the use of RNAse H and the second one based on the use of a three way junction process.

The second objective was to adapt the PUMA assay for protein detection. To that extent, we adapted the conversion module. We achieved detection of human alpha-Thrombin through an aptamer based PEA. Due to poor sensitivity, we then focused on an immunoassay based detection on cytokines, called immuno-PUMA. We demonstrated ultra sensitivity in the femtomolar range. Leveraging our expertise in DNA circuitry, we attempted to build a DNA-based protein classifier for protein signature recognition.

In combination with aptamer, we showed that PUMA can be adapted to the detection of cell surface markers.

In line with the collaborative objective, we explored spatial multiplexing of miRNA: we obtained preliminary results on spatially-localized amplification from DNA-functionalized microbeads.

Chapter 1

Nucleic acid detection

1.1 Résumé du chapitre

Dans ce chapitre, nous décrivons tout d'abord le programme moléculaire d'amplification isotherme utilisé pour la détection des microARN (miARN). Le programme moléculaire est basé sur la boîte à outils Polymerase Exonuclease Nickase Dynamic Network Assembly Toolbox (PEN DNA Toolbox) et est composé de quatre matrices d'ADN. Chacun de ces modèles remplit une fonction spécifique : conversion, amplification, seuillage et rapport. Mélangés avec les enzymes adéquates, ils forment un programme moléculaire de détection de miARN qui peut être utilisé dans des tubes ou dans des compartiments tels que des gouttelettes d'eau dans l'huile. La compartimentalisation permet une quantification digitale absolue donnant directement accès aux concentrations. Nous présentons ensuite une série de miARNs d'intérêt pour les maladies neurodégénératives et les résultats obtenus pour leur détection via ce programme moléculaire. Ensuite, nous nous concentrons sur le greffage de modèles de convertisseurs sur les particules et introduisons une étape de capture. Cette étape de capture est optimisée pour détecter les miARNs extrait du striatum de souris. Puis, nous nous intéressons à une approche de capture intégrant une étape de ligation qui permet de restaurer la fonction du convertisseur, réduisant ainsi la production non spécifique de trigger. Enfin, nous suggérons des stratégies de conversion adaptées à d'autres acides nucléiques en nous focalisant sur les acides nucléiques plus longs, tels que les ARN messagers (ARNm) et les ARN génomiques. Premièrement, avec une approche intégrant la RNAseH. Ensuite, avec un processus de jonction à trois voies.

1.2 Chapter summary

In this chapter, we first describe the isothermal amplification molecular program used for miRNA detection. The molecular program is based on the Polymerase Exonuclease Nickase Dynamic Network Assembly Toolbox (PEN DNA Toolbox) and is composed of four DNA templates. Each of these templates performs a specific function : conversion, amplification, thresholding and reporting. Mixed together with the adequate enzymes, they form a miRNA detection molecular program which can be used in tubes or in compartments such as water-in-oil droplets. The compartmentalization allows absolute digital quantification. We then present a series of miRNAs of interest for neurodegenerative diseases and the results obtained for their detection via the molecular program. Then, we focus on the grafting of converter templates on particles and introduce a capture step. This capture step is optimized to detect miRNA in total miRNA extracted from mouse striatum. We are also interested in a capture approach incorporating a ligation step that restores the function of the converter template, reducing the non-specific production of trigger. Finally, we try to diversify the nucleic acids detected by focusing on longer nucleic acid, such as mRNA and genomic RNA. First, with an approach integrating RNAseH. Secondly, with a three way junction process.

1.3 Introduction: molecular programming for miRNA detection

Our team has previously introduced a new type of in vitro molecular program where modules can be connected together in order to create a DNA network [175]. This toolbox, called «PEN-DNA toolbox» (Polymerase Exonuclease Nickase-Dynamic Network Assembly toolbox), is inspired from gene regulation networks from which it reproduces the modularity and the essential dynamic components. This toolbox is composed of 3 classes of enzymes (polymerase, nickase and exonuclease) and tailored DNA oligonucleotides called templates. Its energy is supplied by dNTPs. It can be seen as a molecular machine whose behaviour is controlled by a DNA software constituted by DNA modules encoded in short oligonucleotides (20 to 30 bases). Those templates can be rationally connected in order to create a DNA network with a predefined function. The communication between templates is realized through a ssDNA called trigger, which design enables it to interact with each template, either by being the input and /or the output. The unspecific degradation of DNA strands induced by the exonuclease keeps the system out of equilibrium. Template's backbone is chemically modified with phosphorothioate (PTO) in order to be protected of the degradation induced by the exonuclease [176].

The isothermal amplification method designed by our group is directly inspired by the principle of the EXPAR method (see section I.5.4). In order to overcome the limitations of EXPAR, our group added a new DNA template reducing the background noise by inactivating unspecifically produced trigger strands stemming from leaky reactions [177]. By doing so, Montagne et al. introduced a bi-stable amplification reaction. The mechanism is detailed in figure 1.1. Briefly, a target DNA strand called trigger can be amplified in presence of an autocatalytic template (aT). After hybridization to the aT, the trigger acts as primer for a polymerisation and nicking cycle while an exonuclease degrades the trigger. This system has an unstable steady state, for no trigger in solution, and a stable steady state at high trigger concentration, when the aT is saturated. Adding a pseudo template (pT), which disables trigger by adding a few bases to it, introduces a second trigger degradation pathway. Those two degradation pathways form a global non linear degradation rate, leading to a system with two stable steady states (respectively for no trigger in solution and at high concentration of trigger, when aT is saturated) and an unstable steady state. This unstable steady state corresponds to the saturation of the pT and leads to a threshold trigger concentration. When the concentration of trigger is below this threshold, no amplification is observed while the amplification occurs when the trigger concentration is above this threshold.

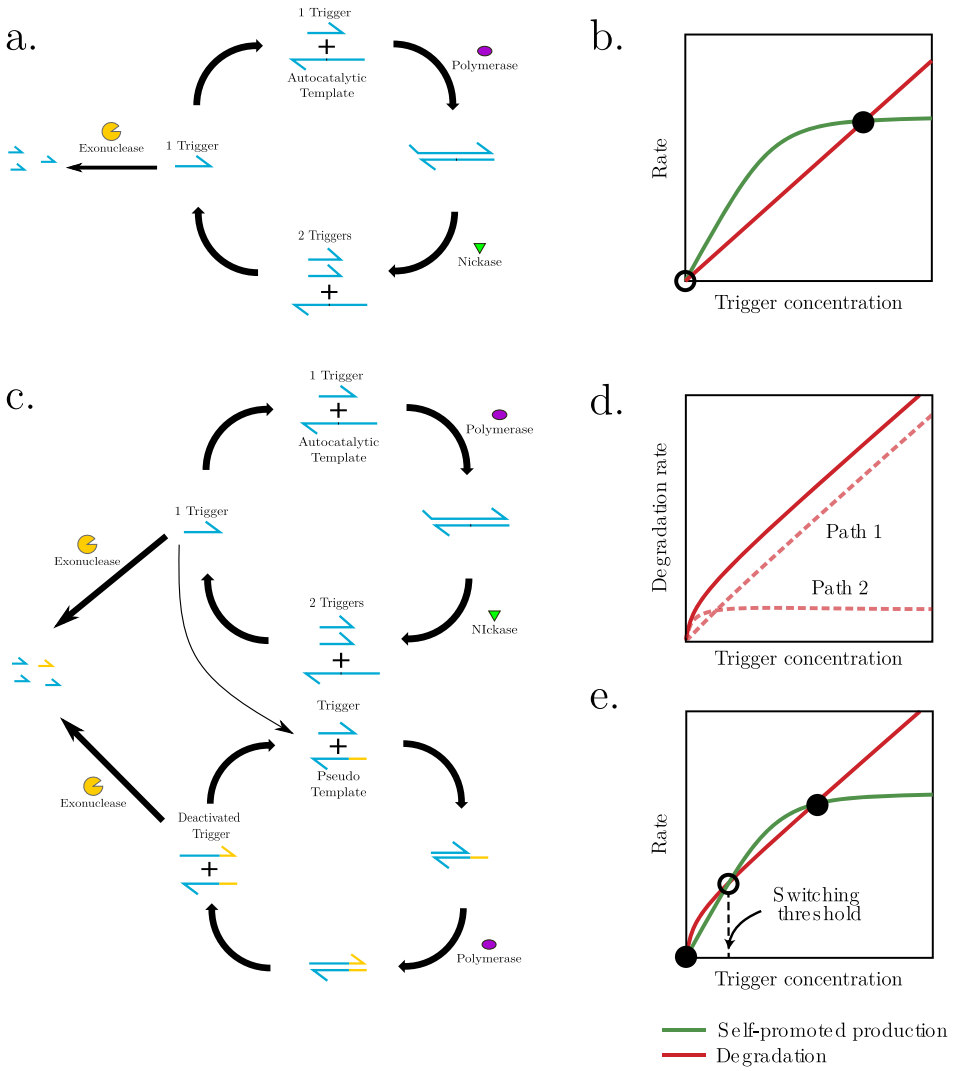

Figure 1.1: **Principle of a PEN DNA Toolbox induced bi-stable switch. a**. A trigger molecule is exponentially amplified by polymerisation and nicking cycles upon an amplification template (autocatalytic template) while an exonuclease degrades the trigger. **b.** Trigger production (green curve) and degradation (red curve) rates in function of trigger concentration for the system described in a. This results in a unstable steady stable in the absence of trigger (black circle) and in a stable steady state at high concentration of trigger (black dot). **c.** A trigger molecule is exponentially amplified by polymerisation and nicking cycles upon an amplification template (autocatalytic template) while an exonuclease and a pseudo template degrade the trigger. **d.** Two different degradation rates are induced by the exonuclease (path 1) and the pseudo template (path 2). The sum of those two degradation rates results in a non linear global degradation rate (red curve). **e.** The superposition of a linear production of trigger (green curve) and a non linear degradation of trigger (red curve) result in a system containing two stable steady (black dots) state and one unstable steady state (black circle). A threshold trigger concentration can thus be defined. When the concentration of trigger is above this threshold, the amplification occurs. However, when the trigger concentration is below this threshold, no amplification is observed. Information & images extracted from [177].

1.3.1 PEN DNA Toolbox mediated miRNA detection

In our case, we are interested in molecular programs for biosensing application. For that purpose, we used a molecular program capable of ultrasensitive miRNA detection via an isothermal amplification mechanism. Such program is composed of 4 templates, each one of them having a specific function [178]:

- **A conversion template (cT):** It converts the molecular signal into a chosen DNA strand, called trigger, which will interact with the other templates (figure 1.2). Thus, it allows the decoupling of the exponentially amplified sequence from the miRNA sequence.
- **An autocatalytic template (aT):** It exponentially amplifies the trigger in isothermal conditions (figure 1.3).
- **A pseudo-template (pT):** It inactivates trigger thus inducing an amplification threshold. If set above the noise, nonspecific amplification is cancelled (figure 1.4).
- **A reporter template (rT):** It generates a specific fluorescent signal from the trigger (figure 1.5).

The cT is designed in such a way that the target miRNA specifically hybridizes to its 3' end. Once captured, the miRNA is used as primer to produce a 12 bases DNA sequence, called trigger, via polymerisation and nicking cycles with a DNA polymerase and Nt.BstNBI. It is the link between the target miRNA and the other modules of the PEN DNA Toolbox. Noteworthy, only the cT (and more precisely, its 3' part complementary to the target) needs to be changed to detect a different miRNA.

The aT and pT are composing a bi-stable switch, which is the core of this molecular program. The aT contains two repeat sequences, respectively at its 3' terminus and at its 5' terminus, leading to the regular doubling of trigger. A trigger hybridizes to the 3' end of the aT and is extended by a polymerase. By design, a Nt.BsmI nicking site is included in the extended product, leading to the release of 2 triggers. The two triggers can then bind to two aTs, leading to a regular doubling of the trigger amount, until the saturation of the available aTs in solution. Noteworthy, the 3' end of the aT is complementary to only 10 bases of the trigger while the 3' end of the pT is complementary to the 12 bases of the trigger, leading to preferential hybridization of trigger to pT. The role of the pT is to linearly deactivate a proportion of trigger to compensate the unspecific production of trigger inherent to all EXPAR system. To do so, the 3' part of the pT hybridizes to the trigger, which then act as a primer and is extended of a few bases by a polymerase. This extended trigger cannot prime the aT anymore and is then degraded by the exonuclease. If enough trigger is produced, the pT deactivation saturates. By overcoming the threshold of trigger concentration imposed by the presence of pT, the exponential amplification of trigger by the aT starts. The threshold of trigger concentration can be modified by changing the pT concentration.

The reporter template (rT) is a hairpin oligonucleotide with a fluorophore at its 5' extremity and the corresponding quencher at its 3' extremity. A part of its sequence is complementary to the trigger, allowing the trigger to hybridize and to be extended by a polymerase. This results in the opening of the rT and the production of a fluorescent signal. This reaction is made reversible by including the Nb.BsmI nicking site in the elongation

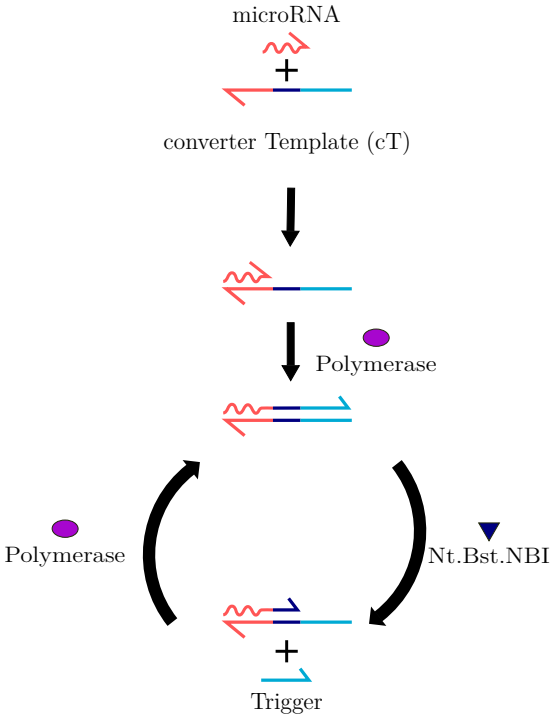

Figure 1.2: **Principle of the converter template.** One miRNA (red) hybridizes to the 3' part of the converter template. This miRNA is extended by a polymerase. The converter template has been designed to contain a Nt.BstNBI nicking site when replicated (dark blue), resulting in the nicking of the polymerisation product and releasing a molecule of trigger (light blue). This whole cycle results in a linear increase of the amount of trigger.

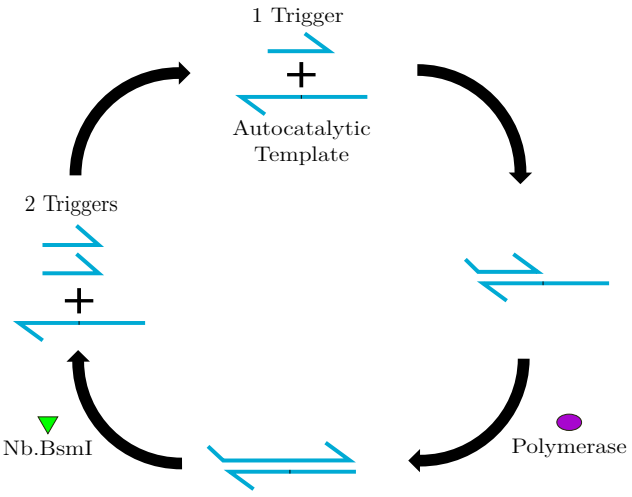

Figure 1.3: **Principle of the autocatalytic template.** One trigger hybridizes to the 3' part of the autocatylic template. This trigger is extended by a polymerase. The trigger has been designed to contain a Nb.BsmI nicking site when replicated, resulting in the nicking of the polymerisation product and releasing two molecules of trigger. This whole cycle results in a regular doubling of the amount of trigger, constituting an exponential amplification

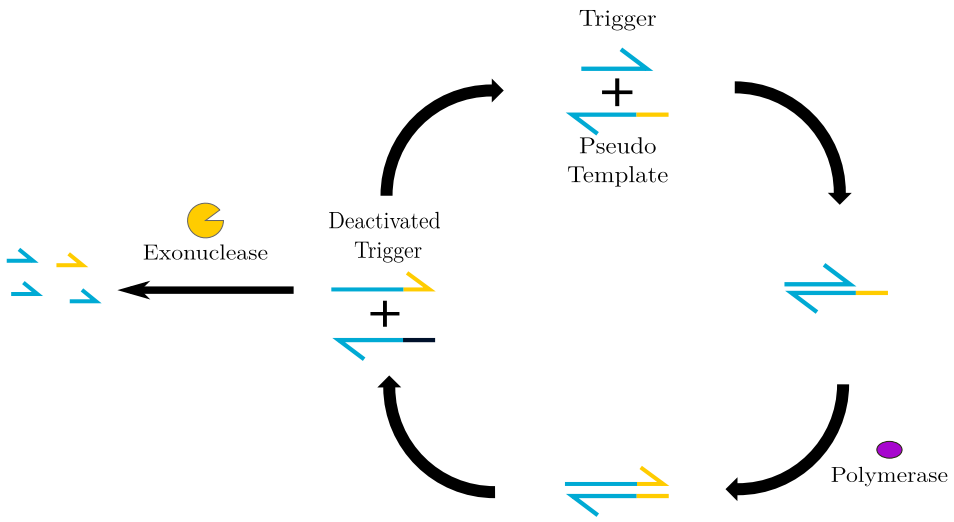

Figure 1.4: **Principle of the pseudo-template.** One trigger hybridizes to the 3' part of the pseudo-template. This trigger is extended by a polymerase, adding a few bases to the 3' part of the trigger. This results in the production of a deactivated trigger unable to be amplified by the autocatalytic template. This deactivated trigger can then be degraded by an exonuclease.

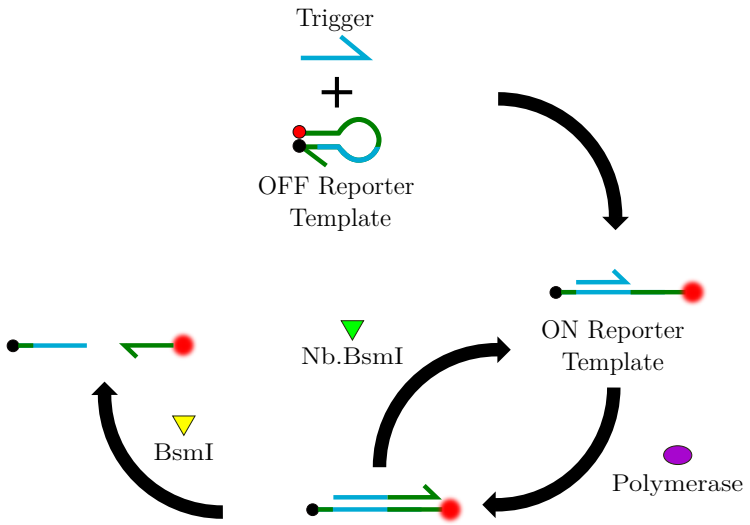

Figure 1.5: **Principle of the reporter template.** The reporter template is a DNA hairpin with a fluorophore at its 5' extremity and a quencher at its 3' extremity. A trigger molecule binds to the hairpin and is then extended by a polymerase, resulting in the opening of the template and in the emission of a fluorescent signal. The extended trigger can be cut by a nickase enzyme, Nb.BsmI or by a restriction enzyme, BsmI.

product. Optionnaly, the restriction enzyme BsmI may be added to the amplification mixture, leading to the cleavage of the double-stranded rT and making fluorescence emission irreversible following amplification. In the absence of trigger sequence, no fluorescence is produced as the rT stays closed.

When those 4 templates are mixed together in optimized concentrations, they form a molecular program able to detect a target miRNA. If the target miRNA is present, the cT produces triggers. If enough cTs are activated, the amount of trigger overcomes the threshold imposed by the pT and the aT starts the exponential amplification. rT is then opened, producing a fluorescence output (figure 1.6). The higher the concentration of the target miRNA, the faster the exponential amplification of the trigger and the sooner the fluorescent signal. Thus, the amplification time is correlated to the miRNA concentration.

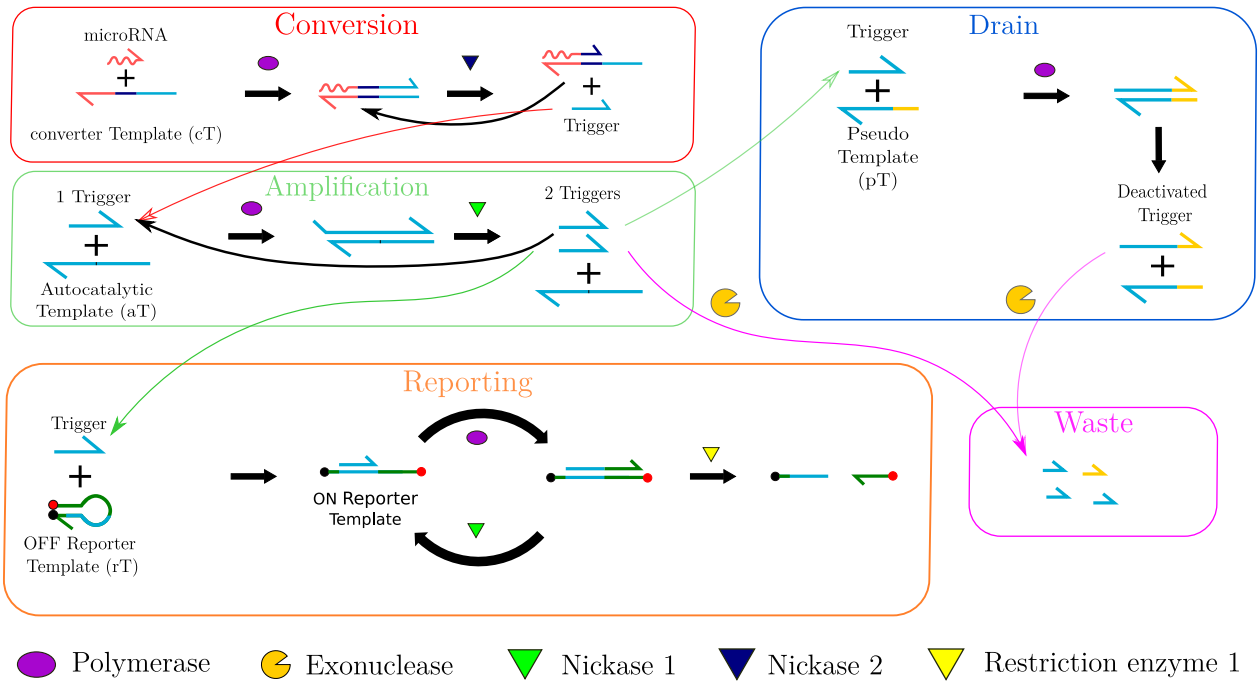

Figure 1.6: **Architecture of the Programmable Ultrasensitive Molecular Amplifier (PUMA) for miRNA detection:** a conversion template (cT) converts the target molecule into a universal DNA trigger; an amplification template (aT) exponentially amplifies this trigger sequence; the background noise, inherent to all exponential amplification mechanism is reduced thanks to the pseudotemplate (pT) that acts as a drain for unspecifically produced trigger strands stemming from leaky reactions; a reporting template (rT) produces a fluorescence output using trigger strands.

In practise, the templates, enzymes, miRNA and reaction buffer are mixed together (figure 1.7 a.). They are then incubated at 50°C and the amplification reaction is monitored in real-time using fluorescent readout (from the reporter template). Our team developed and applied this method to the detection of different miRNAs, including Let7a (figure 1.7.b.i.). All the templates are necessary: if one removes the pT, the limit of detection of Let7a detection is severely reduced (figure 1.7 b..ii.). If one removes the cT (figure 1.7 b..iii.), no amplification takes place, independently of the Let7a concentration. By comparing figure 1.7.b.i. and figure 1.7 b.ii., we can see how the presence of pT greatly improves the limit of detection of the system compared to EXPAR. However, this gain in sensitivity is payed by an increase of the amplification time.

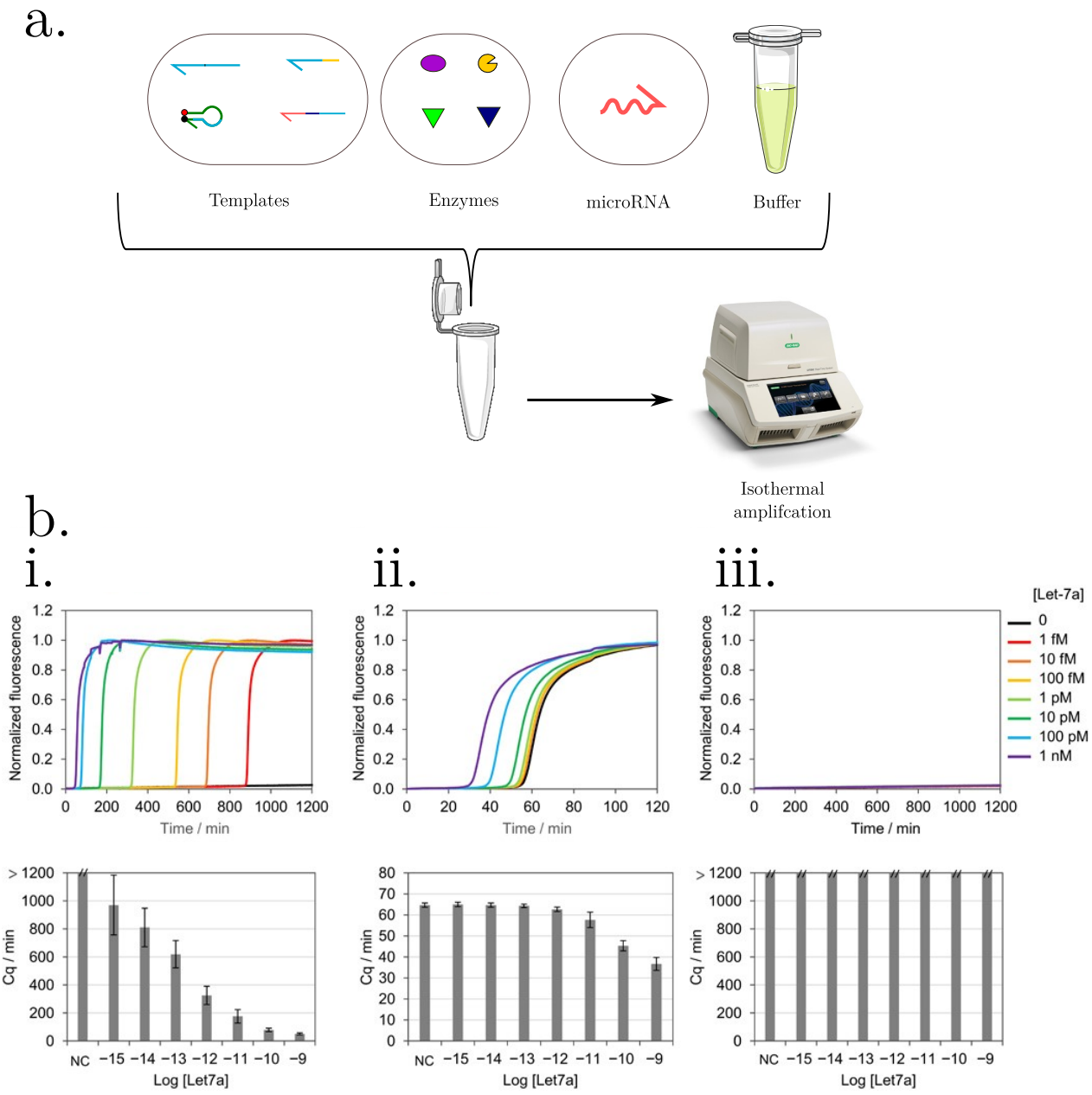

Figure 1.7: **miRNA detection workflow using the PEN DNA Toolbox. a.** DNA Templates, enzymes, miRNA and reaction buffer are mixed together, incubated and monitored by real time fluorescence. **b.** Range of Let7a from 1fM to 1nM in presence, respectively, of the four-template molecular program (**i.**),the molecular program without the pT (**ii.**) or without the cT (**iii.**). The amplification times were extracted and plotted as a function of Let7a concentration. Information and images extracted from [178].

1.3.2 Microfluidics and digital detection

To increase the sensitivity and the accuracy of the method without reaching too long incubation times, the assay has been moved to a digital format (figure 1.8). The previously described mixture containing BsmI is partitioned, in our case into water-in-oil droplets, in such a way that most droplets contain 0, 1 or a few miRNAs according to Poisson distribution. The droplets are generated using single flow or co-flow PDMS on glass chips [179]. Typically, 10 μm diameter droplets are used, leading to a concentration of either 3 pM or 0 pM, respectively, for droplets containing 1 or 0 miRNA. The emulsion is incubated for a few hours at 50°C, sandwiched between sealed glass slides and imaged by fluorescence microscopy. Two kinds of droplets can be distinguished: positive, fluorescent droplets, where the rTs are open, meaning that at least one miRNA molecule is present, and negative, colorless droplets, where the rTs are closed, meaning that no miRNA molecule is present. Images are computer analyzed and the absolute concentration of miRNA is obtained applying Poisson statistics.

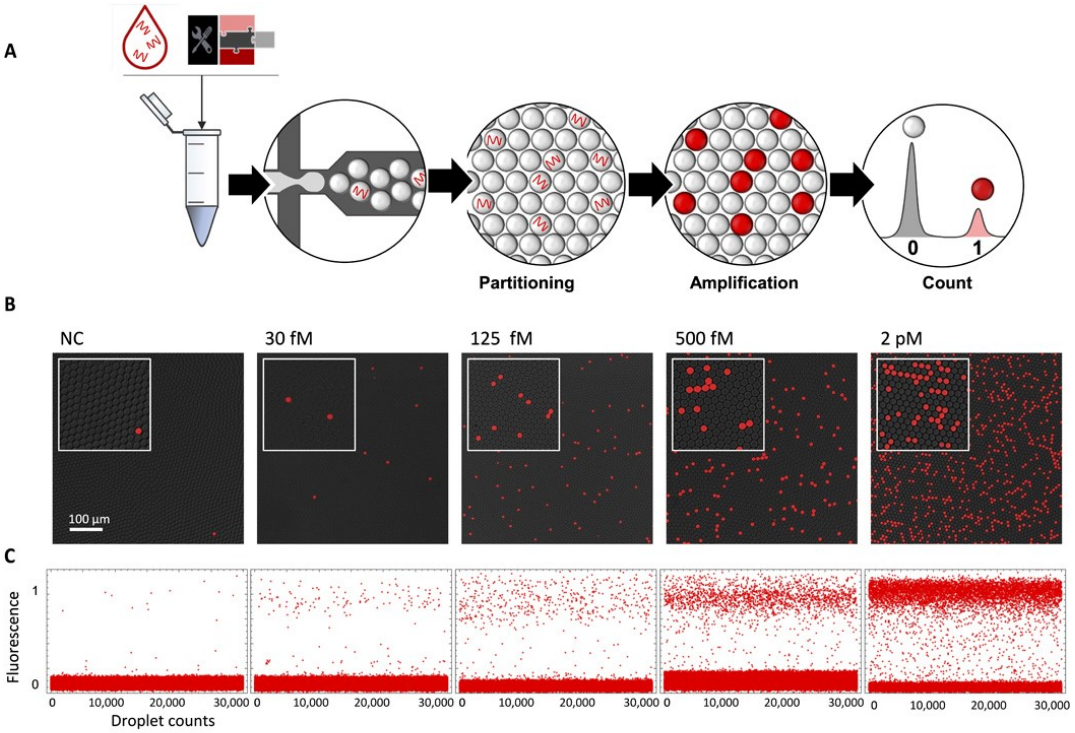

Figure 1.8: **Let7a digital detection. A.** Targeted miRNA molecules are mixed with the templates, enzymes and buffer of the molecular program. Monodiperse water in oil droplets are produced, resulting in the partitioning and random distribution of the miRNA molecules according to Poisson distribution. After incubation, the droplets are imaged by fluorescence microscopy. The droplets containing a least one target display a positive fluorescence signal (1) while the remaining droplets stay negative (0), allowing absolute concentration calculation using Poisson statistics. **B.** Fluorescence microscopy images of an emulsified Let7a range. **C.** Fluorescence level analysis of 30,000 droplets. Information and images extracted from [178].

1.4 Application to miRNA relevant for neurodegenerative diseases

1.4.1 Target miRNAs choice

During this PhD thesis, biomarkers involved in neurodegenerative diseases were targeted. As guts contains neurons [180], the main hypothesis is that biomarkers involved in those diseases could be found in the guts [181] [182] and to further extents, in the feces. We collaborated with the Enteric Nervous System Group, led by Pr. Schäfer at the University of Applied Sciences Kaiserslautern (UASK). It has been decided to use an early symptomatic synuclein (A30P) transgenic mice model [183] and to focus on miRNA. In agreement with Anne Christmann, a PhD student from this group, we decided to target synthetic miRNA already reported in the literature as a first step towards miRNA detection in relevant biological samples. The list of this targeted miRNA can be found in table 1.1. A part of this miRNA has been identified in model mice [183] and a part has been identified in the human brain [184].

1.4.2 Synthetic miRNA detection

The first step towards the detection of miRNA in biological samples was to apply the method described in section 1.3.1 to the detection of synthetic versions of the chosen miRNAs. Vent(exo-) DNA polymerase was used in this set of experiments. For each of them, a specific cT has been designed. Only the miRNA complementary part of each cT is different, all of them producing the α trigger. Mixes containing the miRNA-specific cTs have been prepared and spiked with a varying concentration of the corresponding target, 10 pM, 1 pM, 100 fM and a negative control referred as NC. The experimental data are displayed in figure 1.9. To determine whether a miRNA can be detected or not, we calculated a score taking into account the speed of detection (amplification time, At) and the unspecific production of trigger:

$$Score_{1\,pM} = \frac{Amplification\,time\,of\,the\,no\,target\,control}{Amplification\,time\,of\,the\,1\,pM\,sample}$$

This score was calculated for each miRNA and reported in table 1.1. The higher the score, the better the discrimination between the specific production of trigger due to the miRNA and the unspecific production of trigger. The miRNAs were ranked and sorted into 3 categories. Firstly, the ones with a score greater than or equal to 2, corresponding to miRNAs which can be detected. Secondly, the one with a score superior to 1.2 and inferior to 2, corresponding to miRNAs for which the detection is difficult. Lastly, the one with a score inferior or equal to 1.2, corresponding to miRNAs which cannot be detected. This difference in detection between miRNAs seems to be dependent on sequence effects of the miRNAs. One possible explanation is the presence of secondary structures in some miRNAs. However, this effect alone is not sufficient to explain these differences of detection. Further experiments and analysis would be required to fully characterize this effect.

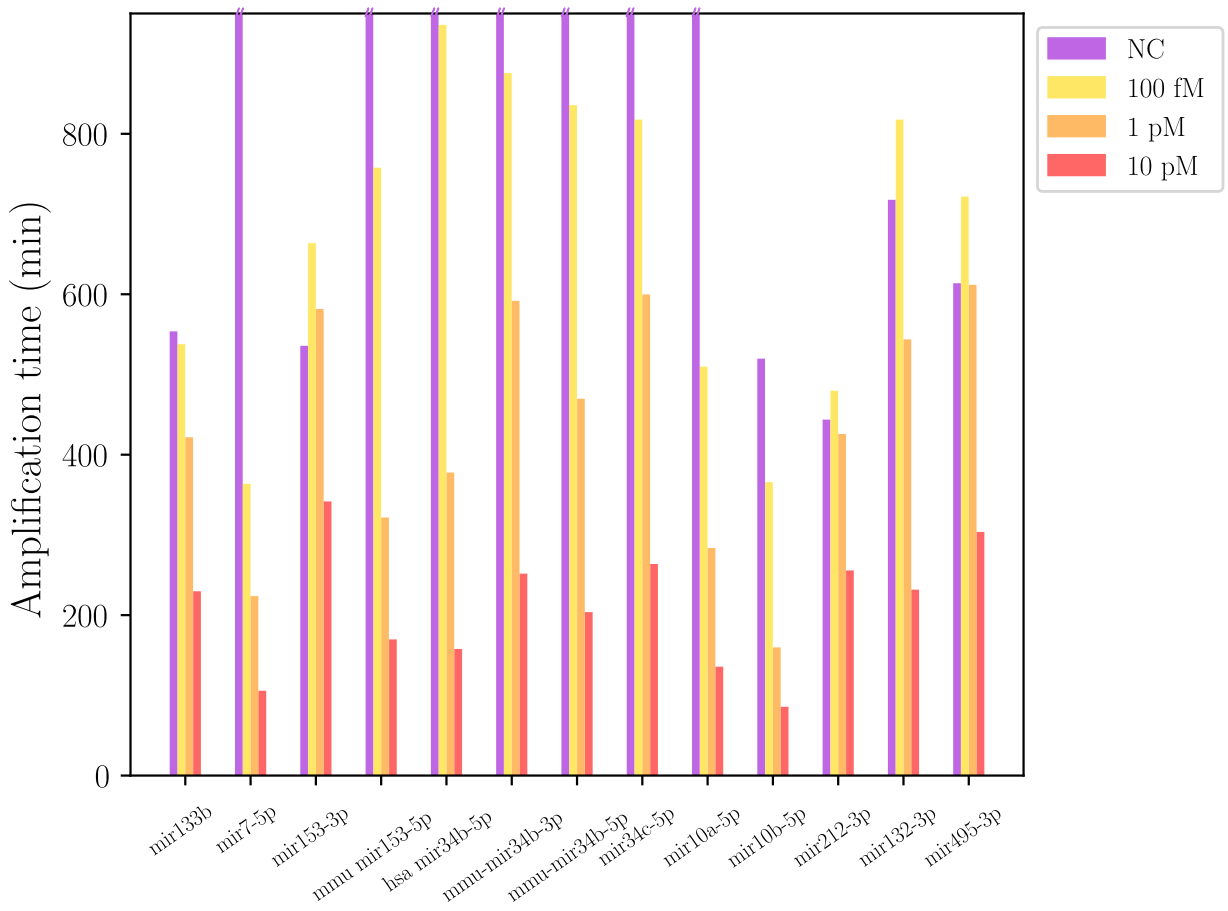

Figure 1.9: **Detection of targeted synthetic miRNAs.** A range of concentration was realized for 13 different synthetic miRNAs. For each targeted miRNA, 0.5nM of the corresponding cT was present in the PUMA. The NC concentration corresponds to a point in absence of synthetic miRNA.

miRNA	$Score_{1pM}$	Comment
mir10a-5p	5,4	Mouse model
mir7-5p	5,1	Human brain
mir10b-5p	3,3	Mouse model
mmu-mir153-5p	3,1	Human brain
hsa-mir34b-5p	2,7	Human brain
mmu-mir34b-5p	2,6	Mouse version of a miRNA found in the human brain
mir34c-5p	2,4	Human brain
mmu-mir34b-3p	1,6	Human brain
mir133b	1,3	Human brain
mir132-3p	1,3	Mouse model
mir212-3p	1,0	Mouse model
mir495-3p	1,0	Mouse model
mir153-3p	0,9	Human brain

Table 1.1: Targeted synthetic miRNAs and their respective scores.

1.4.3 Microfluidics and digital detection

In order to generalize the work previously done by our team to these new miRNAs, the digital detection method described in section 1.3.2 has been applied to miRNAs with a score greater than 2 (cf. table 1.1). Mixes containing the miRNA specific cT were prepared with respectively no miRNA, 40 fM, 200 fM, 1 pM, 5 pM and 25 pM of miRNA. Samples were barcoded using fluorescent dyes and 10 μm droplets were generated using a sample changer [185] which increases generation and analysis throughput with a parallelized process. Droplets were mixed, incubated, imaged and analyzed. The results are displayed on figure 1.10. For each synthetic miRNA, a good correlation between the expected concentration and the experimental concentration was obtained. Noteworthy, the lower the score of the miRNA, the higher the corresponding experimental concentration for no miRNA. This result was expected. Indeed, the lower the score, the smaller the time window to stop the droplet incubation and the more likely droplets without miRNA could start. These results show that the method previously developed by our team allows the digital detection of each selected miRNA and thus to obtain a quantitative and absolute quantification.

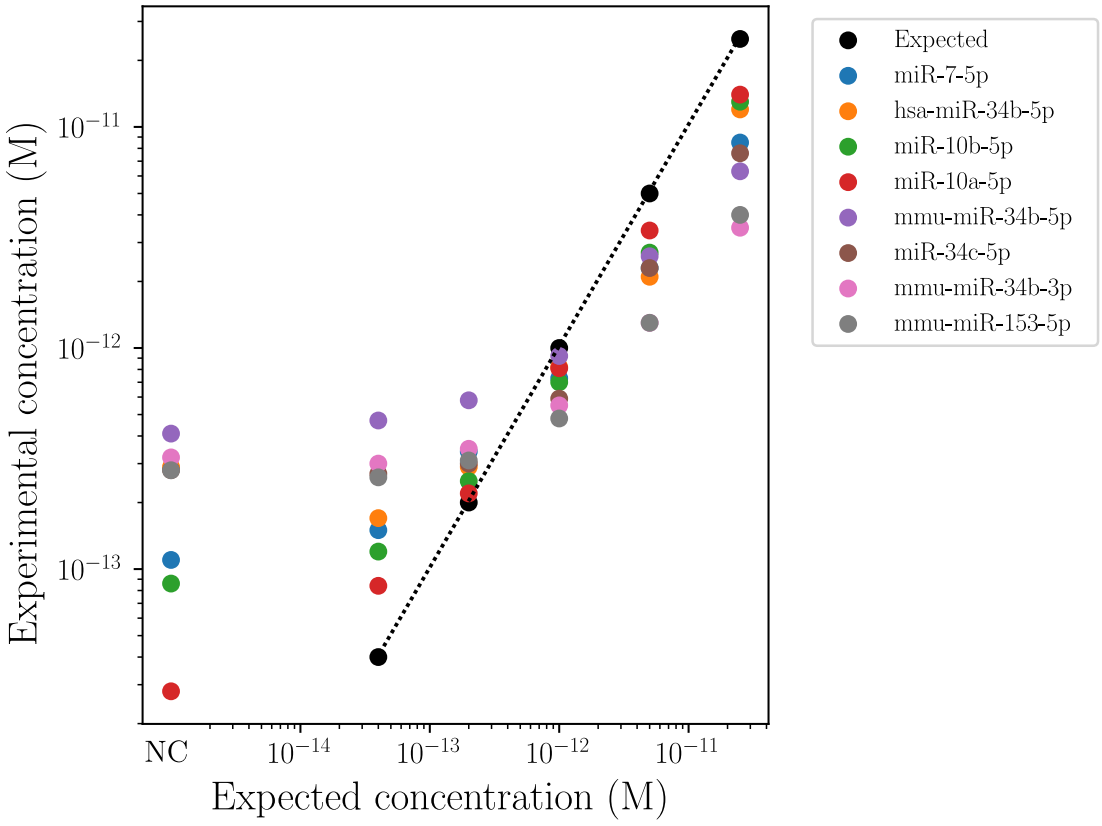

Figure 1.10: **Digital detection of targeted synthetic miRNAs.** Digital detection of different targeted synthetic miRNAs. For each miRNA, the experimental concentration is plotted as a function of the theoretically expected concentration. NC refers to samples containing no targeted miRNA. The dotted line represents the diagonal.

1.4.4 Targeting miRNA in total miRNA extracted from mouse striatum

The second step towards the detection of miRNAs in biological samples was to detect endogenous miRNAs in biological samples from wild type mice. To that extent, Anne Christmann, from UASK, extracted miRNA from mouse striatum with a miRNeasy kit. According to the results obtained in section 1.4.2, Let7a and mir7-5p were targeted in this sample in a tube assay format. For each miRNA, a range of total extracted miRNA was realized. The results are displayed on figure 1.11. Let's focus on Let7a as an example for our analysis (figure 1.11.a.). For Let7a without spiked synthetic miRNA, no amplification is observed for 0 ng.μL^{-1} of total miRNA extract while the amplification is starting for 3.9 ng.μL^{-1}, 7.7 ng.μL^{-1} and 15 ng.μL^{-1}. However, the higher the concentration of total miRNA extract, the higher the concentration of endogenous Let7a but the slower the amplification, suggesting a toxic effect of the matrix. To confirm this hypothesis, 1 pM of synthetic Let7a was spiked in each sample with respectively 0, 3.9, 7.7, 15 and 31 ng.μL^{-1} of total miRNA extract. At low extract concentration (3.9 ng.μL^{-1}), the At is faster than the negative control, suggesting that endogenous Let7a is indeed detected. However, higher extract concentrations induce a delay in the amplification time, indicating the toxicity of the extract (or one of its components) regarding the amplification chemistry. Similar trend is observed for mir7-5p (figure 1.11.b.). A range of extract miRNA was realized: the higher the concentration of extract miRNA, the slower the amplification while without extract miRNA, no amplification was observed. This suggests that endogenous mir7-5p is indeed detected while the miRNA extract has a toxic effect on the amplification chemistry. Then, 1 pM of synthetic mir7-5p has been spiked in each sample with respectively 0, 3.9, 7.7, 15 and 31 ng.μL^{-1} of total miRNA extract. The higher the extract miRNA concentration, the slower the amplification, demonstrating the toxicity of the extract (or one of its components) regarding the amplification chemistry.

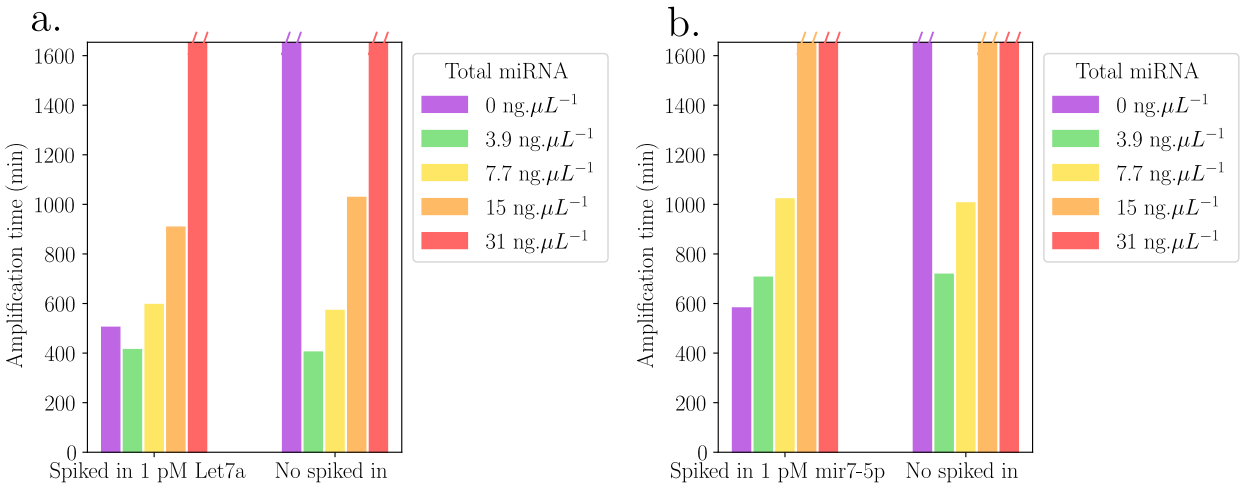

Figure 1.11: **Let7a and mir7-5p detection in total miRNA extracted from mouse striatum**. Total miRNA extracted from mouse striatum range. **a.** Detection of Let7a with and without 1 pM of spiked synthetic Let7a. **b.** Detection of mir7-5p with and without 1 pM of spiked synthetic mir7-5p.

This demonstrates the toxic effect of the total miRNA extract on the PUMA. The fact that this effect is observed for two different target miRNAs suggests that it is not due to a point effect for a specific target sequence but rather that this effect impacts the whole amplification chemistry. While Let7a and mir7-5p can be detected in the total miRNA extract, its toxic effect prevent a quantitative analysis. It is therefore not possible to obtain a robust assay for the detection of miRNA in total miRNA extract by simply adding a portion of the said biological sample directly into the PUMA amplification mixture.

1.5 MiRNA detection: particle-based capture step

In order to get rid of the toxic effect of the total miRNA extract discussed previously, we introduced a capture step on particle. The particles are supposed to capture the targeted miRNAs, be washed and added to the PUMA. In other word, the particles are supposed to allow for capture and concentration of targeted miRNA, while at the time getting rid of toxic components from the sample. To achieve this, our idea is to graft the miRNA specific cT onto particles. By adding these particles to a capture mixture, the present target miRNA hybridizes to the cT and is sequestrated. The particles can then be recovered, washed and added to a PUMA amplification mixture.

1.5.1 Particle choice

The first step was to select suitable particles for this application. We started by testing 30 μm diameter sepharose beads. Those beads have a capacity of 10^{10} streptavidin per bead. In order to visualize the streptavidin site distribution on a bead, 6.10^9 biotinylated oligonucleotides, tagged with an Atto633 fluorophore, were grafted on a sepharose bead which was then imaged by fluorescence microscopy (figure 1.12.a.). The fluorescence intensity profile was extracted and is plotted in figure 1.12.b. The oligonucleotides are distributed in a crown shape: preferentially on the outer part of the beads, as expected from the instantaneous interaction of diffusing oligo with the streptavidin-bound particle. The fact that the oligonucleotides preferentially bind to the outer part of the bead is of prime importance for the desired application. Indeed, the closer the oligonucleotides are to the edge of the bead, the more accessible they are and therefore the more easily the cTs may capture the miRNAs.

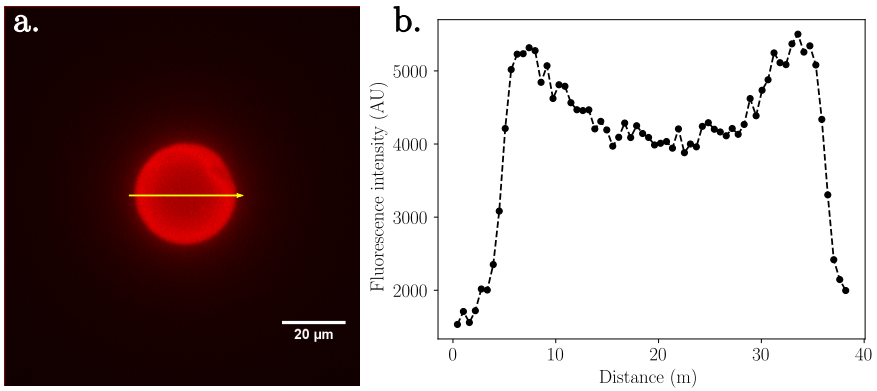

Figure 1.12: **Fluorescent oligonucleotide distribution on a sepharose bead. a.** Image of a T5Atto633Biotin oligonucleotide grafted sepharose bead obtained through fluorescent microscopy (20x). The intensity profile corresponding to the yellow arrow has been extracted. **b.** Fluorescent intensity profile of the T5Atto633Biotin oligonucleotide grafted sepharose bead.

1.5.2 MiRNA detection: on-bead cTs

To test the feasibility of our approach, we first attempted to detect Let7a using a Let7a-specific biotinylated cT grafted onto sepharose beads. We firstly verified that the biotinylated cTs grafted onto the beads were functional. The beads were added to the PUMA mixture, without any capture step, as illustrated on figure 1.13.a.

To study the impact of the number of cTs per sepharose bead, a range of cT per bead has been realized with a constant number of beads added to the PUMA mixture (figure 1.13.b.) and a control with 0.5 nM of cT in solution was realized. For each number of cT per bead, a range of Let7a was carried out, respectively no Let7a, 1 pM and 10 pM, in presence of around 80 sepharose beads. From $1.2.10^4$ to $1.2.10^8$ cT per bead, the amplification time is decreasing, meaning a faster amplification. Beyond $1.2.10^8$ cT per bead, the amplification is slowing down: there is an optimum concentration of cT per bead and the cT in solution. We can suppose that increasing the number of cT per bead allows a faster amplification by easing the hybridization between cTs and miRNAs. However, when a critical number of cT is reached, the beads are too crowded and steric hindrance as well as electronic repulsion are deleterious for the production of trigger. We also see that for $1.2.10^8$ cT per bead, the non-specific trigger production, referred to as leak, is much higher than for the other numbers of cT per bead. This may be due to too many accessible cTs, leading the polymerase to produce trigger even in absence of the targeted miRNA. We chose $1.2.10^7$ cT per bead and decided to decrease the pT concentration to accelerate the detection.

The previous experiment was realized with a concentration of 12 nM pTαT5. A range of pTαT5 was realized (data not shown) and its concentration reduced to 6 nM to speed up the detection for Let7a. A capture step was introduced, and a kinetic realized (figure 1.14). The beads were incubated in a mix containing Let7a in the detection buffer. A duplicate dilution of Let7a RNA version (figure 1.14b.) and a dilution of Let7a DNA version (figure 1.14c.) were incubated 0 h, 1 h or 3 h with the beads. The supernatant was removed and the beads were then transferred to the PUMA amplification mix. No difference

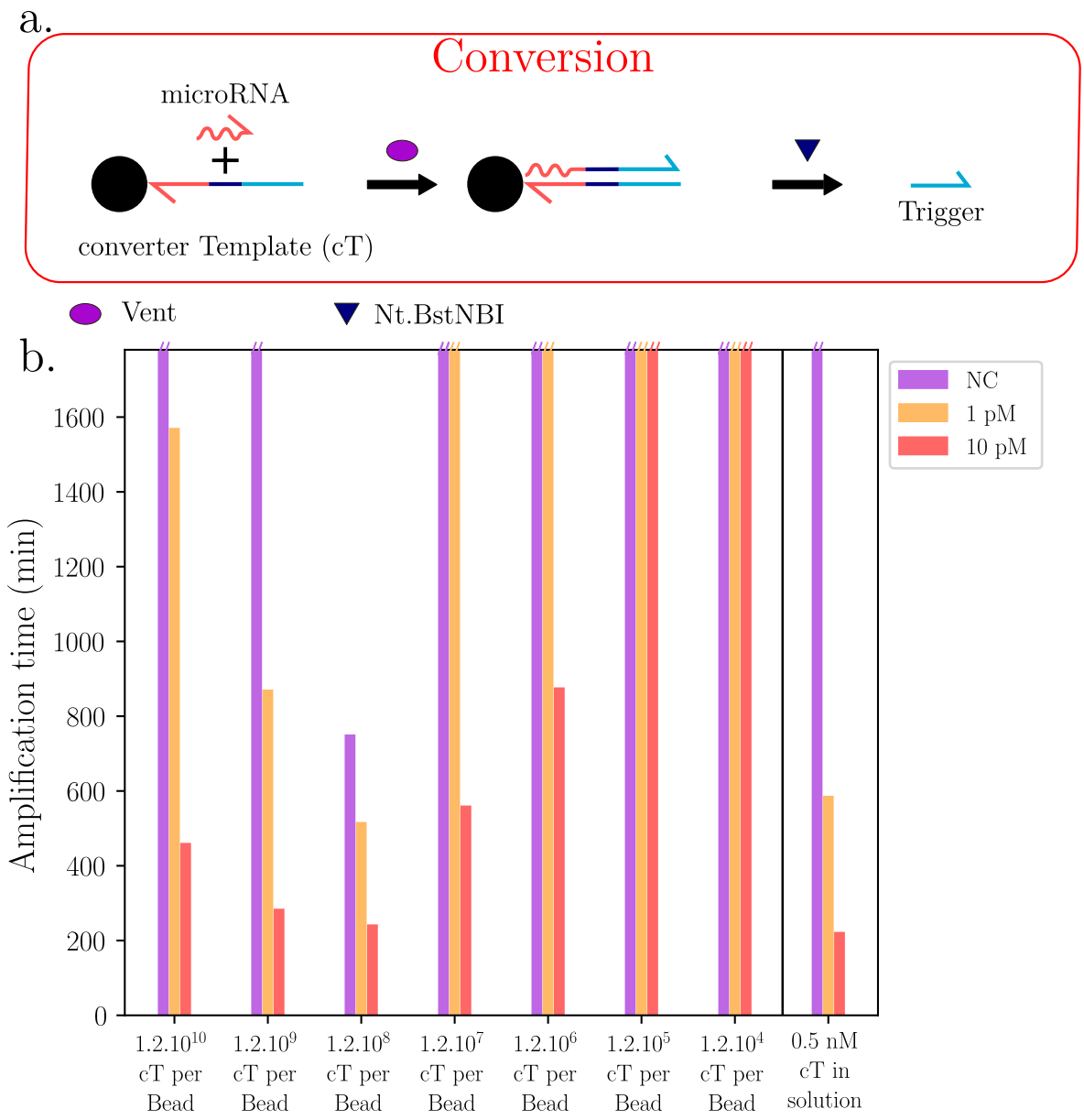

Figure 1.13: **Number of Let7atoαBiot (cT) range for a constant number of sepharose bead.** For each condition, a range of Let7a was realized with 12nM of pT.

was observed between the different incubation times during the capture step, suggesting a fast hybridization kinetic of the target miRNA for the studied concentrations. Introducing a capture step in which the cT carrying beads are incubated in presence of Let7a doesn't improve the detection of Let7a compared to a capture step in presence of Let7a but with no incubation time. Moreover, no difference can be observed between the RNA version and the DNA version of Let7a. Therefore, the fact that we did not observe an effect related to the incubation time of the capture step is not due to the Vent polymerase having issues elongating a RNA primer, as highlighted by Dr.Jet during his thesis [186].

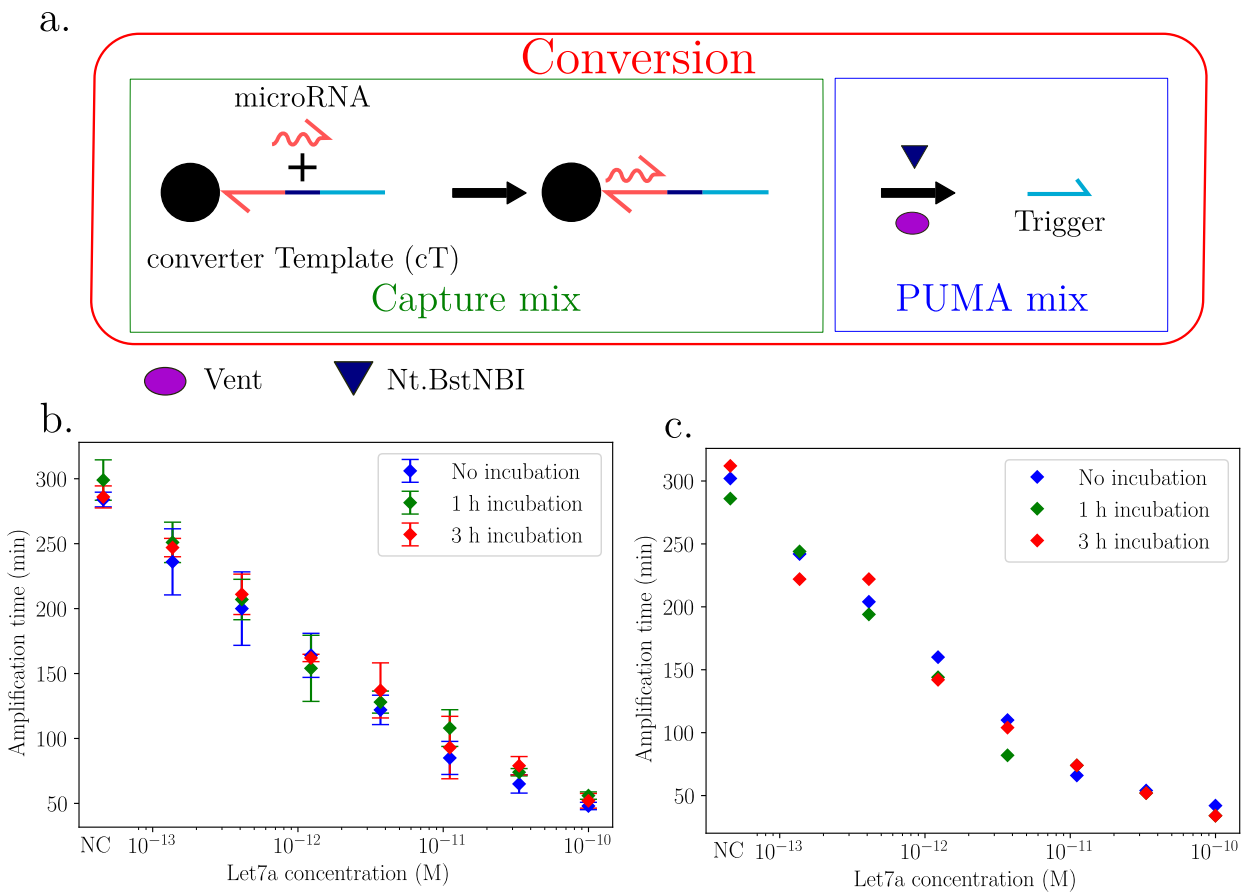

Figure 1.14: **Let7a capture with sepharose beads a.** Converter templates are grafted on beads. The miRNA hybridizes to the cT. The supernatant is removed and the beads added to the PUMA amplification mixture. **b.** Capture kinetic for a 3-fold dilution of the synthetic RNA version of Let7a. Each point is a dilution duplicate. **c.** Capture kinetic for a 3-fold dilution of the synthetic DNA version of Let7a.

1.5.3 Klenow fragment (3'→5' exo-) introduction

According to information provided by our enzyme supplier, Vent polymerase has a low efficiency when working with RNA primers. In the PUMA assay used for miRNA detection, when the miRNA is extended for the first time, Vent polymerase has to work with a RNA primer. To overcome this issue, we decided to add a new polymerase, the Klenow fragment (3'→5' exo-) (referred to as Klenow). Klenow polymerase has the same efficiency when working with RNA primers as well as DNA primers. However, its half life at 50°C is approximately 51 min according to figure 1.15. Klenow polymerase cannot replace Vent polymerase, which is stable at 50°C, but can complement it by realizing the first miRNA elongations.

In order to assess the effect of Klenow addition to the PUMA, a range of Let7a, with on-bead cT directly in the amplification mixture was realized in presence or not of Klenow (figure 1.16.b). The $scores_{1pM}$ obtained for both conditions were calculated and are displayed on figure 1.16.b. The presence of Klenow increase the score from 1.7 to 2.1, thus proving its positive contribution for Let7a detection.

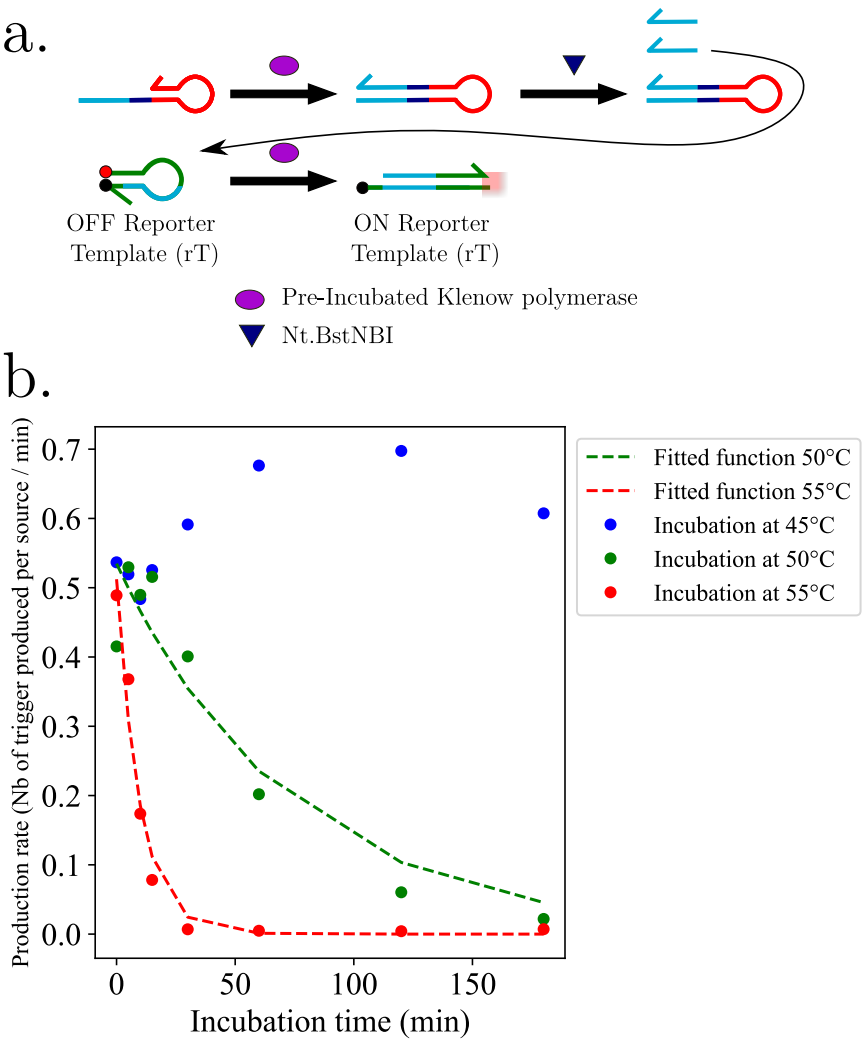

Figure 1.15: **Klenow polymerase deactivation kinetic. a.** Klenow polymerase is pre-incubated a 45, 50 or 55°C and then added to a mix containing a self-activated template, a rT and Nt.BstNBI. The trigger is linearly produced. The opening rate of the rT is correlated to Klenow remaining activity. **b.** Knowing the rT concentration, the initial trigger production rate can be extracted and plotted in function of Klenow pre-incubation time. At 45°C (blue dots), Klenow doesn't lose any activity. At 50°C (green dots) and 55°C (red dots) , Klenow activity can be approximated as a function $y = A.e^{(\frac{-t}{\tau})}$. Data obtained for a pre-incubation at 50 and 55°C were fitted (dotted lines), giving: $A_{50°C} = 0.53\,trigger.min^{-1}$, $\tau_{50°C} = 73.1\,min$, $A_{55°C} = 0.51\,trigger.min^{-1}$, $\tau_{55°C} = 9.9\,min$.

Considering the previously described properties of Klenow, we decided to add it in the capture mix together with dNTPs. The objective is to extend the miRNA on the converter template, giving a structure with an already formed trigger, ready to be nicked. Moreover, the elongated trigger is more stable on the cT as it has more base paring interactions. It should therefore decrease the value of the dissociation constant between the miRNA and the cT, shifting the equilibrium towards more captured miRNA. To assess the efficiency of such

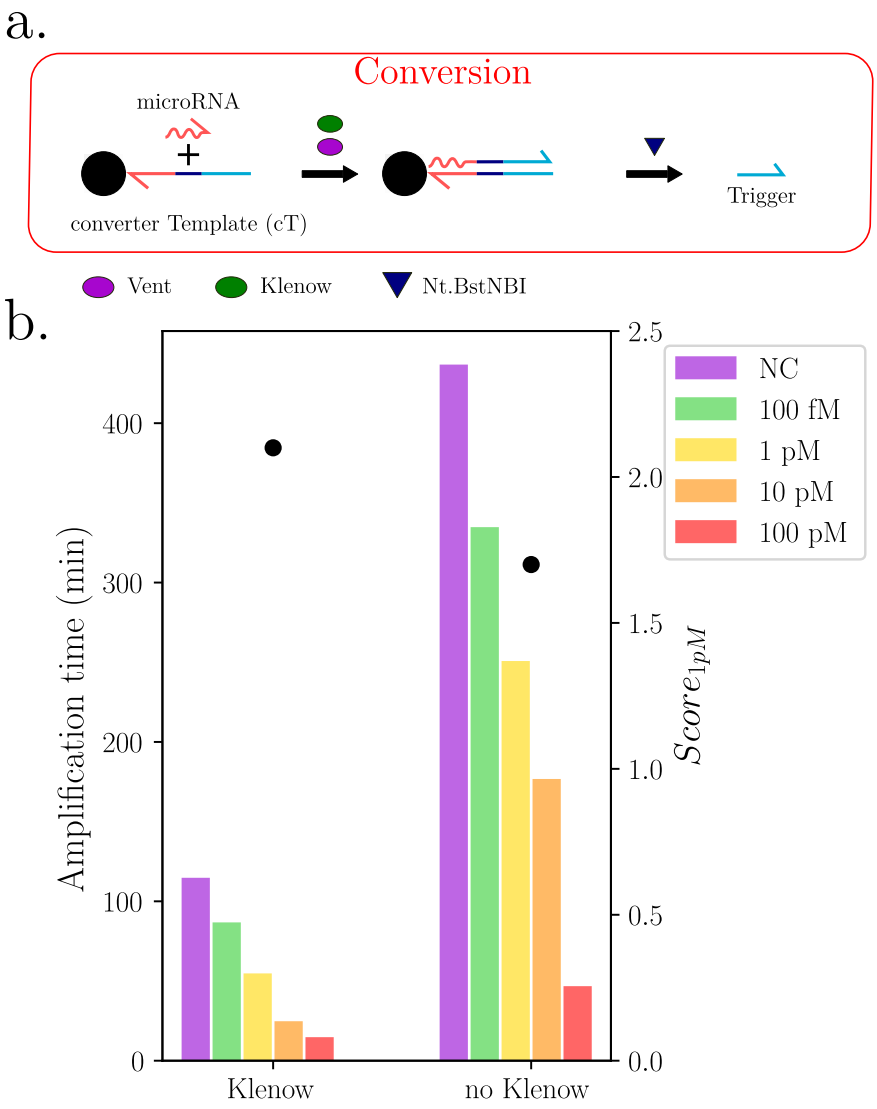

Figure 1.16: **On-bead cT with Klenow. a.** The cT is grafted on sepharose beads. Klenow polymerase is added to the PUMA amplification mixture. The miRNA hybridizes to the cT and undergoes polymerization / nicking cycles producing trigger **b.** Let7a range with and without Klenow in the PUMA mixture. The amplification times for the different Let7a concentrations are given by bar charts (left axis) and the $score_{1pM}$ are given by the black dots (right axis).

a capture step with Let7a specific cT on sepharose beads, the experiment described in figure 1.17 has been performed. Briefly, 3 conditions were compared:

- a Let7a range with a capture step in presence of Klenow.
- a Let7a range with a capture step without Klenow.
- a Let7a range without capture step.

Klenow has also been added to the PUMA amplification mixture. The capture step took place during 30 min at 40°C under agitation. Then, the sepharose beads were transferred into the PUMA amplification mixture. For 10 pM of Let7a, the capture step slightly increases the detection independently of the presence of Klenow during the said capture step. For 1 pM of Let7a, the capture step increases the detection independently of the presence of Klenow during the said capture step. Moreover, the $scores_{1pM}$ obtained for both conditions were calculated and are displayed on figure 1.17. For no capture, the score is around 3, for the capture without Klenow it is around 15 and for the capture with Klenow it is around 22. The capture with Klenow is thus the best condition. For 100 fM of Let7a, the capture step in presence of Klenow increases the detection, while only a slight effect on the detection is observed for a capture step without Klenow. The presence of Klenow during the capture displaces the equilibrium between Let7a, the cT and Let7a hybridized to the cT in favour of the Let7a hybridized to the cT form. This explains the observed results and why the effect of Klenow during the capture increases while lowering Let7a concentration. Adding Klenow during the capture step undeniably increases the effectiveness of the said capture. However, the tested conditions were chosen arbitrarily and need to be optimized.

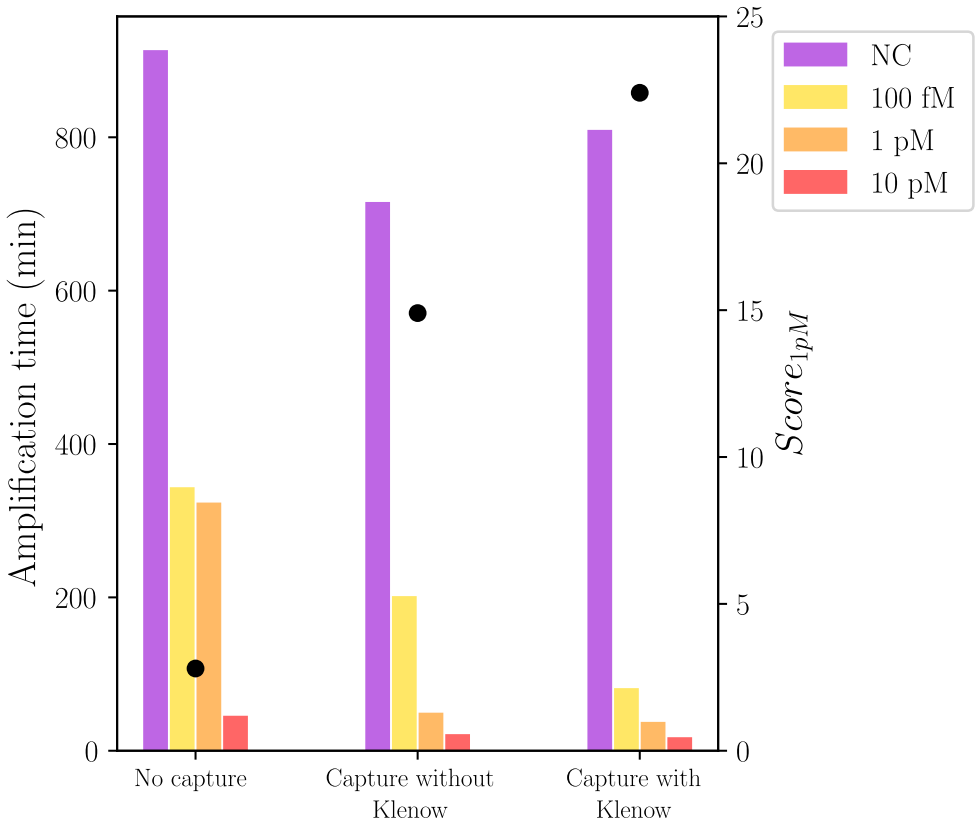

Figure 1.17: **On-bead cT, with or without capture step**. The capture step is realized with and without Klenow. A range of Let7a has been carried out. The amplification times for the different Let7a concentration are given by bar charts (left axis) and the $score_{1pM}$ are given by the black dots (right axis).

1.5.4 Capture step optimization

The preliminary results obtained by introducing a capture step in presence of Klenow seemed to be a promising strategy that we further optimized. We chose to optimize two parameters: the temperature and the duration of the capture step. First, a capture step temperature range was realized for 1 pM and 0 pM of Let7a, between 30°C and 60°C during 30 min under agitation (figure 1.18.b.). The amplification for 1 pM of Let7a started in 30 minutes for 30°C and 40°C, while it started at 38 min for 50°C and at 44 min for 60°C. The $score_{1pM}$ were calculated and as the higher score was obtained at 40°C, we decided to remain at this temperature. Second, a capture step kinetic for 100 fM and no Let7a was performed between 0 and 60 min at 40°C under agitation (figure 1.18.c.). The capture duration has no impact on the amplification time for no Let7a. However, the amplification time drop from about 700 min for 0 min of capture to about 200 min for 30 min of capture. After 30 min, a plateau is reached and the increase in capture time is no longer correlated with a decrease in amplification time. We chose 40 min as the incubation time for the capture step at 40°C.

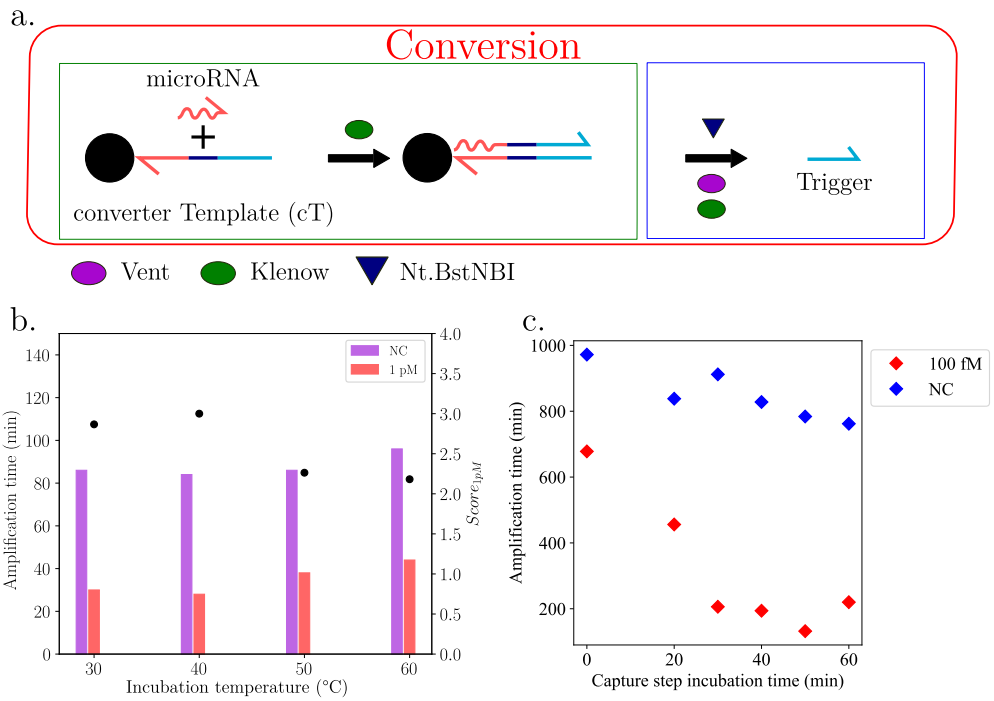

Figure 1.18: **On bead cT, capture step with Klenow a.** The converter templates are grafted on sepharose beads. Klenow polymerase is added to the capture mix. Supernatant is removed and beads are added to the amplification mixture. **b.** Temperature range for the capture step. The amplification times for the different Let7a concentrations are given by bar charts (left axis) and the $score_{1pM}$ are given by the black dots (right axis). **c.** Capture step kinetic for 100 fM (red) and no (blue) Let7a.

To lessen the variability between experiments caused by remaining Klenow on beads [186], a deactivation step was introduced. According to the results obtained in figure 1.15, the capture mix was incubated 30 min at 55°C between capture and washing.

The optimized protocol is as follow:

- Capture step: 20 μL sample volume, 40 min, 40°C, 2000 rpm.
- Klenow deactivation: 30 min at 55°C.
- Removing the supernatant.
- Washing steps if needed.
- Beads transfer into PUMA amplification mixture containing Klenow.

1.5.5 Proof of principle: synthetic miRNA detection

In order to see if the previously optimized parameters can be applied to other miRNAs, the conditions optimized for Let7a have been tested for the detection of other synthetic miRNAs : mir7-5p, mir10a-5p and mir39-ce. Mir7-5p and mir10a-5p are relevent miRNA for neurodegenerative disease. Mir39-ce is a miRNA expressed in *Caenorhabditis elegans*, therefore it is not present in mouse or human samples. It could be spiked in biological sample to mesure the efficiency of the miRNA extraction and for normalization between samples [187]. Ranges from 1 fM to 10 pM of those 3 miRNAs and for Let7a were realized (figure 1.19).

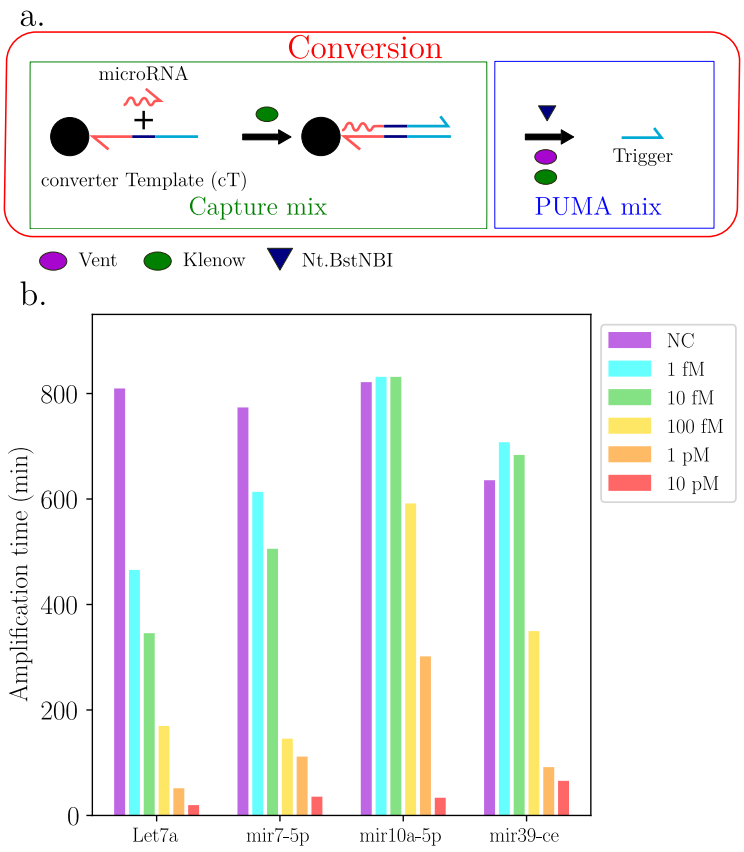

Figure 1.19: **Synthetic miRNA detection with capture step a.** The converter templates are grafted on sepharose beads. Klenow polymerase is added to the capture mix. Supernatant is removed and beads are added to the amplification mix. **b.** Range of synthetic Let7a, mir7-5p, mir10a-5p and mir39-ce.

Let7a and mir7-5p can be detected down to 1 fM. Mir10a-5p and mir39-ce can be

detected down to 100 fM. As it was expected, not all miRNAs can be detected as well as Let7a. However, a LOD of 100 fM is enough for our targeted application, demonstrating that the introduction of the capture step is compatible with reaching a sufficient LOD.

1.5.6 Proof of principle: Let7a detection in total RNA extract

As discussed in section 1.4.4, we observed a toxic effect associated to the background matrix in total miRNA extracted from mouse striatum. While Let7a is indeed detected by the PUMA circuit, the higher the proportion of extracted total miRNA, the slower the amplification (figure 1.20.b.). To overcome this issue, we used the optimized capture step on particles, functionalized with the Let7a-specific cT, in presence of Klenow polymerase. Following capture, the particles were washed and incubated with the PUMA amplification mixture at 50°C. Those experimental conditions removed the toxic effect: the higher proportion of extracted total miRNA, the faster the detection of Let7a (figure 1.20.a.). These results shows the interest of the capture step for the detection of miRNA in total miRNA extract, paving the road for miRNA detection in more complex biological samples.

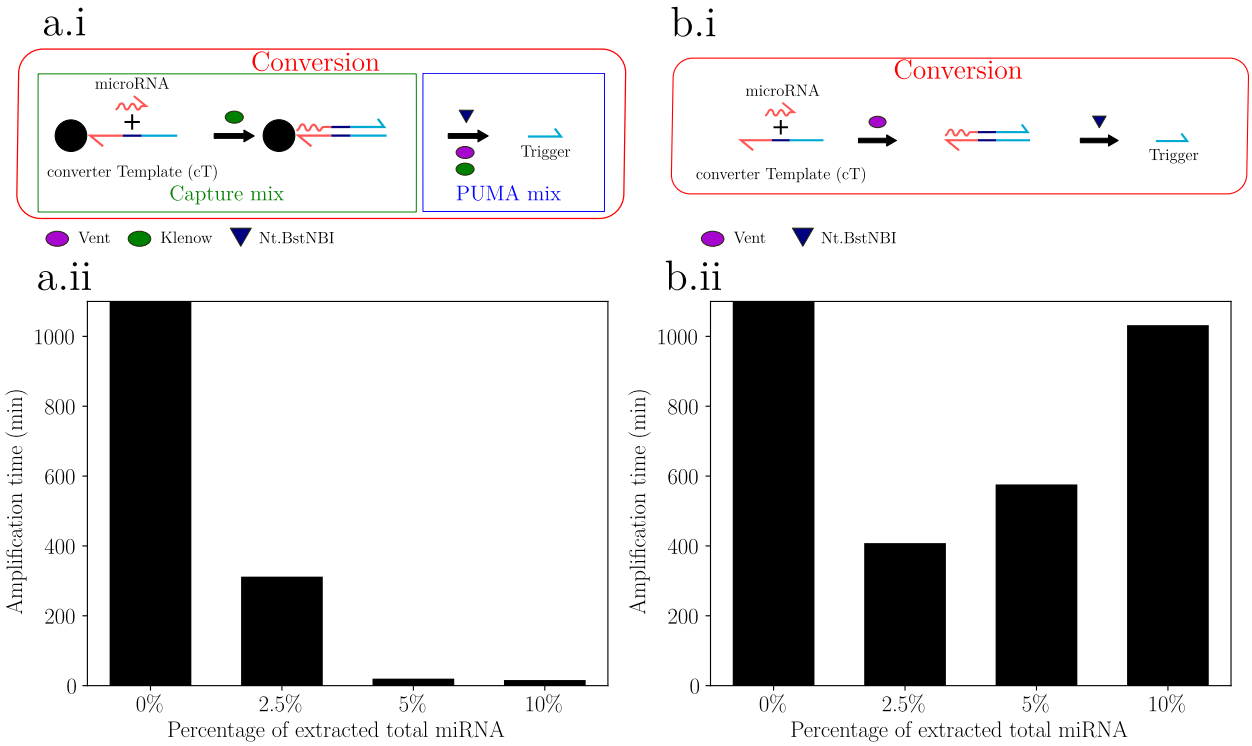

Figure 1.20: **Let7a detection in total miRNA extract with capture step. a.i.** Conversion module with capture step principle. **ii.** Range of total miRNAs, extracted from mouse striatum with a miRNeasy kit, in the capture step. **b.i.** Conversion module principle. **ii.** Range of total miRNAs, extracted from mouse striatum with a miRNeasy kit, in a molecular program without capture.

1.5.7 New set of target miRNAs

So far, the targeted miRNAs have been chosen according to data found in the literature. In order to obtain a miRNA panel of dysregulated miRNAs in the gut of A30P mice, Anne Christmann realized a nCounter miRNA test, based on the nanostring technology [188] with tissue from the colon myenteric plexus or from the mecencephalon in A30P and in wild type mice. Dysregulated miRNAs were identified and their synthetic versions targeted with a PUMA without capture step. The list of those miRNA is given in table 1.2, as well as their $score_{1pM}$ with and without Klenow in the PUMA mixture. The experimental data can be observed in figure 1.21. All the scores obtained in presence of the Klenow polymerase are equal or higher to the scores obtained without the Klenow polymerase, demonstrating again the benefit of adding Klenow to the PUMA amplification mixture.

miRNA	$score_{1pM}$ **without Klenow**	$score_{1pM}$ **with Klenow**	**Comment**
mir17-5p	1.9	2.7	colon myenteric plexus
mir130a-3p	1.0	1.6	colon myenteric plexus
mir134-5p	1.2	1.5	colon myenteric plexus
mir136-5p	1.4	2.1	colon myenteric plexus
mir301a-3p	2.8	7.1	colon myenteric plexus
mmu-mir140-5p	1.2	2.2	mecencephalon
mmu-mir1983	4.5	6.6	mecencephalon
mir-cel-248	1.8	1.8	Spiked in control

Table 1.2: New set of targeted miRNAs and their respective scores.

In order for our team to target these new miRNAs in biological samples of interest, Anne Christmann sent us total miRNA extracted from tissue from the colon myenteric plexus from A30P and wild type mice. She followed the same procedure as the one she carried out for the samples she submitted to the ncounter test. We want to carry detection of miRNA on those samples to see if we find the same dysregulation patterns between samples from healthy and A30P mice. During this procedure, mir-cel-248 was spiked in the different samples, to enable us to normalize the results between different samples.n However, one of the most

dysregulated miRNAs is mir301a-3p, which is about 2.8 times more expressed in A30P than in wild type. This ratio is very low and may be difficult to observe with due to the exponential characteristic of our amplification method.

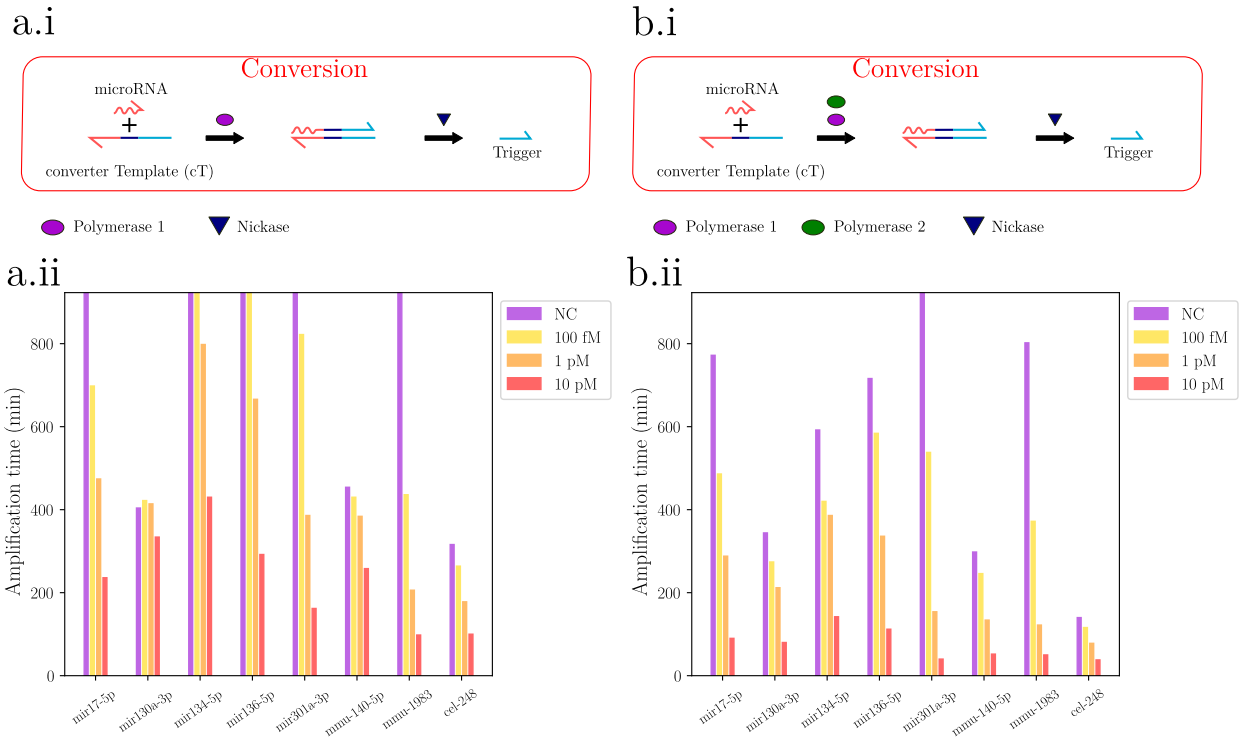

Figure 1.21: **Synthetic miRNA detection with and without Klenow in the PUMA amplification mixture. a.i** Conversion module without Klenow. **ii.** A range of concentration was realized for 8 different synthetic miRNAs. For each targeted miRNA, 0.5nM of the corresponding converter template was present in the PUMA mix. The NC concentration corresponds to a point in absence of synthetic miRNA. **b.i** Conversion module principle with Klenow. **ii.** A range of concentration was realized for 8 different synthetic miRNAs. For each targeted miRNA, 0.5nM of the corresponding converter template was present in the PUMA mix. The NC concentration corresponds to a point in absence of synthetic miRNA.

1.6 miRNA detection: ligation on-particle-based approach

As we can see in figure 1.21, the amplification time of the negative controls is different depending on the cT used. Indeed, the presence of cT is linked to a nonspecific production of trigger, referred to as leak, depending on the sequence of the cT. To get rid of this trigger leak, we decided to separate the cT into two oligonucleotides: lig1 and lig2. Lig1 corresponds to the 3' part of the cT and lig2 to the 5' part of the cT (i.e. the trigger output part). In the presence of the target miRNA, a ligase can bind lig1 and lig2, allowing to recover a complete cT. By attaching lig1 to a bead with a biotin-streptavidin linkage, it would be possible, with

a capture step, to obtain only cTs pre-loaded with miRNA. Indeed, a washing step would make it possible to eliminate non-ligated lig2 oligonucleotides and would consequently avoid the leak inherent to some cTs. In addition, adding Klenow polymerase to the capture mix would result in cTs with extended miRNAs, therefore cTs with triggers ready to be nicked, increasing PUMA efficiency. This is summed up in figure 1.22.

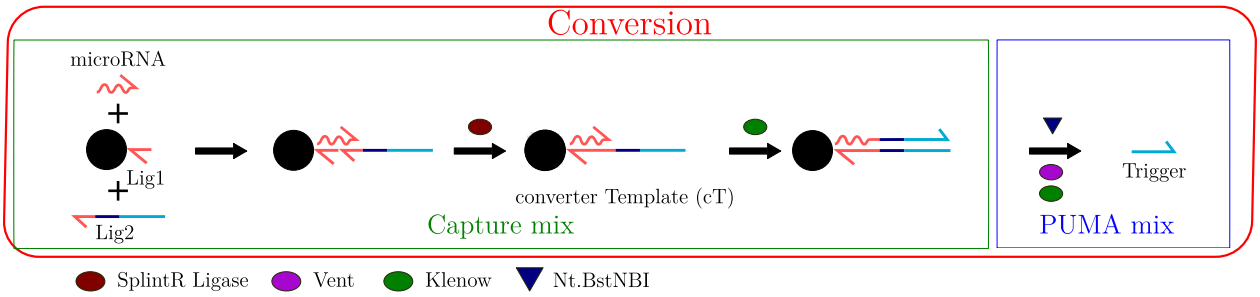

Figure 1.22: **Ligation based capture step conversion module.** The cT is splitted in two oligonucleotides: lig1, corresponding to the 3' end of the cT, and lig2, corresponding to the 5' part of the cT. Lig1 is attached on beads thanks to a biotin-streptavidin link. In presence of the targeted miRNA, lig1 and lig2 are ligated, forming a cT. The miRNA is then extended by a polymerase. The beads are washed, removing the excess of lig2, and added to the PUMA amplification mix.

1.6.1 Leak reduction

To assess the trigger leak caused by different lig2 oligonucleotides, 4 miRNAs and their corresponding cTs were selected: Let7a, mir31-3p, mir301a-3p and mir-cel-248. Mir31-3p is a miRNA that we know is difficult to detect, due to the leak of its cT [186]. Mir301a-3p and mir-cel-248 were presented earlier. A range of each lig2 oligonucleotide was made from 20 pM to 2 nM, as shown in figure 1.23. As expected, the leak induced by the lig2 oligonucleotides (figure 1.23) is correlated to the leak observed for the corresponding cT (figure 1.21). The Le7a-specific cT as well as the specific lig2 oligonucleotide do not cause an important leak. As mir31-3p, mir301-3p and mir-cel248 cTs are more leaky, we observe that 2 nM of their respective lig2 oligonucleotides induce a significant leak. From 20 pM of lig2 oligonucleotide and below, the leak can be considered as negligible. This information is used to calibrate the number and volume of washes required after the capture stage.

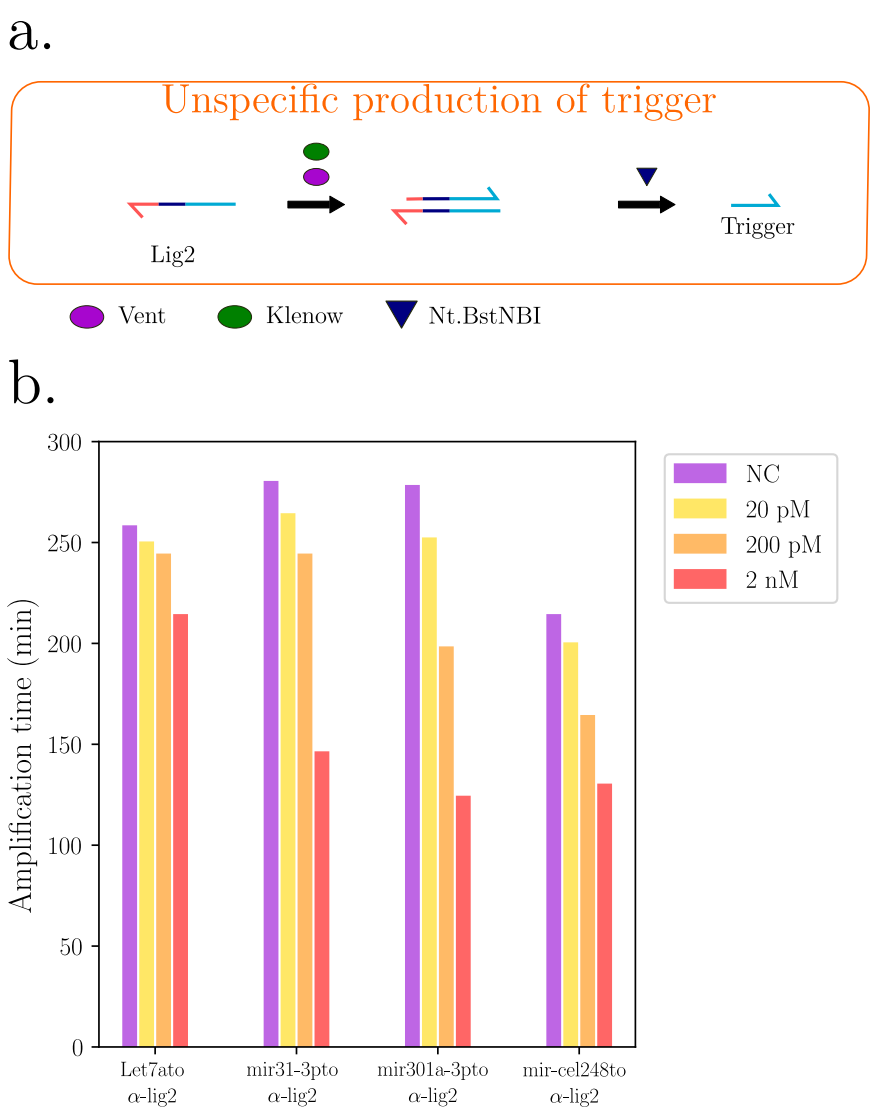

Figure 1.23: **Unspecific production of trigger induced by lig2 oligonucleotides. a.** Polymerases extend the complementary of lig2 oligonucleotide even without primers, resulting in the unspecific production of trigger. **b.** Range of lig2 oligonucleotides for 4 different corresponding cTs.

1.6.2 Ligation in bulk

The first step towards an on-bead ligation capture step was to test the ligation approach in tube, without beads, for the detection of Let7a and mir301a-3p. A ligase, SplintR ligase, as well as the oligonucleotides lig1 and lig2 corresponding to the different cTs were added to the PUMA instead of the full cT (figure 1.24). For each miRNA, a control was performed without lig1. In both cases, a range of miRNA is detected in presence of the lig1 oligonucleotide (figure 1.24 b. and c.). In contrast, there is no detection of miRNA without the lig1 oligonucleotide. To explain this result, the K_d of the involves species was calculated (see appendix A). At 50°C, the K_d between Let7a and its cT is around 500 fM while the K_d between Let7a and its lig2 oligonucleotide is around 1.7 μM. At the same temperature, the K_d between mir301a-3p

and its cT is around 14 fM while the K_d between Let7a and its lig2 oligonucleotide is around 87 nM. There is thus 7 orders of magnitude between the K_d of a miRNA and its cT and the K_d of a miRNA and its lig2 oligonucleotide. In absence of the lig1 oligonucleotide, no cT is formed, the miRNA cannot hybridize significantly to the lig2 oligonucleotide and no trigger is produced. The fact that miRNAs can be detected in presence of lig1 oligonucleotides indicates that cT is formed, leading to trigger production.

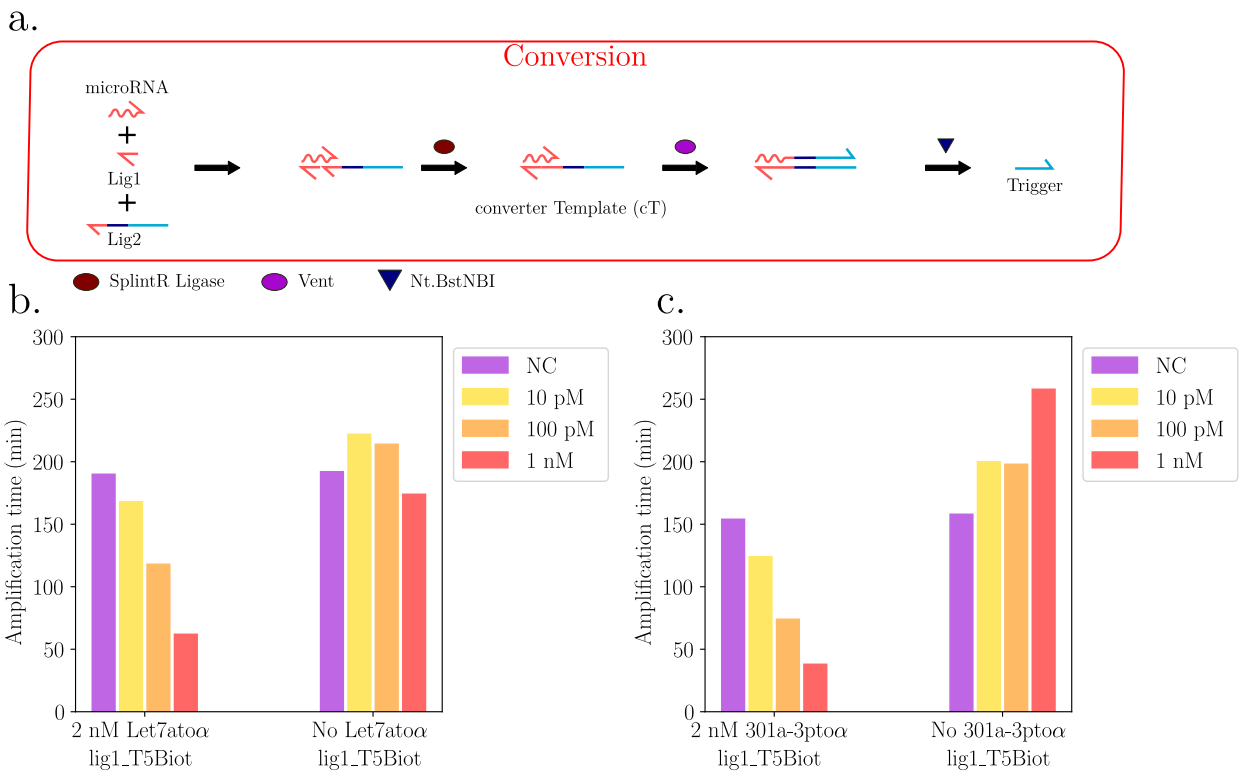

Figure 1.24: **Ligation in tube, without capture. a.** In presence of the target miRNA, lig1 and lig2 are ligated, forming a cT. The miRNA undergoes polymerization / nicking cycles, thus producing triggers. **b.** Let7a range, with and without Let7atoα_lig1_T5Biot. **c.** mir301a-3p range, with and without 301a-3ptoα_lig1_T5Biot.

1.6.3 On-bead ligation

1.6.3.1 Proof of principle

The lig1 oligonucleotide was then attached to sepharose beads via a biotin-streptavidin linkage. The beads were incubated during 1 h at 25°C in SplintR ligase buffer in presence of the targeted miRNA, SplintR ligase, Klenow and the lig2 oligonucleotide. 4 miRNAs were targeted: Let7a, mir31-3p, mir301a-3p and mir136-5p (figure 1.25).

For Let7a and mir301a-3p, two cT designs were tested, and thus two lig2 oligonucleotide designs. During his thesis, Dr.Jet introduced a new class of cT displaying a poly(T) spacer between the miRNA binding site and the Nt.BstNBI recognition site. His experiments demonstrated that the addition of a poly(T) spacer as short as 5 nucleotides increases the

trigger production rate of the supporter cT [186]. Thus, we decided to compare this two classes of cT for the detection of Let7a and mir301a-3p. As expected, the detection was faster for the new class of cT, which was also tested for mir31* and mir136-5p. However, this improvement did not lead to the detection of mir136-5p with the ligation approach while it was detected with the full cT approach (figure 1.21). Noteworthy, as there is no more leak of the cT in this experiment, the pT concentration could then be reduced to allow a faster amplification without impacting the LOD of the system.

During his thesis, Dr. Jet grafted the cT on Dynabeads from Thermo Fisher Scientific, which are coated with streptavidin. Those are magnetic beads, easier to handle and especially easier to wash than sepharose beads. We thus decided to move to dynabeads while the capture step conditions remained unchanged. To determine the efficiency of the ligation for cT production, we compared beads carrying the lig1 oligonucleotide, with lig2 and SplintR ligase in the capture mix, and beads carrying the lig1 oligonucleotide plus the full cT. As shown in figure 1.26, mir301a-3p and mir-cel248 ranges were realized. For mir301a-3p, the ligation approach seems to be working. For 20 pM of mir-cel248 the ligation strategy also seems to be working. However, for 2 pM and below, the ligation method is less efficient than the full cT approach. These first results show that miRNA detection via a ligation-mediated capture step is feasible. However, optimization is still required to achieve similar performance to the one obtained with a full cT-mediated capture step.

1.6.3.2 Optimization

The preliminary results obtained for the ligation-based capture step in presence of Klenow seemed promising. We tried to optimize the conditions of the capture step. 3 polymerase mixes, with a corresponding concentration of pT, were tested in the PUMA amplification mix:

- Vent, with 5 nM of pT
- Vent and Klenow with 8nM of pT
- Bst 2.0 WS with 15 nM of pT.

The $scores_{2pM}$ were calculated and are displayed on figure 1.27. The best results were obtained by Vent and Klenow with 8 nM of pT (figure 1.27). However, to simplify the protocol, it was decided to continue with Wind and 5 nM pT. Indeed, Klenow leakiness would be a problem in the case of a droplet experiment, leading to a too high percentage of false negatives. Noteworthy, with Bst 2.0 WS in the amplification mix, the reaction is complete in less than 20 minutes, highlighting the polymerization speed of this polymerase.

Dr. Jet designed a washing procedure, referred to as "Hard Wash" composed of 2 resuspension/ ultrasound sonication/supernatant discarding cycles in a salty buffer followed by 2 resuspension/supernatant discarding cycles in the storage buffer to restore salts concentrations compatible with the molecular program [186]. With this washing procedure, there is no need for thermally deactivation of Klenow after the capture step. To assess the utility of the Klenow deactivation step that we introduced, we realized the detection of mir301a-3p with the ligation on-bead approach. A population of beads was directly washed with the hard wash while a second population was incubated 30 min at 55°C before washing. The results were similar (figure 1.28.b.). As the Klenow deactivation step showed no more benefit, it was removed from the protocol.

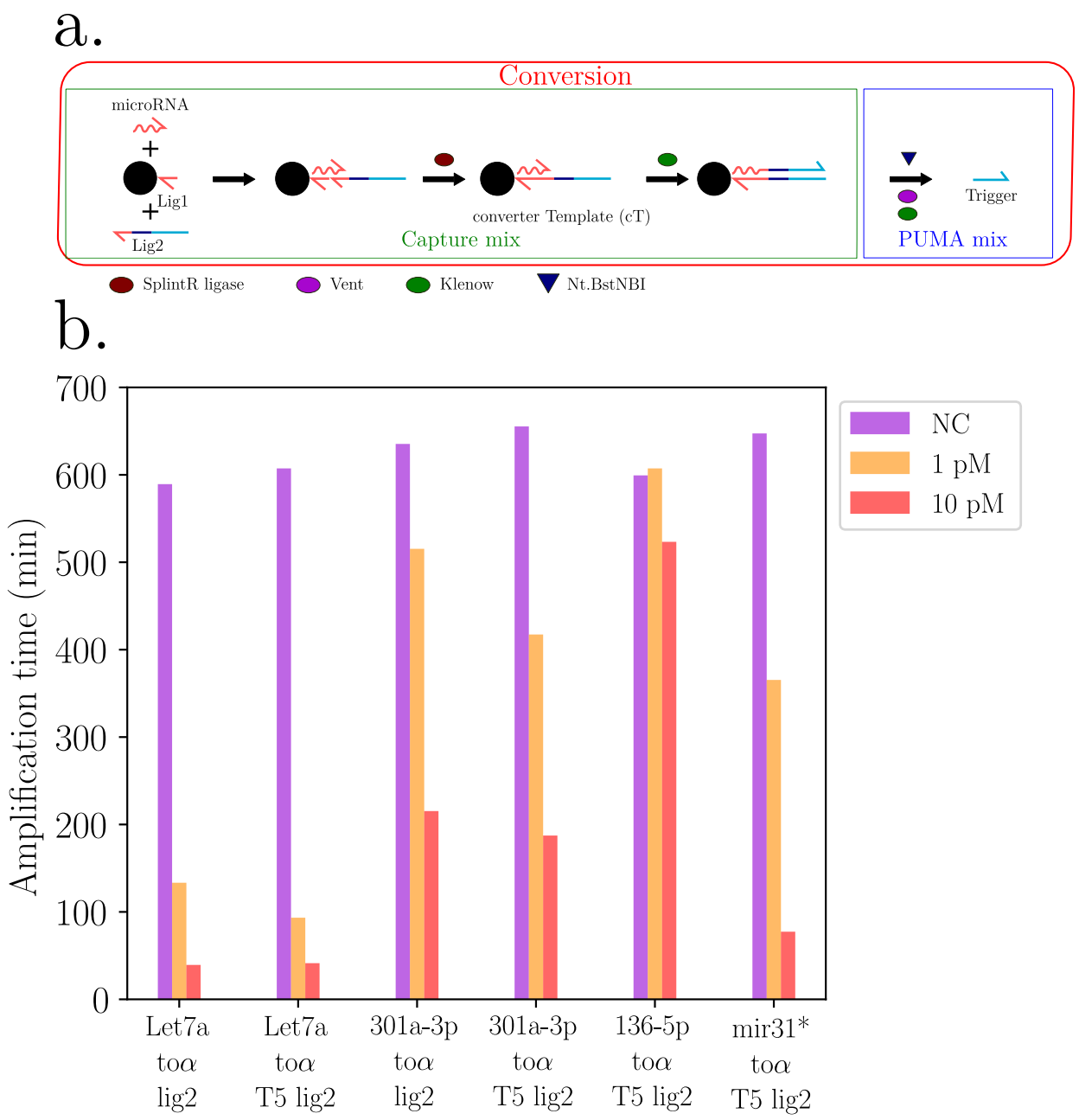

Figure 1.25: **Synthetic miRNA ranges. Capture step with ligation. a.** In presence of the targeted miRNA, on-bead biotinylated lig1 and lig2 oligonucleotides are ligated, forming a cT. The miRNA is elongated by a polymerase. The beads are washed and added to the PUMA amplification mix. **b.** Synthetic miRNA ranges. The capture mixture was containing the corresponding lig1 oligonucleotide. The "T5" mention indicates that a poly(T) spacer is present between the miRNA binding site and the Nt.BstNBI recognition site.

A capture temperature range has been made, from 25°C to 50°C, for a 10 min capture with 0 and 2 pM of mir301a-3p. We observed the greatest discrimination between 0 and 2 pM of target for 35 °C and 40 °C. Therefore, it was decided to use 37°C for the capture step in

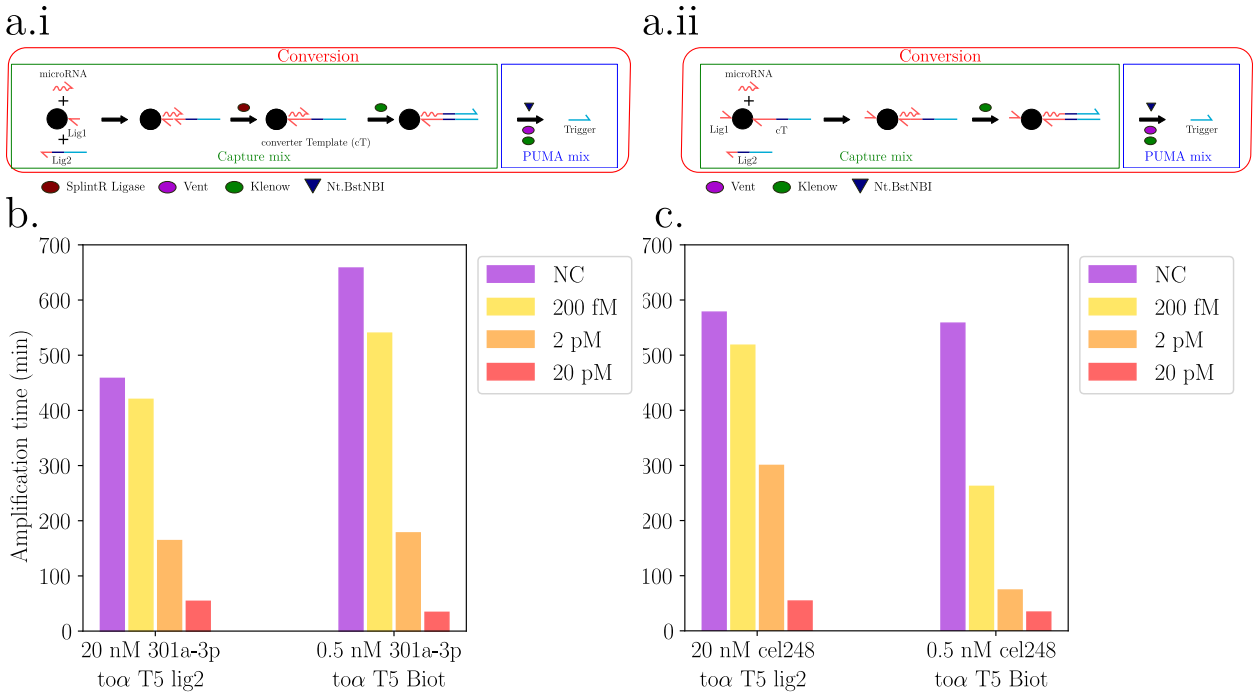

Figure 1.26: **Comparison between capture step with ligation and without ligation. a.i.** In presence of the targeted miRNA, on-bead biotinylated lig1 and lig2 oligonucleotides are ligated, forming a cT. The miRNA is elongated by a polymerase. The beads are washed and added to the PUMA amplification mix. **ii.** The targeted miRNA hybridizes to an on-bead cT. The miRNA is elongated by a polymerase. The beads are washed and added to the PUMA amplification mixture. **b.** Synthetic mir301a-3p range. Comparison between capture step with ligation to form cT (5 nM pT) or capture step with full cT (8 nM pT). **c.** Synthetic mir-cel248 range. Comparison between capture step with ligation to form cT (5 nM pT) or capture step with full cT (8 nM pT).

the next experiments (figure 1.28.c.). A capture step kinetic for 2 pM and no mir301a-3p, at 37°C, has been performed between 0 and 60 min (figure 1.28.d.). The capture seems finished at 10 min. The optimized protocol is as follow:

- Capture step: 10 min, 37°C, 2000 rpm in SplintR Ligase Buffer
- Hard Wash
- Beads transfer into PUMA amplification mixture.
- PUMA amplification mixture: Vent and 5 nM of pT in mirBuffer.

Those optimized conditions were used for the detection of mir301a-3p and mir-cel-248 (figure 1.28.e.) The results obtained for mir301a-3p were satisfying, while the results obtained for mir-cel248 were mixed. Indeed, even 2 pM of mir-cel248 could hardly be discriminated from no mir-cel248 while it could be detected before the optimization process. The conditions optimized for mir301a-3p are not suitable for mir-cel248. Further optimization is required to achieve conditions that are also suitable for the detection of mir-cel-248.

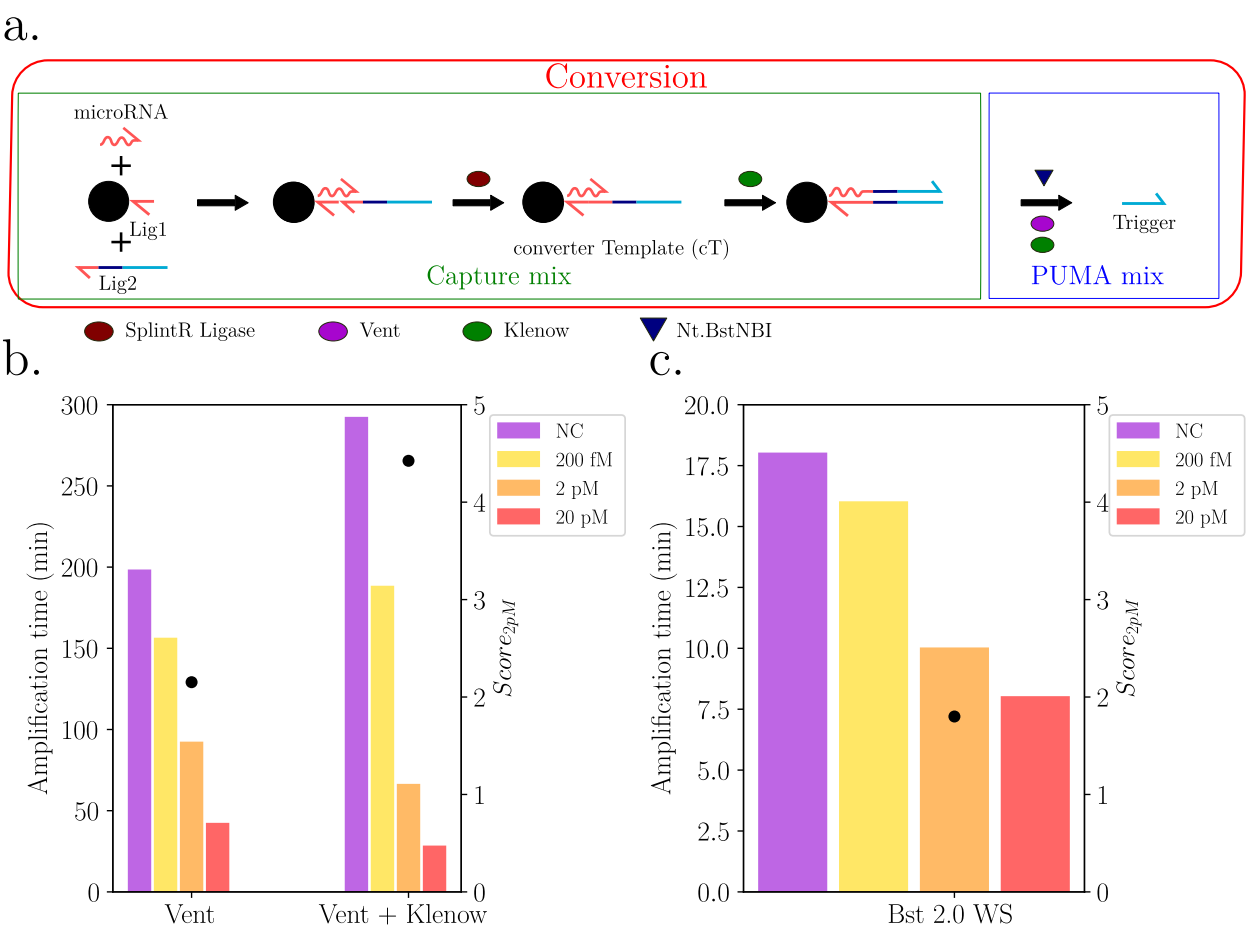

Figure 1.27: **Capture step with ligation for synthetic mir301a-3p detection, different polymerases in the PUMA amplification mixture. a.** In presence of the targeted miRNA, on-bead biotinylated lig1 and lig2 oligonucleotides are ligated, forming a cT. The miRNA is elongated by a polymerase. The beads are washed and added to the PUMA amplification mixture. **b.** Range of synthetic mir301a-3p. PUMA amplification mixture contains Vent or Vent and Klenow. The capture took place for 1 h at 25°C. The amplification times for the different Let7a concentrations are given by bar charts (left axis) and the $scores_{2pM}$ are given by the black dots (right axis). **c.** Range of synthetic mir301a-3p. PUMA amplification mixture contains Bst 2.0 WS. The capture took place for 1 h at 25°C. The amplification times for the different Let7a concentrations are given by bar charts (left axis) and the $scores_{2pM}$ are given by the black dots (right axis).

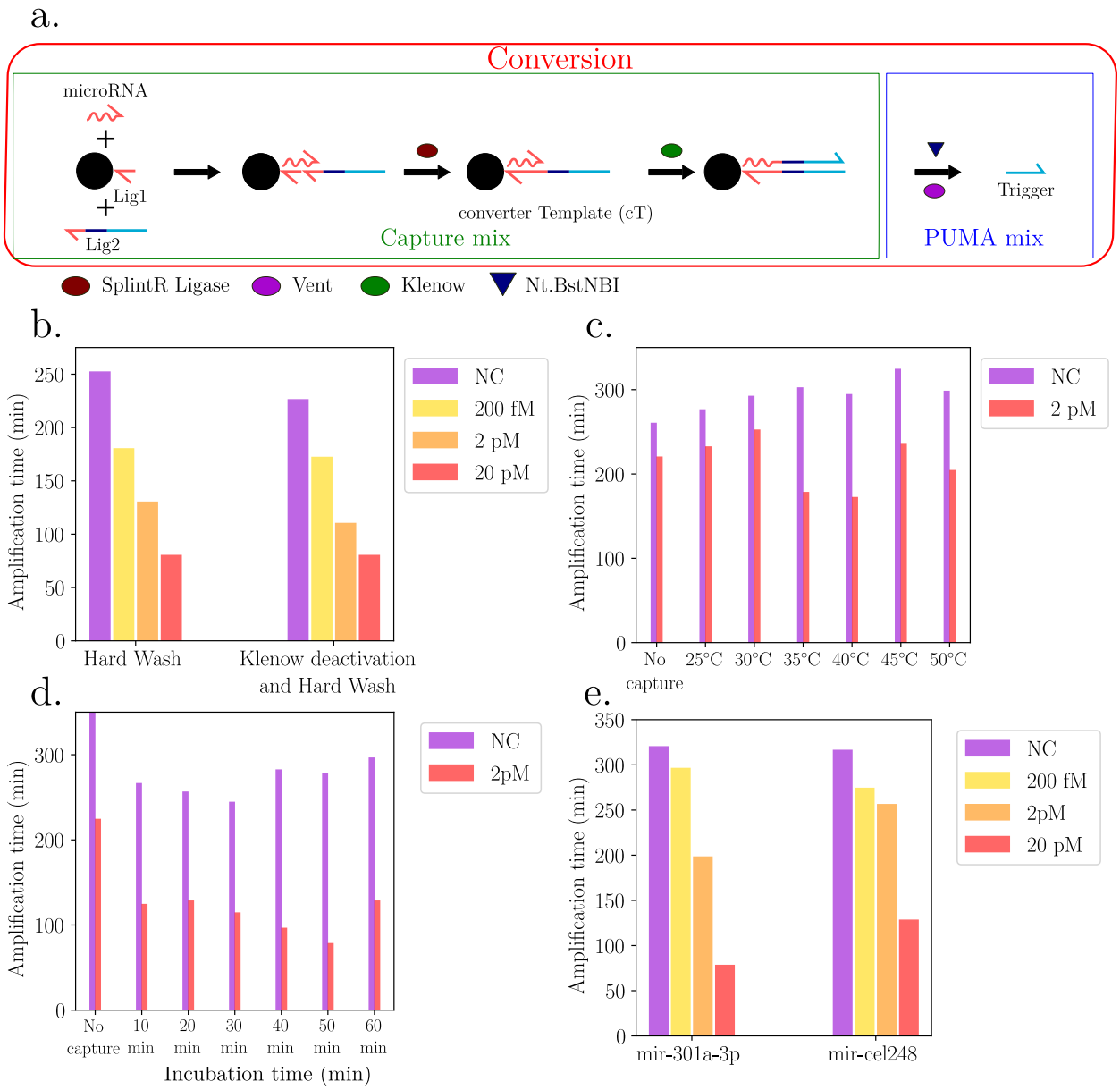

Figure 1.28: **Ligation-based capture step optimization. a.** In presence of the targeted miRNA, on-bead biotinylated lig1 and lig2 are ligated, forming a cT. The miRNA is elongated by a polymerase. The beads are washed and added to the PUMA amplification mix. **b.** Range of synthetic mir301a-3p. Captur step with Ligation, with and without Klenow deactivation before hard wash. The capture occurred for 10 min at 37°C. **c.** Capture step incubation temperature range with respectively 2 pM and no synthetic mir301a-3p. The capture took place during 10 min. **d.** Ligation capture step incubation kinetic at 37°C with respectively 2 pM and no synthetic mir301a-3p. **e.** mir301a-3p and mir-cel248 ranges, the capture step took place during 10 minutes at 37°C in presence of lig1 and lig2 oligonucleotides. Beads were then washed and mixed with a PUMA amplification mixture.

1.7 Long nucleic acid detection

Due to the SARS-CoV-2 pandemic and the resulting sanitary context, we decided to focus on long nucleic acid detection, in particular genomic RNA detection. Indeed, the detection of genomic RNA is of prime importance for virological testing and early diagnosis [189].

Developing a method to detect long nucleic acid could also allow the detection of new biomarkers. For example, long noncoding RNAs have been identified as promising biomarkers in the early detection of cancer [190]. The detection of mRNA could also be an interesting path. For instance, the modulation of mRNA stability plays a role in drug discovery and therapeutic intervention [191].

The results presented in this section were obtained in the framework of the FindCov ANR project in collaboration with the team of Dr. Genot, CNRS researcher at LIMMS, University of Tokyo.

1.7.1 Rnase H introduction for RNA detection

The approach developed for the detection of miRNA was not usable in its current state for the detection of long RNA or DNA sequences. Indeed, we use the target miRNA as a primer, adding bases in 3' of the miRNA with a polymerase. For genomic RNA, there is a clear need for targeting areas other than the 3' region.

A tailored conversion strategy had to be design for long RNA. Our idea was to adapt the cT-based approach by adding RNASe H to the PUMA. RNAse H is an enzyme that recognizes a DNA:RNA duplex, it hydrolyzes the RNA strand by releasing the 3'-OH and 5'-phosphate ends [192]. By cutting the RNA in the targeted area, this releases a 3' part with an OH, which can be used as primer by a polymerase. Since the added bases are coming from dNTPs, the newly created DNA strand cannot be cleaved by RNAse H, leaving the cT activated and leading to trigger production (figure 1.29). Depending on the nicking location in the target sequence, the primer created will be extended only if it is long enough to remain hybridized to the cT. In addition, it is possible for the targeted RNA region to be nicked at several locations, generating primers of only a few bases. To improve our chances of success, the Klenow polymerase was added to the detection mix for its affinity for RNA primers, as explained earlier.

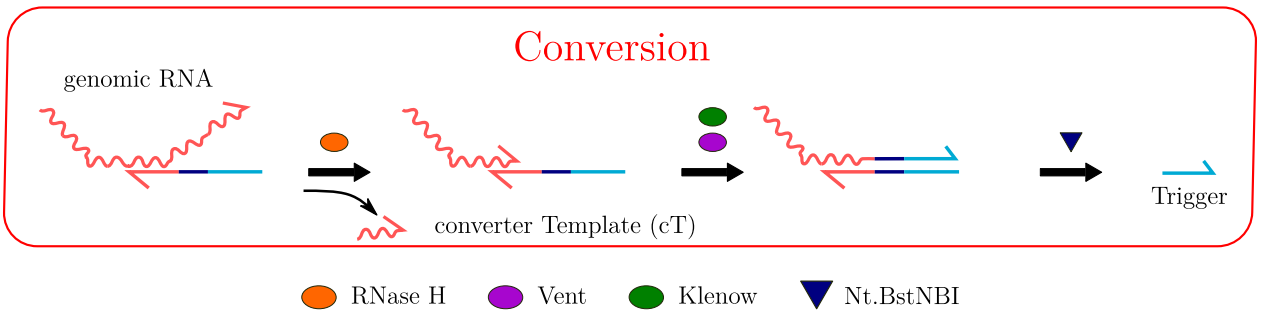

Figure 1.29: **Long RNA detection with a cT and RNAse H principle.** The targeted RNA hybridizes to the cT and is cut by RNAse H. The resulting primer is extended by a polymerase then nicked, producing triggers.

1.7.1.1 Proof of principle on a modified miRNA

In order to obtain a proof of principle, we headed to the detection of the Let7a miRNA with 5 extra bases at its 3' extremity that mismatch with the cT (referred to as Let7a++). These 5 extra bases are not complementary to the cT, therefore Let7a++ is unable to activate the production of trigger unless the mismatching tail is removed by the RNAseH activity. Thus, it is necessary to nick Let7a++ to obtain a primer that can be extended by a polymerase to lead to trigger production. The principle is illustrated in figure 1.30.a.

The first step was to perform an RNAse H range with or without 1 pM of Let7a ++. As we can see in figure 1.30.b., there is an optimum of RNAse H. Indeed, if there is not enough of it, Let7a++ will not be nicked fast enough. On the contrary, if there is too much of it, Let7a++ will be nicked into a multitude of fragments, leaving no primer long enough to remain hybridized on the cT and to be extended by the polymerases. A range of Let7a++ was then made with the optimized concentration of RNAseH. As it can be seen in figure 1.30.c., it is possible to detect down to 1 fM of Let7a++. The proof of principle of the detection of a short RNA with this technique was thus obtained.

1.7.1.2 Towards MS2 detection

In order to see if the results obtained for the detection of Let7a++ were transferable to genomic RNA, we tested this approach for the detection of MS2 genomic RNA (figure 1.31a.), which is commercially available. We started by choosing different regions of this genomic RNA that possess minima secondary struture most suitable for effective detection, that we decided to target. The corresponding cTs were tested with synthetic RNA targets of about 20 bases. These RNA targets were not completely complementary to the cTs and had 2 base mismatches, on the same principle than Let7a++ and its cT. The results obtained are available in figure 1.31.b. Out of the 5 cT/target combinations tested, 2 targets were detected down to 100 fM and were selected for further validation: MS2-t4 and MS2-t7. Ranges of these two targets were then performed in presence of their corresponding cT. (figure 1.31c.). The detection limits for these targets were in the high femtomolar range, which is higher than the one achieved for Let7a++, but these results were good enough to attempt to detect MS2. MS2 ranges were performed in the presence of MS2-t4toβ or MS2-t7toβ, using ms2t4 and ms2t7 as positive controls, respectively (figure 1.31d. and e.). As we can observe, MS2 is not detected while the positive controls, MS2-t4 and MS2-t7 targets, were detected with similar LODs than obtained previously (figure 1.31c.). Therefore, this system does not detect MS2.

To explain these results, we first investigated a possible toxicity of MS2 genomic RNA to PUMA. We performed a Let7a++ detection assay with 0 or 100 pM of MS2 (figure 1.32.b.). The similar results obtained under these two conditions allowed us to eliminate this hypothesis. We then assumed that the secondary structure of MS2 made it difficult for cT hybridization. We were inspired by the work of Lopez et al. to introduce helper strands (HS) [193]. In their work, they designed helper strands (60 nt) to help unfold the RNA secondary structure by hybridizing to regions adjacent to the targeted one. We designed our own HSs and performed an annealing between MS2, different cTs and HSs. The product of this annealing was then added to the PUMA mixture containing RNAse H. A control was performed without HSs (figure 1.32.c.). This approach did not allow the detection

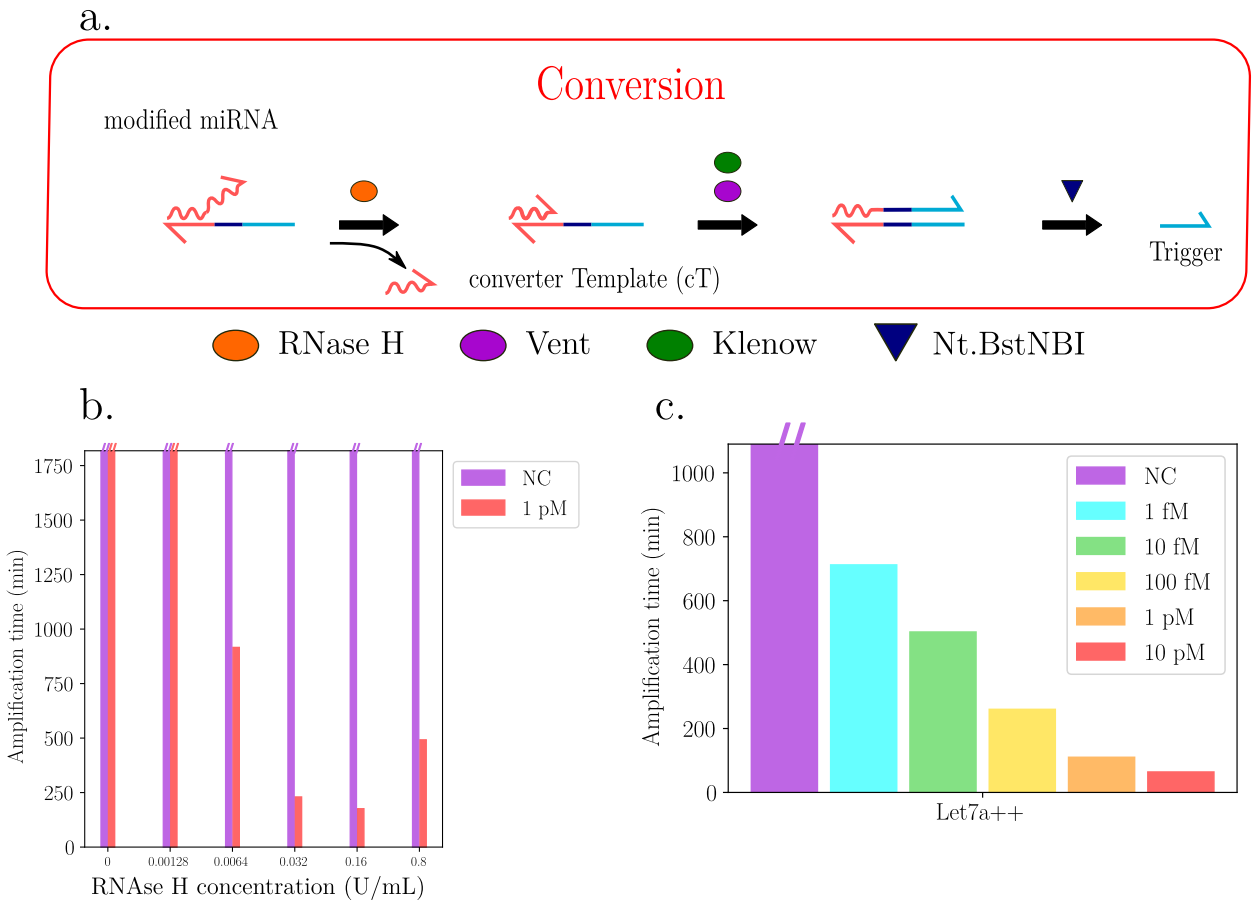

Figure 1.30: **Proof of principle on an extended miRNA. a.** A modified version of Let7a with two more bases, Let7a++, unable to be extended on the cT is targeted. This modified miRNA hybridizes to the cT and is cut by RNAse H. The resulting primer is extended by a polymerase then nicked, producing triggers. **b.** A RNase H range was realized with respectively no Let7a ++ and 1 pM of Let7a++. **c.** A range of Let7a++ was realized with the previously optimized RNAse H concentration in the PUMA mixture.

of MS2. Then, in order to pre-cut MS2 and release the targeted area, we performed an annealing followed by a 1 h incubation at 50°C between MS2, HSs and thermostable RNAse H. The concentration of thermostable RNAse H was previously optimized (figure 1.32.d.). The product of this incubation was added to the PUMA containing the cTs. This approach did not allow the detection of MS2 (figure 1.32.e.).

These different approaches aiming to overcome the possible secondary structures of MS2 did not give the expected results. Nevertheless, in view of the results obtained for the detection of Let7a++, it seems possible to detect MS2. Further experiments are needed, including targeting other MS2 sequences and trying to detect other viral RNAs to see if the problem persists.

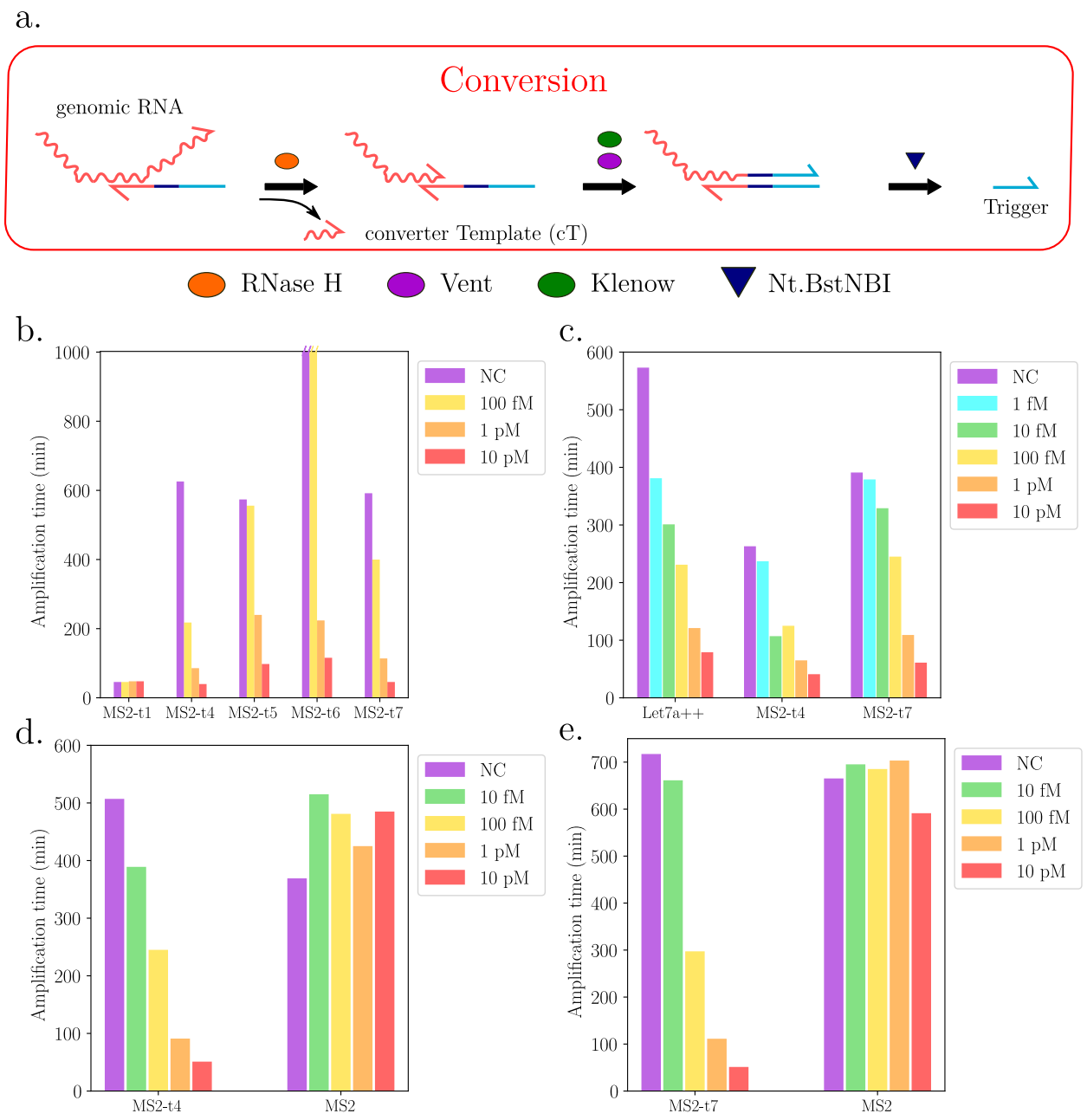

Figure 1.31: **Optimization for MS2 detection.** **a.** Principle scheme. The targeted genomic RNA hybridizes to the cT and is cut by RNAse H. The resulting primer is extended by a polymerase then nicked, producing triggers. **b.** Different regions of MS2 genomic RNA were targeted. Ranges of synthetic corresponding regions were targeted with 0.5 nM of the specific cTs. **c.** Ranges of Let7a++, MS2-t4 and MS2-t7 in presence of their specific cTs. **d.** Ranges of MS2-t4 and MS2 were realized in presence of the cT MS2-t4toβ.e. Ranges of MS2-t7 and MS2 were realized in presence of the cT MS2-t7toβ.

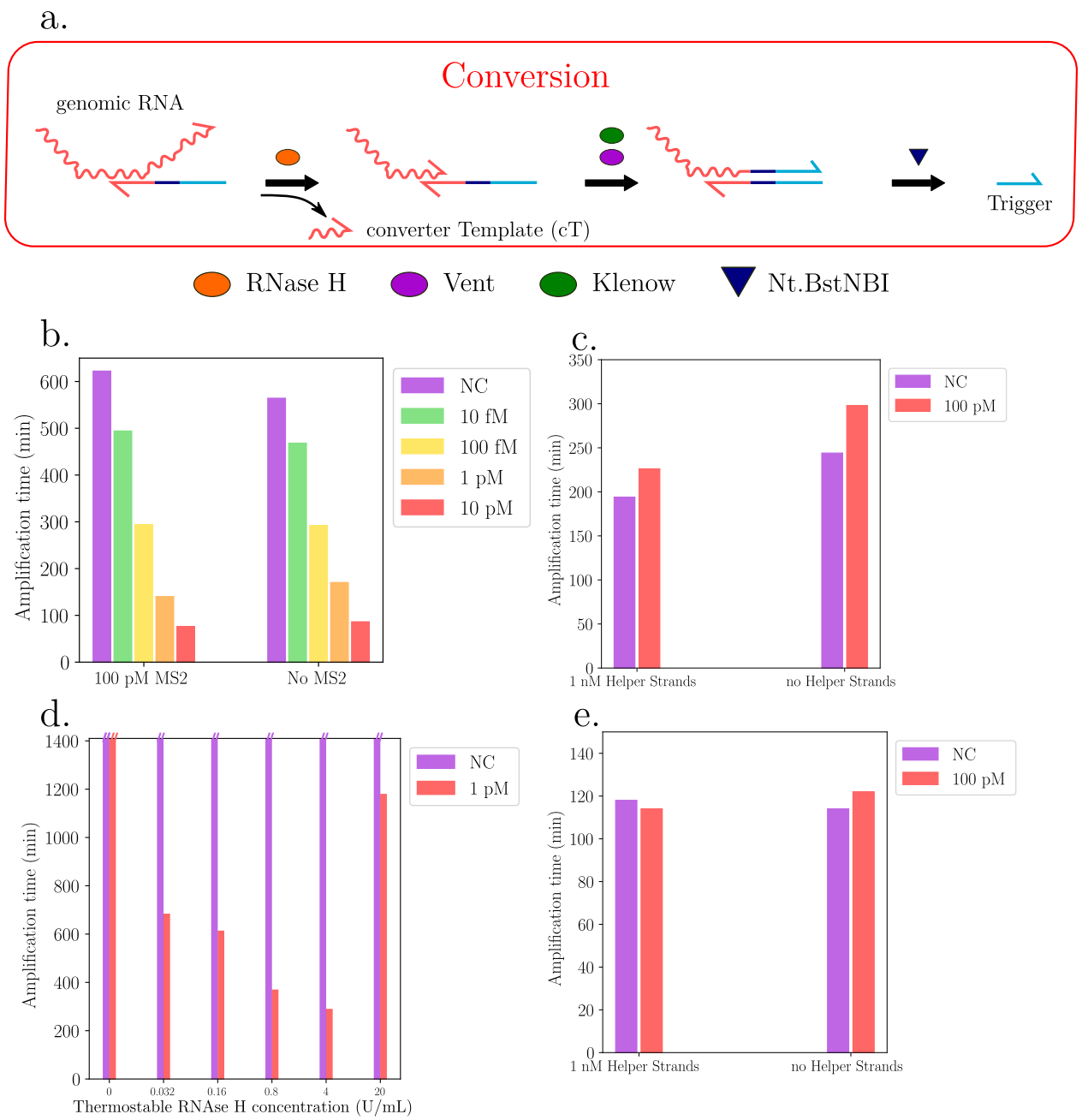

Figure 1.32: **Different strategies for MS2 detection. a.** Principle scheme. The target genomic RNA hybridizes to the cT and is cut by RNAse H. The resulting primer is extended by a polymerase then nicked, producing triggers. **b.** To assess the toxicity of MS2 on the PUMA, a range of Let7a++ was carried out in presence or not of MS2. **c.** MS2 was annealed with the cTs and the helper strands before being added to the PUMA. A control was realized without helper strands. **d.** A thermostable RNase H range was realized with respectively no Let7a ++ and 1 pM of Let7a++. e. MS2 was annealed with the helper strands and incubated with thermostable RNAse H before being added to the PUMA. A control was realized without helper strands.

1.7.1.3 Towards mRNA detection

In order to beter understand what was going on with MS2 RNA, we tried to detect a mRNA. A mRNA is shorter than a viral genomic RNA, and it expected to have less secondary structures, which are troublesome for its detection. We synthesized the GFP messenger RNA, which will be referred to as mGFP. Different cTs were tested, either alone or mixed together, targeting different mGFP regions (figure 1.33.b.). However, no mGFP region was detected: we were not able to detect mGFP by this process. This may be due to the secondary structures of mGFP. To verify this, further experiments should be performed, including targeting other mGFP regions and trying to detect other mRNA to see if the problem persists. So far, it has not been possible to detect long sequences with this approach. However, the results obtained for the detection of Let7a++ show that the concept works. One direction to explore is the denaturation of secondary structures for long RNAs. However, the presence of denaturing agents, such as urea [194], could affect the PUMA performances.

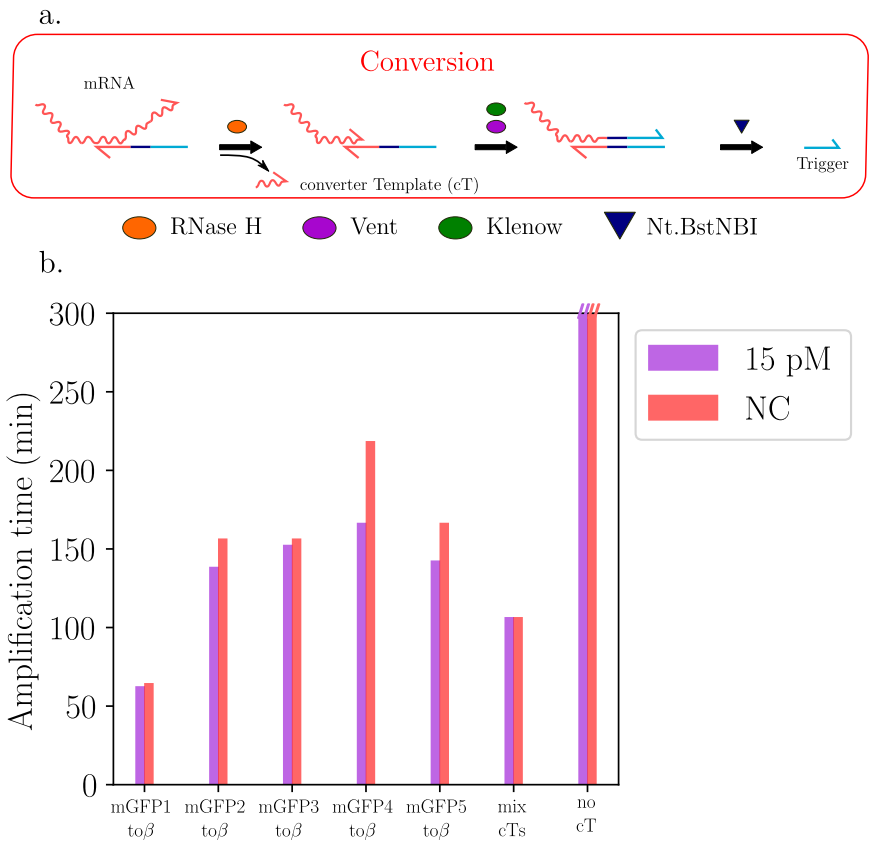

Figure 1.33: **mRNA detection principle. a.** Principle scheme. The targeted mRNA hybridizes to the cT and is cut by RNAse H. The resulting primer is extended by a polymerase then nicked, producing triggers. **b.** Different region of mGFP were targeted thanks to their corresponding cT. The "mix cTs" condition corresponds to a mix of the 5 designed cTs.

1.7.2 Three way junction for long RNA or DNA detection

In order to detect long ssRNA or ssDNA, we got interested in the three way junction (3WJ) approach. This approach is based on the use of two detection strands: the 3WJ Template and the 3WJ Primer. In the presence of the target strand, the 3WJ Template and the 3WJ Primer hybridize first to adjacent regions of the target strand, and only then to each other due to a small overlap between their sequences. The main advantage compared to the cT-based PUMA is that it has no cT, so no leak induced by the presence of cT. A proof of principle has been realized by Wharam et al. for the detection of ribosomal ribonucleic acid (rRNA) of *Escherichia coli K-12 MG1655* with the 3WJ junction method [195]. It has been used to generate primers for rolling circle amplification (RCA) [196] and more recently coupled to EXPAR [197]. Our goal is to couple the 3WJ detection approach with an on-bead target capture, as illustrated on figure 1.34. Additionally, the capture strands may serve as HS, thus facilitating the detection of the target.

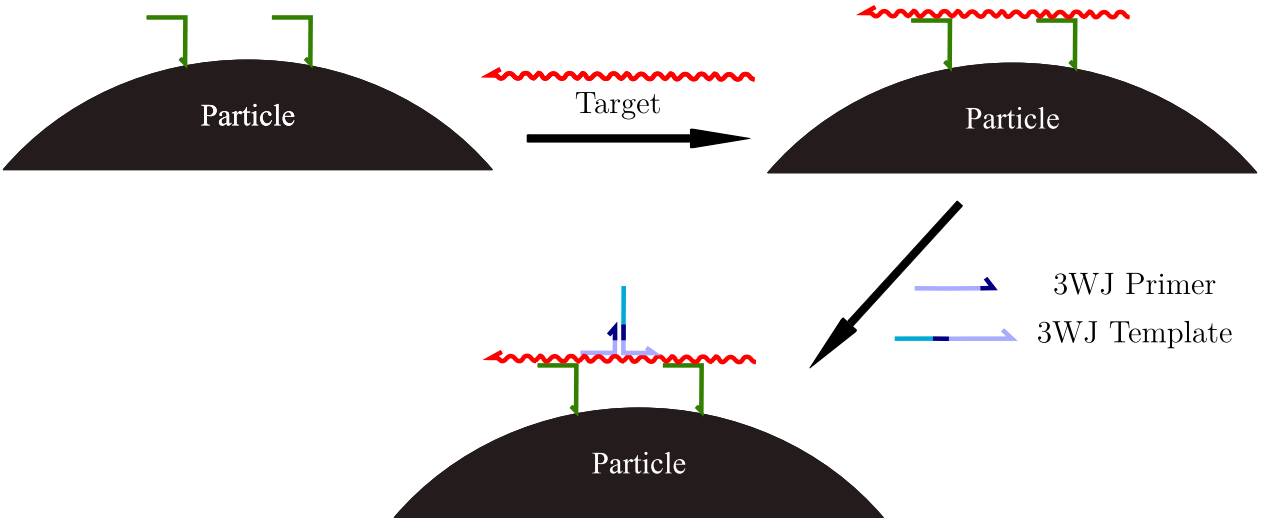

Figure 1.34: **On-bead 3WJ detection principle.** Capture strands are grafted on particles. The targeted RNA or DNA strand hybridizes to capture strands. The 3WJ Template and 3WJ Primer hybridize to the target and only after to each other due to the small overlap between them.

To obtain a proof of principle, we decided to target a 108 nt long DNA strand, which is the DNA version of a part of mGFP. The first step was the design of the two 3WJ oligonucleotides: the 3WJ Primer and the 3WJ Template. The 3WJ Template contains the Nt.Bst.NBI nicking site and the complementary trigger sequence (figure 1.35.a.i). Since the overlap of the two oligonucleotides is necessary, the number of overlapping nucleotides had to be optimized. Indeed, if it is too long the oligonucleotides will hybridizes even in absence of the target (figure 1.35.a.ii). On the contrary, if it is too short, the polymerases won't be able to elongate it. To find a compromise, a range of equimolar mixtures of the template and the primer was performed with and without target. As Li et al. chose a 6 nt overlap for their design [198], we decided to test 6 and 8 overlapping nucleotides with an amplification mixture containing Vent and Klenow polymerases (respectively figure 1.35.b and figure 1.35.c.). The ratio between the amplification times obtained for the templates

with (signal) and without target (background) were calculated and are given in table 1.3. From those results, we decided to go on with an overlapping of 6 nucleotides.

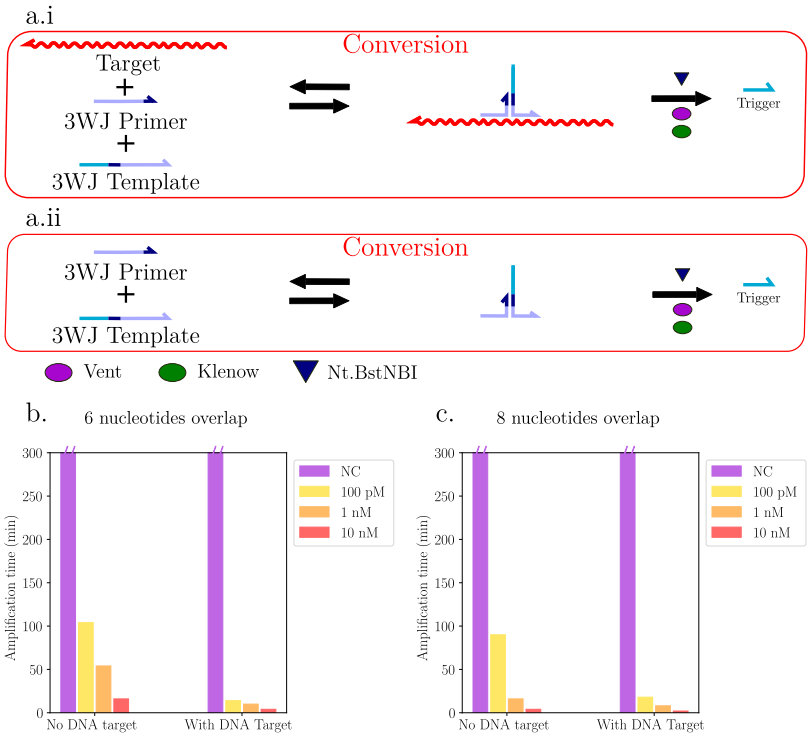

Figure 1.35: **3WJ Template and 3WJ Primer overlap. a.i.** The 3WJ Template and 3WJ Primer hybridize to the target and only after to each other due to the small overlap between them. By design, the 3WJ template contains the Nt.BstNBI nicking site and the trigger complementary sequence. Thus, the formation of the 3WJ results in the production of trigger. **a.ii.** If the overlap between the 3WJ Template and 3WJ Primer is too important, they can hybridize to each other leading to trigger production. **b.** Equimolar 3WJ Template and Primer range with and without target in equal concentration. The overlap is 6 nucleotides long. **c.** Equimolar 3WJ Template and 3WJ Primer range with and without target in equal concentration. The overlap is 8 nucleotides long.

Template / Primer concentration	**6 nucleotides overlap**	**8 nucleotides overlap**
100 pM	7.4	5.0
1 nM	5.4	2.0
10 nM	4.0	2.0

Table 1.3: Signal over background ratio for equimolar 3WJ Template and 3WJ Primer concentrations. The experiment was realized in presence or not of the DNA Target in equal concentration to the 3WJ template/primer set. The experiment was realized in solution, without particles. The ratio was calculated for 6 and 8 nucleotides overlap between the 3WJ Template and the 3WJ Primer.

We then coupled the 3WJ detection approach with an on-bead target capture (figure 1.36.a.). Dynabeads were used with capture strands and the previously optimized oligonucleotides were used to detect the mGFP-3WJ DNA target. A range of the DNA target was carried out and 3 different PUMA amplification mixture were tested. The first one containing Klenow and Vent, the second one containing Bst 2.0 WS (figure 1.36 b.) and the last one containing only Vent (figure 1.36 c.). As it can be observed, the mixture containing only Vent didn't allow the DNA target detection while the two other mixtures allowed it. Our main hypothesis to explain this is that a 6 bases primer is too short to be extended efficiently by the Vent polymerase.

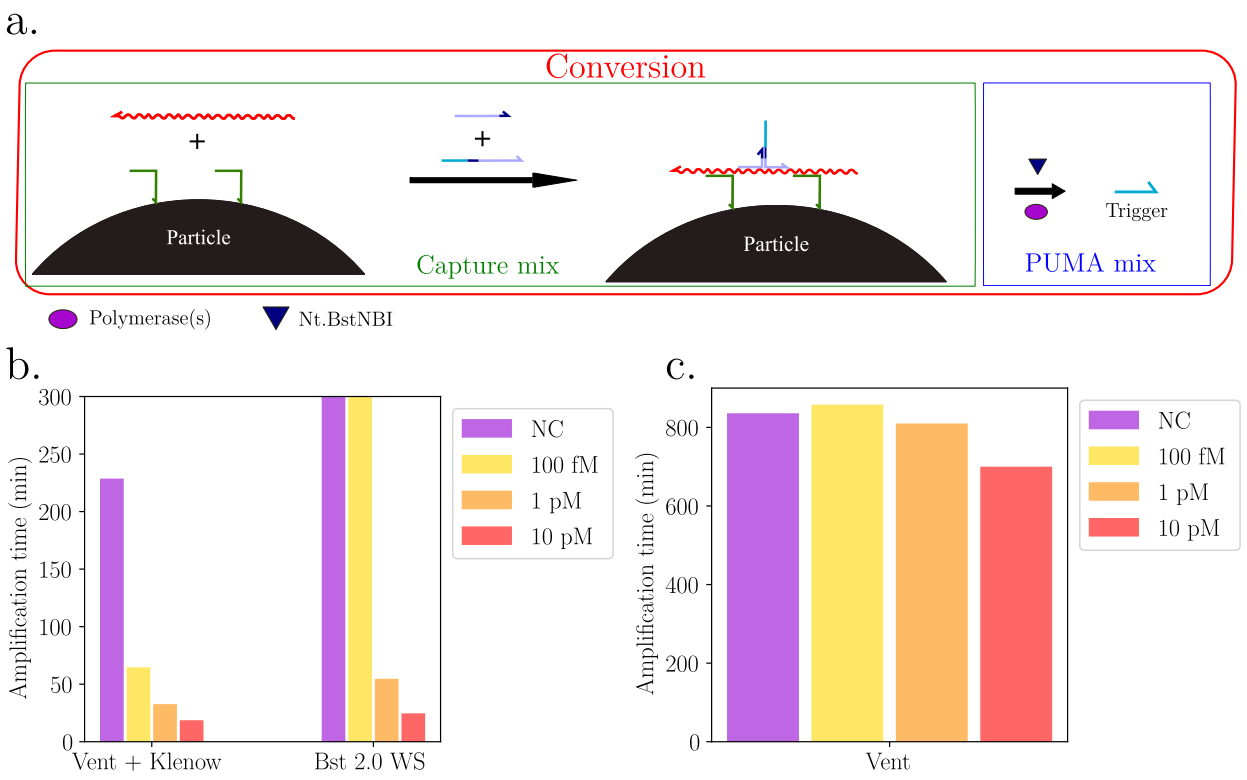

Figure 1.36: **On-bead 3WJ detection: polymerases test. a.** Capture strands are grafted on dynabeads. The targeted DNA strand hybridizes to capture strands. The 3WJ Template and 3WJ Primer hybridize to the target and only after to each other due to the small complementary region between them. The beads are washed and added to the PUMA amplification mix leading to trigger production. **b.** DNA target range. Detection with either Vent and Klenow or Bst 2.0 Ws in the PUMA amplification mix. **c.** DNA target range. Detection with Vent in the PUMA amplification mix.

The detection of a DNA target was successfully realized. This preliminary result shows that this approach has the potential to detect longer DNA or RNA targets. Further experiments are needed to see if the detection of mRNA and then genomic RNA is feasible.

1.8 Discussion

The main aim of the work presented in this first chapter was to detect miRNAs involved in neurodegenerative diseases.

We firstly selected a series of miRNA found in the literature and showed that a part of them can be detected in tube as well as in water-in-oil droplets, following our team's work.

We then demonstrated that by grafting the converter templates on particles and by introducing a capture step, we can detect Let7a and mir7-5p in total miRNA extracted from mouse striatum while removing the inherent toxic effect of the biological matrix.

Based on Anne Christmann's nanostring results, we refocused on a new set of dysregulated miRNAs in mouse models. Among those miRNAs, we chose mir301a-3p, the most promising one, to optimize a capture step integrating a ligation phase to reconstitute an operational cT, thus reducing the non-specific production of trigger. However, mir-cel248 couldn't be detected as effectively as mir301a-3p with the optimized ligation capture step. This is unfortunate because mir-cel248 was spiked into the extracted miRNA samples that we received to allow us to normalize the results.

However, mir-cel-248 detection is satisfying enough to move to digital detection and, later, to multiplexed digital detection. Briefly, lig1 oligonucleotides as well as a population specific barcode could be grafted on beads. Those beads could be mixed with the miRNA containing sample in presence of the lig2 oligonucleotides, a ligase and a polymerase to capture the targeted miRNAs. The beads could be washed if necessary, then mixed with the PUMA components, encapsulated in droplets, incubated, imaged and finally computer analyzed. They could also be analyzed by flow cytometry. In addition, the use of the Bst 2.0 WS polymerase drastically reduces the amplification times. However, this polymerase induces a very strong non-specific amplification in presence of a cT. Although we did not have time to pursue in this direction, the use of Bst 2.0 WS for the bead ligation approach seems, in the long run, to be a promising path.

Due to the SARS-CoV-2 pandemic and the resulting sanitary context, we decided to focus on long nucleic acid detection, in particular genomic RNA detection. We firstly tried a process involving RNase H in the PUMA mixture. By nicking the targeted RNA on the cT, it would free a 3' end which could be used as primer by a polymerase. This approach worked on an extended miRNA, but not on mRNA or on genomic RNA, probably due to the secondary structures.

Secondly, we tried a a three way junction process. We got successful results for the detection of a 108 nucleotides DNA target. It needs to be tested on a RNA version and then designed new oligonucleotides for the SARS-CoV-2 genomic RNA. Its detection could then be tried in digital format. Briefly, capture strands would be grafted on beads. Those beads would be mixed with the targeted RNA containing sample in presence of the 3WJ template and the 3WJ primer. The beads could be washed if necessary, then mixed with the PUMA components, encapsulated in droplets, incubated, imaged and finally computer analyzed. They could also be analyzed by flow cytometry. Different designs of 3WJ Template and 3WJ Primer could be tested, to vary the dissociation constants between the two templates, between the 3WJ Template and the target DNA strand or between the 3WJ Primer and the target DNA strand. Similarly, other capture strand designs could be tested. Thanks to the different washing steps, reducing non-specific amplification, the use of Bst 2.0 WS is a path

to be explored. Indeed, it would allow to significantly reduce the amplification times, down to less than 30 minutes according to the preliminary results displayed in this chapter.

Chapter 2

Protein detection

2.1 Résumé

Dans ce chapitre, nous allons présenter les différentes approches testées pour la détection de protéines. La structure du PUMA présentée en chapitre 1 a été conservée, seul le module de conversion a été adapté. Nous avons commencé par nous intéresser à l'utilisation d'aptamères, des séquences d'acides nucléiques dont la conformation spatiale leur permet d'interagir avec les molécules ciblées. Premièrement, nous avons essayé, sans succès, de détecter un changement de conformation d'un aptamère en présence de la protéine ciblée. Puis, nous avons utilisé une approche d'extension de proximité, en modifiant deux aptamères pour leurs permettre d'interagir avec le PUMA. Cela a permis la détection de l'alpha-thrombine humaine.

Ensuite, nous sommes passés à l'utilisation d'anticorps, en particulier à l'adaptation d'un kit ELISA. Nous avons commencé par fonctionnaliser un anticorps de détection biotinylé avec un oligonucléotide détectable par un cT. Puis, après une phase d'optimisation, nous avons fonctionnalisé un anticorps de détection avec un oligonucléotide auto-activé. Ceci nous a permis de gagner 3 ordres de grandeurs sur la limite de détection d'IL-12 p70 par rapport à un test ELISA traditionnel. Cette approche a été utilisé pour la détection de deux autres protéines : IL-4 et INFg.

Nous avons finalement tenté d'obtenir un classificateur prenant en entrée deux concentrations en protéines pour donner un unique signal de sortie. Ces deux protéines peuvent avoir le même effet sur le PUMA : l'activer ou l'inhiber. Elles peuvent aussi avoir une action contraire : l'une l'activant, l'autre l'inhibant. Nous avons montré qu'il est possible d'obtenir un tel classificateur avec des oligonucléotides greffés sur des anticorps, mais nous n'avons pas réussi à obtenir un classificateur avec des protéines : un échange d'oligonucléotide entre les anticorps de détections est observé, nuisant à la spécificité du signal.

2.2 Summary

In this chapter, we will present the different approaches tested for protein detection. The PUMA structure presented in Chapter 1 has been retained, only the conversion module was adapted. We started by looking at the use of aptamers, nucleic acid sequences whose spatial conformation allows them to interact with the target molecule. First, we tried, without success, to detect a conformational change of an aptamer in presence of the targeted protein. Then, we used a proximity extension assay, modifying two aptamers to allow them to interact with PUMA. This led to the detection of human alpha-Thrombin.

We then moved on to the use of antibodies, in particular the adaptation of an ELISA kit. We started by functionalizing a biotinylated detection antibody (Ab) with a cT-detectable oligonucleotide. Then, after an optimization phase, we functionalized a detection antibody with a sT. This allowed us to gain 3 orders of magnitude on the detection limit of IL-12 p70 compared to an ELISA. This approach was used for the detection of two other proteins: IL-4 and INFg.

Finally, we attempted to obtain a classifier that takes two protein concentrations as input to give a single output signal. These two proteins can have the same effect on PUMA: activate or inhibit it. They can also have an opposite action: one activating it, the other inhibiting it. We have shown that it is possible to obtain such a classifier with oligonucleotides grafted onto antibodies, but we have not succeeded in obtaining a classifier with proteins: an exchange of oligonucleotides between the detection antibodies is observed, affecting the specificity of the signal.

2.3 Introduction

As proteins are composed of amino acids, their detection using a PUMA approach is not as straightforward as nucleic acid detection. In order to connect a protein to a PUMA circuit, two main paths have been explored: antibodies and aptamers. In this chapter are presented the different approaches tested for protein detection with a PUMA circuit.

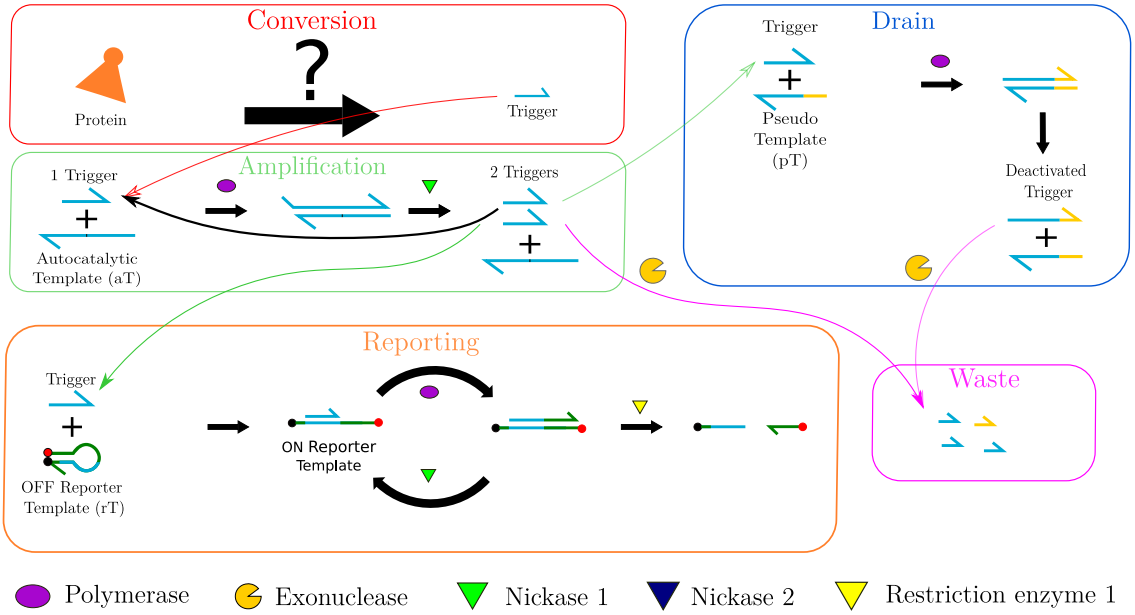

Figure 2.1: **Architecture of the Programmable Ultrasensitive Molecular Amplifier (PUMA) for protein detection.** A conversion module converts the target protein into a universal DNA trigger; an amplification template (aT) exponentially amplifies this trigger sequence; the background noise, inherent to all exponential amplification mechanism is reduced thanks to the pseudotemplate (pT) that acts as a drain for unspecifically produced trigger strands stemming from leaky reactions; a reporting template (rT) produces a fluorescence output using trigger strands.

As illustrated on figure 2.1, the main body of the PUMA used for miRNA detection have been conserved: a conversion module, an amplification module, a drain module and a reporting module are composing the PUMA circuit. While the structure of the amplification module, the drain module and the reporting module remain unchanged, different conversion module were tested. We will present them and discuss their pros and cons in this chapter.

2.4 Nucleic acid aptamer based-PUMA design for one-step detection

Our first idea was to try nucleic acid aptamers. Indeed, nucleic acid aptamers are small three-dimensional structures of oligonucleotides selected to bind to a target of interest with high affinity and specificity [53]. The connection between the PUMA circuit and nucleic acid aptamers would be straightforward.

2.4.1 Converter template-based approach

Aptamers change conformation when binding to their target [199]. We therefore tried to detect a change of aptamer conformation thanks to a cT. The idea is that by adding a nucleic acid aptamer in the PUMA, its conformation will change in presence of the targeted protein. Two changes of conformation would be interesting for us: one freeing the 3' part of the aptamer and one sequestrating it. However, only a few protein-aptamer structures are known, making it difficult to predict a conformational change of interest for our detection method. Nevertheless, we selected an aptamer for VEGF165 detection, SL2B [200] [201], to test this idea.

With the reported K_d value of the aptamer with its target, corresponding to the equilibrum described in equation 2.1, it is possible to calculate the concentration of free aptamer in solution knowing the concentration of protein and the total concentration of aptamer in solution. Indeed, the K_d value is given by the equation 2.2.

$$Aptamer - Protein <=> Aptamer + protein \tag{2.1}$$

$$K_d = \frac{[Aptamer].[Protein]}{[Aptamer - Protein]} \tag{2.2}$$

A schematic illustration is available in figure 2.2. for the case where the aptamer is sequestered by the protein, making its detection impossible. The reported K_d value of SL2B with VEGF165 is 0.5 nM [201]. Therefore, it is possible to calculate the concentration of free SL2B in solution in function of the initial concentration of SL2B and VEGF165. The concentration of free SL2B in solution was calculated for a range of VEGF165 from 0 to 70 nM and for a range of SL2B from 5 pM to 500 pM. The results were reported in table 2.1. Interestingly, the concentration of free SL2B of solution is changing of 2 orders of magnitude between no VEGF165 and 70 nM of VEGF165. Such concentrations of target can be detected with a PUMA, as presented in chapter 1. This means that if only one form of SL2B, either free in solution or bond to VEGF165, can be detected, we would be able to detect the presence of VEGF165 in solution.

	5 pM SL2B	50 pM SL2B	500 pM SL2B
$7.00.10^{-8}$ M VEGF165	$3.55.10^{-14}$ M	$3.55.10^{-13}$ M	$3.57.10^{-12}$ M
$7.00.10^{-9}$ M VEGF165	$3.34.10^{-13}$ M	$3.35.10^{-12}$ M	$3.55.10^{-11}$ M
$7.00.10^{-10}$ M VEGF165	$2.09.10^{-12}$ M	$2.13.10^{-11}$ M	$2.60.10^{-10}$ M
0.00 M VEGF165	$5.00.10^{-12}$ M	$5.00.10^{-11}$ M	$5.00.10^{-10}$ M

Table 2.1: Free SL2B in solution in function of SL2B and VEGF165 concentrations.

A range of VEGF165 was performed in presence of 0, 5, 50 and 500 pM of SL2B to see if we could detect a change of free SL2B concentration. A cT with 8 bases complementary to the 3' part of SL2B was present (figure 2.3.a.). Once extended by Vent polymerase and nicked by Nt.BstNBI, the resulting extended aptamer stays hybridized to the cT, ready to be extended again. This design is irreversible: once the aptamer is extended, the cT continuously produces triggers. With 500 pM of SL2B, the amplification time increases for 70 nM of VEGF165, suggesting that free SL2B can be detected, while SL2B bond to VEGF165 cannot. This effect is not observed for less SL2B. Noteworthy, the lower the temperature, the faster the nonspecific amplification. This is due to the fact that by lowering the temperature, the trigger binds more to the pT, reducing its catalytic activity and thus its effectiveness.

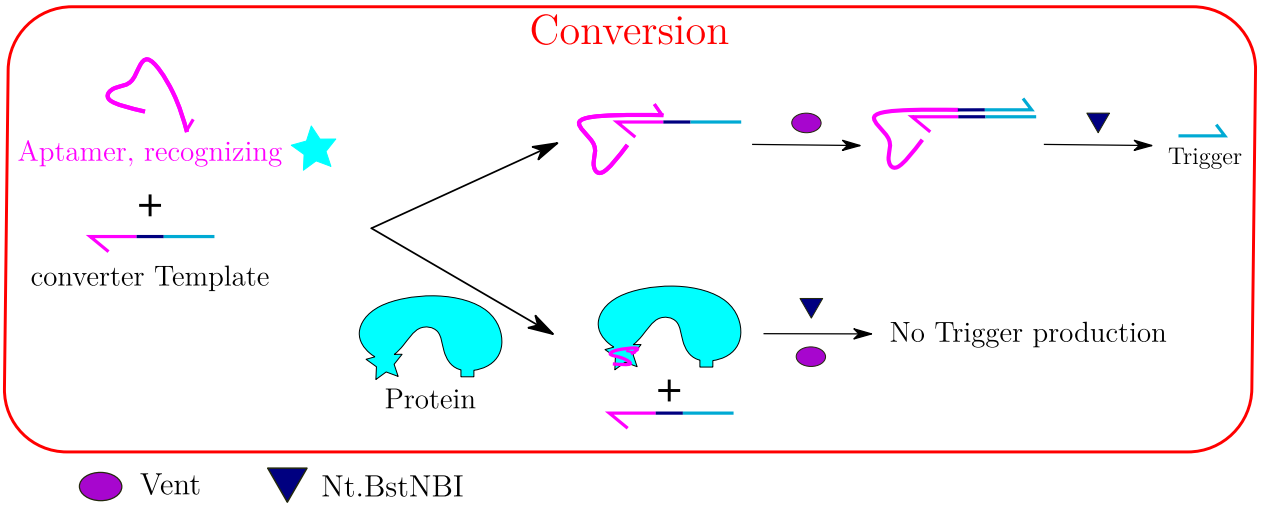

Figure 2.2: **Scheme principle of VEGF165 detection with SL2B and cT a.** A specific aptamer (pink) recognizes a part of a protein, represented by the the turquoise star. An aptamer specific cT is designed. In absence of the targeted protein, the aptamer hybridizes to the cT, undergoes nicking / polymerizing cycles resulting in trigger production. In presence of the targeted protein, the aptamer binds preferentially to the protein. By doing so, the aptamer does not hybridize to the cT and no trigger is produced.

Next, two cTs were tested: one with 8 bases complementary to the 3' part of SL2B (figure 2.3.b.) and one with 10 bases complementary to the 3' part of SL2B (figure 2.3.c.). For each of them, 4 temperatures were tested: 45°C, 46°C, 48°C and 50°C. The cT with 10 complementary bases induces too much baseline trigger production, with amplification times between 40 and 60 minutes. The cT with 8 complementary bases seems correct and the best compromise in terms of temperature is 48°C in these conditions.

A range of VEGF165 was performed with these optimized conditions, in presence of 500 pM SL2B or in presence of scrambled SL2B. Scrambled SL2B has the same G,T,A and C base composition as SL2B and all its bases, except the 8 in 3', were randomly distributed. Therefore, it shouldn't bind to VEGF165 but it should still be able to activate the cT. As it can be observed in figure 2.3.d., similar results were obtained for SL2B and scrambled SL2B. The amplification time delay for high concentrations of VEGF165 is not caused by the sequestration of the aptamer but is an inherent toxic effect of the protein.

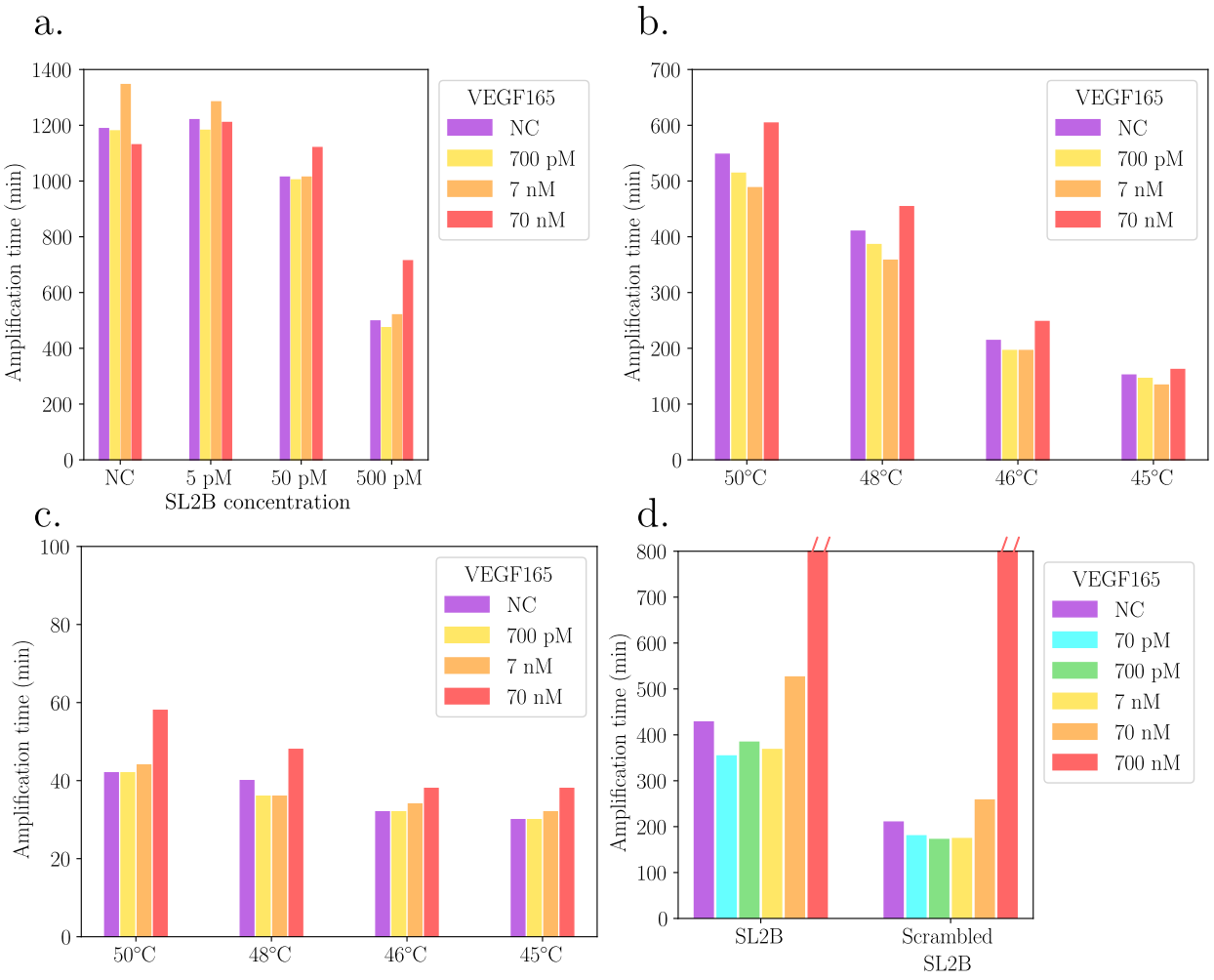

Figure 2.3: **VEGF165 detection with SL2B and cT. a.** A protein / aptamer couple was chosen: VEGF165 and SL2B. A range of VEGF165 was realized for different concentrations of SL2B in presence of 0.5 nM of a cT with 8 complementary bases to SL2B. **b.** Range of VEGF165 in presence of 500 pM of SL2B as well as 0.5nM of a cT with 8 complementary bases to SL2B. Different temperatures were tested for the PUMA incubation. **c.** Range of VEGF165 in presence of 500 pM of SL2b as well as 0.5 nM of a cT with 10 complementary bases to SL2B. Different temperature swere tested for the PUMA incubation. **d.** Range of VEGF165 realized with 500 pM of SL2B or 500 pM of scrambled SL2B. The PUMA mixture contained 0.5 nM of a cT with 8 complementary bases to SL2B.

2.4.2 Caged trigger approach

We tried to detect a change of aptamer conformation thanks to a new template: a caged trigger. A caged trigger refers to a trigger modified with a 3' tail that prevents its amplification. The 3' portion of the target nucleic acid hybridizes to the 3' of the caged trigger and is extended by a polymerase. By design, the caged trigger contains the nickase site of Nb.BssSI, leading to its release. This mechanism is not catalytic, a caged trigger can only yield one trigger, thus it should allow to reduce the nonspecific production of trigger. Indeed,

once activated, a cT continuously produces triggers, this is not the case of a caged trigger.

As in section 2.4.1, the idea is that by adding a nucleic acid aptamer in the PUMA, its conformation will change in presence of the targeted protein. The same two changes of conformation would be interesting for us: one freeing the 3' part of the aptamer and one sequestrating it. To test our idea, we selected an aptamer for human alpha-Thrombin : the 15mer [163]. The 15mer have a K_d of 0.5 nM. Therefore, it is possible to calculate the concentration of free 15mer in solution in function of the initial concentration of 15mer and human alpha-Thrombin. The concentration of free 15mer in solution has been calculated for a range of human alpha-Thrombin from 0 to 1 μM and for a range of 15mer from 400 pM to 3.2 nM. The results has been reported in table 2.2. Interestingly, the concentration of free 15mer in solution is changing of 3 orders of magnitude between no and 1 μM of human alpha-Thrombin. This means that if only one form of 15mer, either free in solution or bonded to human alpha-Thrombin, can be detected, we will be able to detect the presence of human alpha-Thrombin in solution.

	400 pM 15mer	800 pM 15mer	1.6 nM 15mer	3.2 nM 15mer
$1.00.10^{-6}$ M human alpha-Thrombin	$2.00.10^{-13}$ M	$4.00.10^{-13}$ M	$8.01.10^{-13}$ M	$1.60.10^{-12}$ M
$1.00.10^{-7}$ M human alpha-Thrombin	$2.00.10^{-12}$ M	$4.01.10^{-12}$ M	$8.09.10^{-12}$ M	$1.64.10^{-11}$ M
$1.00.10^{-8}$ M human alpha-Thrombin	$1.98.10^{-11}$ M	$4.11.10^{-11}$ M	$8.90.10^{-11}$ M	$2.13.10^{-10}$ M
$1.00.10^{-9}$ M human alpha-Thrombin	$1.59.10^{-10}$ M	$3.73.10^{-10}$ M	$9.46.10^{-10}$ M	$2.37.10^{-9}$ M
$1.00.10^{-10}$ M human alpha-Thrombin	$3.58.10^{-10}$ M	$7.40.10^{-10}$ M	$1.52.10^{-9}$ M	$3.11.10^{-9}$ M
0.00 M human alpha-Thrombin	$4.00.10^{-10}$ M	$8.00.10^{-10}$ M	$1.60.10^{-9}$ M	$3.20.10^{-9}$ M

Table 2.2: Free 15mer in solution in function of 15mer and human alpha-Thrombin concentrations.

A schematic illustration is available in figure 2.4. for the case where the aptamer is sequestered by the protein, making its detection impossible. Firstly, 3 caged triggers with respectively 4, 6 and 8 bases complementary to the 3' part of the 15mer were tested. The K_d of the 15mer with 15mer toα 8 bases, 15mer toα 6 bases and 15mer toα 4 bases have been calculated using Nupack (see appendix A), giving a K_d of respetively, 74 nM, 2.0 μM and 1.0 mM at 48°C. However, the presence of Vent polymerase in the amplification mixture

can significantly displace these equilibria by extending the 15mer when it hybridizes to a caged trigger. To determine if this was the case, a range of 15mer was performed in presence of 0.5 nM of each of these caged triggers (figure 2.5.a.). Only the caged trigger with 8 complementary bases had a response correlated to the concentration of 15mer, this caged trigger will be referred to as 15mertoα 8 bases. These experimental results are in agreement with the calculated K_d values. Possibly, 4 and 6 bases is too short to be used as primer by Vent polymerase.

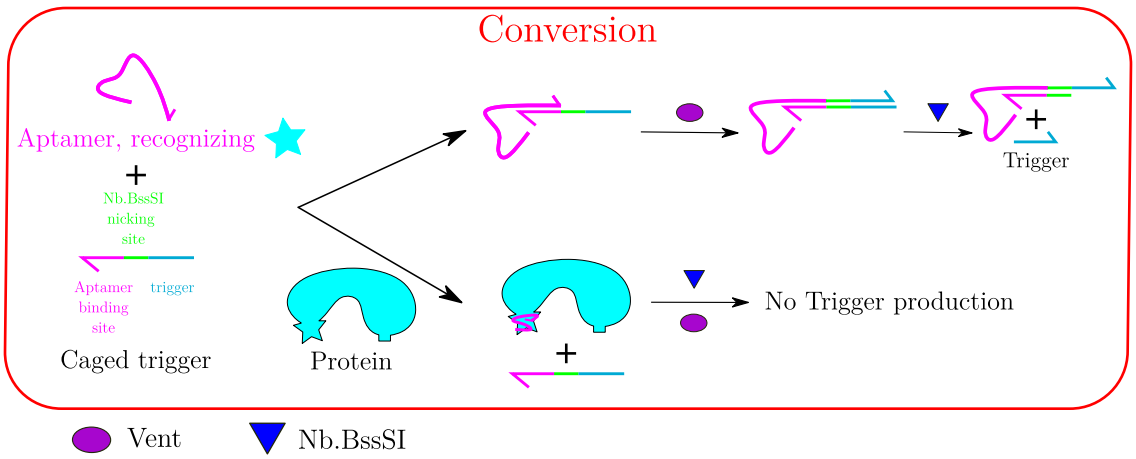

Figure 2.4: **Scheme principle of human alpha-Thrombin detection with 15mer and caged trigger.** A chosen aptamer (pink) recognizes a part of a protein, represented by the the turquoise star. An aptamer specific caged trigger is designed: it contains a 3' extremity complementary to the 3' extremity of the aptamer (pink), a Nb.BssSI nicking site (green) and a trigger (light blue). In absence of the target protein, the aptamer hybridizes to the caged trigger, undergoes polymerisation and nicking, resulting in trigger release. In presence of the target protein, the aptamer binds preferentially to the protein. By doing so, the aptamer doesn't hybridize to the caged trigger and no trigger is released.

Then, a human alpha-Thrombin range was performed in presence of 0.5 nM of 15mertoα 8 bases. Different concentrations of 15mer were tested: 400 pM, 800 pM, 1.6 nM, 3.2 nM (figure 2.5.b.). A range of human alpha-Thrombin was then carried out with 0.5 nM of 15mertoα 8 bases and 400 pM of 15mer. Different reaction temperatures were tested: 45°C, 46°C, 48°C and 50°C. The best temperature is 48°C in these conditions (figure 2.5.c.).

Finally, a range of Human alpha-Thrombin was performed with these optimized conditions, in presence of 400 pM 15mer or in presence of scrambled 15mer. As it can be observed in figure 2.5.d., similar results were obtained for 15mer and scrambled 15mer. Again, the amplification time delay for high concentrations of human alpha-Thrombin is not caused by the sequestration of the aptamer but is an inherent toxic effect.

Trying to detect the conformational change of an aptamer with a cT (or a caged trigger) does not seem to be a suitable method for the detection of a relatively weak molecular interaction (aptamer-protein). The irreversible process of cT activation, even non catalytic in the case of a caged trigger, causes too much background trigger production.

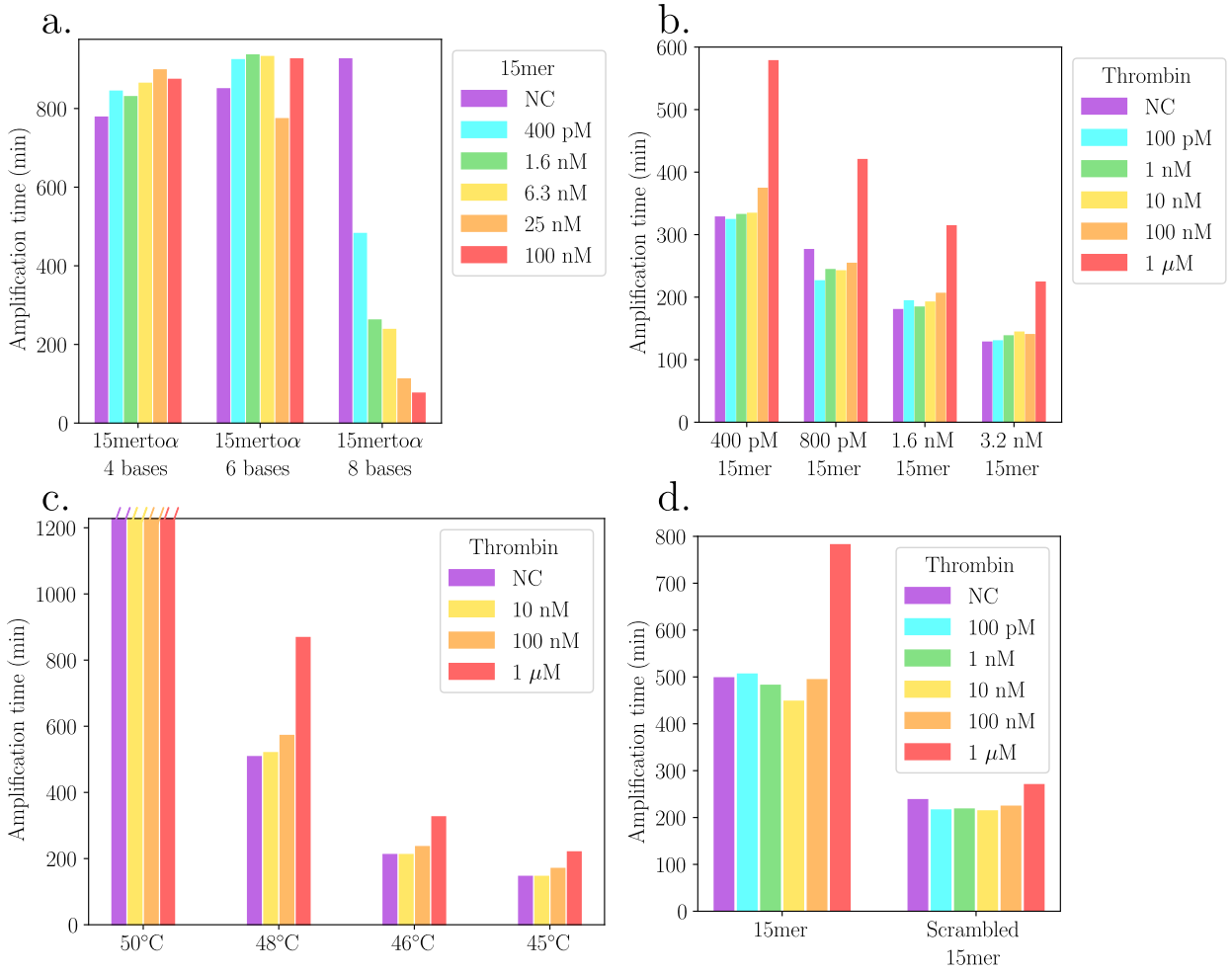

Figure 2.5: **Human alpha-Thrombin detection with 15mer and caged trigger. a.** A couple protein / aptamer has been chosen: human alpha-Thrombin and 15mer. A range of 15mer wsa realized in presence of 0.5 nM of 3 different caged triggers matching the 15mer aptamer on 4, 6 and 8 bases respectively. **b.** Range of human alpha-Thrombin in presence of 0.5 nM of 15mertoα 8 bases. Different concentrations of 15mer have been tested. **c.** Range of human alpha-Thrombin in presence of 400 pM of 15mer as well as 0.5 nM of 15mertoα 8 bases. Different temperatures have been tested for the PUMA incubation. **d.** Range of human alpha-Thrombin with 400 pM of 15mer or 400 pM of Scrambled 15mer. The PUMA mixture contained 0.5 nM of 15mertoα 8 bases. The amplification took place at 48°C.

2.4.3 Proximity extension assay-based approach

Since the attempt to detect the conformational change of an aptamer using a cT did not work, we got interested in the detection of proteins thanks to a proximity extension assay (PEA) (see section I.6.2.2). Briefly, a matched pair of antibodies or aptamers linked to specific oligonucleotides binds to the targeted protein, locally increasing the concentration of the two oligonucleotides of the pair. The two oligonucleotides come in close proximity, hybridize to each other and one of them is extended by a polymerase, creating a DNA amplicon. In our approach, the specific oligonucleotides are an activator and its specific cT. The DNA

amplicon is a trigger molecule, interacting with the PUMA circuit.

2.4.3.1 Nb.BsmI-based design

Dr. Banerjee, a postdoctoral fellow at LBC, worked on optimizing the sequences of the activator and its cT for protein detection through a matched pair of antibodies (data not shown). This design works with the Nb.BsmI nickase enzyme, at 37°C in FS Buffer 1x and with the Bst Large Fragment (Bst LF) polymerase (see section 3.4 for explanations on temperature and buffer optimization). The cT and the activator are hybridizing to each other on 9 bases. Due to the Nb.BsmI nicking site sequence, the design is reversible. In that case, when the activator hybridizes to the cT, is extended by a polymerase and then nicked to release a trigger, the oligonucleotides return to their initial state, i.e. as before the elongation by the polymerase. Trigger production therefore does not shift the equilibrium between the two oligonucleotides, reducing background amplification.

For a proof of principle with aptamers, we decided to target the human alpha-Thrombin with two aptamers: the 15mer and the 29mer, reported in the same review [163]. The activator and cT sequences optimized by Dr. Banerjee, as well as a T12 linker were added to the sequences of the two selected aptamers, as illustrated on figure 2.6. The cT is added at the 5' extremity of the aptamer while the activator is added at the 3' extremity. The K_d of the 15mer-activator (15mer-act) / 29mer-cT as well as the K_d of 15mer-cT / 29mer-act have been calculated (see appendix A), giving a K_d of 104 nM at 37°C for both of the oligonucleotide sets.

The first step has been to carry a range of human alpha-Thrombin, respectively 0, 1, 10 and 100 nM in presence of 0, 1, 10 and 100 nM of an equimolar mix of 15mer-act / 29mer-cT (figure 2.7.a.) or in presence of 0, 1, 10 and 100 nM of an equimolar mix of 15mer-cT / 29mer-acT (figure 2.7.b.).

The combination 15mer-act / 29mer-cT did not allow human alpha-Thrombin detection. However, 10 nM and 100 nM of 15mer-cT / 29mer-act allowed the detection of 100 nM of human alpha-Thrombin. 0 and 1 nM of 15mer-cT / 29mer-act did not allow human alpha-Thrombin detection. The $scores_{100nM}$, for the detection of 100 nM of human alpha-Thrombin, have been calculated and reported on figure 2.7.b. The highest score was obtained with 10 nM of 15mer-cT / 29mer-act, we therefore selected this condition for further optimization. The necessity to test both combinations 15mer-cT / 29mer-act and 15mer-act / 29mer-cT is illustrated: it it possible, due to the spatial conformations of the oligonucleotides, that only one of these combinations works. Moreover, it is also possible that adding a linker, a cT or an activator to an aptamer modifies its properties, thus preventing its binding to the targeted protein.

Following these very promising preliminary results, we tried to optimize the experimental conditions. As Dr. Banerjee performed his assay in FS Buffer 1x (see section 3.4), we decided to realize a range of human alpha-Thrombin, with 10 nM of 15mer-cT / 29mer-act, in FS Buffer 1x and in miRBuffer 1x (figure 2.8.a.). The $scores_{100nM}$, for the detection of 100 nM of human alpha-Thrombin, have been calculated and reported on the figure. As the highest score was obtained in FS Buffer 1x, we decided to continue to perform the PEA in this buffer. Noteworthy, the LOD is lower than for the results of figure 2.7.c. This is due to the use of new low binding pipet tips, Corning, allowing us to realize more precise protein

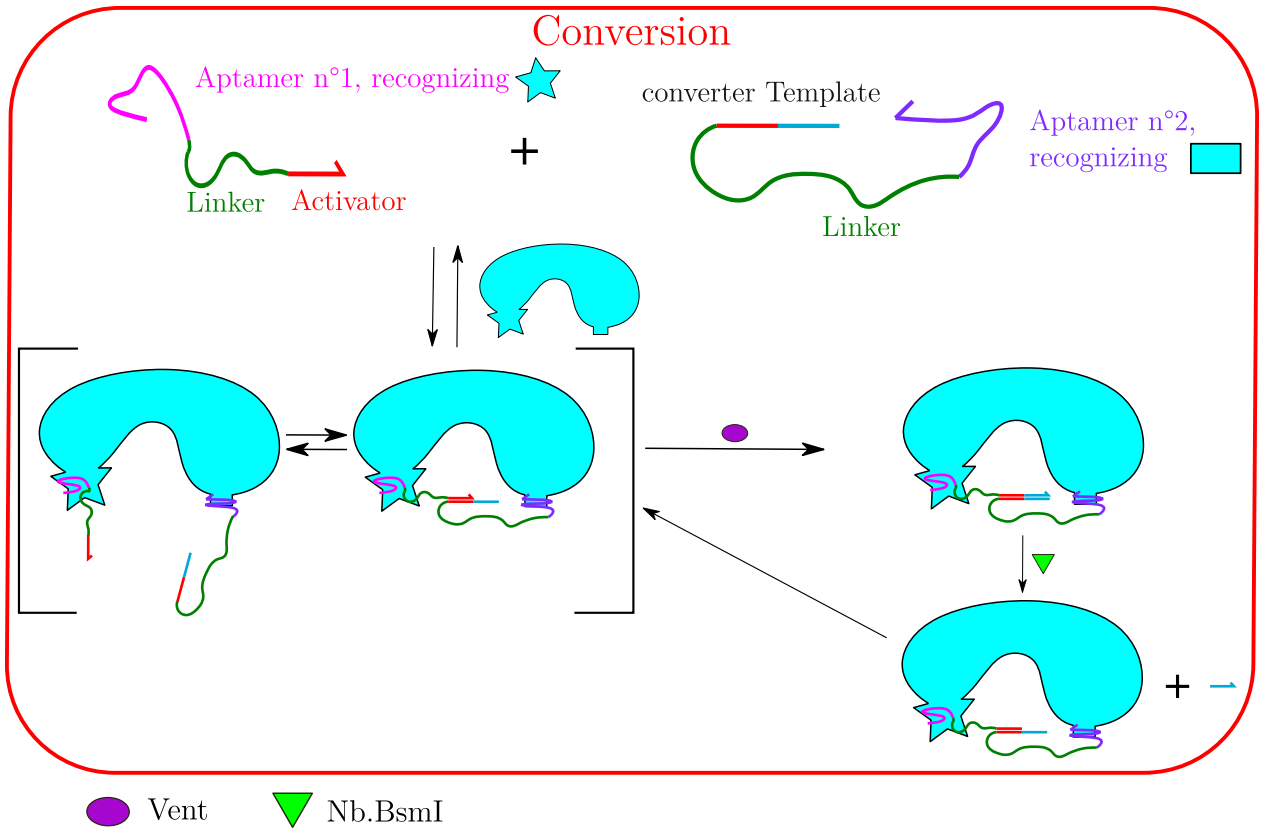

Figure 2.6: **Principle scheme of proximity extension assay based PUMA.** Two aptamers (pink and purple) recognising parts of a protein, respectively represented by the the turquoise star and the turquoise rectangle, are chosen. One of the aptamer is carrying a cT at its 5' extremity while the other one is carrying an activator, able to hybridize to the cT, at its 3' end. A linker is present between the aptamers and the cT or activator. In presence of the targeted protein, the aptamers bind to their respective target first, bringing the cT and the activator close. Then, the activator hybridizes to the cT, is extended by a polymerase and nicked to produce a trigger molecule. The oligonucleotides return to their initial states as the design is reversible. In absence of the targeted protein, the activator and the cT doesn't hybridize, leading to no trigger production.

dilution. Moreover, a toxic inherent effect appears for 1 μM of Human alpha-Thrombin, as already observed when trying to detect the Human alpha-Thrombin with a caged trigger approach (see section 2.4.2).

In order to reduce the nonspecific production of trigger, we compared the detection of human alpha-Thrombin with 10 nM of 15mer-cT and 10 nM of either 29mer-act of 29mer-act-V2. The 29mer-act-V2 has an activator which matches the cT on 8 bases, one base less than the 29mer-act (figure 2.8.b.). This missing base is in 5' of the activator and thus can not be recovered by polymerase extension. The $scores_{100nM}$ have been calculated and reported on the figure. The score is higher for the 15mer-cT / 29mer-act oligonucleotide set. Moreover, the detection of 10 nM of human alpha-Thrombin with 15mer-cT / 29mer-act-V2 is approximately 5 times slower than the detection with 15mer-act / 29mer-cT. The K_d of

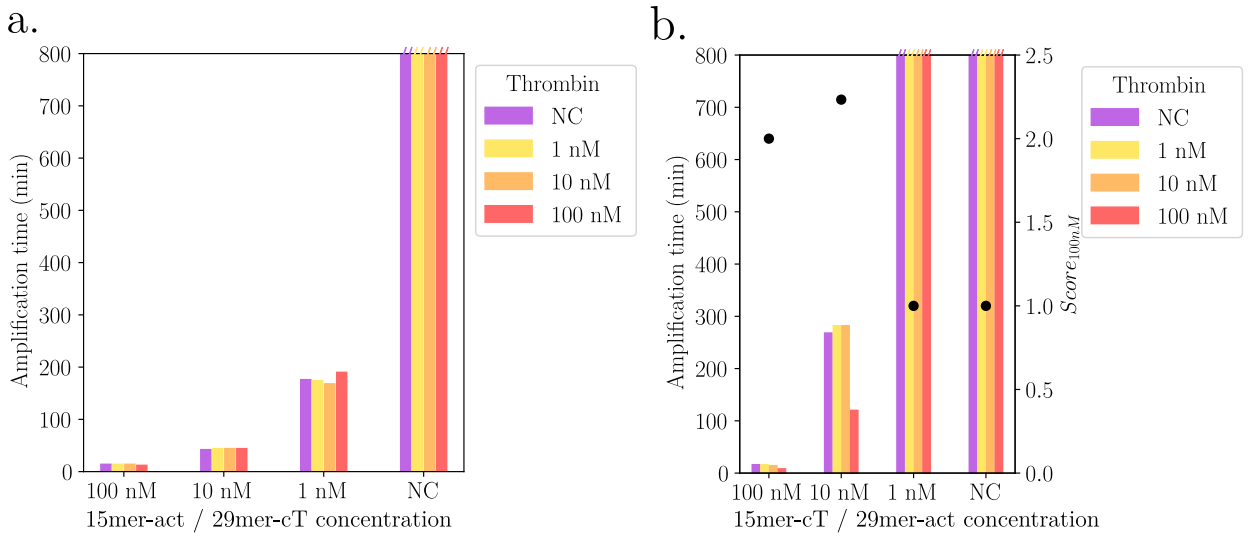

Figure 2.7: **Proximity extension assay: different aptamer combinations for human alpha-Thrombin detection. a.** The 15mer and the 29mer, two aptamers, were chosen for the detection of human alpha-Thrombin. A range of Human alpha-Thrombin has been realized while the 15mer was carrying the cT and the 29 mer the activator. An equimolar range of aptamer was conducted. **b.** Range of human alpha-Thrombin while the 15mer was carrying the activator and the 29 mer the cT. An equimolar range of aptamer was conducted. The amplification times for the different human alpha-Thrombin concentrations are given by bar charts (left axis) and the $scores_{100nM}$ are given by the black dots (right axis).

the 15mer-cT / 29mer-act-V2 were calculated (see appendix A), giving a K_d of 156 nM at 37°C. With a higher K_d than the 15mer-cT / 29mer-act oligonucleotide set, it is logic for the production of trigger to be slower and thus for the amplification times to be higher.

Finally, a range of human alpha-Thrombin was realized in FS Buffer containing 10 nM of 15mer-act and 29mer-cT. Controls with 10 nM of scrambled aptamers have been realized. Scrambled aptamers are indicated by the "S" before the name of the aptamer (figure 2.8.c.). The detection of 100 nM of human alpha-Thrombin was achieved only for the aptamers, not for the scrambled versions, demonstrating the specificity of the detection.

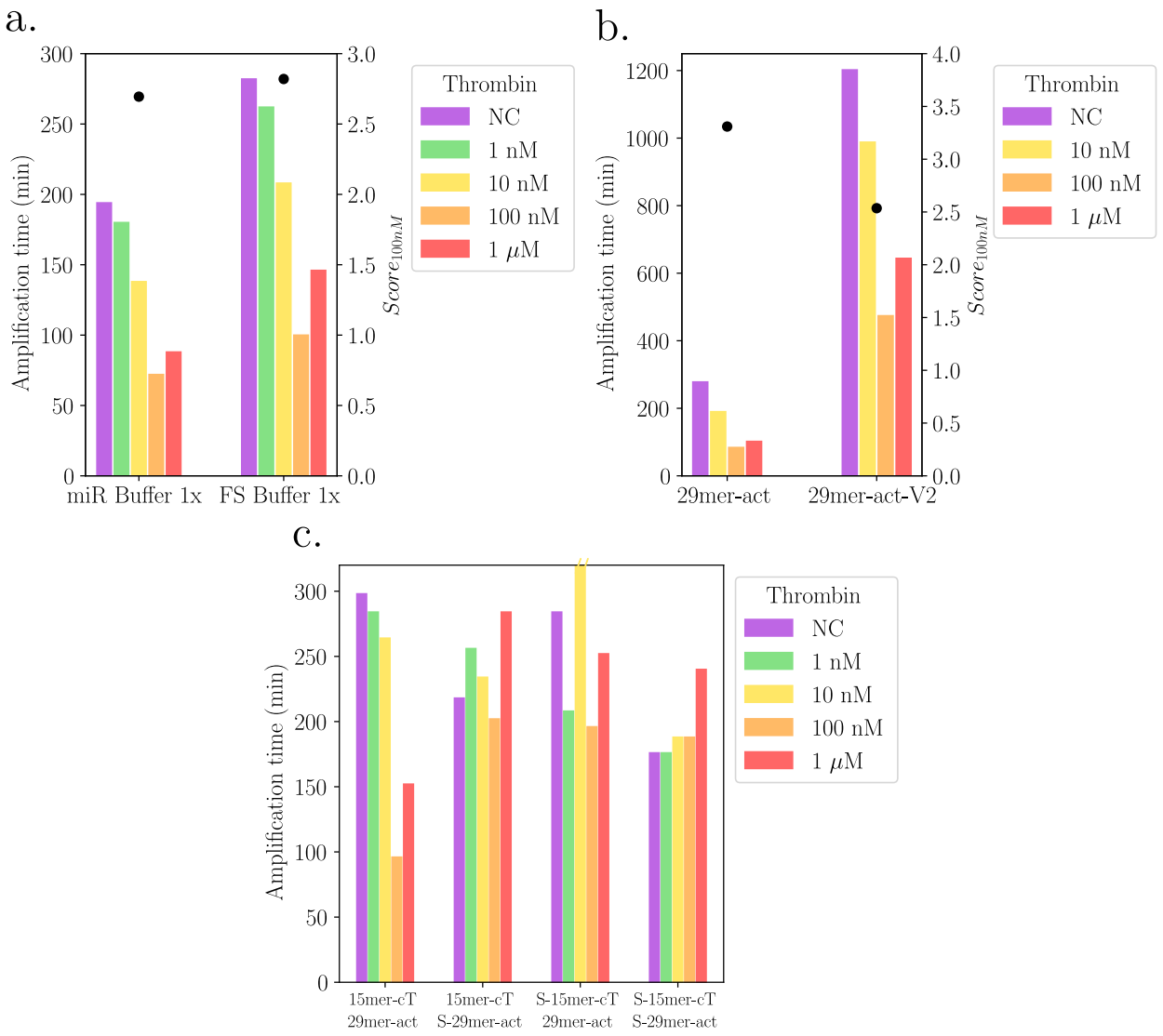

Figure 2.8: **Proximity extension assay: human alpha-Thrombin detection optimization. a.** A range of human alpha-Thrombin was realized in mirBuffer 1x or in FS Buffer 1x in presence of 100 nM of 15mer-activator (15mer-act) and 29mer-cT. **b.** A range of human alpha-Thrombin was realized in FS Buffer 1x, in presence of 10 nM of 29mer-cT and 10 nM of either 15mer-act or 15mer-act-V2. The 15mer-act-V2 matches the cT on one base less than the 15mer-act. The amplification times for the different human alpha-Thrombin concentrations are given by bar charts (left axis) and the $scores_{100nM}$ are given by the black dots (right axis). **c.** A range of human alpha-Thrombin was realized in FS Buffer containing 10 nM of 15mer-act and 29mer-cT. Controls with 10 nM of scrambled aptamers have been realized. Scrambled aptamers are indicated by the "S" before the name of the aptamer.

Once this proof of principle obtained for human alpha-Thrombin detection, we tried to apply the PEA approach to other proteins. The first one was VEGF165: we selected two aptamers, the 25mer and VEAP121 used by Kariper et al. [202]. We realized a range of VEGF165 with 1 and 10 nM of 25mer-act / VEAP121-cT (figure 2.9.a.) and with 1 and

10 nM of 25mer-cT / VEAP121-act (figure 2.9.b.). However, none of the tested conditions allowed the detection of VEGF165.

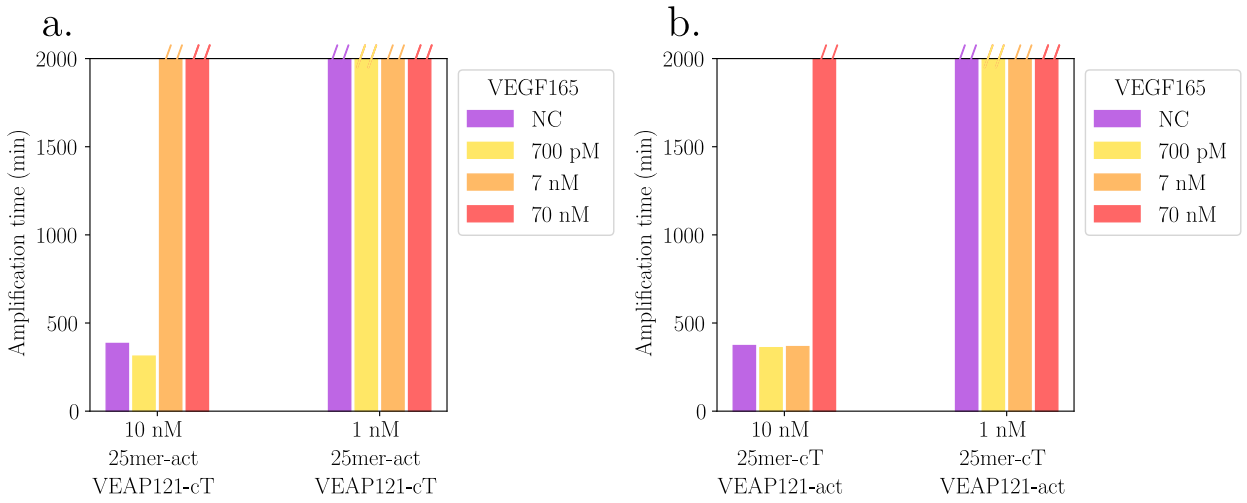

Figure 2.9: **Proximity extension assay: VEGF165 detection.** In order to detect VEGF165, two aptamers were selected: respectively the 25mer and the VEAP121. **a.** A range of INFg has been carried out for two different equimolar concentrations of 25mer-act and VEAP121-cT. **b.** A range of INFg has been carried out for two different equimolar concentrations of 25mer-cT and VEAP121-act.

The second one was Interferon γ (INFg): we selected two aptamers reported in the literature, the 25mer [203] and the 34mer [204]. We realized a range of INFg with 1 and 10 nM of 34mer-act / 25mer-cT (figure 2.9.a.) and with 1 and 10 nM of 34mer-cT / 25mer-act (figure 2.9.b.). However, none of the tested conditions allowed the detection of INFg.

The failure to detect VEGF165 and INFg suggests that further optimization is required. Indeed, it is possible that the conditions used, notably in terms of buffers and temperatures, are too different from those used for the selection of these aptamers. In addition, it is possible that the addition of the linker, the cT or activator may modify the properties of the chosen aptamers. Finally, it is possible that the chosen linker, a T12, is not adapted to the structure of the targeted proteins, preventing the cT and activator from hybridizing.

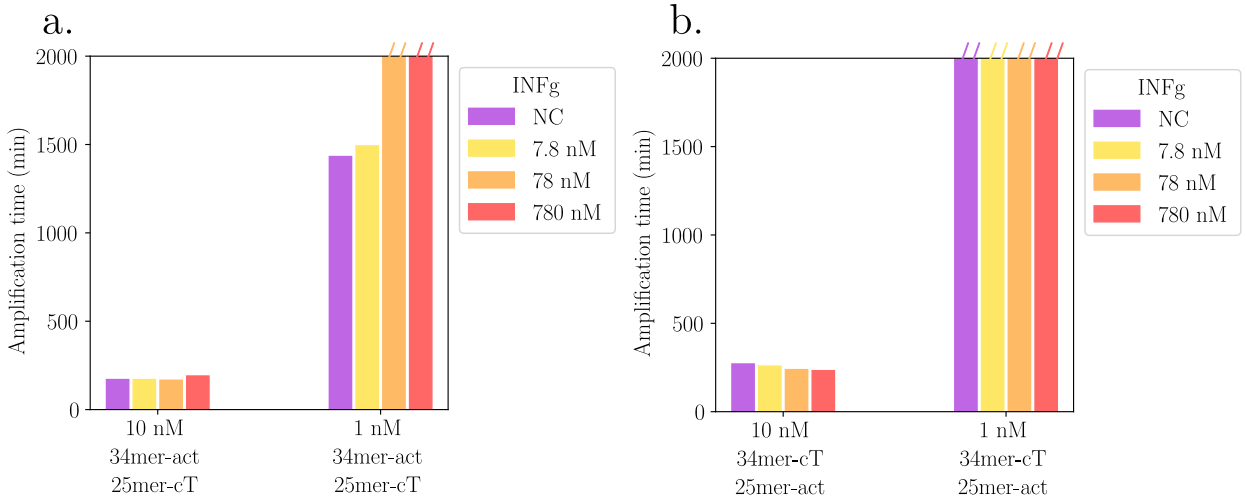

Figure 2.10: **Proximity extension assay: INFg detection.** In order to detect INFg, two aptamers were selected: respectively the 25mer and the 34mer. **a.** A range of INFg was carried out for two different equimolar concentrations of 34mer-act and 25mer-cT. **b.** A range of INFg was carried out for two different equimolar concentrations of 34mer-cT and 25mer-act.

2.4.3.2 Nt.BstNBI-based design

In an attempt to accelerate the speed of detection of human alpha-Thrombin, we designed two sets of activator / cT working with Nt.BstNBI: one containing the sequence GAGA between the trigger complementary and the Nt.BstNBI nicking site and one containing the sequence GATT (See section 2.5.3.4 for more explanations on the sequences choices). The K_d of the GAGA activator / cT and the GATT activator / cT sets were calculated (see appendix A), giving K_d of respectively 29 and 69 nM at 37°C. The lower the K_d, the higher the affinity of the two oligonucleotides and the more likely the nonspecific production of trigger. It is to be noted that the Nt.BstNBI PEA design is not reversible. Therefore, the nonspecific trigger production is increased compared to the Nb.BmsI design.

Those two sets were tested (figure 2.11). The GAGA activator / cT set is faster than the GATT activator / cT set with and without human alpha-Thrombin. The $scores_{1uM}$, for the detection of 1 μM of human alpha-Thrombin, have been calculated and reported on the figure. The higher score is obtained for the GAGA oligonucleotide set. Moreover, the GAGA oligonucleotide set allows the detection of 10 nM of human alpha-Thrombin and is not sensitive to the toxic effect induced by 1 μM of human alpha-Thrombin. The GATT oligonucleotide set does not allow the detection of 10 nM of human alpha-Thrombin and is sensitive to the toxic effect induced by 1 μM of human alpha-Thrombin.

So far, the GAGA oligonucleotide set is the best optimization that we have been able to achieve using Nt.BstNBI. However, only 2 sets of oligonucleotides have been tested. It would be interesting to test other sequences to acquire more data, allowing a better understanding of PUMA coupled to a PEA conversion module systems. Moreover, while the detection with Nt.BstNBI based on the GAGA oligonucleotide set is faster than the detection using Nb.BsmI, it shows a reduced sensitivity.

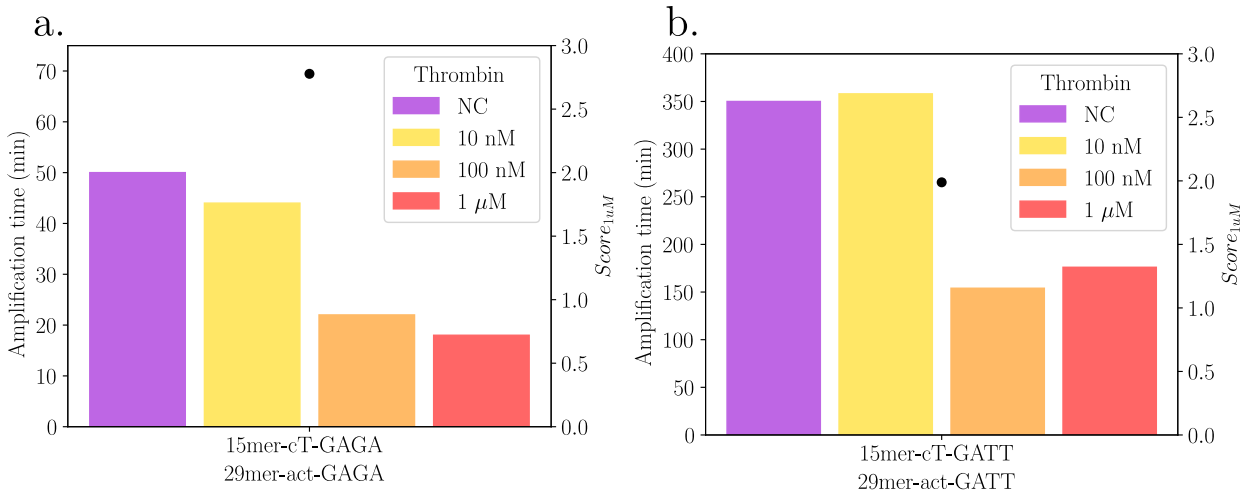

Figure 2.11: **Proximity extension assay: human alpha-Thrombin detection. Nt.BstNBI-based designs.** A range of human alpha-Thrombin was realized in FS Buffer with 100nM of 15mer-cT-GAGA / 29mer-act-GAGA (**a.**) and with 100nM of 15mer-cT-GATT / 29mer-act-GATT (**b.**). The amplification times for the different human alpha-Thrombin concentrations are given by bar charts (left axis) and the $scores_{1uM}$ are given by the black dots (right axis).

PEA based aptamers does not seem suitable for sensitive detection of proteins. This is likely related to the high K_d of the aptamers with the target protein. A possibility is to replace them with antibodies, which have lower K_d, as reported in the literature (see section I.4.1). A better understanding of the spatial conformations and interactions is required. However, the binding site and conformation of aptamers are poorly described in the literature. Although this solution approach stays relevant, for example, for the detection of secreted proteins, we decided to turn to a supported approach, similar to ELISA, for which we hope to achieve better sensitivities.

2.5 Immuno-PUMA design for two-step detection

2.5.1 ELISA approach

We then turned our attention to the use of antibodies and more particularly to the adaptation of the ELISA principle. Briefly, for a traditional sandwich ELISA, a target protein binds to a capture antibody grafted on a surface and is then recognized by a detection antibody functionalized with a biotin and added in a second step (see section I.4.2). A labelled enzyme, such as avidin-HRP, is then added, allowing a substrate to be transformed into a product that can be detected by absorbance or fluorescence measurement (figure 2.12.a.). For our first experiments, we got interested in the detection of mouse IL-12 p70 protein. Monitoring this interleukin provides information on the immune response [205]. To realize our experiments, we used a commercial ELISA kit from Biolegend. We started by making a range of IL-12 p70 (figure 2.12.b.) to test the kit. With this kit, detection is achieved by the conversion of a commercial substrate, called substrate D, by HRP to a product which absorbance is measured at 595 nm. This allowed us to conclude that the LOD of the commercial kit is around 500 fM, following the provider's procedure.

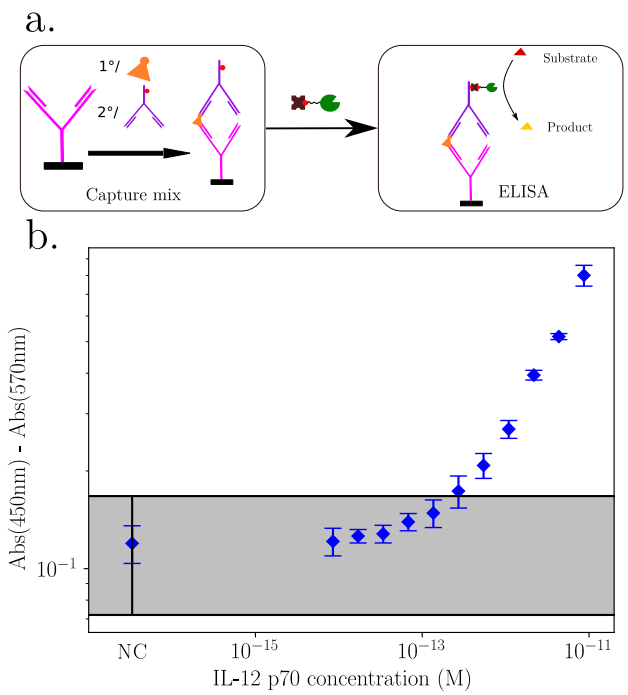

Figure 2.12: **IL-12 p70 detection via an absorbance ELISA. a.** Principle of the absorbance ELISA. The target protein (orange) binds to a capture antibody grafted on a surface (pink) and is then recognized by a detection antibody (purple) functionalized with a biotin and added in a second step. Avidin-HRP is then added, allowing a substrate to be transformed into a product that can be detected by absorbance measurement. **b.** A two-fold dilution range of IL-12 p70 was realized. Detection was performed using avidin-HRP and substrate D. All data points were obtained through dilution triplicate. The shaded area represents 3 times the standard deviation of the NC.

As the PUMA reporting system is based on fluorescence, we adapted the commercial ELISA kit to obtain a fluorescent signal. Indeed, fluorescent reporting system have been proved to be more sensitive than absorbance reporting system [206] in ELISA tests. Thus, to compare the LOD of the ELISA kit to the LOD obtained via a PUMA, we needed to remove this bias. For this purpose, we replaced the substrate D with *Amplex*^{TM}Red (Thermofisher). HRP converts *Amplex*^{TM}Red to resorufin, which is excited at 550 nM and the fluorescence is measured at 585 nM (figure 2.13.a.). A range of IL-12 p70 has been realized in those conditions (figure 2.13.b.), allowing us to determine a LOD around 500 fM for this system. The fluorescent reporting system did not improve the LOD of the commercial ELISA kit in this case.

Following these results, we investigated the possibility of coupling the antibodies capture approach to a PUMA.

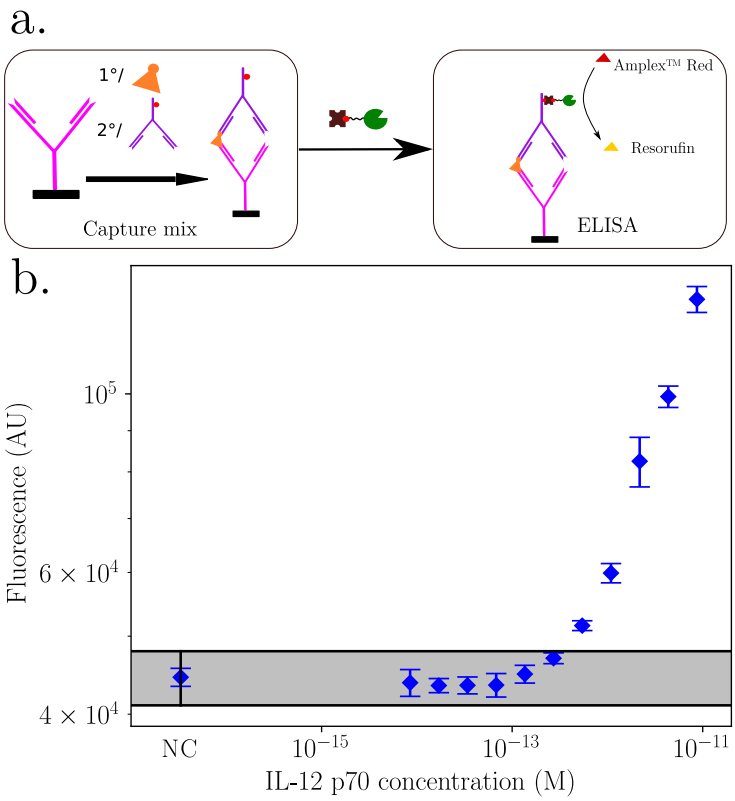

Figure 2.13: **IL-12 p70 detection via a fluorescence ELISA. a.** Principle of the fluorescence ELISA. The target protein (orange) binds to a capture antibody grafted on a surface (pink) and is then recognized by a detection antibody (purple) functionalized with a biotin and added in a second step. Avidin-HRP is then added, allowing *Amplex*^{TM}Red to be transformed into resorufin, which can be detected by fluorescence measurement. **b.** A two-fold dilution range of IL-12 p70 was realized. Detection was performed using avidin-HRP and *Amplex*^{TM}Red. All data points were obtained through dilution triplicate. The shaded area represents 3 times the standard deviation of the NC.

2.5.2 Converter template-based approach

2.5.2.1 Total Seq A oligonucleotide

We first considered a cT approach, as used previously for miRNA detection (see section 1.3.1). Our ELISA kit supplier, Biolegend, offers antibodies with two labelled DNA oligonucleotides carrying a free 3' end: Total Seq A (TSA) and Total Seq B (TSB). In addition, a commercial version of TSA with a streptavidin exists and can be grafted onto a biotinylated antibody (TotalSeq-A0951 PE Streptavidin). We started by making a range of these labels with the corresponding cTs: a range of polyA (corresponding to the 3' extremity of TSA) and a range of TSB were carried out (figure 2.14.). Both oligonucleotides were detected, the $scores_{1pM}$ calculated and reported on the figure. The TSB-specific cT induces a higher background signal than the TSA-specific cT. We also note that the detection of polyA is slower than the one of TSB. As the TSA specific cT does not leak much, we were able to decrease the pT concentration.

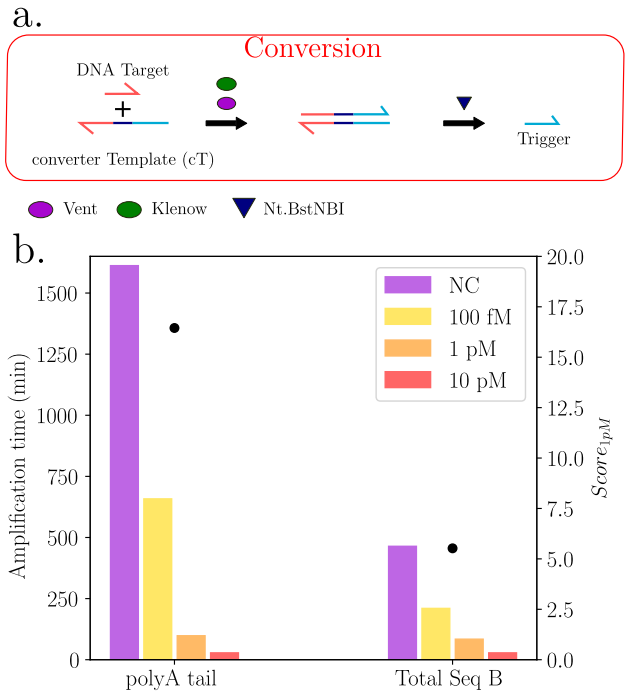

Figure 2.14: **PolyA and Total Seq B ranges. a.** Conversion module for DNA strand detection. **b.** PolyA tail and Total Seq B ranges. The amplification times for the different oligonucleotide concentrations are given by bar charts (left axis) and the $scores_{1pM}$ are given by the black dots (right axis).

We then adapted an ELISA kit for a PUMA detection of IL-12 p70, in an approach referred to as cT-based immuno-PUMA. Briefly, a target protein binds to a capture antibody grafted on a high binding polystyrene plate and is then recognized by a detection antibody functionalized with a biotin and added in a second step. TotalSeq-A0951 PE Streptavidin is then added, allowing a detection with a PUMA containing the TSA-specific cT (polyAtoα). The polystyrene plate is then incubated in a plate reader at 50°C and the fluorescence monitored in real-time. A range of IL-12 p70 has been realized (figure 2.15). A LOD around 130

fM was obtained, i.e. almost 4 time lower than the ELISA test. Then, we wanted to know if this LOD was imposed by the antibodies or if it was a limit imposed by the PUMA. For this, two strategies were tested: increasing the concentration of pT to decrease the LOD, and trying to add Klenow, as done previously for the detection of miRNA (see section 1.5.3).

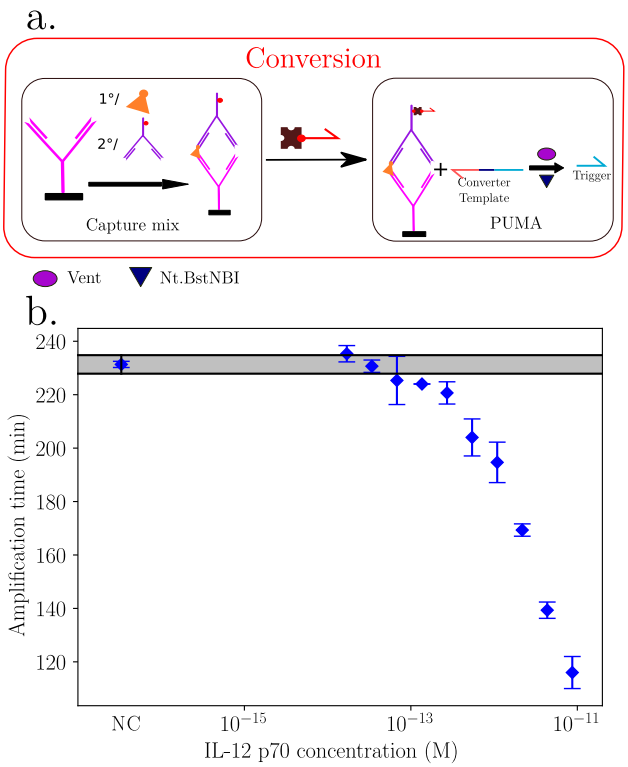

Figure 2.15: **IL-12 p70 detection via a cT-based immuno-PUMA circuit. a.** Principle of the PUMA-converter template based protein detection, optimized with a capture step. The target protein (orange) binds to a capture antibody grafted on a surface (pink) and is then recognized by a biotinylated detection antibody (purple) added in a second step. The detection antibody is then functionalized with an input strand. The other components of the PUMA assay are then added and the amplification is monitored in real-time. **b.** A two-fold dilution range of IL-12 p70 was realized. Detection was performed with the oligonucleotide TotalSeq-A0951 PE Streptavidin and the cT polyAtoα. All data points are dilution triplicates. The shaded area represents 3 times the standard deviation of the NC.

2.5.2.2 Klenow introduction

We therefore tested the detection of IL-12 p70 in presence of Klenow, assuming that it would decrease the LOD as done previously for miRNA detection (see section 1.5.3). We adjusted the pT concentration and performed a new IL-12 p70 range with and without Klenow (figure 2.16.a., b.). As it can be observed, the adjustment of pT concentration did not allow to improve the LOD. Surprisingly, adding Klenow led to a very fast amplification, 52 minutes for no IL-12 p70, and no decrease of LOD. This fast amplification was not expected.

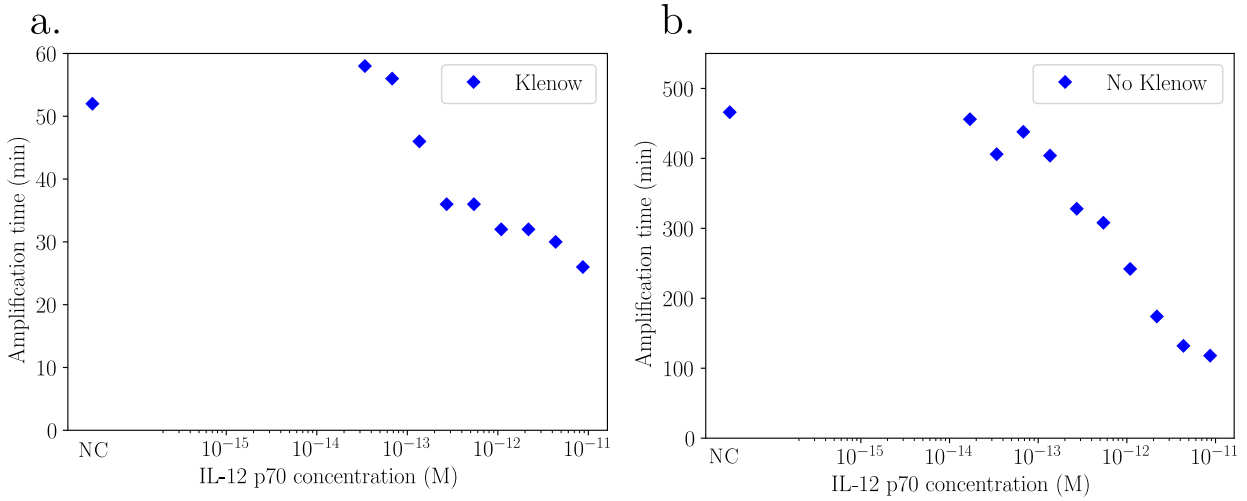

Figure 2.16: **IL-12 p70 detection via a cT-based immuno-PUMA circuit with and without Klenow. a.** A two-fold dilution range of IL-12p70 was realized. Detection was performed with the oligonucleotide TotalSeq-A0951 PE Streptavidin and the cT polyAtoα. The PUMA amplification mixture contained Klenow polymerase. **b.** A two-fold dilution range of IL-12p70 was realized. Detection was performed with the oligonucleotide TotalSeq-A0951 PE Streptavidin and the cT polyAtoα. The PUMA amplification mixture did not contain Klenow polymerase.

To explain this result, we decided to measure the temperature into a well of a polystyrene plate placed in the plate reader at 37°C and 50°C. The results are displayed in figure 2.17. The temperatures can be fitted as a function $T(t) = T_i + (T_f - T_i).(1 - e^{(\frac{-t}{\tau})})$, with T_i the initial temperature, T_f the final temperature and τ the characteristic time of the system. For such a system, it takes $5.\tau$ to achieve a temperature rise of 95% of $T_f - T_i$. The characteristic time is around 5.5 min in both cases meaning that during 27.5 min the system is out of thermal equilibrium. In comparison, in the thermocycler, temperature equilibrium is achieved in a matter of seconds, almost instantaneously. Combined with the results of figure 1.15, this implies that Klenow polymerase is deactivated more slowly in the plate reader than in the thermocycler, leading to a faster nonspecific production of trigger. In the thermocycler, the tube is in contact with the heating wall, whereas in the plate reader, the plate is placed in a heated cavity. This explains the difference in kinetics observed for the temperature in the tube and its impact on Klenow polymerase. This explains also the fast nonspecific amplification: it is not possible to use Klenow in experiments carried out in the plate reader.

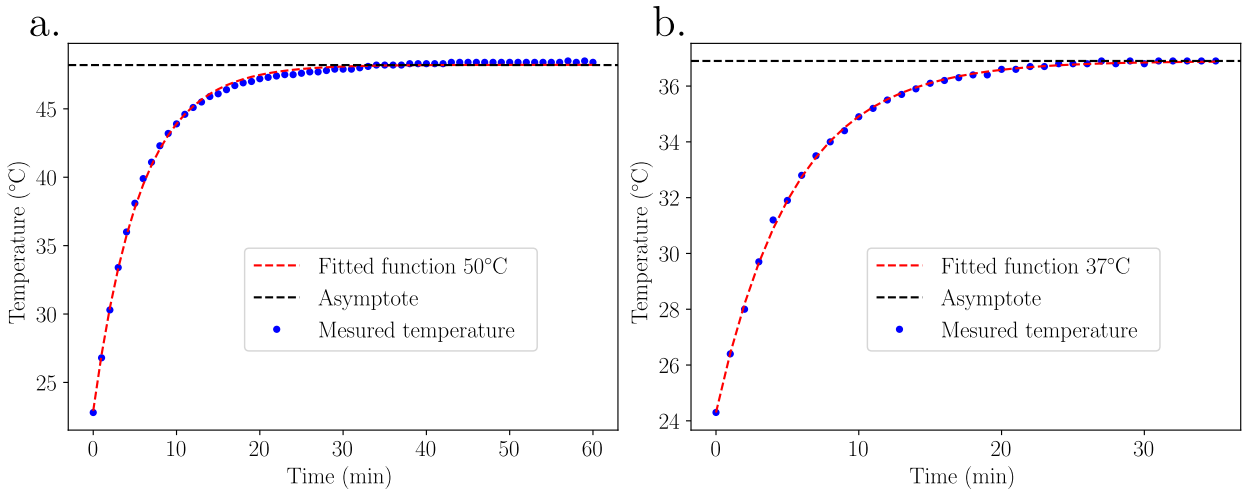

Figure 2.17: **Plate reader temperature kinetic.** A plate was introduced in the plate reader at time 0. The temperature was measured in one well of the plate thanks to a thermocouple and the temperature in the well in function of time was fitted as a function $T(t) = T_i + (T_f - T_i).(1 - e^{(\frac{-t}{\tau})})$. **a.** The temperature of the plate reader was set to 50°C. The fitted parameters are: $T_i = 22.9°C$, $T_f = 48.2°C$, $\tau = 5.7\,min$. **b.** The temperature of the plate reader was set to 37°C. The fitted parameters are: $T_i = 24.3°C$, $T_f = 36.9°C$, $\tau = 5.4\,min$.

2.5.3 Self-activated template based approach

2.5.3.1 Principle and interests

As we have seen before (see section 1.6.1), the cT is the main component responsible for the nonspecific amplification of triggers. To avoid this, we can test different cTs or move towards a method without cT. We chose the second option. Indeed, by taking advantage of the washing steps of the immuno-PUMA, we can include a self-activated template (sT). This template is composed of 3 parts, respectively in the 5' to 3' order: a part complementary to the trigger, the Nt.BstNBI nicking site and a stem loop allowing the 3' extremity to hybridize to the nicking site and to be ready to be extended by a polymerase (see figure 2.18). A biotin must be added to the 5' of the sT in order to bind it to a biotinylated antibody via a streptavidin. Thus, in presence of the target protein, the sT is present, whereas in absence of the target protein, it is absent. The various PUMA components are then added, allowing trigger production from the sT. The principle is illustrated on figure 2.18.

2.5.3.2 Template optimization

We investigated the effect of the environing bases of the nicking recognition site on the production of trigger. To do this, we chose a sequence of sT (sequence n°1 in table 2.3) and we ordered 48 sequences with 2 bases modification compared to the sequence n°1. We then looked at the amplification time (figure 2.19.b) for 1 pM of sT with a PUMA and we looked at the linear trigger production rate (figure 2.19.c) for 1 nM of sT. We then plotted the production rate in function of the inverse of the amplification time to see if they were

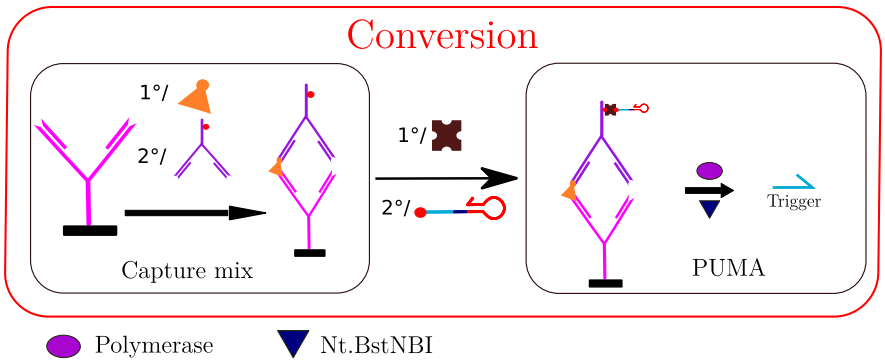

Figure 2.18: **Protein detection via a self-activated template-based immuno-PUMA circuit principle.** Principle of the PUMA sT-based protein detection, optimized with a capture step. The targeted protein (orange) binds to a capture antibody grafted on a surface (pink) and is then recognized by a detection antibody (purple) functionalized with a streptavidin (brown) and a sT. The other components of the PUMA assay are then added and the amplification is monitored in real-time.

correlated (figure 2.19.d). As expected, there is a correlation between these two parameters: the higher the production rate, the lower the amplification time. This confirms that the production rate of a sT is a relevant parameter to assess the efficiency of its detection by a PUMA. We also observed very strong disparities in terms of production rates depending on the sequences (table 2.3). This reinforced our idea of optimising these bases. We thus tried to use this set of data to create a computer model, based on linear approximation. This model assumes that the bases have additive independent effects on the production rate. This is for sure an oversimplification. The model was trained with the production rates presented in table 2.3. Then the fitted model was tested on 3 production rates which were not used to train the model (sequences n°47 and 49). Finally, we selected 5 sequences (n° 50 to 54) not previously used in the model, ordered them and tested them. This is represented on figure 2.21. The green dots correspond to the predicted sTs. As we can see, the estimated production rates were overestimated.

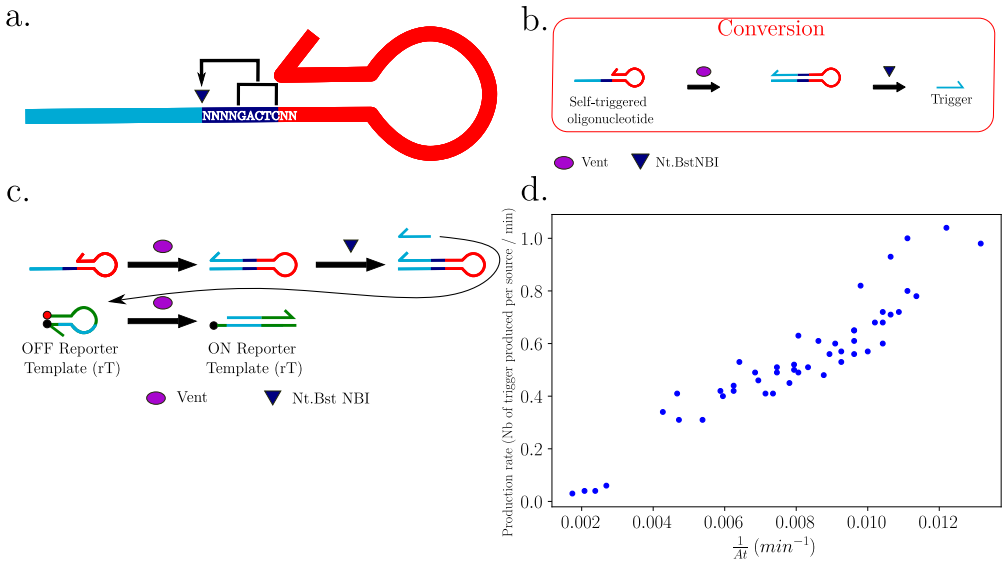

Figure 2.19: **sT optimization. a.** Scheme of a self-activated temaplate. 4 bases are present between the Nt.Bst.NBI nicking site and the trigger complementary sequence. N denotes either a A, T, C or G base. **b.** Conversion module used for the PUMA: a sT undergoes polymerisation / nicking cycles, thus producing trigger. **c.** Principle of the production rate experiment. A sT undergoes polymerization / nicking cycles in presence of a rT. The trigger is linearly produced and the opening rate of the rT is correlated to the production rate of the sT. **d.** Production rate in function of the inverse of amplification time obtained for each tested sequence.

n°	**Sequence**	**Production rate with Vent** (number of trigger produced per sT per minute)	**Production rate with Bst 2.0 WS** (number of trigger produced per sT per minute)
1	GAAT-GACTC-AC	0.68	3.36
2	AAAT-GACTC-AC	0.03	0.01
3	ATAT-GACTC-AC	0.04	0.04
4	AGAT-GACTC-AC	0.53	2.46
5	ACAT-GACTC-AC	0.45	1.41
6	TAAT-GACTC-AC	0.06	0.06
7	TTAT-GACTC-AC	0.04	0.05
8	TGAT-GACTC-AC	0.63	3.21
9	TCAT-GACTC-AC	0.31	1.3
10	GTAT-GACTC-AC	0.42	2.22
11	GGAT-GACTC-AC	0.57	2.99

12	GCAT-GACTC-AC	0.60	2.99
13	CAAT-GACTC-AC	0.50	0.96
14	CTAT-GACTC-AC	0.41	1.52
15	CGAT-GACTC-AC	0.72	1.38
16	CCAT-GACTC-AC	0.65	1.45
17	GAAA-GACTC-AC	0.72	2.25
18	GAAG-GACTC-AC	0.42	2.23
19	GAAC-GACTC-AC	0.51	3.48
20	GATA-GACTC-AC	0.56	3.26
21	GATT-GACTC-AC	0.41	3.01
22	GATG-GACTC-AC	0.60	3.42
23	GATC-GACTC-AC	0.53	3
24	GAGA-GACTC-AC	1.04	1.56
25	GAGT-GACTC-AC	0.98	3.17
26	GAGG-GACTC-AC	0.68	3.07
27	GAGC-GACTC-AC	0.78	3.09
28	GACA-GACTC-AC	0.80	4.07
29	GACT-GACTC-AC	0.57	3.68
30	GACG-GACTC-AC	0.61	3.41
31	GACC-GACTC-AC	0.40	2.44
32	GAAT-GACTC-AA	0.49	2.67
33	GAAT-GACTC-AT	0.46	2.68
34	GAAT-GACTC-AG	0.52	2.79
35	GAAT-GACTC-TA	0.49	2.59
36	GAAT-GACTC-TT	0.93	1.82
37	GAAT-GACTC-TG	0.56	2.44
38	GAAT-GACTC-TC	1.00	1.42
39	GAAT-GACTC-GA	0.41	2.43
40	GAAT-GACTC-GT	0.31	1.44
41	GAAT-GACTC-GG	0.44	2.68
42	GAAT-GACTC-GC	0.49	3
43	GAAT-GACTC-CA	0.34	1.99
44	GAAT-GACTC-CT	0.61	2.79
45	GAAT-GACTC-CG	0.51	2.65
46	GAAT-GACTC-CC	0.82	1.01
47	GGTT-GACTC-AC	0.65	3.19
48	GGAA-GACTC-AC	0.71	2.89
49	GTTT-GACTC-AC	0.48	4.46
50	GGGA-GACTC-TC	0.57	Not applicable
51	CGGA-GACTC-TC	0.25	Not applicable

52	GGGA-GACTC-TT	0.62	Not applicable
53	GCGA-GACTC-TC	0.51	Not applicable
54	GGGA-GACTC-TG	0.94	Not applicable

Table 2.3: sT production rate in function of sT sequence for two different polymerases. The green bases are the ones differing from sequence n°1.

We then looked at the possibility of adding phosphorotioates to the 5' extremity of the sT to accelerate trigger production by lowering the melting temperature between the produced trigger and the self-triggered oligonucleotide [207]. To this end, we performed a production rate experiment (figure 2.21. a.) by adding from 1 to 6 phosphorotioates to the same self-triggered oligonucleotide (figure 2.21.b.). The results are displayed on figure 2.21.c. We found that the presence of phosphorotioates does not further increase the production rate. This suggests that the release of triggers from the sT is not limited by the dehybridization rate of the output.

As mentioned earlier, we wanted to graft this sT onto the detection antibody via a biotin-streptavidin linkage. Thus, we needed to add a biotin to the sT. We tested 2 locations for this biotin: at the 5' extremity, with a T5-Sp18 linker (figure 2.22.a.i.) and at the inner position of the loop via an amino-dT building block (figure 2.22.a.ii.). Ranges of these two different oligonucleotides were performed in presence or absence of 0.25 streptavidin equivalent. As it can be seen in figure 2.22.b, without streptavidin, there is no significant difference between the two possibilities. However, in presence of streptavidin, the oligonucleotide with a biotin at the 5' extremity is much better detected than the oligonucleotide with a biotin at the internal position (figure 2.22.c). As already showed by our team, the presence of a biotin-streptavidin group on an oligonucleotide can hinder the polymerase [208]. The T5-Sp18 linker at the 5' extremity of the sT does not seem to induce steric hindrance.

These different observations were combined and we decided to work with an oligonucleotide containing the GAGA-GACTC-AC sequence, without phosphorotioate and with a biotin at the 5' extremity with a T5-Sp18 linker. We used this new sT for the detection of several proteins. Briefly, the targeted protein binds to a capture antibody grafted on a surface and is then recognized by a detection antibody. It is then functionalized with a streptavidin and the optimized sT. The other components of the PUMA assay are then added and the amplification is monitored in real-time (figure 2.23.a.). This method was applied to the detection of IL-12 p70 (figure 2.23.b.), IL-4 (figure 2.23.c.) and INFg (figure 2.23.d.). The achieved LODs are respectively around 530 attoM, 9 fM and 450 attoM. Noteworthy, the reached LOD for IL-12 p70 is lower than the one reached with the immuno-PUMA cT-based approach or with the absorbance ELISA. This approach allowed us to gain two orders of magnitudes in the detection of IL-12 p70. The data obtained for IL-4 and INFg suggest that this is also the case for IL-4 and INFg. Indeed, according to the supplier's data sheets, the dynamic range of absorbance ELISA is 143 fM - 8.9 pM for IL-4 and 462 fM - 29.6 pM for INFg.

The specificity of the different detection antibodies were investigated (figure 2.23.d.).

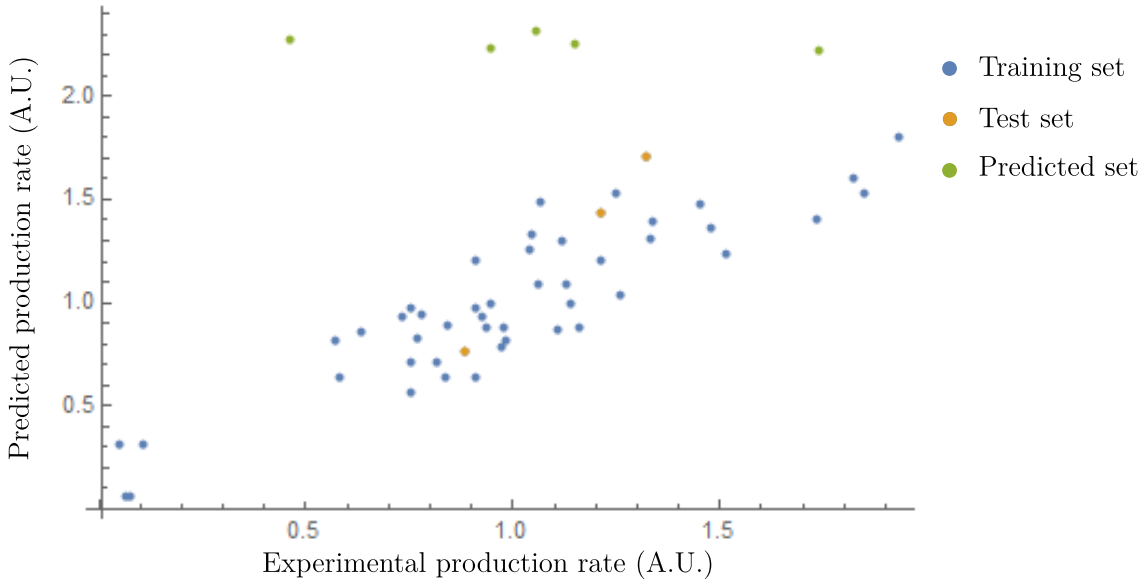

Figure 2.20: **sT production rate modelization.** The production rates presented in table 2.3 were used for training a mathematical model. The blue dots correspond to the training set. The orange dots correspond to the test set. The green dots correspond the predicted set.

To that extent, no protein, 8.7 pM IL-12 p70, 8.9 pM IL-4 and 29.6 pM INFg were captured by their specific capture antibodies, stained with IL-12 p70 detection Ab, IL-4 detection Ab or INFg detection Ab then functionalized with streptavidin and a biotinylated self-triggered oligonucleotide. As expected, the proteins were detected only when stained with their specific detection Ab, demonstrating their specificity.

This increase in sensitivity comes with an increase in experiment time: 1 pM of IL-12 p70 is detected in approximately 6h with the sT-based immuno-PUMA against 5h with a classical ELISA test. We then tried to optimize the assay time.

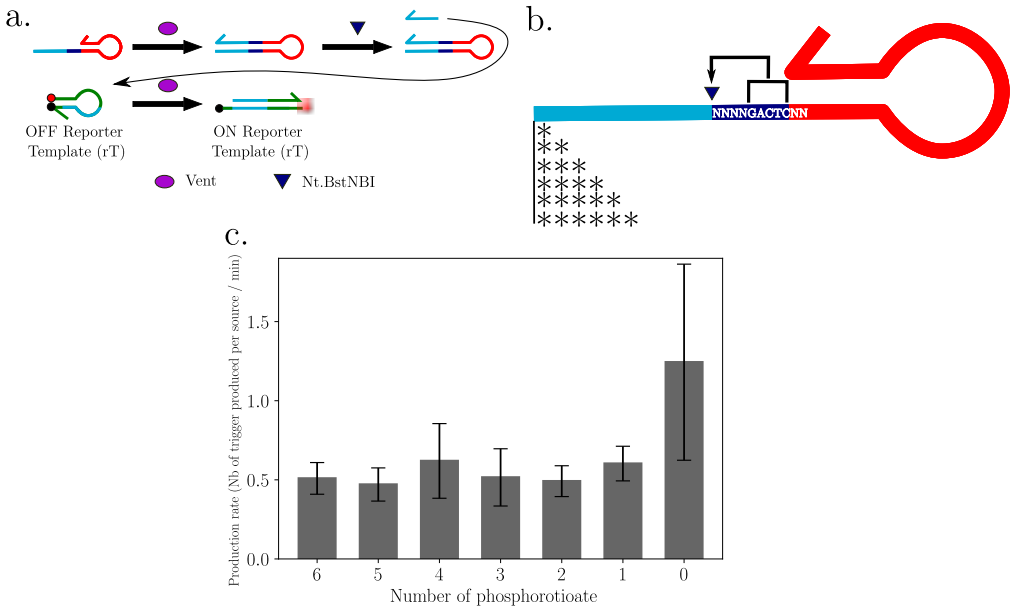

Figure 2.21: **Self-activated template: phosphorotioates optimization. a.** Principle of the production rate experiment. A sT undergoes polymerisation / nicking cycles in presence of a rT. The trigger is linearly produced and the opening rate of the rT is correlated to the production rate of the sT. **b.** Scheme of a sT. Phophorotioates, symbolized by "*", can be added to the backbone of the sT. The choice has been made to add some at its 5' extremity, corresponding to the trigger complementary part. **c.** Production rate in function of the number of phosphorotioates added to the sT backbone. Except the number of phosphorotioates, the sequences of the sTs were the same for all tested conditions.

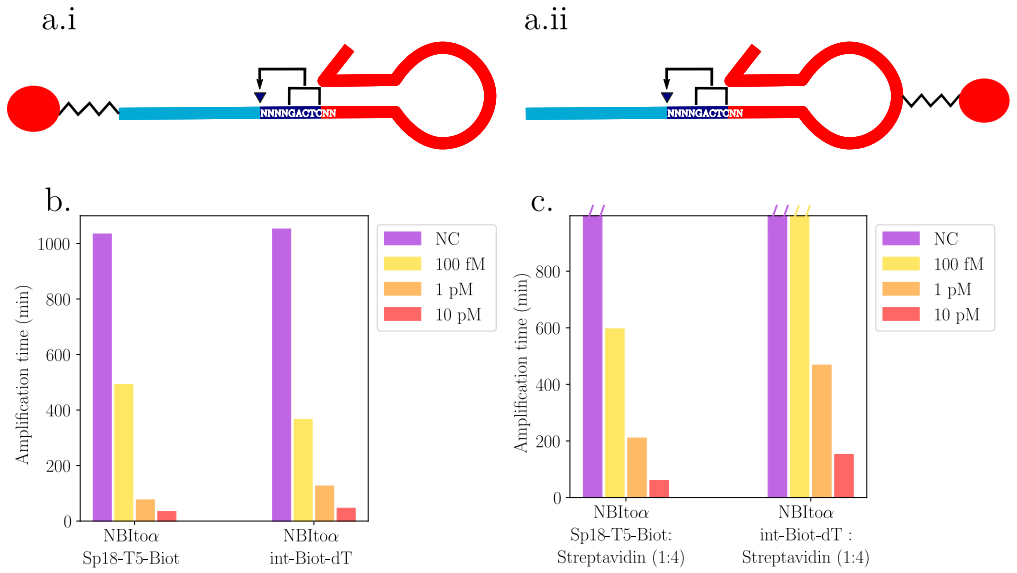

Figure 2.22: **Self-activated template: biotin position optimization. a.** *s*T biotin (red circle) positions. The biotin has been placed either at the 5' extremity (**i.**), via a T5-Sp18 linker, or inside the stem loop of the self-triggered oligonucleotide (**ii.**) via an amino-dT building block. **b.** sTs ranges. **c.** sTs ranges in presence of streptavidin.

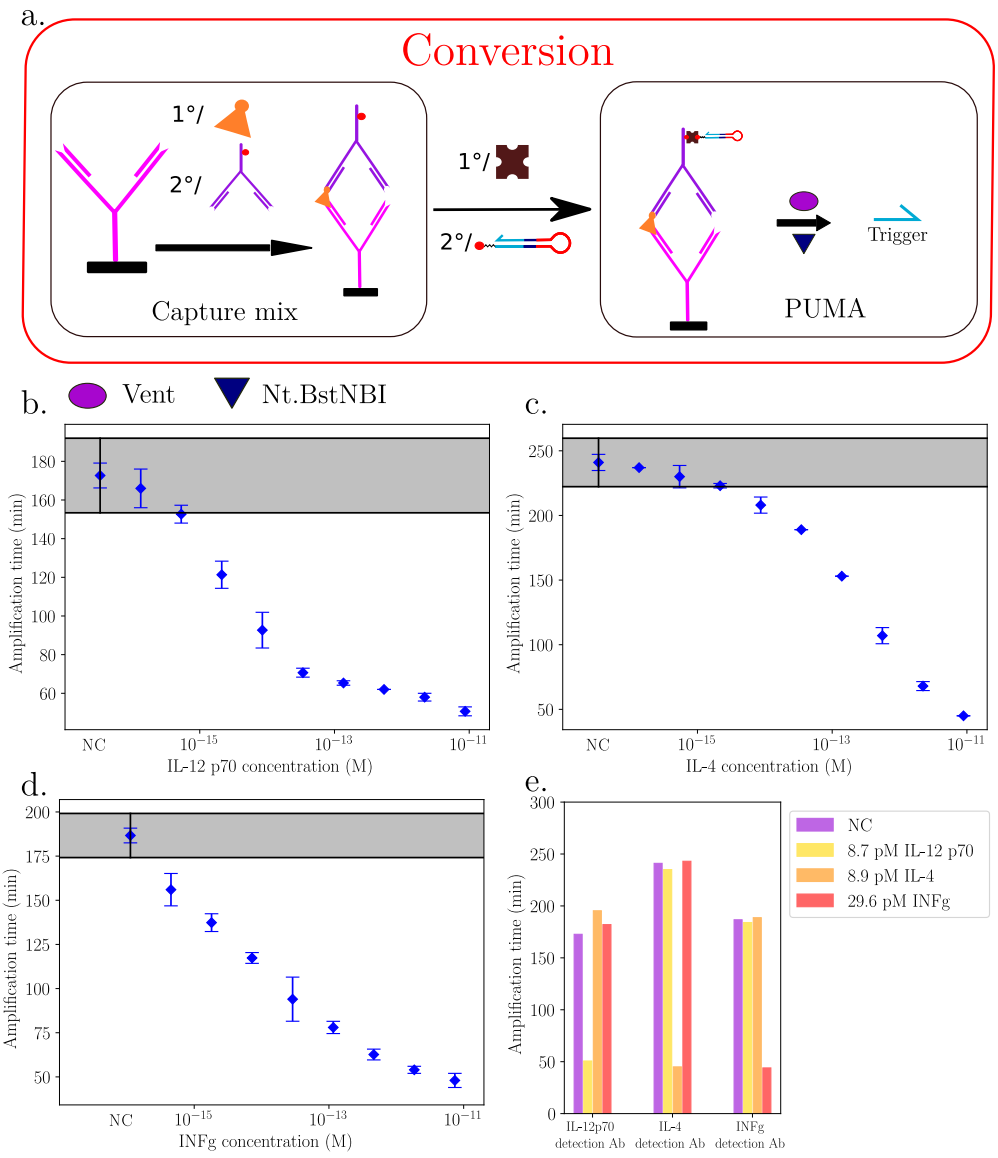

Figure 2.23: **Protein ranges: sT-based immuno-PUMA a.** Principle of the sT-based immuno-PUMA, optimized with a capture step. The targeted protein (orange) binds to a capture antibody grafted on a surface (pink) and is then recognized by a detection antibody (purple) functionalized with a streptavidin (brown) and the optimized biotinylated sT. The other components of the PUMA assay are then added and the amplification is monitored in real-time. **b.** A four-fold dilution range of IL-12 p70 was realized. The detection was carried out with the optimized biotinylated sT. All points are dilution triplicates. The shaded area represents 3 times the standard deviation of the NC. **c.** A four-fold dilution range of IL-4 was realized. The detection was carried out with the optimized biotinylated sT. All points are dilution triplicates. The shaded area represents 3 times the standard deviation of the NC. **d.** A four-fold dilution range of INFg was realized. The detection was carried out with the optimized biotinylated sT. All points are dilution triplicates. The shaded area represents 3 times the standard deviation of the NC. **e.** Specificity test of the different antibodies: no protein, 8.7 pM IL-12 p70, 8.9 pM IL-4 and 29.6 pM INFg were detected using the optimized biotinylated sT and IL-12 p70 detection Ab, IL-4 detection Ab or INFg detection Ab.

2.5.3.3 Bst 2.0 WS

In an attempt to get faster detection, we then looked at the use of another polymerase: Bst 2.0 WS. We started by making a range of Bst 2.0 WS in presence of 0 and 10 pM of a self-triggered oligonucleotide. As we can see in figure 2.24.a., the best compromise is 0.5% of Bst 2.0 WS. Indeed, at higher concentration, the nonspecific trigger production is too important. Moreover, 10 pM is detected in ten minutes while it takes approximately 30 minutes in the optimized conditions with Vent(exo-). We then performed a production rate experiment in presence of 0.5% Bst 2.0 WS as well as in presence of 4% Vent(exo-) for all the sequences presented in table 2.3. As it can be seen in figure 2.24.b, for a large majority of the tested sequence, the production rate is higher in presence of Bst 2.0 WS. This is encouraging for the detection of a sT. Noteworthy, the production rate obtained with Bst 2.0 WS does not strongly correlate with the production rate obtained with Vent(exo-) except for a few sequences that are very slow in both cases. This suggests that the influence of the sequence of the self-triggered oligonucleotide on the production rate is mostly due to the polymerase.

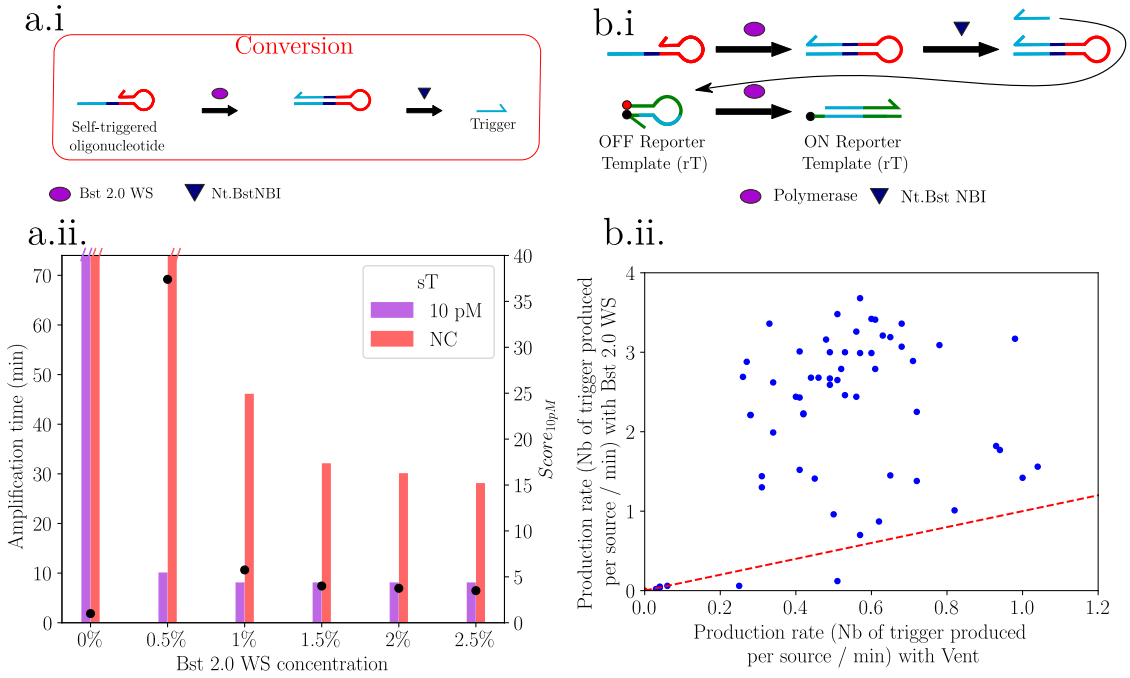

Figure 2.24: **Bst 2.0 WS range and production rate with sT a.i** Conversion module used for the PUMA: a sT undergoes polymerisation / nicking cycles, thus producing trigger. **ii.** Bst 2.0 WS range in presence of 0 and 10 pM of sT. After 74 minutes, the presence of parasites was observed and the experiment stopped. The amplification times for the different oligonucleotide concentrations are given by bar charts (left axis) and the $scores_{10pM}$ are given by the black dots (right axis). **b.i.** Principle of the production rate experiment. A sT undergoes polymerisation / nicking cycles in presence of a rT. The trigger is linearly produced and the opening rate of the rT is correlated to the production rate of the sT. **ii.** Production rates obtained with Bst 2.0 WS in function of the production rates obtained with Vent for different sTs. The dotted red line represents the equality of production rates: the points above have a higher production rate with Bst 2.0 than with Vent(exo-).

We then looked at the use of this polymerase for the detection of a sT with a biotin and a T5-Sp18 linker at its 5' extremity. For this purpose, a range of the optimized sT, whose sequence has been defined previously, was performed. Three conditions were tested: the biotinylated sT alone, the biotinylated sT in absence of streptavidin and the biotinylated sT in presence of streptavidin and a biotinylated antibody. As it can be seen in figure 2.25, the presence of streptavidin negatively impacts the detection of the oligonucleotide. Furthermore, the presence of the antibody and streptavidin has the same impact. We can conclude that Bst 2.0 WS is more sensitive to steric hindrance than Vent(exo-). Moreover, the impossibility to detect 100 fM of sT does not allow us to consider using this method for the detection of proteins: the detection limit is too high. It would be interesting, at a later stage, to test different linker allowing us to free ourselves from this steric hindrance. However, we did not have the time to test this.

2.5.3.4 Nt.BstNBI nicking site sequence optimization for γ switch

Building on the results obtained on sT sequence optimization for the α switch at 50°C, we investigated the possibility of transposing them to the γ switch, operating at 37°C. We thus looked at the trigger production rate of γ trigger obtained with Bst LF at 37°C in function of the production rates of α trigger obtained with Vent at 50°C for different sT. We tested 5 different sequences for the bases environning the Nt.BstNBI nicking site of the sT. These sequences are given in table 2.4. As we can see in figure 2.26, the results are quite similar between the two production rates: the sequence with the higher production rate for the γ trigger is also the one given the higher production rate with the α trigger. It is surprising to obtain similar results between the Bst LF polymerase at 37°C and the Vent polymerase at 50°C. However, only 5 sequences were tested, this can bias the observation. This results were then used to design the oligonucleotide for the PEA approach for human alpha-Thrombin detection (see section 2.4.3.2).

n°	**Environning nicking site sequence**	**Production rate with Vent at 50°C** (number of trigger produced per sT per minute)	**Production rate with Bst LF at 37°C** (number of trigger produced per sT per minute)
1	TCAT GACTC AC	0.31	0.34
2	GATT GACTC AC	0.41	0.66
3	GAGA GACTC AC	1.04	1.45
4	GAGT GACTC AC	0.98	0.80
5	GAGC GACTC AC	0.78	0.83

Table 2.4: sT production rate in function of sT sequence for two different triggers.

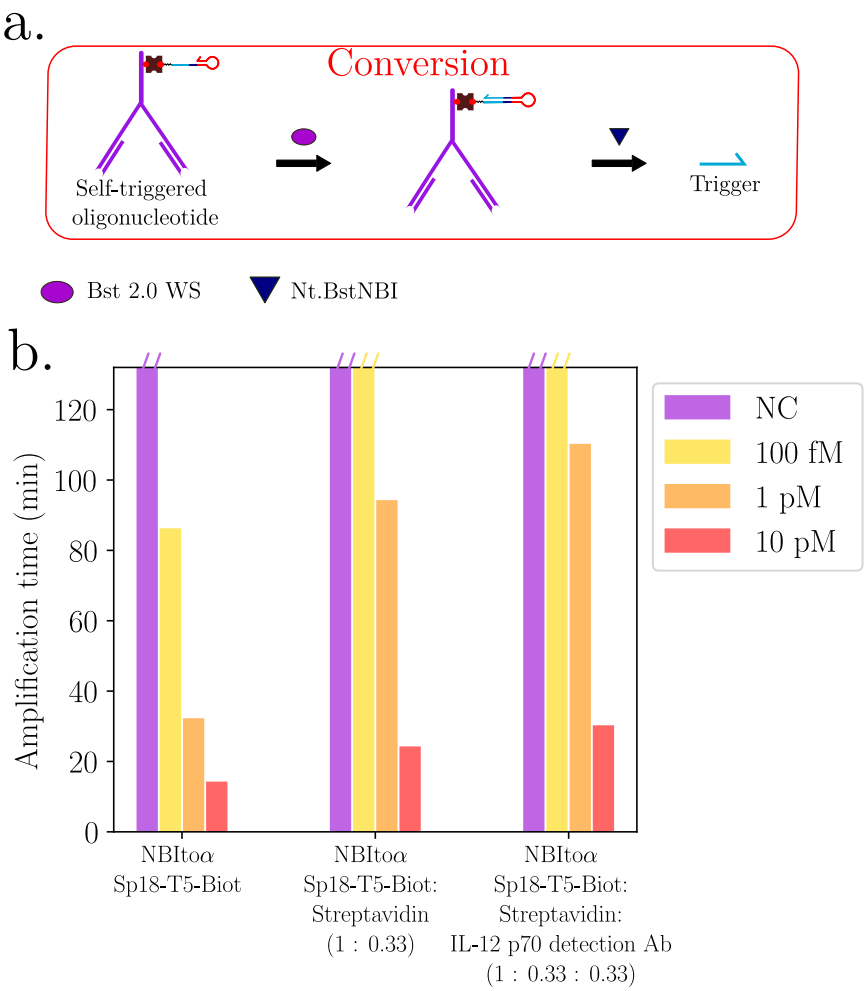

Figure 2.25: **Bst 2.0 WS self-triggered oligo on Ab. a.** Conversion module used for the immuno-PUMA: a sT, linked to an antibody via a streptavidin-biotin linkage, undergoes polymerisation / nicking cycles, thus producing trigger. **b.** Ranges of NBItoα-Sp18-T5-Biot, NBItoα-Sp18-T5-Biot : streptavidin (1 : 0.33) and NBItoα-Sp18-T5-Biot : streptavidin : IL-12 p70 detection Ab (1 : 0.33) : 0.33). After 132 minutes, the presence of parasites was observed and the experiment stopped.

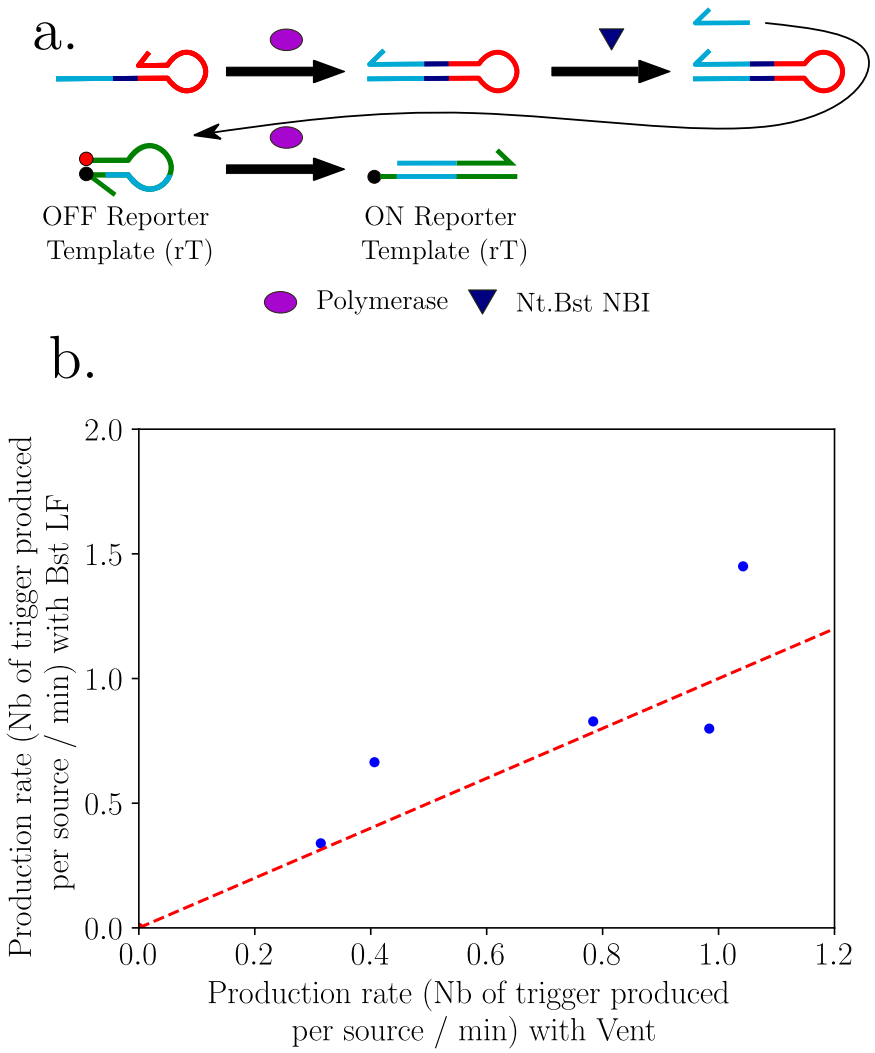

Figure 2.26: **sT production rates with Bst LF and Vent. a.** Principle of the production rate experiment. A sT undergoes polymerisation / nicking cycles in presence of a rT. The trigger is linearly produced and the opening rate of the rT is correlated to the production rate of the self-triggered oligonucleotide. **b.** Production rates of γ trigger obtained with Bst LF at 37°C in function of the production rates of α trigger obtained with Vent at 50°C for different self-triggered oligonucleotide. The dotted red line represents the equality of production rates.

2.6 Towards a two-input classifier

As our amplification method is oligonucleotide-based, we have access to the computational arsenal of DNA nanotechnology. One of the possibilities is to realized molecular classification [209][40]. Following the results obtained previously, we decided to look at a PUMA system that could take into account two inputs. Our goal is to be able to take into account the concentrations of two proteins to provide a single output. To do this in a general way, we needed to introduce a conversion module with a negative weight: we used a killer template (kT), as already introduced by our team [210][211]. Its principle will be explained later in this section.

2.6.1 Antibodies quantification

In view of the system presented above, we need to graft orthogonal oligonucleotides onto the antibodies before staining the plate containing the capture antibodies and the proteins. Indeed, it is not possible to perform this in 3 steps as for sT-based immuno-PUMA. We therefore quantified the antibodies used with a Bradford test [212]. A standard range was performed and the detection antibodies of the IL-12 p70, IL-4 and INFg ELISA kit were quantified as shown in figure 2.27. The concentrations of the detection antibodies were respectively 179 μM, 173 μM and 142 μM for the 200x stock solution of IL-12 p70, IL-4 and INFg detection Ab, respectively.

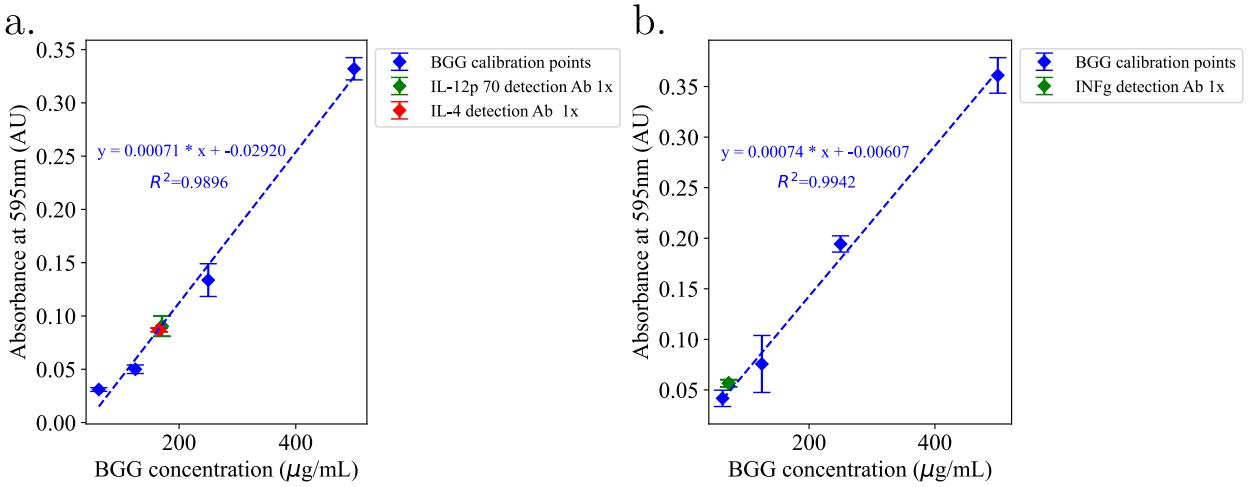

Figure 2.27: **Bradford assay for Ab quantification a.** A Bradford calibration curve (blue) has been realized with BGG. IL-12 p70 detection Ab (green) and IL-4 detection Ab (red) have been quantified. All points are dilution triplicates. **b.** A Bradford calibration curve (blue) has been realized with BGG. INFg detection Ab (green) has been quantified. All points are dilution triplicates.

2.6.2 Negative weight implementation

Implementing a negative weight enables to reverse the logic set with cT. It thus allows to take into account the absence or presence of each target. We build on previously described kT design to implement negative weight in our circuit architecture. The 5' end of the kT is complementary to a DNA target, then comes the nicking site of Nt.BstNBI and finally a part complementary to a pT (figure 2.28). Thus, detection of the target induces the production of pT. This will delay the trigger amplification: we are in the case where the more target, the longer the amplification time.

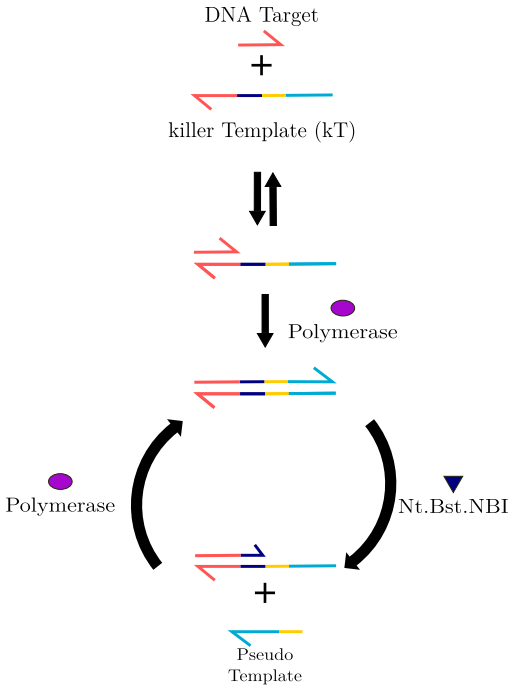

Figure 2.28: **kT principle.** A DNA target (red) hybridizes to the 3' part of the killer template. This DNA target is extended by a polymerase. The killer template has been designed to contain a Nt.BstNBI nicking site when double-stranded (dark blue), resulting in the nicking of the polymerization product and releasing a molecule of pT. This whole cycle results in a linear increase of the amount of pT.

2.6.2.1 α switch

We first optimized a kT for TSB detection (figure 2.29.a.) for the α switch, working at 50°C. We tested kTs with different inhibition strength [210]. To do this, we tested different kTs which respectively produce a pT with 2, 3 or 4 A bases in 5' of the trigger complementary sequence, thus producing deactivated trigger with 2, 3 or 4 T bases at its 3' extremity. A range of each of them was performed in presence of 100 pM of TSB figure (figure 2.29.b.). The results show that the kTs producing pT with 2 or 3 A bases have the expected effect. However, the kT producing pT with 4 bases A has no effect on the PUMA. This can be explained by the K_d of the different produced pT and their respective kTs (see appendix A). The K_d are respectively 1.8 nM for TSBtopTαA4P, 0.7 nM for TSBtopTαA3P and 0.3 nM

for TSBtopTαA2P. Indeed, the longer the pT, the higher the affinity of the produced pT for its kT, shifting the equilibrium between the pT hybridized to the kT and the pT in solution. Furthermore, the longer the pT produced, the longer for the polymerase to assemble it from the kT. Once the pT released, the same mechanism applies to trigger deactivation. These two effects add up, explaining why the longer the produced pT, the slower its turnover, thus the lower its inhibition.

We then compared 5 kTs producing respectively a pT containing 2 A-bases, 1 A-base, 1 T-base, 1 G-base or 1 C-base to the pT (figure 2.29.c.). As expected, the kT producing pT containing a G base at its 5' extremity is in fact a cT: the trigger with a C base at its 3' is still able to interact and be extended by the aT. To determine the inhibition strength of a kT, we calculated a score taking into account the unspecific production of trigger in presence of 0 and 10 pM of the kT DNA target:

$$ScorekT_{10\,pM} = \frac{Amplification\,time\,of\,the\,10\,pM\,sample}{Amplification\,time\,of\,the\,no\,target\,control}$$

The scorekT were calculated for the different tested kT and reported on the figure 2.29.c. We note that the best kT is the one producing a pT with a C base. This is a sequence effect, demonstrating the interest of testing the possible base combinations to select the more suitable for our target application.

We have therefore selected the kT TSBtopTαC1P and carried out a range of it in presence of 0 and 1 pM of TSB (figure 2.29.d.). The best concentration appears to be 1.6 nM of TSBtopTαC1P. To take into account the results of figure 2.17, we realized a range of TSB, respectively no, 1 pM, 10 pM and 100 pM, in the thermocycler and in the plate reader. As it can be observed in figure 2.29.e, 10 pM of TSB is detected in the thermocycler but not in the plate reader. As the temperature is lower in the plate reader for 25 min, less pT can be released from the kT, resulting in a less delayed amplification which can not be differentiated from no TSB. This effect adds up with the increase of leak in the plate reader because of the temperature, as demonstrated in section 2.5.2.2.

2.6.2.2 γ switch

We then designed a kT for the γ switch, working at 37°C (figure 2.30.a) Taking into consideration the results obtained for the α switch, we tried a kT leading to the production of a pT containing 1 A base at its 5' extremity, adding a thymine to the trigger. A range of TSBtopTγA1P was realized in presence of 0 and 10 pM of TSB (figure 2.30.b). The results show that 1.25 nM of this kT is the best concentration. However, the discrimination between no and 10 pM of TSB is very low. A range of TSB has then been carried out in the plate reader (figure 2.30.c). Surprisingly, the detection of 10 pM of TSB was way better in the plate reader than in the thermocycler. However, 1 pM of TSB could not be detected. We also observe that the response is non linear, which is expected for a kT.

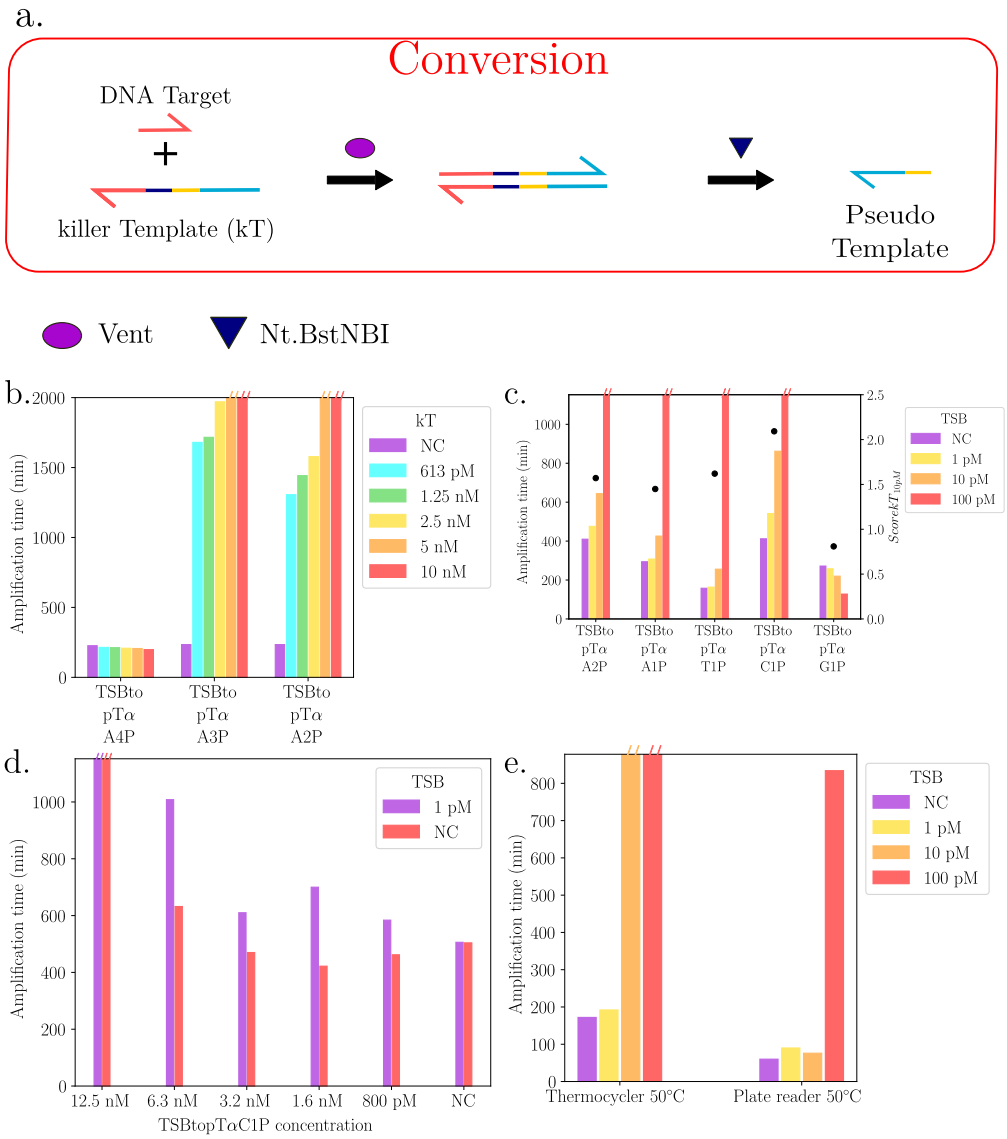

Figure 2.29: **TSB-specific kT optimization for α switch. a.** Conversion module used for the PUMA: DNA target hybridizes to the kT and undergoes polymerization / nicking cycles, thus producing pT. **b.** Ranges of various kT differing in the lenght of the pT output in presence of 100 pM of TSB. 3 kTs have been tested, leading to pT which have respectively 2, 3 or 4 A bases at their 5' extremity. The "P" in the name of the kT indicates the presence of a phosphate at the 3' end of the kT. **c.** TSB ranges in presence of 2.5 nM of kT. 5 kT have been tested, leading to pT which have respectively 2 bases A, 1 base A, 1 base T, 1 one C or one base G at their 5' extremity. The amplification times for the different TSB concentrations are given by bar charts (left axis) and the $scorekT_{10pM}$ are given by the black dots (right axis). **d.** TSBtopTαC1P range in presence of 0 and 1 pM of TSB. **e.** TSB range in presence of 1.6 nM of TSBtopTαC1P. The amplification mixtures have been split between tubes placed either in a thermocycler at 50°C or in a plate reader at 50°C.

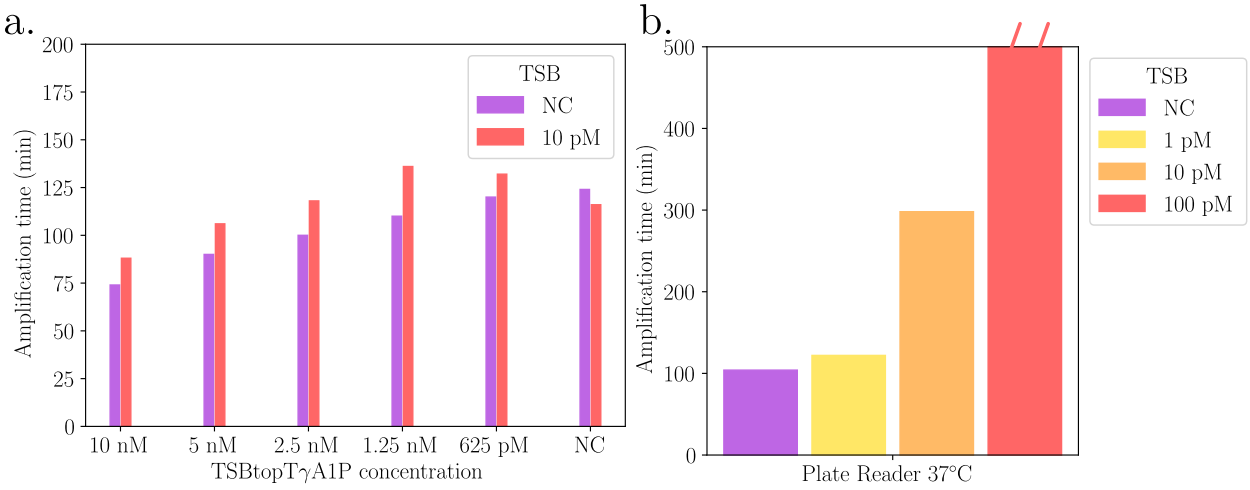

Figure 2.30: **TSB-specific kT optimization for γ switch. a.** TSBtopTγA1P range in presence of no and 10 pM of TSB. **b.** TSB range in presence of 1.25 nM of TSBtopTγA1P. The experiment took place in a plate reader at 37°C.

2.6.3 Classifier

2.6.3.1 DNA classifier

We took advantage of the development of a kT adapted for the α switch to test the implementation of a PUMA with two inputs. The final goal is to obtain a classifier taking in input 2 proteins, with the possibility of modulating the PUMA according to the desired configuration. 4 possibilities are considered: both proteins activate the switch (+/+), both proteins inhibit the switch (-/-), one protein activates and the other inhibits (+/-) or (-/+). For each of these possibilities, an oligonucleotide is assigned to each detection antibody and the corresponding cTs / kTs added to the PUMA amplification mixture.

The first step is to have a classifier that works in presence of two target DNA strands. These ones would later be grafted on target-specific Ab. Consider the case where we assign a positive coefficient to target DNA strand 1 and a negative coefficient to target DNA strand 2. The detailed functioning of the corresponding PUMA is illustrated in figure 2.31.

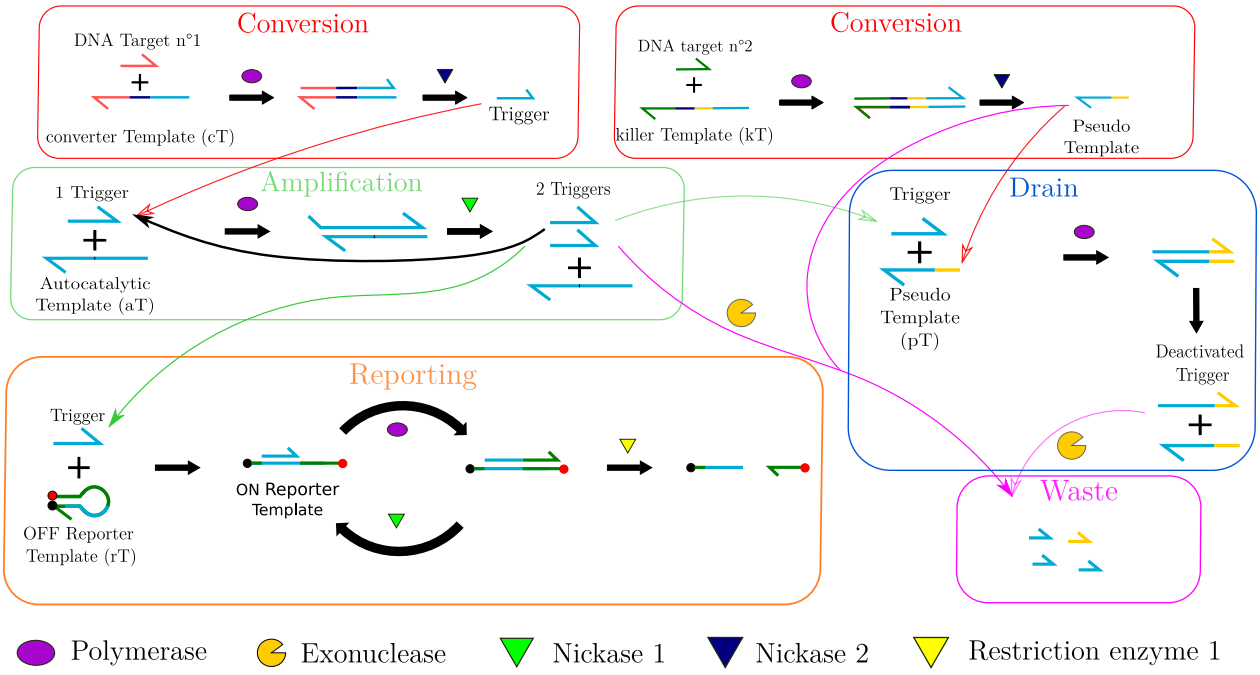

Figure 2.31: **PUMA architecture for two-inputs detection:** a conversion template (cT) converts the first target molecule into a universal DNA trigger; a killer template (kT) converts the second target molecule into a pseudo template; an amplification template (aT) exponentially amplifies this trigger sequence; the background noise, inherent to all exponential amplification mechanism is reduced thanks to the pseudotemplate (pT) that acts as a drain for unspecifically produced trigger strands stemming from leaky reactions; a reporting template (rT) produces a fluorescence output using trigger strands.

For the reasons explained above, we decided to target 2 oligonucleotides: TSB and polyA. We incorporated a TSB specific kT and a polyA specific cT into the PUMA (figure 2.32.a.). A concentration matrix was carried out, with respectively 0, 1 pM, 10 pM and 100 pM of each of the oligonucleotides. The result obtained is available in figure 2.32.b. We

can see that we obtain the expected behaviour: when the TSB concentration increases, the amplification time increases, when the polyA concentration increases, the amplification time decreases. This is very encouraging for the next step: the classifier is working, now we have to connect it to the 2 protein inputs.

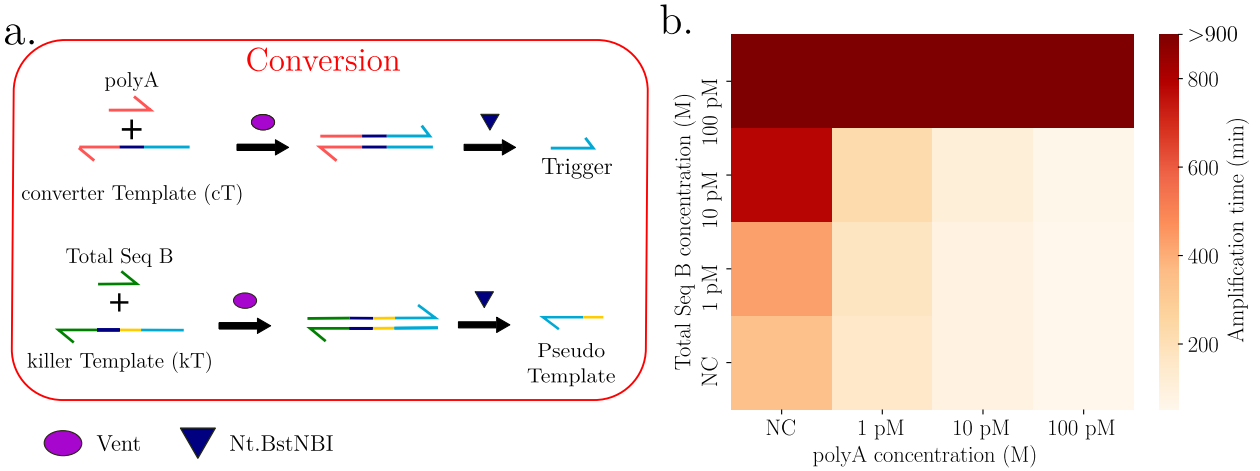

Figure 2.32: **Two-oligonucleotide inputs classifier. a.** Conversion module used for the two-input PUMA. PolyA (red) hybridizes to the cT and undergoes polymerisation / nicking cycles, thus producing trigger. TSB (green) hybridizes to the kT and undergoes polymerisation / nicking cycles, thus producing pT. **b.** Amplification times obtained for a polyA and TSB matrix ranges.

We therefore tested the same PUMA amplification mixture when biotinylated version of these oligonucleotides were grafted onto detection antibodies. Two antibodies were chosen: IL-12 p70 detection antibody for TSB and IL-4 detection antibody for polyA. 0.33 equivalent of these biotinylated antibodies were mixed with 0.33 equivalent of streptavidin and 1 equivalent of the corresponding oligonucleotide. Therefore, IL-12 p70 detection antibody should be detected with a negative weight while IL-4 detection antibody should be detected with a positive weight. A concentration matrix was carried out, with respectively 0, 1 pM, 10 pM and 100 pM of each of the biotinylated oligonucleotides and the corresponding antibody. The results obtained are available in figure 2.33. We can see that we obtain the expected behaviour: when the IL-12 p70 concentration increases, the amplification time increases, when the IL-4 concentration increases, the amplification time decreases. We can deduce that the presence of detection antibodies does not interfere with the classifier.

2.6.3.2 Protein classifier

Finally we tested the classifier for the detection of 2 proteins. We chose to target the IL-12 p70 and IL-4 proteins. We coated a plate with a mix of capture antibodies for these two proteins and then performed a concentration matrix of these two proteins. Finally, a staining was performed with a mix of capture antibodies carrying the biotinylated oligonucleotides polyA and TSB, prepared as previously explained. The PUMA amplification mixture contained a polyA-specific cT and a TSB-specific kT. Therefore, the presence of IL-4 should activate the

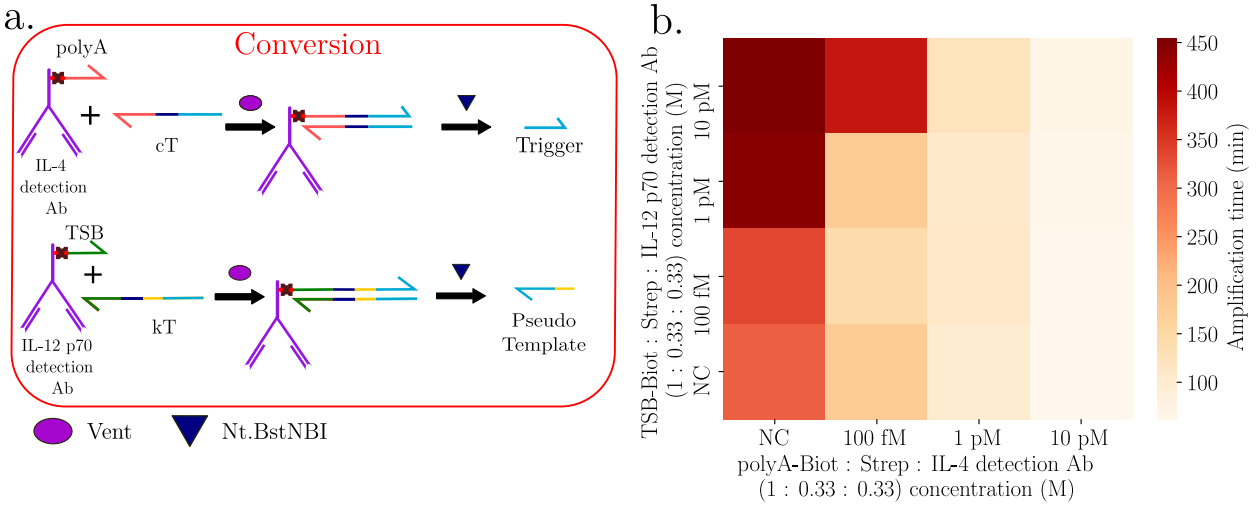

Figure 2.33: **Two oligonucleotide on antibody inputs classifier. a.** Conversion module used for the two-inputs PUMA. PolyA : streptavidin : IL-4 detection Ab (1 : 0.33 : 0.33)(red) hybridizes to the cT and undergoes polymerisation / nicking cycles, thus producing trigger. TSB : streptavidin : IL-12 p70 detection Ab (1 : 0.33 : 0.33) (green) hybridizes to the kT and undergoes polymerisation / nicking cycles, thus producing pT. **b.** Amplification time obtained for a PolyA : streptavidin : IL-4 detection Ab (1 : 0.33 : 0.33) and TSB : streptavidin : IL-12 p70 detection Ab (1 : 0.33 : 0.33) matrix ranges.

switch, while the presence of IL-12 p70 should inhibit it. The results obtained are available in figure 2.34. The expected behaviour is observed for IL-12 p70: the amplification time increases when the concentration of IL-12 p40 increases. However, we observe that when the concentration of IL-4 increases the amplification time also increases: this is contrary to what is expected. We speculate that this result is due to an exchange of biotinylated oligonucleotides between detection antibodies, leading to a loss of signal specificity.

To overcome this oligonucleotide exchange situation, we thought about using di-biotinylated oligonucleotides because the stability of the linkage with the streptavidin bound antibody should be higher. We decided to work with the γ switch at 37°C. Rather than using a di-biotinylated oligonucleotide, we used 2 complementary oligonucleotides: one with a biotin at its 5' end and the other with a biotin at its 3' end. A schematic figure is available in figure 2.35.a. There are two possibilities: to use either a cT or a kT as an oligonucleotide with a biotin at its 5' end. The oligonucleotide with a biotin at its 3' end is an activator. A range of each of the duplexes obtained was carried out and the results are available in figure 2.35.b. We see that this approach makes it possible to obtain two behaviours: a di-biotinylated duplex activating the switch and a di-biotinylated duplex inhibiting the switch.

We then evaluated the exchanges of di-biotinylated duplexes between antibodies. A plate was coated with the IL-4 detection antibody. 0 and 8.7 pM of IL-4 were added. Finally, 350 nM of IL-4 detection antibody with 1 equivalent of streptavidin and 1 equivalent of the di-biotinylated oligonucleotide NBItoγ-DiBiot were used for staining the detection step, in presence of a range of IL-12 p70 detection antibody with 1 equivalent of streptavidin and 1 equivalent of the di-biotinylated oligonucleotide NBItopTγA1-DiBiot (figure 2.36.a.). If

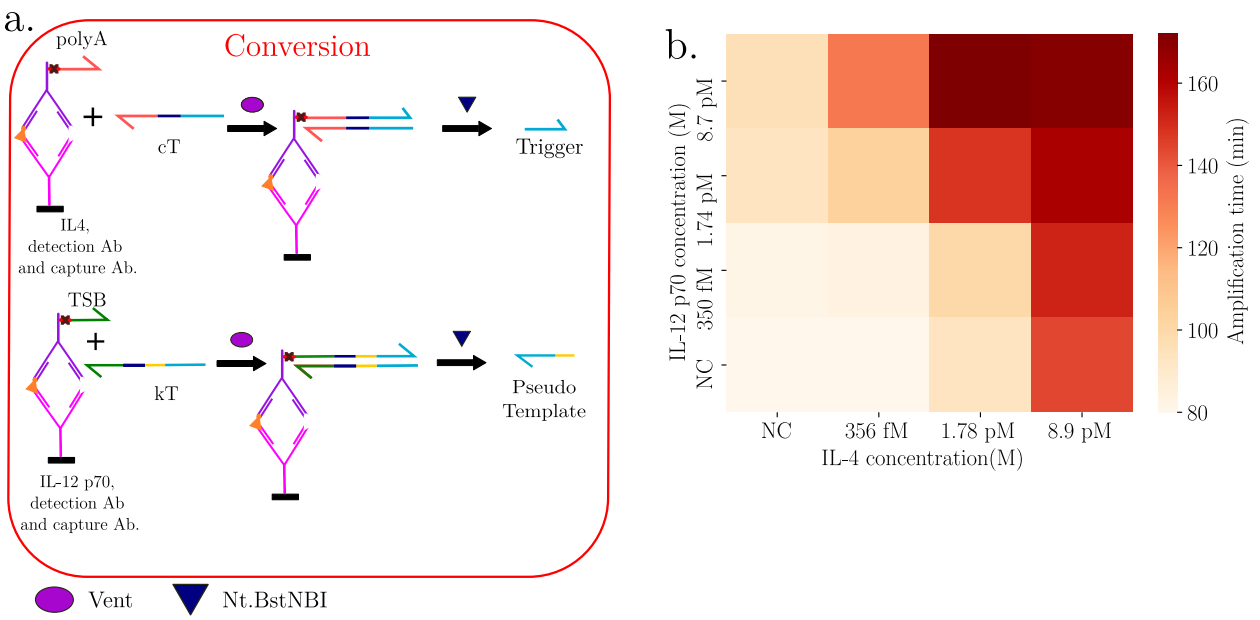

Figure 2.34: **Two-protein inputs classifier. a.** Conversion module used for the two-inputs PUMA. Each targeted proteins (orange) binds to a specific capture antibody grafted on a surface (pink) and is then recognized by a specific detection antibody (purple) functionalized with a streptavidin (brown) and single stranded DNA oligonucleotide. IL-4 and IL-12 p70 have been targeted. PolyA : streptavidin : IL-4 detection Ab (1 : 0.33 : 0.33)(red) hybridizes to the cT and undergoes polymerisation / nicking cycles, thus producing trigger. TSB : streptavidin : IL-12 p70 detection Ab (1 : 0.33 : 0.33) (green) hybridizes to the kT and undergoes polymerisation / nicking cycles, thus producing pT. **b.** Amplification time obtained for a IL-4 and IL-12 p70 matrix ranges.

there is no exchange under these conditions, the concentration of the IL-12 p70 detection antibody should have no influence on IL-4 detection. As we can see in figure 2.36.b., this is not the case. Surprisingly, the higher the concentration of di-biotinylated oligonucleotide NBItopTγA1-DiBiot, the earlier the amplification starts. Moreover, for 350 and 175 nM of IL-12 p70 detection antibody, no discrimination can be made between 0 and 8.7 pM of IL-4. This is counter-intuitive, as we expected the opposite effect. It seems that an interaction between the two di-biotinylated oligonucleotides takes place, preventing the washing away of excess oligonucleotides. Further experiments are needed to fully explain and characterize this effect.

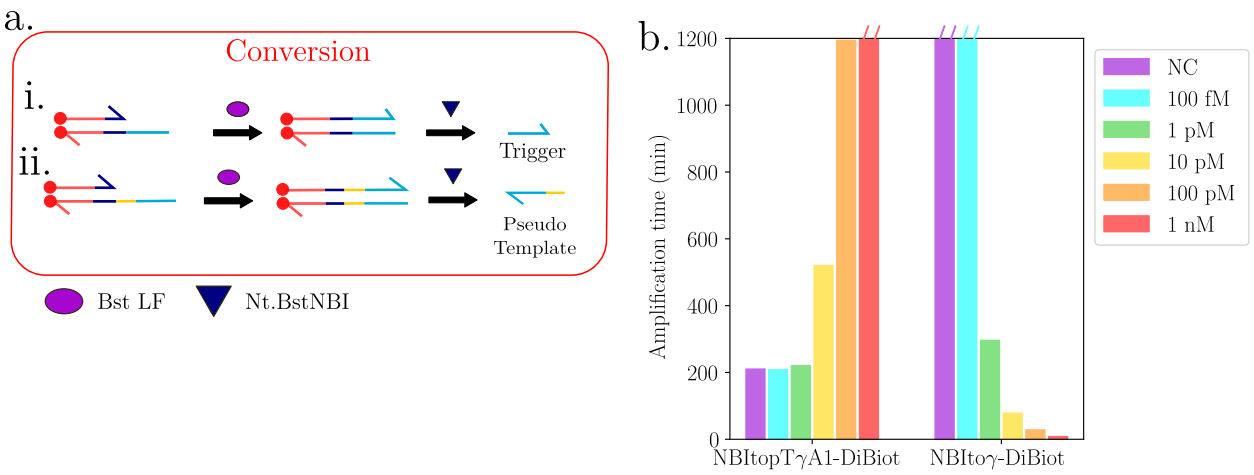

Figure 2.35: **Di-biotinylated oligonucleotides principle scheme. a.i.** Conversion module used for the PUMA. A 5' biotinylated activator oligonucleotide hybridizes to a 3' biotinylated converter template and undergoes polymerisation / nicking cycles, producing trigger. **b.** NBItopTγA1-DiBiot range in presence of 5 nM of pTγ. NBItoγ-DiBiot range in presence of 10 nM of pTγ.

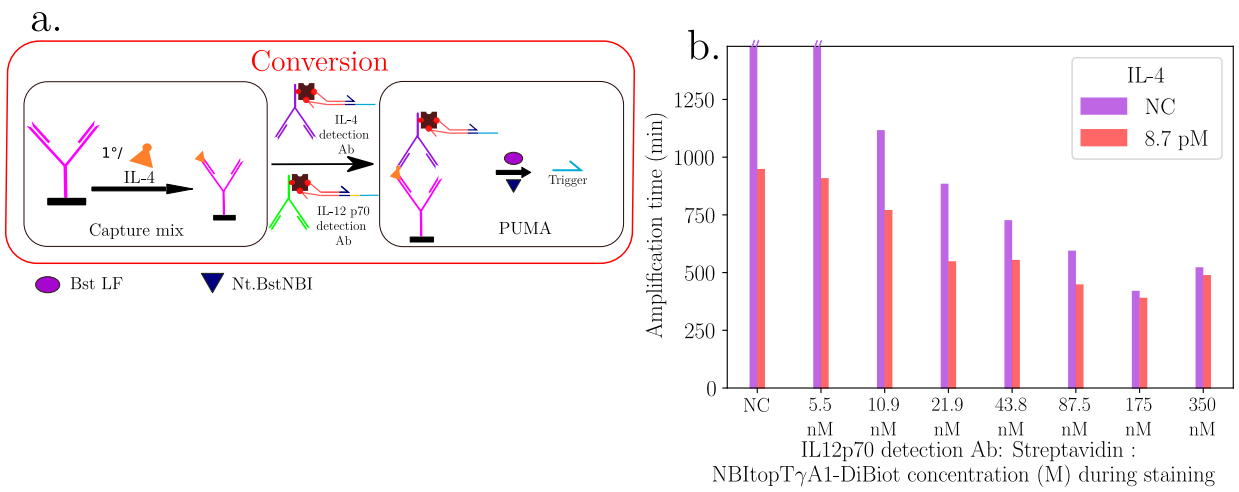

Figure 2.36: **Dibiotinylated oligonucleotide exchange.** Conversion module used for the PUMA. The targeted IL-4 protein (orange) binds to a specific capture antibody grafted on a surface (pink). A mix of NBItoγ-DiBiot : Streptavidin : IL-4 detection Ab (1 : 1 : 1) and NBItopTγA1-DiBiot : Streptavidin : IL-12 p70 detection Ab (1 : 1 : 1) has been used to recognize the IL-4 protein. The other component of the PUMA were then added. **b.** No and 8.7 pM of IL-4 were targeted. The staining step has been realized with 350 nM of NBItoγ-DiBiot : Streptavidin : IL-4 detection Ab (1 : 1 : 1) and a range of NBItopTγA1-DiBiot : streptavidin : IL-12 p70 detection Ab (1 : 1 : 1).

2.7 Discussion

In this chapter, we obtained a proof of principle for human alpha-Thrombin detection using a PEA approach. For this purpose, two aptamers have been modified: an activator was added at the 3' extremity of the 29mer and a cT was added at the 5' extremity of the 15mer. Designs with Nb.BsmI and Nt.BstNBI nickase enzymes were tested. While the detection with Nt.BstNBI is faster, the detection with Nb.BsmI is more sensitive, allowing to detect as low as 10 nM of human-alpha Thrombin. Further experiments are needed to improve this design. On the molecular programming part, the sequences of the used activator and cT could be optimized by trying a new set of bases between the Nt.BstNBI nicking site and the trigger complementary.

However, the main optimization remains on the aptamer selection. Indeed, the selected aptamers are used in a buffer and at a temperature different of the ones used for their selection. Moreover, adding a cT or an activator as well as a T12 linker to their sequences can reduce their affinity to the protein. All those effects considered, it is highly likely that the effective K_d of the aptamers with their targeted protein is increased, also increasing the LOD of the system. To address this, it would be possible to evolve and select a pair of aptamers under the conditions used for molecular programs while imposing the presence of a cT and an activator. It would be possible, for example, to carry out a SELEX [213] with a selection step carried out by a PEA. A first step could be to use the sequences used for the detection of Thrombin to carry out a mutation/selection cycle.

We then got interested in the bases around the Nt.Bst.NBI nicking site and their influence on the trigger production. We focused on sT but those results could be used for trigger production by a cT, as done for the PEA approach.

Using an optimized sT, we achieved the detection of IL-12 p70, IL-4 and INFg down to low femtomolar concentrations using a sT-based immuno-PUMA. These LODs are 2 to 3 orders of magnitude lower than the LODs obtained with classical ELISA tests. Other proteins could be detected by changing the set of used antibodies.

Moving to digital detection of proteins is a path to be explored. It would be possible to graft capture antibodies on particles and then to use these particles at a concentration where each particle can capture 0, 1 or a few proteins. Then, the particles would be stained with a biotinylated detection Ab, streptavidin and a biotinylated sT. Finally, beads would be mixed with a PUMA amplification mixture and compartmentalize in wtaer-in-oil droplets. After incubation, the droplets could be analyzed by fluorescent microscopy and the protein concentration calcultated using Poisson distribution.

Concerning the protein classifier, it has been shown that the classifier in itself is working, the main issue is to link the classifier to the protein concentration. For this, a biotin-streptavidin linkage has been tried but resulted in an exchange of oligonucleotide between detection antibodies during the detection antibodies staining. A possibility to overcome this would be to covalently graft the oligonucleotides on the detection antibodies. However, our supplier cannot provide unmodified versions of the biotinylated antibodies. This means that we would have to try different antibodies to see if they could be used as detection antibodies for an ELISA. As our supplier has certainly optimized the set of used antibodies, changing one of them could result in a loss of sensitivity.

Chapter 3

Cells phenotyping

3.1 Résumé

Dans ce chapitre, nous nous sommes intéressés à l'utilisation d'aptamères pour la détection de protéines à la surface d'une cellule. En utilisant un aptamère spécifique d'une protéine de surface caractéristique des cellules cible, il est possible de phénotyper une population de cellules. Une séquence connue, qui peut être choisie arbitrairement, est ajoutée en 3' de l'aptamère spécifique. Ici, nous avons choisi TSB et utilisé un cT spécifique de cette séquence.

Premièrement, le PUMA a été optimisé pour fonctionner à 37°C dans un buffer compatible avec des étapes ultérieures de biologie moléculaire, par exemple une rétro transcription. Ensuite, deux aptamères ont été testés pour la reconnaissance des cellules Ramos : TE02 et TD05. TD05 donnant le meilleur résultat, il a ensuite été utilisé. Une portion de milieu de culture utilisé pour les cellules Ramos a été ajouté au PUMA, augmentant la viabilité des cellules sans impacter la détection des cellules. Il a également été montré qu'une détection non spécifique des cellules est possible en marquant les cellules avec un oligonucléotide portant une molécule de cholestérol à son extrémité 5'.

3.2 Summary

In this chapter, we focused on the use of aptamers for the detection of cell surface protein markers. Such method could be applied to cell phenotyping. A known sequence that can be chosen arbitrarily is added at the 3' extremity of the specific aptamer. Here we chose TSB and used a TSB-specific cT.

Firstly, the PUMA was optimized to work at 37°C in a buffer compatible with subsequent molecular biology steps, e.g. reverse transcription. Secondly, two aptamers were tested for Ramos cell recognition: TE02 and TD05, the latter giving the best results. A fraction of the culture medium used for Ramos cells was added to the PUMA, increasing the viability of the cells without impacting the detection of the cells. It was also shown that non-specific cell detection is possible by labelling the cells with an oligonucleotide carrying a cholesterol molecule at its 5' extremity.

3.3 Introduction: Interest of molecular programming for isothermal live cell detection

In this chapter, we looked at the possibility of phenotyping cells by focusing on surface proteins. As reported in the literature, cell surface proteins have already been used to program an aptamer-based biomolecular reaction network [214], an aptamer-based DNA-Based logic platform [215], an aptamer displacement reaction from live-cell surfaces [216] or an antibody based dynamic DNA gates for multiplexed cell sorting [217]. Therefore, given the results of the precedent chapter, the possibility of phenotyping cells using aptamer seemed to be an interesting direction.

The use of PUMA for cell phenotyping would allow to obtain a signal amplification from a specific cell surface marker. Combined with the PUMA high sensibility, detection of poorly expressed cell surface markers could be achieved. The produced signal could also be used for subsequent molecular biology steps.

The results presented in this chapter have been used for a patent application.

Our goal is to detect cell surface protein markers using aptamers. Our main idea is to add an arbitrarily known sequence at the 3' extremity of a specific aptamer. This sequence could then be detected using a PUMA.

3.4 Temperature and buffer optimization

The first step was to choose a known sequence and to optimize the PUMA to detect it at 37°C in a buffer suitable for reverse transcription. We selected the TSB sequence, already introduced in the precedent chapter (see section 2.5.2.1).

A previously used molecular program, referred as α switch, which only performs between 42°C and 50°C [176], [175], [218] was adapted to work at 37°C. A range of temperature was realized for a molecular program optimized to detect TSB at 50°C. As it can been seen in figure 3.1.a., there is a clear dose response between the concentration of TSB target and the amplification time at high temperature (>46.3°C). At lower temperature, there is no substantial difference between the amplification time of the samples with different concentration of TSB, highlighting the importance of the temperature on this amplification system. In particular, we observed that the lower the temperature, the sooner the amplification of negative control (called false positive, in absence of target). The false positive is due to spurious reactions that produce a few trigger oligonucleotides nonspecifically. This phenomenon, known as leak, is increased when the temperature is lower and prevents the sensitive detection of the TSB target. Additionally, the enzymes, when used much below their optimal temperature, loose activity and become prone to product inhibition. Altogether, we can conclude that the classic PUMA designs (α switch) does not perform at 37°C.

Despite the fact that the α molecular program does not operate at 37°C, we used it to optimize the new buffer. Indeed, to ensure compatibility with subsequent step of the process, for example transcriptomic analysis of cellular RNA, it was necessary to use a different buffer than the one used classically for PUMA systems [178], and to change it to a buffer compatible with reverse transcription. It was first necessary to supplement the RT buffer with dNTPs and $MgSO_4$. A range of $MgSO_4$ was realized in order to calibrate the concentration that

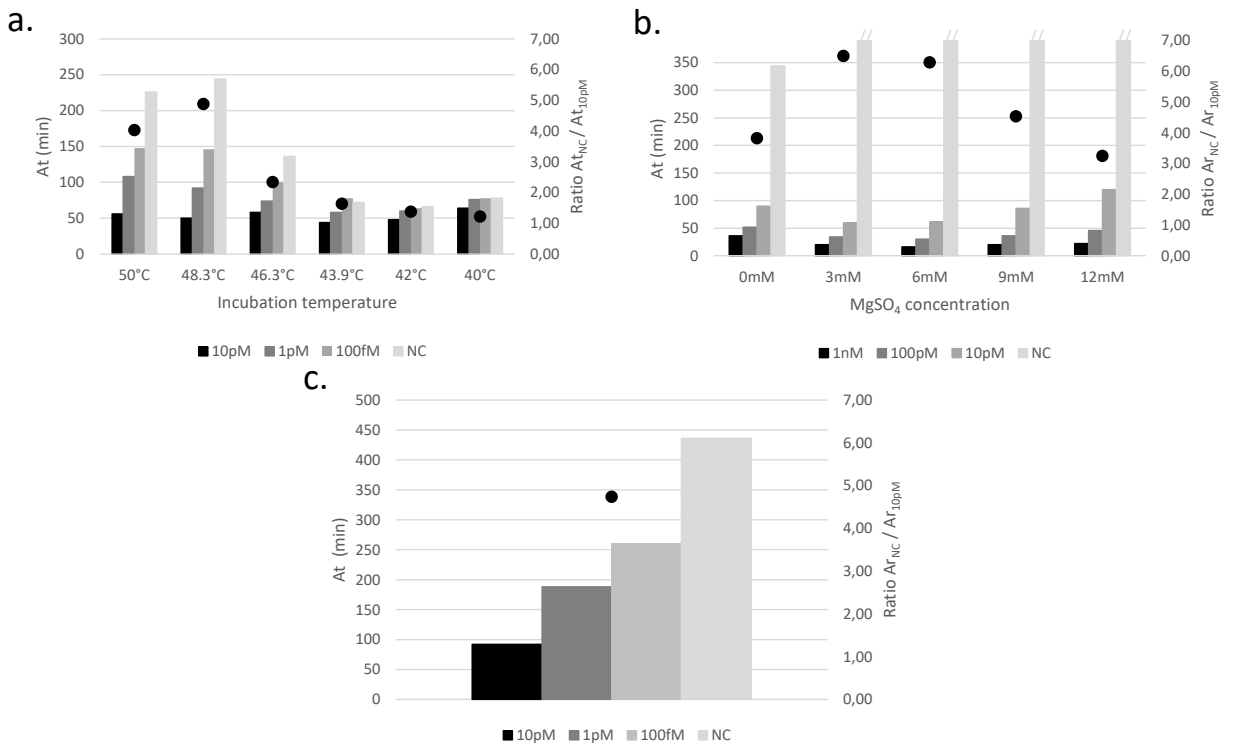

Figure 3.1: **Adapting PUMA to work at 37°C in FS Buffer 1x. a.** A range of temperature was used for a molecular program optimized to detect TSB at 50°C. The ratio At_{NC} / At_{10pM} characterizes the efficiency of the detection: the higher the ratio, the better the detection of TSB. There is a clear dose response between the concentration of TSB target and the amplification time (A_t) at high temperature (>46.3°C). At lower temperature, there is no substantial difference between the amplification time of the samples with different concentrations of TSB, highlighting the importance of the temperature on this amplification system. **b.** A range of $MgSO_4$ was realized at 46°C for the same molecular program than in panel a but in a buffer close to the one used for Reverse-Transcription . The ratio At_{NC} / At_{10pM} characterizes the efficiency of the detection: the higher the ratio, the better the detection of TSB. In this case, 3 mM of $MgSO_4$ seems to be the best choice. **c.** A range of TSB was realized at 37°C with the switch γ in a buffer optimized for one pot PUMA and retro transcription reaction. The output of the PUMA is correlated to the concentration of TSB: the lower the A_t, the higher the concentration of TSB.

was needed (figure 3.1.b). Supplementing the buffer with 3 mM of $MgSO_4$ gives the best signal-to-noise ratio.

In order to obtain a molecular program operating at 37°C, we switched to another set of templates, designed to work at this temperature [219], referred to as γ switch. This molecular program was conceived by decreasing the melting temperature of the trigger on the corresponding autocatalytic template, which can be obtained by shortening the trigger or adjusting their sequence toward higher AT/GC content. The consequence of the lower melting temperatures is that triggers produced nonspecifically now dynamically exchange

between aT and pT, and thus get an opportunity to be deactivated if the concentration is below the threshold [177]. Additionally, this change also solved the enzyme issue since nicked products can spontaneously dehybridize, avoiding enzyme inhibition.

Finally, a range of TSB was realized at 37°C in the optimized buffer, with the γ switch (figure 3.1.c). It was observed that the higher the concentration of TSB, the lower the At, demonstrating the efficient sensing of the target down to 100 fM at 37°C, temperature compatible with cell integrity, in a buffer suitable for reverse transcription.

3.5 Aptamer-mediated live cell phenotyping

3.5.1 Aptamer choice

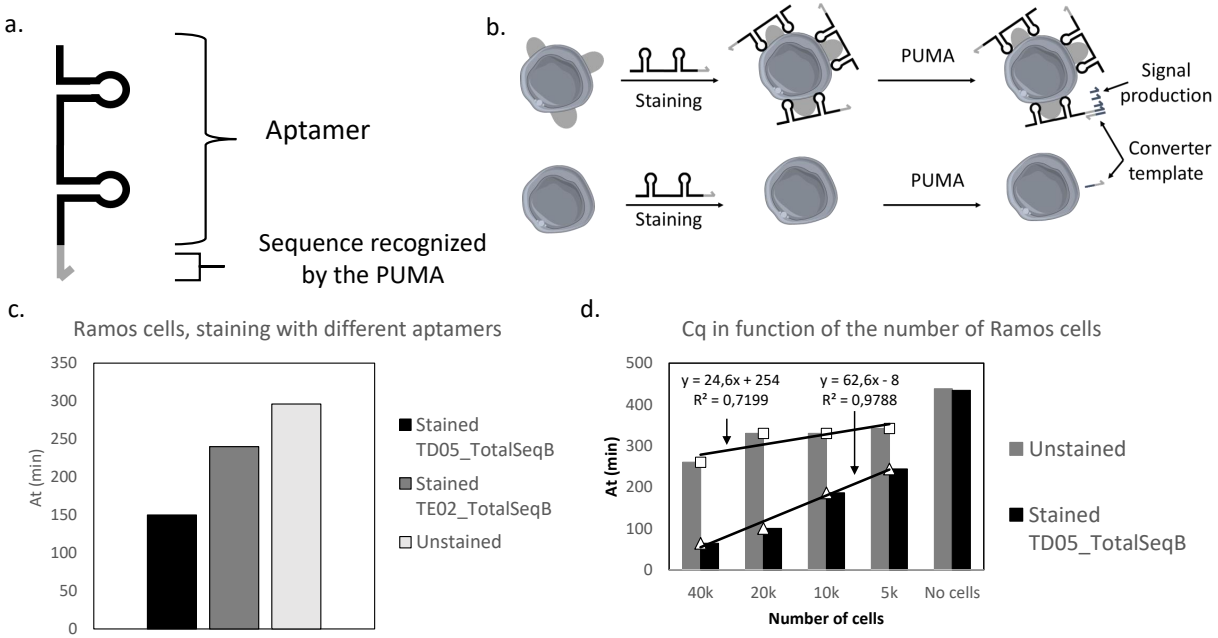

Figure 3.2: **Detection of cells stained with a cell-specific aptamer. a.** Schematic structure showing the way the aptamers were modified to activate the PUMA: a specific sequence (TSB) was added in 3' of reported aptamer sequences. **b.** Cells are stained with a specific aptamer. If the cell presents the targeted markers, the aptamer binds to it and can therefore be used as input by the PUMA. **c.** Both aptamers bind to the Ramos cells, as suggested by the lower A_t in comparison to unstained cells. TD05-TSB was shown to best initiate the amplification. **d.** A range of TD05-TSB stained Ramos cells was realized: the output of the PUMA is proportional to the quantity of cells while it is not the case for stained without aptamer Ramos cells, as suggested by the correlation coefficient of the A_t in function of the number of cells.

Once the molecular program optimized to detect TSB at 37°C in the new buffer, we appended the TSB sequence to the 3' extremity of two Ramos-specific aptamers (TD05

and TE02) (figure 3.2.a.) reported in the literature [220]. In presence of a TSB-specific cT, the presence of one of the aptamer should lead to the production of trigger γ (figure 3.2.b.). Ramos cells were stained with either of the aptamers (see section 6.7.3 for the protocol) and we observed that the amplification occurred sooner than with unstained cells. The effect was significantly higher with TD05 in comparison to TE02, demonstrating the specific triggering of the amplification by cell-bound TD05. (figure 3.2.c). Figure 3.2.d. shows the amplification start in presence of an increasing concentration of Ramos cells, either unstained or stained with TD05-TSB strand. For each cell concentration > 0, stained cells induced faster amplification (lower At) in comparison to unstained cells. Furthermore, higher concentrations of stained cells were correlated with earlier amplification. Altogether, these results demonstrate that we succeeded in staining cells with the modified specific aptamer, and that the cell-bound modified aptamer is able to specifically trigger the amplification.

3.5.2 Adding a proportion of cellular media

As the optimized buffer contains only salts and dNTPs, we studied the survival rate of the cells in this buffer, which is different from the culture medium used for cell culture. We thus estimated cell death without or with 12.5% of cellular media in FS Buffer 1x with 3 mM $MgSO_4$. Ramos and 3T3 cells were let 5 hours at 37°C in those two buffers and stained with propidium iodide. Cells were analyzed through flow cytometry and proportions of alive and dead cells were calculated (Figure 3.3.b., 3T3 cells (i) and Ramos cells (ii)). We observed that in presence of 12.5% cellular media, the proportion of alive cells is increased from 55% to 87% for 3T3 cells and from 0.7% to 9% for Ramos cells. It is clear that adding a fraction of cellular media to the buffer improves cell survival over time.

We then tried to add a proportion of cellular media in the molecular program buffer in order to maintain cell viability. First, a range of cellular media (RPMI + 10% FBS + 1 % penicillin/streptomycin [P/S]) was realized with respectively 0, 1 and 10 pM of TSB in order to assess the effect of the cellular media on the amplification reaction (figure 3.3.a.). Atto633 and EvaGreen fluorescences were used to monitor the starting time of the amplification and a potential unspecific DNA production of the system (called "divergence" [221]) respectively. It has been shown that at 12.5% of cellular media and below, specific amplification from the molecular program occurred and no divergence was observed. However, at 25 %, divergence was observed and at 50 %, divergence and no specific amplification took place.

Finally, we performed the detection of Ramos cells, either unstained or stained with TD05-TSB (see section 3.5), with the molecular program in the presence of 12.5% of cellular media (figure 3.3.c.). For each cell concentration > 0, stained cells induced faster amplification (lower At) in comparison to unstained cells. Furthermore, higher concentrations of stained cells were correlated with earlier amplification. These results demonstrate that it is possible to use the molecular program for specific detection of cell bound oligonucleotides, while maintaining cell viability by inclusion of cellular media in the reaction buffer.

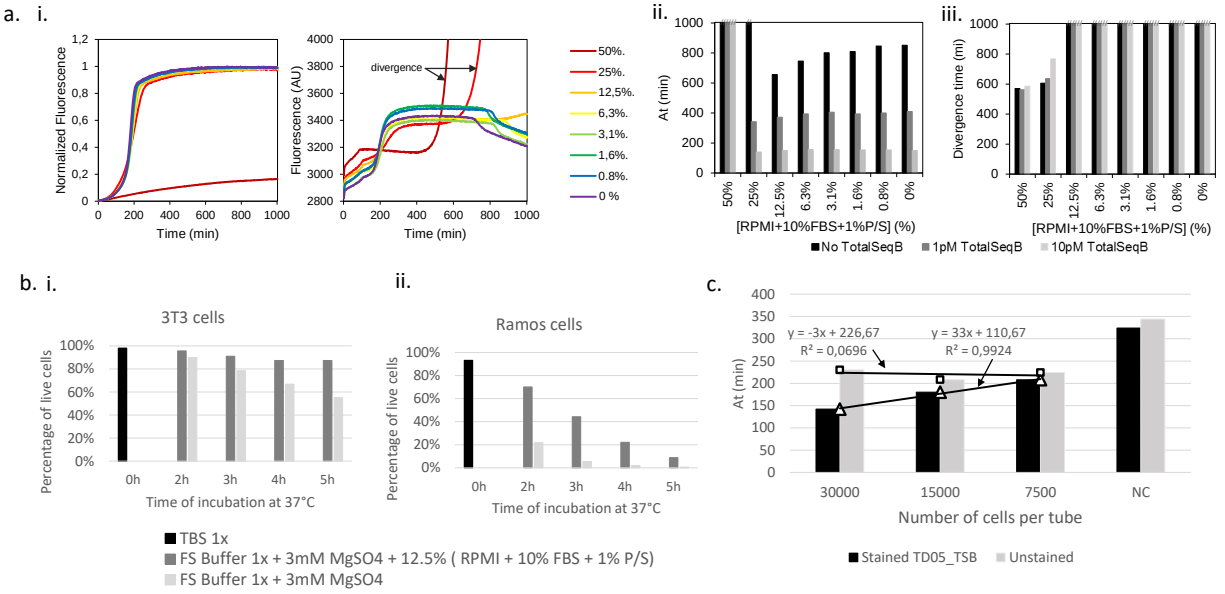

Figure 3.3: **Impact of cellular media on both cell viability and the amplification reaction from the molecular program. a.** A range of cellular media (RPMI + 10% FBS + 1% P/S) was realized with respectively no TotalSeq B, 1pM of TSB and 10pM of TSB. Atto633 fluorescence was monitored (recorded time: 1002 minutes). (i) Amplification curves for Atto633 (left) and Evagreen intercalating dye (right) for 10 pM TSB samples. From these curves are extracted the amplification starting time (At, ii) and the divergence time (iii): at 50% of cellular media, no amplification started, from 25% and below, the cellular media did not hamper the amplification reaction triggered by the TSB sequence. At 50% and 25%, divergence was observed while at 12.5% and below, no divergence was observed. **b.** Effect of the buffer on the cell survival. A kinetic of degradation of 3T3 (i) and Ramos (ii) cells at 37°C was realized in FS Buffer 1x with 3mM $MgSO_4$ supplemented or not with 12.5% of cellular media. Cells were stained with propidium iodide and analyzed by flow cytometry to extract the proportions of alive and dead cells. Adding 12.5 % of cellular media increased the proportion of live cells from 55% to 87% (i) and from 0.7% to 9% (ii) for 3T3 and Ramos cells respectively after 5h of incubation. The proportions of live cells a 0h were obtained from cells stored in 1x TBS. **c.** A range of unstained or TD05-TSB-stained Ramos cells was incubated with the amplification mixture containing 12.5% of (RPMI + 10% FBS + 1% P/S) : the output of the PUMA is correlated to the quantity of cells, as suggested by the negative correlation coefficient of the A_t in function of the number of cells, while no amplification was observed independently of the concentration of unstained cells. The cellular media does not have an impact on the detection of stained cells.

3.6 Nonspecific live cell phenotyping

We then got interested in the possibility of detecting cells nonspecifically. The staining and

detection of cells using a cholesterol-conjugated oligonucleotide (DLet7aT10ChoPro) was demonstrated (figure 3.4.a.). Due to its properties, it is already known that the cholesterol moiety inserts into the cell membranes [222] thereby attaching the oligonucleotide to its surface (figure 3.4.b.). The 3' part of DLet7aT10ChoPro oligonucleotide was used as input for the cT Let7atoγ, inducing the production of B11a trigger (figure 3.4.c.). Figure 3.4.d. depicts an experiment where various concentrations of Ramos cells, either unstained or stained with the cholesterol-modified oligonucleotide, were incubated together with the amplification mixture. While no amplification was observed with unstained cells (up to 730 minutes), the stained cells could trigger the amplification. Moreover, the concentration of stained cells was inversely correlated to the amplification time (i.e. the more cells, the sooner the amplification). These results demonstrate the specific triggering of the amplification by cell-anchored DNA strands.

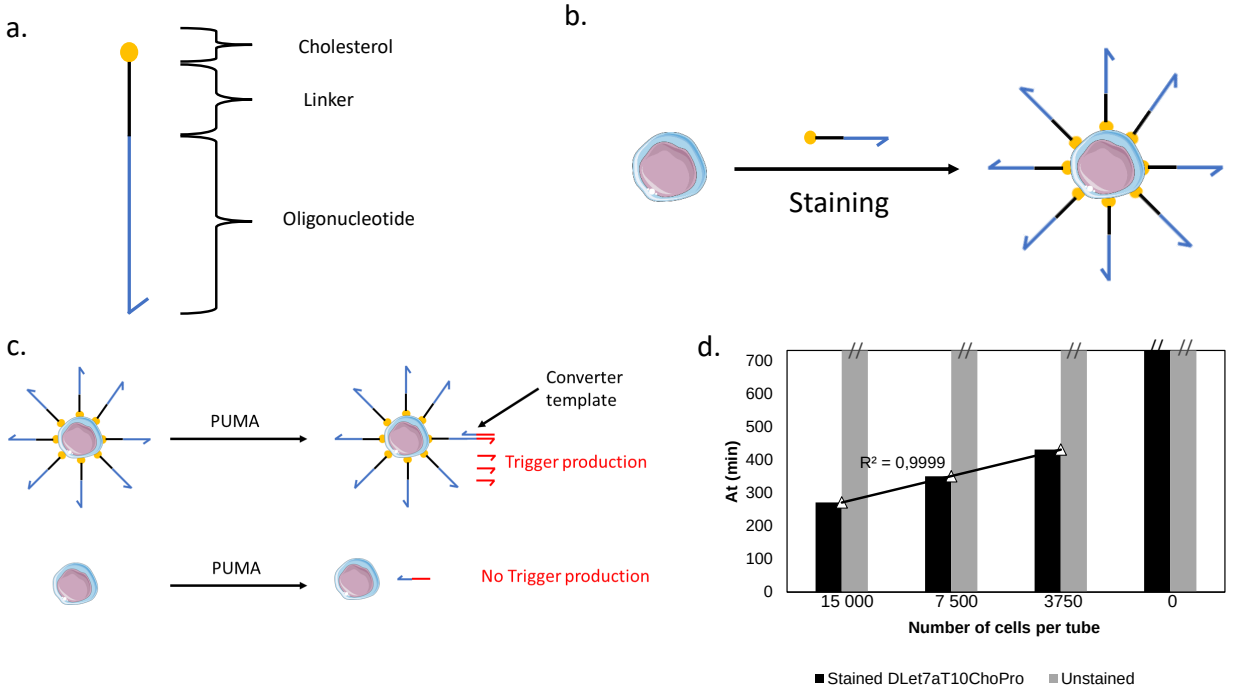

Figure 3.4: **Detection of cells stained thanks to oligonucleotide conjugated with cholesterol. a.** Schematic structure of the used oligonucleotide: a cholesterol molecule is attached to the 5' extremity of the desired oligonucleotide using a T10 linker. **b.** Cells are stained with a cholesterol-modified oligonucleotide. Due to its properties, the cholesterol inserts in the cell membrane. **c.** Cells stained with the cholesterol-modified oligonucleotide can be detected with the PUMA: the cholesterol modified oligonucleotide is used as input. If the cells are not stained with this oligonucleotide, there is no input for the PUMA. **d.** A range of unstained or DLet7aT10ChoPro-stained Ramos cells was incubated with the amplification mixture: the output of the PUMA is correlated to the quantity of cells, as suggested by the correlation coefficient of the At in function of the number of cells, while no amplification was observed independently of the concentration of unstained cells.

3.7 Discussion

In this chapter, we obtained a proof of principle for the phenotyping of Ramos cells with a specific aptamer, TD05, to which we added the TSB sequence in order to be able to detect it with a cT. Other cell types could be targeted using different aptamers. Although we were able to differentiate stained cells from unstained cells, further experiments are required. First, adding a population of stained cells with a scrambled aptamer, to ensure the specificity of the aptamer. In addition, to obtain a more convincing proof of principle, we could stain an initial population composed of several cell types. Only the cells bearing the targeted specific surface marker would trigger PUMA amplification. So far, only immortalised cell lines have been targeted. An important step would be to target cells from biological tissues, known as primary cells.

As we have seen, the incorporation of a fraction of cellular media to the PUMA significantly increases cell viability. However, approximately 30% of Ramos cells die within two hours of incubation at 37°C in the presence of 12.5% cellular media. This proportion could be reduced with further buffer optimisation or by accelerating the reaction.

In order to speed up detection and reduce non-specific trigger production, it is also an option to add a sT to the specific aptamer. Different designs are possible, such as adding it to the 3' extremity of the aptamer with a non-nucleic acid linker separation. The effect of different linker types still have to be assess. Another design would be to add the different parts of the sT to the aptamer sequence in such a way that the conformational change due to the presence of the target surface protein induces formation of a functional sT.

A limitation of the described method is that it is targeting only one surface marker. In order to target two protein surface markers at the same time, we can consider the possibility of performing an aptamer based PEA. It is also conceivable to detect secreted proteins using a PEA: the faster the targeted protein is secreted, the earlier the PUMA starts.

Designing a classifier similar to the one presented in chapter 2, it would be possible to extend even further the number of target surface marker. It would thus allow to detect specific signature of protein surface markers.

Chapter 4

Towards an integrated microfluidic chip

4.1 Résumé

Dans ce chapitre, nous nous sommes intéréssés à la possibilité d'obtenir un départ spatiallement localisé du PUMA dans une chambre micro-fluidique. Le but est d'obtenir une détection spatiale multiplexée de plusieurs biomarqueurs. Pour cela, nous avons commencé par tester le comportement du PUMA utilisé pour la détection de Let7a dans des chambres micro-fluidiques en verre, passivées avec de la BSA ou de l'huile novec 1720 et scellées avec de la colle époxy. Ensuite, des chambres micro-fluidique en PMMA scellés avec de la graisse à vide ont été testées et selectionnées. Des matrices auto-activées biotinylées ont été greffés sur des billes en sépharose, menant à l'observation d'un départ localisé du PUMA autour de ces billes. Ensuite, dans l'optique d'utiliser un hydrogel fonctionnalisé avec des matrices de conversion spécifiques à des miARN ciblés, nous avons fontionnalisé des billes de THA avec une matrice de conversion spécifique à Let7a. Ces billes ont été ajoutées à une mixture d'amplification PUMA, permettant une amplification spécifique en présence du miRNA ciblé. Ce résultat démontre la possibilité de greffer une matrice de conversion sur l'hydrogel choisi tout en conservant sa fonction de conversion.

Enfin, l'interfacage du PUMA avec des transistors à effet de champ sensibles aux ions basés sur des nanofils de silicium a été étudié avec nos collaborateurs. Un bref résumé de ces travaux est presenté. Cela a permis d'obtenir un signal de sortie électrique pour le PUMA.

4.2 Summary

In this chapter, we investigated the possibility of obtaining a spatially localized amplification of PUMA in a microfluidic chamber. The final aim is to obtain a multiplexed spatial detection of several biomarkers. To this end, we first tested the behaviour of the PUMA used for Let7a detection in glass microfluidic chambers, coated with BSA or novec 1720 oil and sealed with epoxy glue. Subsequently, PMMA microfluidic chambers sealed with vacuum grease were tested and selected. A biotinylated sT was grafted onto sepharose beads, leading to the observation of a localized start of PUMA around these beads. Then, in order to use a

hydrogel functionalized with specific cTs for targeted miRNAs, we functionalized THA beads with a Let7a-specific cT. These beads were added to a PUMA amplification mixture, allowing specific amplification in the presence of the targeted miRNA. This result demonstrates the possibility of grafting a cT onto the chosen hydrogel while maintaining its cT function.

Finally, the interfacing of PUMA with ion-sensitive field-effect transistors based on silicon nanowires (NW) was studied with our collaborators. A brief summary of this work will be presented. This resulted in the demonstration of the possibility of obtaining an electrical output signal for the PUMA.

4.3 Desired microfluidic chip

Our goal is to obtain a microfluidic chip allowing a multiplexed miRNA detection with an electrical readout.

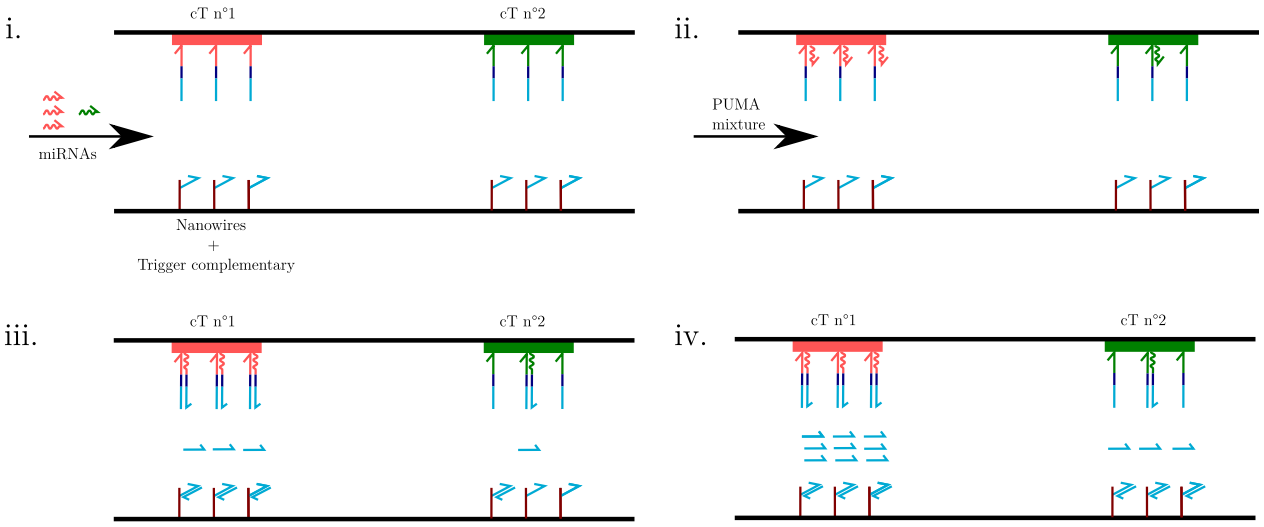

Figure 4.1: **Principle scheme of the desired microfluidic chip.** cTs specific for miRNA n°1 are grafted onto a chip wall in a localized spot. Similarly, cTs specific to miRNA n°2 are grafted onto the same wall of the chip, in a second localized spot. Silicon nanowires, carrying the trigger complementary DNA strand, are grafted onto the opposite wall. A sample is flushed into the chip, allowing the cTs to capture their specific miRNAs (**i.**). A wash step is performed and a PUMA amplification mixture is introduced. The chip is then incubated, leading to trigger production (**ii.**). The higher the initial concentration of miRNA, the faster the PUMA amplification, saturating the silicon trigger nanowires. Thus, the local concentration of DNA strands induces a change in the negative charge density around the nanowires, allowing the detection of an electrical signal. In this example, there is more miRNA n°1, so the corresponding nanowires will be saturated first (**iii.**), then the nanowires corresponding to miRNA n°2 will be saturated in a second time (**iv.**).

For that purpose, we decided to focus on a spatial multiplexing: different spots of cTs would be present on the chip (figure 4.1). Thus, each cT target and capture a specific miRNA. After a washing step, the PUMA amplification miture is introduced, leading to a spatiallized start of the PUMA, around the miRNA specific cT.

In order to obtain an electrical readout, silicon nanowires, carrying the trigger complementary DNA strand, would be grafted onto the opposite wall. The PUMA amplification produce trigger, part of which binds to the complementary DNA strand on the nanowires. Thus, the local concentration of DNA strands induces a change in the negative charge density around the nanowires, allowing the detection of an electrical signal.

We have therefore separated this objective into two parts: obtaining a spatially localized start of the PUMA and obtaining an electrical output signal.

4.4 Spatially localized start

In this section, we focused on obtaining a spatially localized start.

4.4.1 Glass chip

The first step was to choose a microfluidic chamber suitable for observing a spatially localized start of the PUMA. We started by working with homemade glass chambers: a parafilm layer was carved to the chamber dimensions and sandwiched between two glass slides. The sandwich is put on a hot plate at 60°C allowing the parafilm to melt and tighly stick to the glass. The chamber is then filled with the PUMA mixture, sealed with epoxy glue and incubated. The fluorescence intensity of the PUMA readout can be monitored in real time via fluorescence microscopy, giving information on the start of the PUMA in two dimensions of space (figure 4.2.a.).

As it has been reported in the literature that glass inhibits the activity of the Nt.BstNBI nickase [223], we got interested in the impact of chamber coating on the PUMA. We started by looking at the coating of glass chambers with bovine serum albumin (BSA) at 2 mg/mL: at this concentration, BSA aggregates and passivates the glass surface, making it highly unlikely for Nt.BstNBI to meet the bare glass surface. The detection of 0 or 10 pM of Let7a was performed in BSA-coated and non coated chambers (figure 4.2.b.). The amplification started only for 10 pM of Let7a in the BSA-coated chamber. For each chamber, the fluorescence intensity of a space region has been averaged and plotted in function of time (figure 4.2.c. for the non coated chambers, figure 4.2.d. for the BSA-coated chambers). A part of each PUMA mixture was placed in tubes in a thermo-cycler (figure 4.2.e.), allowing the comparison of the amplification curves obtained in chambers and in the thermo-cycler. Finally, amplification times for the detection of 10 pM and no Let7a in coated or non coated chambers and in tubes in a thermocycler (hereafter referred as the bulk reaction) were extracted from the fluorescent intensity curves (figure 4.2.f.).

As observed in the chambers, no amplification took place in 450 min in the non coated chambers while an amplification was observed for 10 pM of Let7a in the BSA-coated chamber. This illustrates the necessity of processing glass prior to use to carry a PUMA. However, by comparing the amplification curves obtained in the BSA-coated chambers and in the tubes in the thermo-cycler, we can observed differences in the PUMA behaviour. Firstly, the amplification for 10 pM of Le7a starts at 78 min in the thermo-cycler while it starts at 375 min in the BSA-coated chamber. Secondly, the amplification takes approximately 30 minutes in the thermo-cycler while it is still not finished after 75 minutes in the BSA- coated

chamber. This allows us to conclude that amplification is at least 60% slower in the BSA-coated chambers. This is coherent with the higher amplification time in the BSA-coated chambers. Altogether, those data allow us to conclude that the BSA coating reduces the toxicity of the glass for the PUMA but but does not eliminate it completely.

In order to remove completely the toxicity of the glass for the PUMA, we then looked at the coating of glass chambers with an hydrophobic solution (Novec 1720). This solution makes the glass surface hydrophobic, disfavoring the aggregation of hydrophilic protein on the glass surface. To assess the behaviour of a PUMA in chambers, a PUMA for the detection of 10 pM and not Let7a was performed in novec 1720 oil coated and non coated chambers (figure 4.3.a.). The amplification started only for 10 pM of Let7a in the novec 1720 oil coated chamber.

As observed in the chambers, no amplification took place in 720 min in the non coated chambers (figure 4.3.b.) while an amplification was observed for 10 pM of Let7a in the novec 1720 oil coated chamber (figure 4.3.c.). This illustrates, again, the necessity of processing glass prior to use to carry a PUMA. However, by comparing the amplification curves obtained in the novec 1720 oil coated chambers and in the tubes in the thermo-cycler (figure 4.3.d.), we can observed differences in the PUMA behaviour. Firstly, the amplification for 10 pM of Le7a starts at 110 min in the thermo-cycler while it starts at 210 min in the BSA-coated chamber. Secondly, the amplification takes approximately 30 minutes in the thermo-cycler while it takes approximately 60 min in the novec 1720 oil coated chamber (figure 4.3.e.). This allows us to conclude that amplification is 50% slower in the novec 1720 oil coated chambers. Moreover, a turn-over, caused by the degradation of triggers by the exonuclease when the dNTPs are exhausted, can be observed in the novec 1720 oil coated chamber, showing that the PUMA is working properly in the coated chambers even if it is slower than in a thermo-cycler. Compared with the results obtained for BSA-coated chamber, the novec 1720 oil coating seems to be better. However, there seems to be residual toxicity for the PUMA.

To explain the difference in amplification times between the thermo-cycler and the novec 1720 oil coated chamber results, we got interested in the toxicity of the epoxy glue used to seal the chambers. For this purpose, a range of Let7a was performed in tubes in the thermo-cycler. Epoxy glue coated tubes were compared to tubes without treatment (figure 4.4.b.). The result is clear: there is no amplification in the tubes containing epoxy glue whereas amplification normally takes place in the untreated tubes. The epoxy glue therefore has a toxic effect on PUMA.

As an alternative to the epoxy glue, we tested the use of vacuum grease to seal our chamber, as previously reporter [224]. We first confirmed that the grease is not toxic for the PUMA reaction by performing a range of Let7a in tubes containing vacuum grease and in untreated tubes (figure 4.4.c.). No significant difference was observed, suggesting that sealing these chambers with vacuum grease would be less toxic than sealing the chambers with epoxy glue.

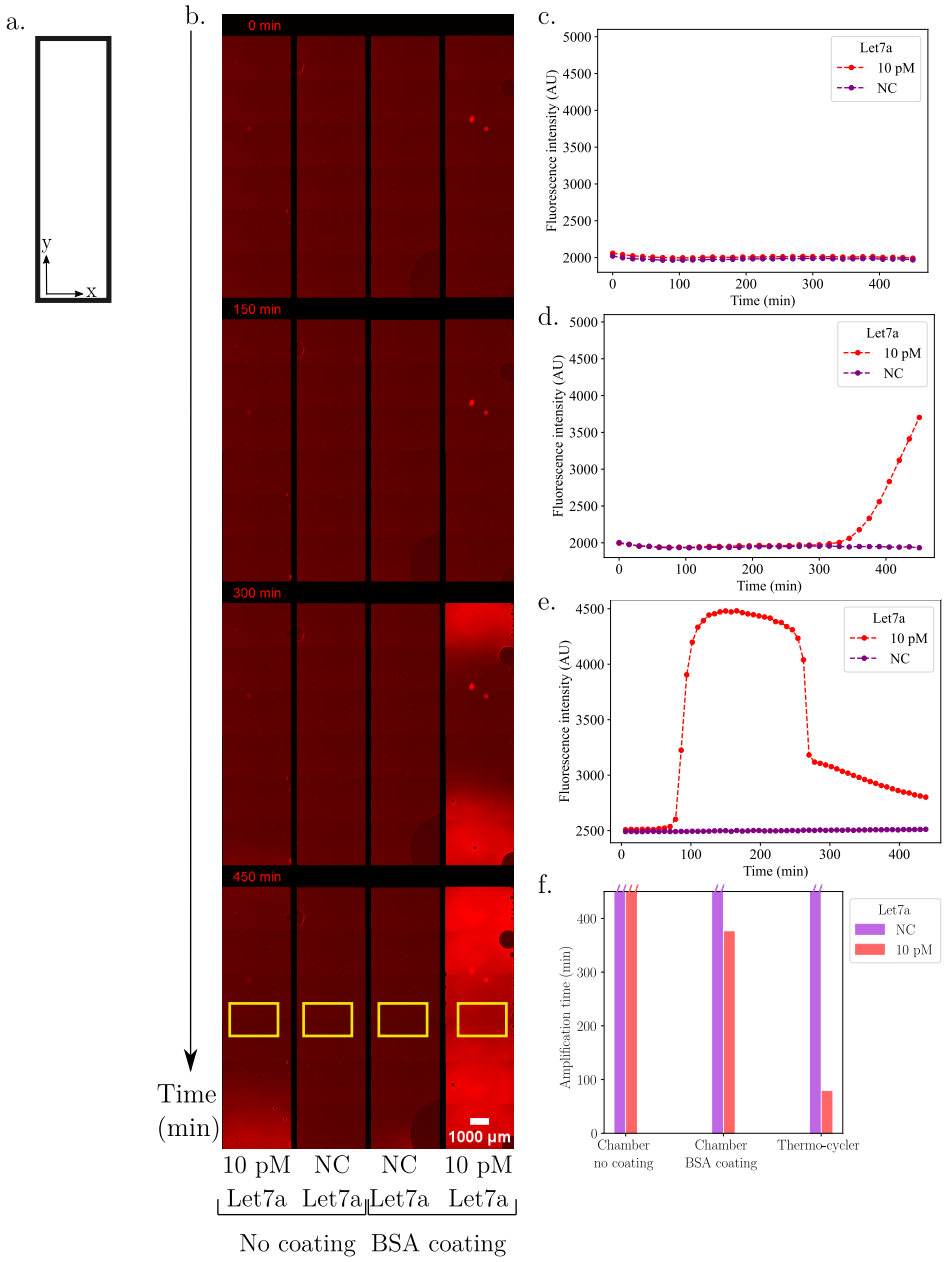

Figure 4.2: **Let7a detection in BSA-coated glass chambers. a.** A chamber is observed in 2 spatial dimensions: x and y. **b.** Glass chambers were coated or not with BSA. PUMA amplification mixtures containing 10 pM and no Let7a were introduced in the chambers, which were then sealed with epoxy glue. The chambers were incubated at 50°C and fluorescence intensity was monitored in real-time via fluorescence microscopy. For each chamber, the fluorescence intensity in the yellow boxes has been averaged for each time point. **c.** Average fluorescence intensity in the non coated chambers in function of time for 10 pM and no Let7a. **d.** Average fluorescence intensity in the BSA-coated chambers in function of time for 10 pM and no Let7a. **e.** Fluorescence intensity in function of time for 10 pM and no Let7a in a thermo-cycler. **f.** Amplification times for the detection of 10 pM and no Let7a in coated or non coated chambers and in tubes in a thermo-cycler.

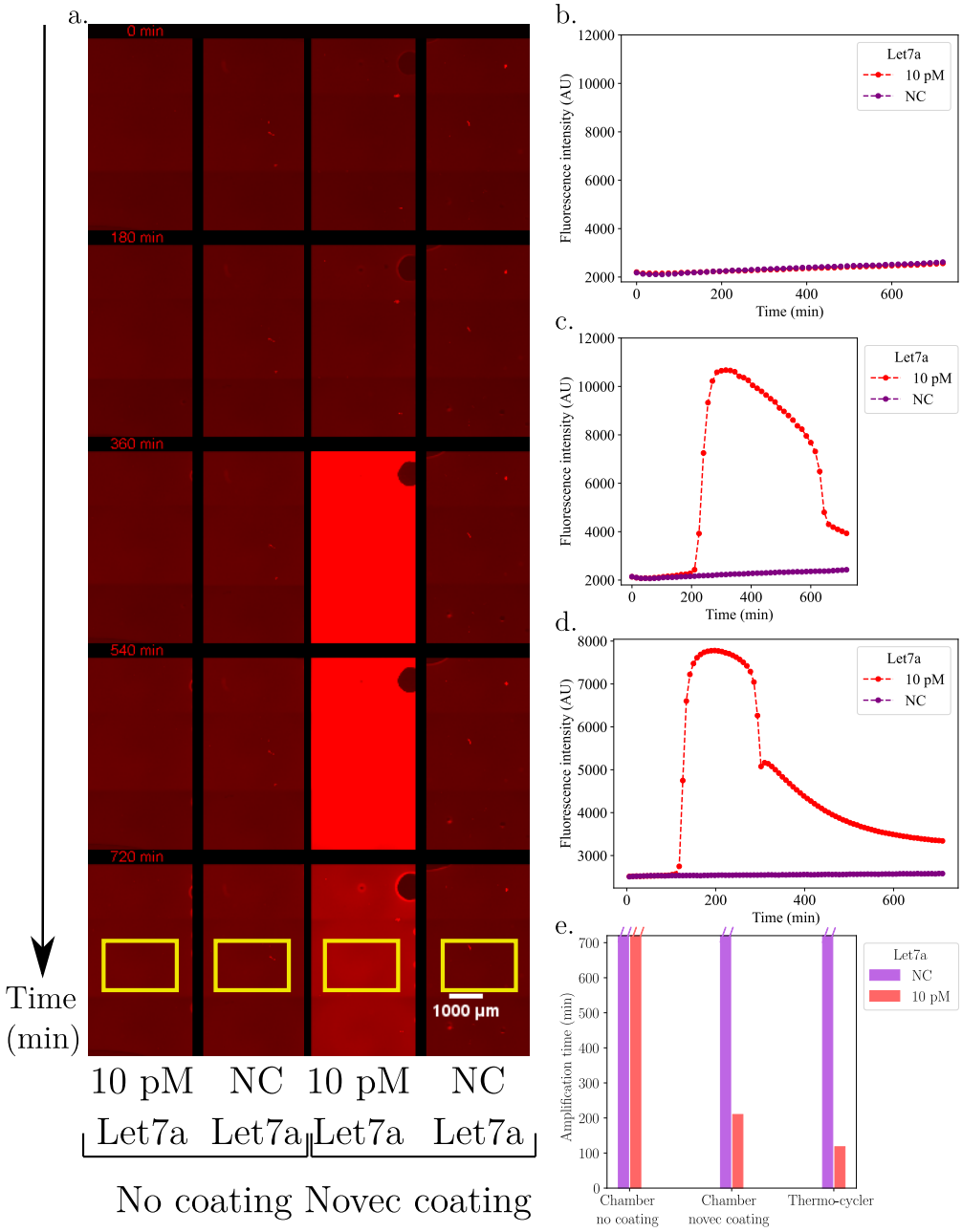

Figure 4.3: **Let7a detection in novec 1720 oil-coated glass chambers.** **a.** Glass chambers were coated or not with novec 1720 oil. PUMA amplification mixtures containing 10 pM and no Let7a were introduced in the chambers, which were then sealed with epoxy glue. The chambers were incubated at 50°C and fluorescence intensity was monitored in real-time via fluorescence microscopy. For each chamber, the fluorescence intensity in the yellow boxes has been averaged for each time point. **b.** Average fluorescence intensity in the non coated chambers in function of time for 10 pM and no Let7a. **c.** Average fluorescence intensity in the novec 1720 oil coated chambers in function of time for 10 pM and no Let7a. **d.** Fluorescence intensity in function of time for 10 pM and no Let7a in a thermo-cycler. **e.** Amplification times for the detection of 10 pM and no Let7a in coated or non coated chambers and in tubes in a thermo-cycler.

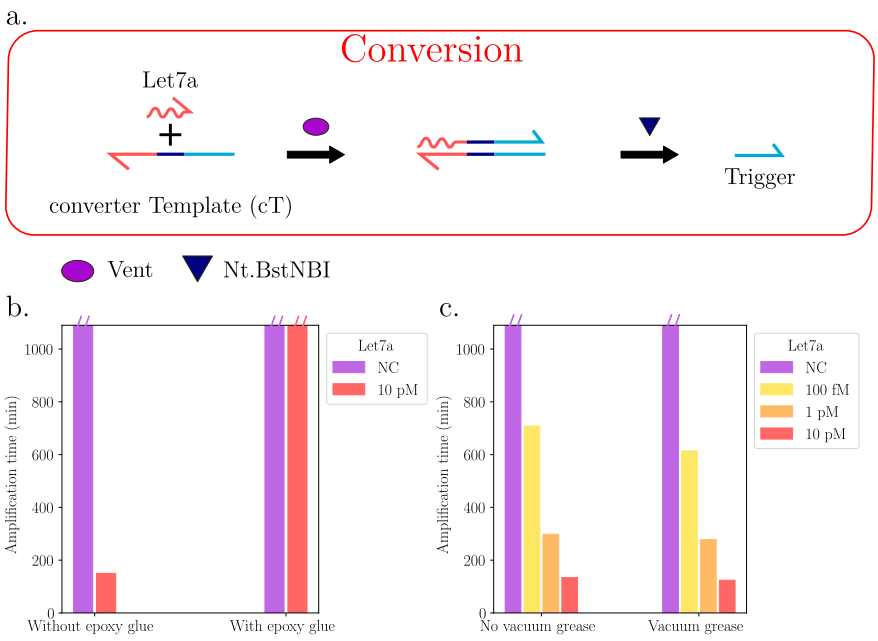

Figure 4.4: **Epoxy glue and vacuum grease toxicity assessment. a.** Principle of the conversion module. **b.** Let7a range. The tubes were coated or not with epoxy glue before adding the PUMA used for Let7a detection. The experiment was realized in tubes in a thermo-cycler. **c.** Let7a range. The tubes were coated or not with vaccum grease before adding the PUMA used for Let7a detection. The experiment was realized in tubes in a thermo-cycler.

4.4.2 PMMA ship

To avoid the manufacture of glass chambers and the passivation protocol, we then tested chambers made of poly (methyl methacrylate) (PMMA) materials that have no impact on PUMA activity. To assess the behaviour of a PUMA in those chambers, a PUMA for the detection of 10 pM and not Let7a was performed in PMMA chambers sealed with vaccum grease (figure 4.5.a.). The amplification started for 10 pM and no Let7a in PMMA chambers.

As observed in the chambers, amplifications were observed for 10 pM of Let7a in 150 min and for no Let7a in 240 min in the PMMA chambers (figure 4.5.b.). Meanwhile, in the thermo-cycler, the amplification started only for 10 pM of Let7a in 174 min (figure 4.5.c.). Moreover, a turn over can be observed in the PMMA chamber, showing that the PUMA is working properly in the PMMA chambers even if it is slower than in a thermo-cycler. Compared with the results obtained for novec 1720 oil coated chamber sealed with epoxy glue, the PMMA chambers sealed with vaccum grease seems to be better: the amplification for 10 pM of Let7a is starting almost at the same time than in the thermo-cycler (figure 4.3.d.). As it can be seen on figure 4.5.a., air bubbles have entered the chambers, causing a drop in the temperature and leading to an early nonspecific trigger production. With greater care in closing the chambers, this problem can easily be solved, delaying the nonspecific amplification of trigger.

To assess the possibility of obtaining a spatially localized start of the PUMA, biotinylated sT as well as Atto488 fluorescent dye were grafted on sepharose beads and placed in a PMMA chamber, sealed with vacuum grease, with a PUMA amplification mix (figure 4.6.a). As we can see in figure 4.6.b, from 10 min onwards, a localized departure can be observed on the beads carrying the biotinylated sT while no amplification is observed for the beads without template. This demonstrates the feasibility of localized PUMA start in a microfluidic device. However, this was realized for 3.10^8 self-triggered oligonucleotides per bead. For comparison, it corresponds to the number of miRNA in 10 μL at 50 pM. As we are targeting hundreds of femtomolar or picomolar concentrations, such experiment still has to be optimized to work with approximately 10 to 100 less self-triggered oligonucleotides and then with a miRNA / cT couple.

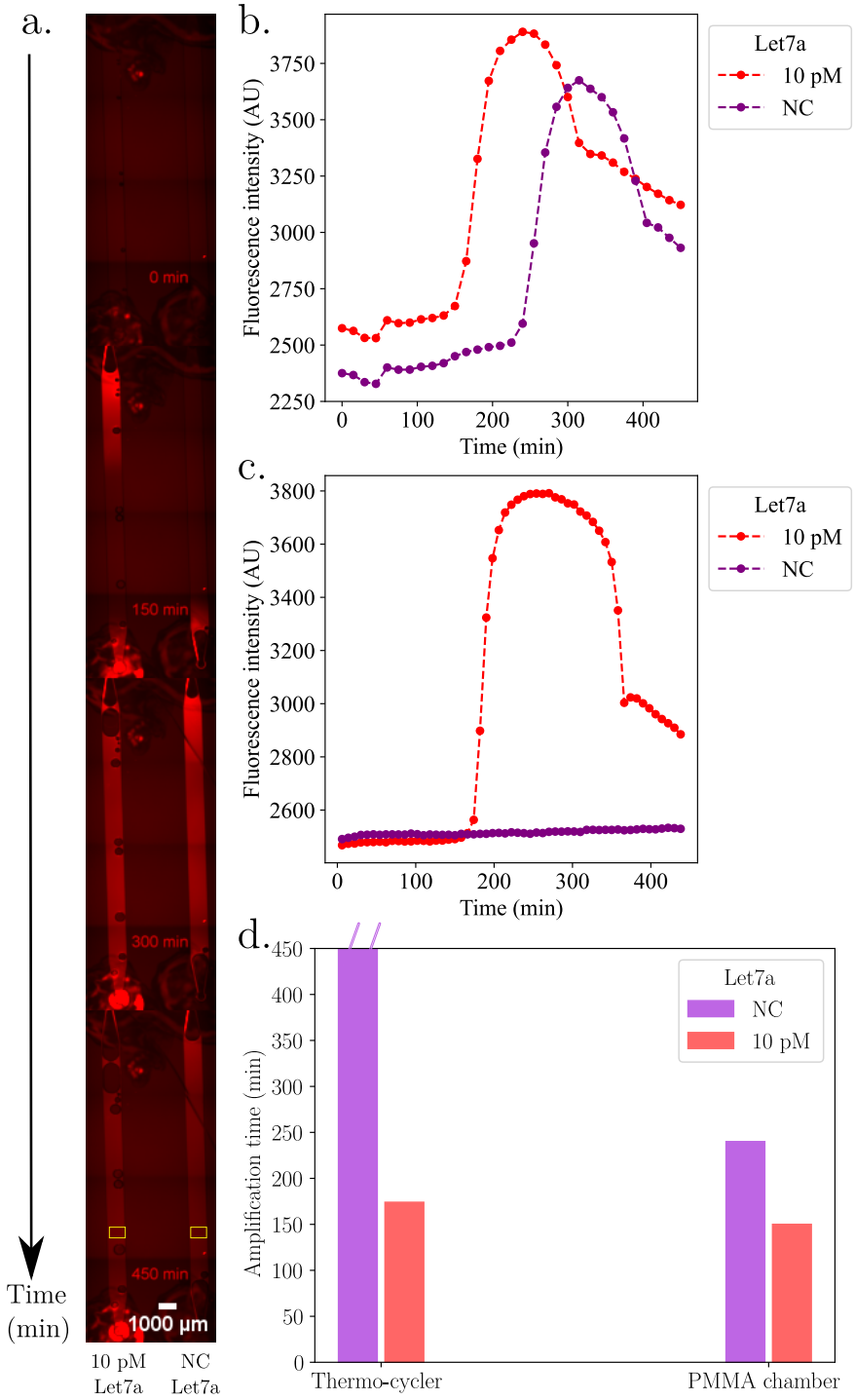

Figure 4.5: **Let7a detection in PMMA chambers. a.** PUMA amplification mixtures containing 10 pM and no Let7a were introduced in the PMMA chambers, which were then sealed with vacuum grease. The chambers were incubated at 50°C and fluorescence intensity was monitored in real-time via fluorescence microscopy. For each chamber, the fluorescence intensity in the yellow boxes has been averaged for each time point. **b.** Average fluorescence intensity in the PMMA chambers in function of time for 10 pM and no Let7a. **c.** Fluorescence intensity in function of time for 10 pM and no Let7a in a thermo-cycler. **d.** Amplification times for the detection of 10 pM and no Let7a in PMMA chambers and in tubes in a thermo-cycler.

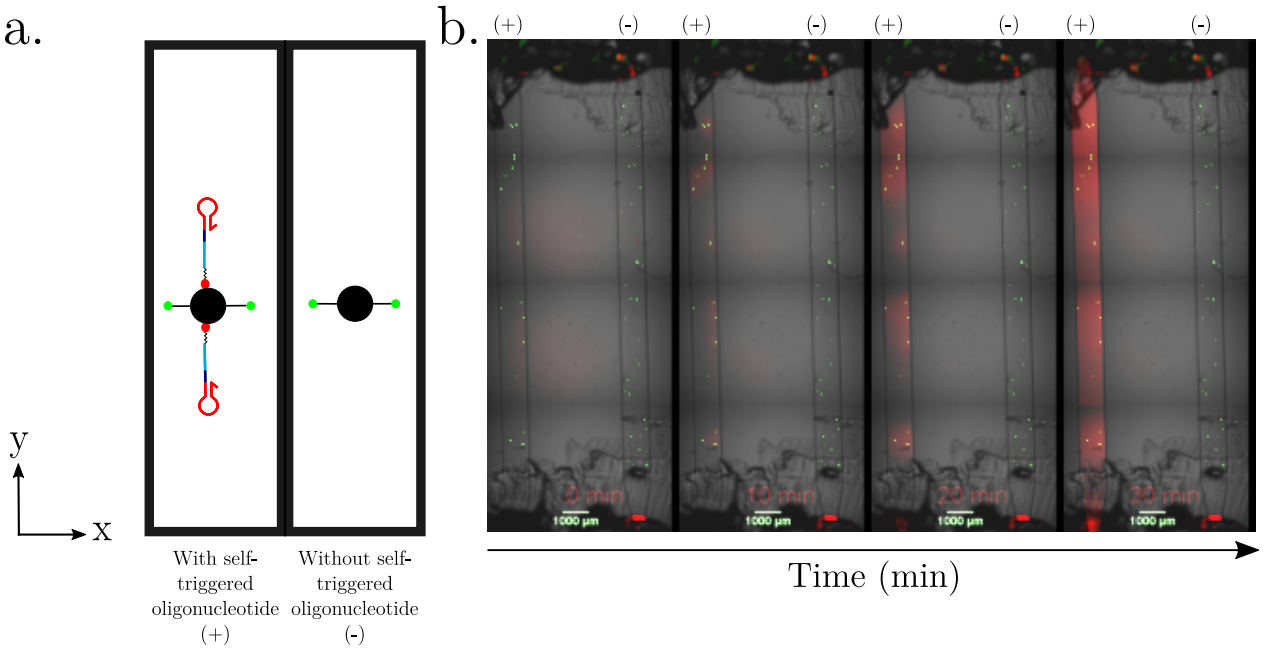

Figure 4.6: **On-bead sT in PMMA chambers. a.** Self-triggered oligonucleotide as well as Atto488 fluorescent dye were grafted on sepharose beads and placed in a PMMA chamber with a PUMA amplification mix (+). Atto488 fluorescent dye was grafted on sepharose beads and placed in a PMMA chamber with a PUMA amplification mix (-). **b.** A PUMA amplification mixture containing self-triggered oligonucleotide grafted fluorescent sepharose beads was introduced in a PMMA chamber (+) while a PUMA amplification mixture containing fluorescent sepharose beads was introduced in a PMMA chamber (-). The chambers were then sealed with vacuum grease, incubated at 50°C and fluorescence intensity was monitored in real-time via fluorescence microscopy.

4.4.3 Towards hydrogel grafting

Once the proof of principle of a localized start was obtained on beads, we decided to study the possibility of grafting a hydrogel onto a wall of a microfluidic chip and to functionalize this hydrogel. In the long term, our goal is to obtain a localized start around a hydrogel spot. We were interested in thiolated hylaronic acid (THA) [225], as our team has already acquired know-how in the synthesis and use of this hydrogel [211].

The first step was to see if it was possible to graft maleimide oligonucleotides onto THA beads synthesized by Dr. Sieskind. To do this, THA beads of 10 µm diameter and a fluorescent maleimide oligonucleotide were placed in a medium containing tris(2-carboxyethyl)phosphine (TCEP), reducing the disulfide bonds and thus leaving a thiol group on the hyaluronic acid which undergoes a Michael addition on maleimide groups. These beads were washed and imaged by fluorescence microscopy (figure 4.7.a.) The fluorescence intensity profile of a bead was extracted and plotted (figure 4.7.b.). We can see that it is possible to graft maleimide oligonucleotides after the production of the hydrogel by following this procedure.

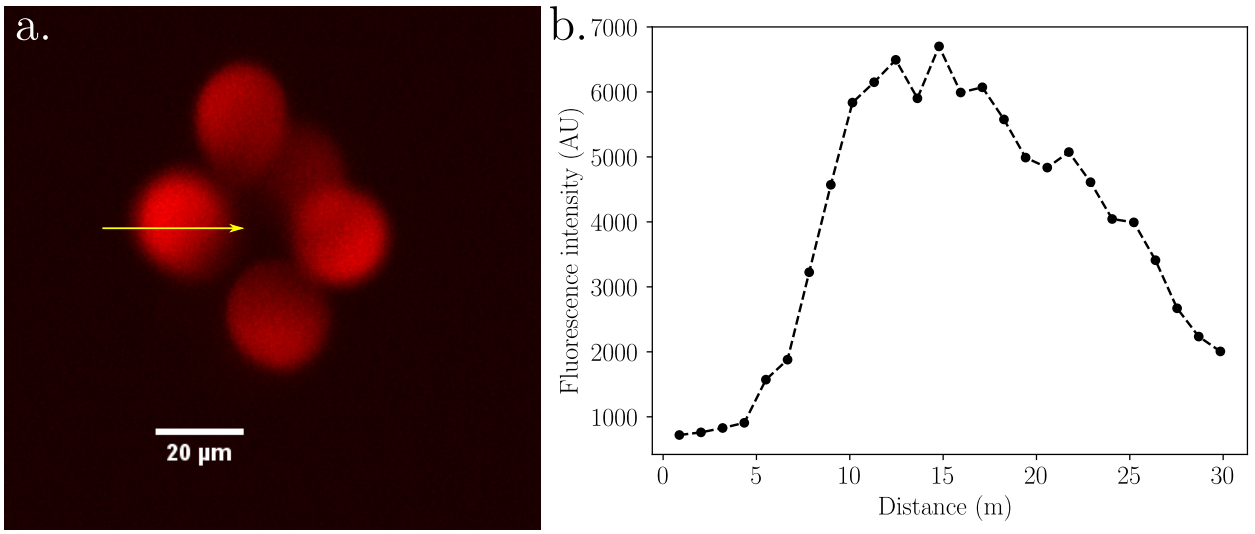

Figure 4.7: **Fluorescent oligonucleotide repartition on THA beads. a.** Image of a maleimide Cy5 oligonucleotide grafted THA beads obtained through fluorescent microscopy (20x). The intensity profile corresponding to the yellow arrow has been extracted. **b.** Fluorescent intensity profile of the maleimide Cy5 oligonucleotide grafted THA beads.

The second step was to functionalize THA beads with maleimide cTs. The beads were then introduced into a PUMA amplification mixture and a corresponding miRNA range was performed (figure 4.8.a.) This was done for 3 miRNAs: Let7a (figure 4.8.b.), mir17-5p (figure 4.8.c.) and mir132-3p (figure 4.8.d.). For each miRNA, two quantities of beads were tested: 800 and 25 000 beads. 25 000 beads enables the detection of 10 pM of each miRNA, which is not the case for 10 pM of mir132-3p with 800 THA beads. However, the higher the number of beads, the more cT and the faster the nonspecific amplification of trigger. Thus, 25 000 beads seems to be the best compromise but further experiments would be needed to find the optimum number of THA beads. Noteworhy, the increase of amount of beads, and thus of cT

is not correlated with an increase of leak for the mir132-3p-specific cT. Combined with the lack of sensitivity for mir132-3p detection, this suggests that this design is not very active. However, the results obtained for Let7a and mir17-5p detection demonstrates that miRNA detection is possible using maleimide cT grafed on THA. This is an important step towards the desired final microfluidic device.

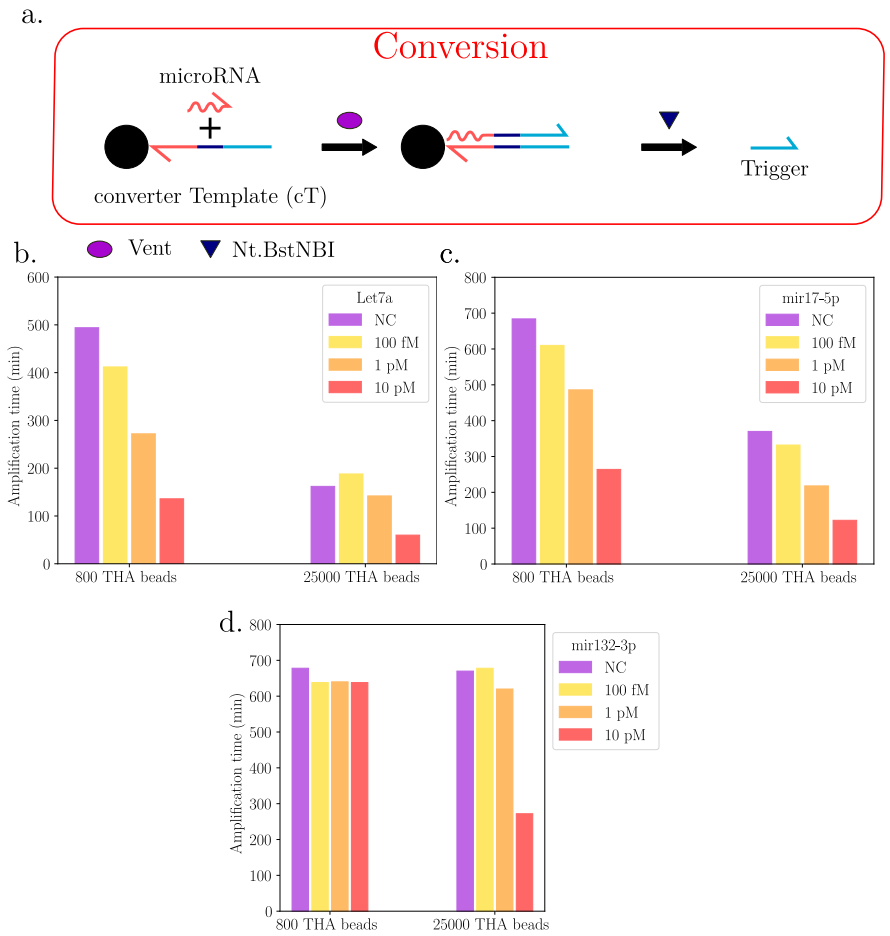

Figure 4.8: **miRNA detection with functionalized THA beads. a.** Conversion module principle. Converter templates are grafted on THA beads. The miRNA hybridizes to the cT, is extended by Vent polymerase and nicked by Nt.BstNBI, thus producing triggers. **b.** Let7a range in presence of 800 and 25 000 Let7a specific cT grafted THA beads. **c.** mir17-5p range in presence of 800 and 25 000 mir17-5p specific cT grafted THA beads. **d.** mir132-3p range in presence of 800 and 25 000 mir132-3p specific cT grafted THA beads.

Then, we decided to see if it was possible to incorporate a maleimide-Cy5 oligonucleotide in the THA polymer during its polymerisation in order to get a homogeneous repartition of this oligonucleotide. According to the protocol optimized by Dr. Sieskind, a mixture of THA with dylight405-maleimide and an malemide-Cy5 oligonucleotide in presence of TCEP was prepared and mixed with a solution of poly(ethylene glycol) divinyl sulfone (PEGDVS). The dylight405-maleimide is incorporated in the polymer to see the THA with fluorescent microscopy. As it can be observed in figure 4.9, the fluorescent images of the THA layer

obtained for the dylight405 and the Cy5 channels displayed the same pattern, showing an inhomogeneous repartition of malemide-Cy5 oligonucleotide in the polymerized THA.

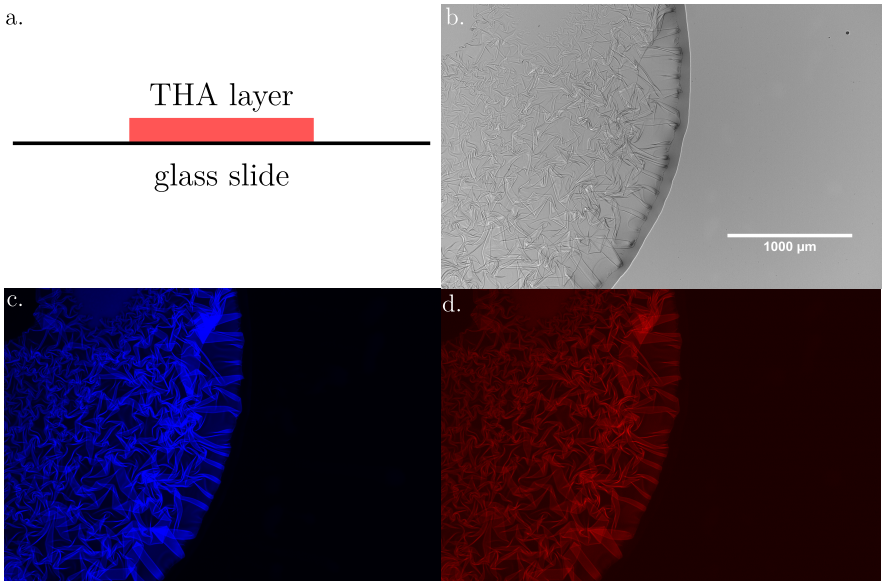

Figure 4.9: **THA polymerisation on a glass slide. a. b.** Bright Field image of the THA spot. **c.** Cascade Blue image of the THA spot. **d.** Cy5 image of the THA spot.

4.5 Silicon nanowires

In order to obtain an electrical output signal, the PUMA was interfaced with silicon nanowire based ion-sensitive field-effect transistors (ISFET) [226]. In this section will be shortly presented the principle of the performed experiments. The results presented in this section have been obtained with our calloborators at IEMN and at Aachen in the framework of the global ANR project.

Briefly, a ssDNA complementary to the PUMA produced trigger is grafted on the silicon nanowires. As the PUMA amplification takes place, trigger strands are produced and a fraction binds to its complementary grafted on silicon nanowires, leading to an accumulation of negative charge on the nanowires [227]. Thus, there is an increase of the density of negative charges at the solid-liquid interface, delineating the shift in the threshold voltage of the FET.

The interfacing between the PUMA with the silicon nanowire based ISFET has been realized step by step. First, only the amplification module (aT and pT) and the rT were present and the PUMA was activated by 1 nM or no trigger (figure 4.11). This allowed to compare the readout obtained by fluorescence in a thermo-cycler and the readout obtained with nanowire based ISFET set-up. A slight difference in amplification times was observed, most likely due to temperature control limitation in the nanowire based ISFET set-up. Then, Let7a and its corresponding cT were added to the PUMA, allowing the detection of 10 pM of Let7a (figure 4.12). Finally, the detection of 10 pM of Let7a was achieved in a media containing 10% of FBS, media used to mimic a physiological sample (figure 4.13).

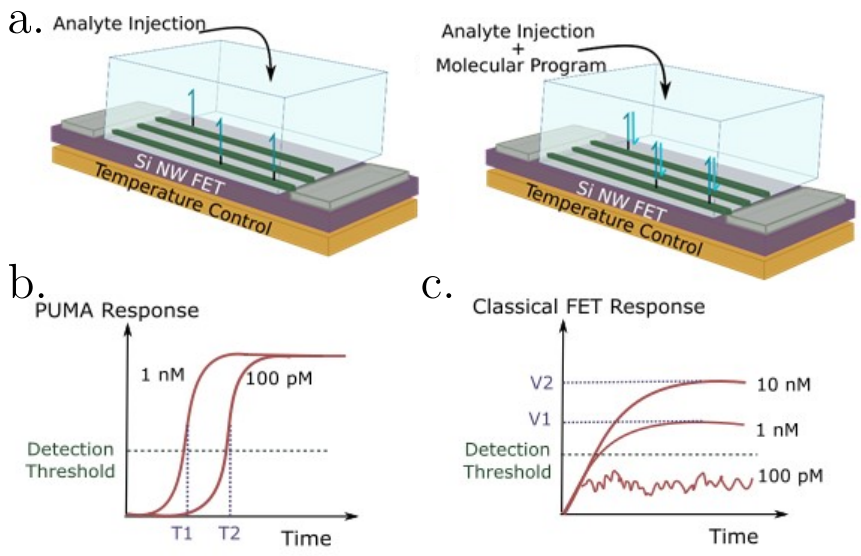

Figure 4.10: **PUMA coupling to Si NW FET principle. a.** The trigger complementary is grafted on silicon nanowires. In absence of the PUMA, injection of the targeted analyte will not induce trigger production (left). In presence of the PUMA, injection of the targeted analyte will induce trigger production, which will hybridizes to its complementary, locally increasing the negative charges around the nanowires (right). **b.** The output signal for the ISFET-PUMA is an amplification time which is correlated to the analyte concentration. **c.** The output signal for a classical FET system is a voltage value. Figure realized by Dr. Kaur.

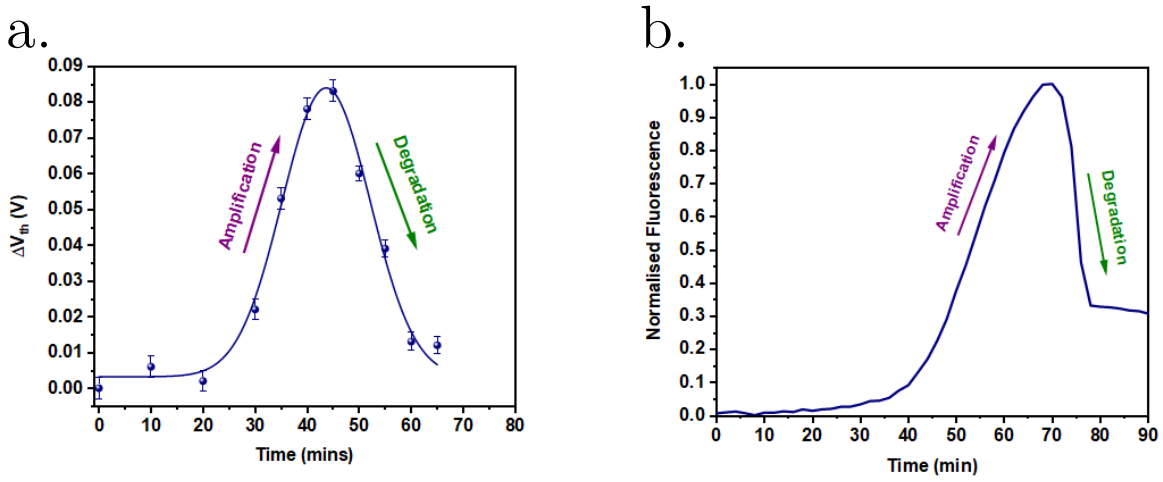

Figure 4.11: **Detection of trigger with PUMA coupled to Si NW FET.** A comparison of the PUMA's response as followed by **(a)** NW FET based readout and **(b)** standard fluorescence readout. Experiments and figure realized by Dr. Kaur.

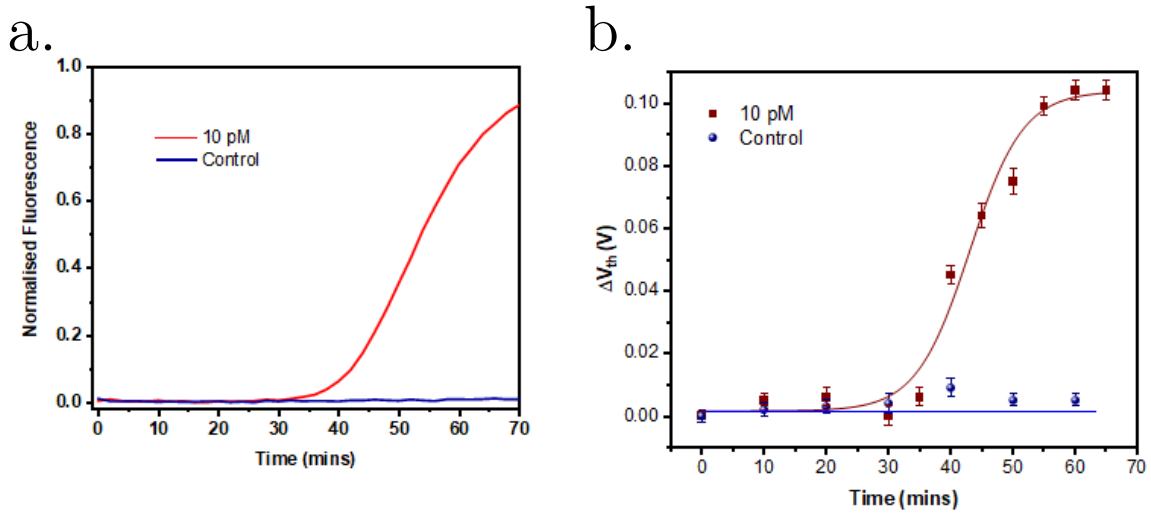

Figure 4.12: **Detection of Let7a with PUMA coupled to Si NW FET. a.** Time encoded electrical measurements for the PUMA with 10 pM Let7a and negative control (no miRNA) on Si NW FET and **b.** the corresponding fluorescent measurement in a thermocycler. Experiments and figure realized by Dr. Kaur.

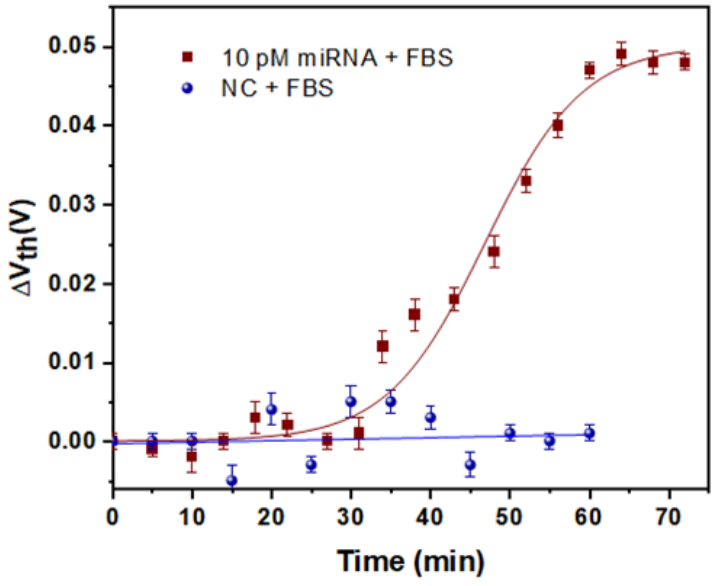

Figure 4.13: **Detection of Let7a in FBS with PUMA coupled to Si NW FET.** Si NW FET readout of 10 pM miRNA (brown) and negative control (blue) in Fetal Bovine Serum (10%). The lines are fitted to the time evolution of the system. Experiments and figure realized by Dr. Kaur.

4.6 Discussion

In this chapter, we have shown that coating of microfluidic glass chambers reduces the toxicity of glass on PUMA, coating with novec 1720 oil giving better results than coating with BSA, but is still not optimal. In addition, the material used to seal the chamber is important: epoxy glue is toxic while vacuum grease is not. Next, PMMA microfluidic chambers were tested. Sealed with vacuum grease, they showed no toxicity to PUMA. These chambers were used to obtain a localized start around beads carrying self-triggered oligonucleotides. However, the number of oligonucleotides was high: 3.10^8 oligonucleotides per bead. In comparison, this would correspond to capturing all the miRNA contained in 10 µL of sample at 50 pM on 1 bead. We therefore see that further experiments are needed to optimize the system and attempt to obtain a localized start with 10 to 100 times less oligonucleotides.

A first step was made towards grafting oligonucleotide onto a wall of a microfluidic chip. We want to use a hydrogel to achieve this: we chose THA. We were able to graft cTs onto THA beads, while retaining their functionality, and achieved the detection of miRNA in tubes. Furthermore, it was shown that it is possible to graft THA containing oligonucleotides onto a glass surface. Further experiments are needed to achieve grafting of cTs and to obtain a localized start around the THA spot. Ultimately, it seems possible to multiplex this approach, with different hydrogel spots each containing a different cT. Thus, PUMA activation around a hydrogel spot would provide information on the concentration of the corresponding targeted miRNA. The chemical diffusion rate could be problematic by imposing a large distance between each cT spot. To overcome this problem, it is possible to compartmentalize each THA spot after repartition of the PUMA amplification mixture.

Finally, the proof-of-principle obtained for the coupling of PUMA with ISFET based on silicon nanowires allows to obtain an electrical output signal. For an integrated chip, it is easier to implement an electronic readout than an optical one, thus greatly simplifying the needed set-up. This could allow the possibility of obtaining many different output signals if required, overcoming the current limitations of rT imposed by fluorophores [210].

Chapter 5

Conclusion and perspectives

5.1 Conclusion

miRNAs and proteins are promising biomarkers for early diagnosis of neurodegenerative diseases. The aim of this PhD project was to design a multiplexed detection method for the co-detection of miRNA and proteins.

In the first chapter, we introduced a cT-based capture step on particles, which made it possible to detect Let7a and mir7-5p in total miRNA extracted from mouse striatum while removing the inherent toxic effect of the biological matrix. We then explored a ligation-based capture step that restores the function of the converter template, reducing the non-specific production of trigger. We then tried to detect long nucleic acid sequence. We were able to detect at synthetic 108 nucleotides DNA target via a three-way junction approach.

In the second chapter, we presented an aptamer-based PEA method for human-alpha Thrombin detection down to 10 nM. To increase the sensitivity of the method, we moved to a supported approach. To that extent, we used a pair of antibodies, one to capture the target protein and the second one, biotinylated, to detect the protein. This last antibody was functionalized by oligonucleotides, allowing to interface the presence of the protein with our nucleic acid amplification chemistry. Substituting a traditional cT by a sT allowed to gain 3 orders of magnitude (LOD of 530 attoM) as compared to conventional ELISA test for mouse IL-12 p70 detection. This approach was used for the detection of two other proteins: IL-4 and INFg. Lastly, we attempted to design a protein classifier, to take into account several input signals, compute them resulting in one single output signal. The chemistry of the classifier is working with oligonucleotide inputs but is not fully optimal for the classification of protein signatures. Future work will aim at optimizing the grafting chemistry for the classifier to work with input proteins.

In the third chapter, we exposed a Ramos cells phenotyping proof of principle using a specific aptamer, TD05, to which we added a cT-detectable sequence. We showed that it is possible to discriminate TD05-TSB stained from unstained Ramos cells. We demonstrated that adding a percentage of cellular media in the PUMA amplification mixture increases the survival rate of the cells without impacting the detection performance. A nonspecific cell detection was also achieved using a cholesterol-labelled oligonucleotide.

In the fourth chapter, we compared PUMA behaviour into homemade microfluidic glass chambers and commercial PMMA chambers. We finally chose the PMMA chambers in

which a localized start of the PUMA was observed around sT-carrying sepharose beads. Finally, a THA layer containing maleimide fluorescent oligonucleotides was obtained, mapping the road towards a cT containing THA layer and, in longer term, the possibility to spatially multiplex miRNA detection using different THA spots.

5.2 Perspectives

Several directions can be explored in future works. Firstly, for miRNA detection, work remains to be done to optimized the ligation-based on particle capture step for miRNA detection. Ideally, the Bst 2.0 WS polymerase would be used, allowing to reach a quantitative detection in approximately 30 minutes. This results could then be used to detect relevant miRNAs, such as mir-301a-3p in the biological samples received from our collaborators of UASK. Finally, it would be interesting to detect these miRNAs in mouse feces.

Concerning the detection of long nucleic acids, the three-way junction process seems to be a promising path. Further experiments are needed to optimize the design of the 3WJ template and primer. As for miRNA detection, an improvement would be to use Bst 2.0 WS to reduce the amplification time.

Regarding protein detection, the sequences used for the PEA approach can be optimized, especially for sequences based on Nt.Bst.NBI nicking site. Indeed, we had time to test only two of them, which led to two very different results, highlighting the need to deepen our understanding of the PEA chemistry by combining a systematic experimental approach with a theoretical model of this proximity assay. Concerning the sT-based immuno PUMA, sT sequence and linker could be further optimized to further reduce the LOD. For the protein classifier method, there is a clear need for another type of linkage between antibodies and oligonucleotides. Indeed, though simple to implement, the biotin-streptavidin linkage is reversible and results in oligonucleotide exchange between the two target-specific detection antibodies. To circumvent this issue, covalent grafting of oligonucleotides should be implemented to hopefully lead to a functional protein classifier.

On the matter of cells phenotyping, it would also be possible to use the output of the PUMA to perform downstream molecular biology steps, for exemple RNA sequencing. To do so,it would be possible to co-encapsulate a cell and a hydrogel bead carrying DNA strands consisting of a unique molecular identifier (UMI) and reverse transcription primers. While in a standard RNA-sequencing pipeline, all cells that are coencapsulated with a bead are sequenced, PUMA-assisted sequencing would direct the sequencing only on the cells that display a given -user-selected - phenotype: the PUMA circuit will interpret the level of specific cell markers and in turn trigger (or not) the production of a DNA strand used to release the bead-bound reverse sequencing primers. Following reverse transcription, the emulsion is broken and only the free-floating cDNA products would be sequenced, after the beads are pulled down. By sequencing this mixture, one obtains the transcriptome only of the cells with the targeted phenotype. This application is particularly attractive in the case of rare cell sequencing, as it eliminates the tedious step of cell enrichment while reducing the sequencing background load.

In other words, the PUMA triggers the release of primers allowing to sequence only the cells with the desired phenotype. The resulting emulsion would then be broken, the

mixture centrifuged, and the supernatant recovered. This supernatant would contain only the reverse transcription data from cells with the targeted phenotype.

Several steps remains to be achieved before reaching spatial multiplexing for simultaneous detection of proteins and miRNAs. The first one is to obtained a localized start of the PUMA on a cT containing THA spot. Once this achieved, multiplexed miRNA detection could be reached. Then, in order to detect proteins, a capture antibody or aptamer could be grafted on a THA spot. By successive steps, a protein could be captured, labelled with sT-conjugated antibody or an aptamer and detected via the localised start of the PUMA on the THA spot.

Another way of multiplexing the detection of proteins and miRNA is to use barcoded particles. Different populations of particles, each of them targeting a different miRNA or protein could be mixed with a sample containing the target biomarkers. After a capture step, particles would be washed, recovered and added to a PUMA amplification mixture. Finally, the said mixture would be partitioned using water-in-oil droplets to get 0, 1 or a few particles per droplet, achieving digital detection. After droplet incubation, readout could be obtained by fluorescence microscopy or flow cytometry.

In the longer term, the industrialisation of one of these two multiplexing methods seems possible. In the case of spatial multiplexing, a microfluidic chip could be sold. A liquid biopsy sample would be loaded for a capture step. Then, a washing step would take place and the PUMA reconstituted from an enzyme premix and a template premix would be introduced. The chip would finally be incubated and an integrated electrical detection system would provide the result. In the case of particle-based multiplexing, kits of premixed particle subpopulations, designed to target a panel of miRNAs and proteins, would be prepared. These particles could then be mixed with a liquid biopsy sample for a capture step. The particles would then be washed and introduced in a reconstituted PUMA amplification mixture. The mixture would be partitioned using a microfluidic device included in the kit. After incubation, the readout could be obtained by automated flow cytometry.

For all methods presented, in the case of multiplexed detection, each target is quantified separately and a signature can be established by combining the results of the analyses. This is appropriate for the discovery of disease signatures but is laborious for the routine identification of these signatures in patients. Building on the information-processing of DNA circuits, complementary approaches could be developed to take into account the concentrations of different molecules and give a single output signal. Briefly, a DNA circuit is built to take integrate the concentration of the difference markers, such as miRNAs or proteins, process this information in-moleculo to finally report an output signal depending on the input concentrations (e.g. a fluorescent signal in the case where the disease signature is recognized). Such complex DNA circuits can adopt a boolean architecture [228] [229] [230] or mimick neural network classifiers [209] [193] [40]. This is a very recent field and work remains to be done to increase the sensitivity of these DNA circuits to reach concentrations relevant to medical diagnosis. Nevertheless, it looks promising and would transfer the complexity of the various methods currently used to amplification chemistry, allowing for low-cost, point of care tests.

Chapter 6

Material and methods

6.1 Chemicals

Oligonucleotides were purchased from Biomers (Germany) and Eurofins (Luxembourg). The sequences were purified by high-performance liquid chromatography (HPLC) and checked by matrix-assisted laser desorption/ionization mass spectrometry. Table 6.1 recapitulates all the sequences used throughout the study. All enzymes, except ttRecJ, were pruchased from New England Biolabs (NEB).

A 10-fold dilution of Nt.BstNBI was prepared by dissolving the stock enzyme in diluent A (NEB) supplemented with 0.1% Triton X-100.

6.2 Oligonucleotide sequences

Oligo name	**Sequence**	**Function**
α	GAATGACTCAC	Trigger
αtoα	C*A*G*T*CCAGAATGCAGTCCAGAA p	aT
pTα	T*T*T*T*TCAGTCCAGAATG p	pT
rTα	Atto633 *A*T*TCTGAATGCAGTCCAGAAT BHQ2	rT
Let7atoα	TGCAGTCCAGAAGTTTGACTCAAA-CTATACAACCTACTACCTCA p	cT
Let7atoα T7 biot	TGCAGTCCAGAAGTTTGACTCAAACTATA-CAACCTACTACCTCA TTTTTTT Biot	On-bead cT
133btoα	TGCAGTCCAGAA-GTTTGACTCA -TAGCTGGTTGAAGGGGACCAAA p	cT
7_5ptoαP	TGCAGTCCAGAA-GTTTGACTCA-AACAACAAAATCACTAGTCTTCCA p	cT
7_5ptoα T7 biot	TGCAGTCCAGAA-GTTTGACTCA-AACAACAAAATCACTAGTCTTCCA TTTTTTT Biot	On-bead cT
153_3ptoαP	TGCAGTCCAGAA-GTTTGACTCA-GATCACTTTTGTGACTATGCAA p	cT

mmu153_5ptoαP	TGCAGTCCAGAA-GTTTGACTCA-AGCTGCAACGTCACAAAAATGAC p	cT
hsa34b_5ptoαP	TGCAGTCCAGAA-GTTTGACTCA-CAATCAGCTAATGACACTGCCTA p	cT
mmu34b_5ptoαP	TGCAGTCCAGAA-GTTTGACTCA-ACAATCAGCTAATTACACTGCCT p	cT
mmu34b_3ptoαP	TGCAGTCCAGAA-GTTTGACTCA-GATGGCAGTGGAGTTAGTGATT p	cT
34c_5ptoαP	TGCAGTCCAGAA-GTTTGACTCA-GCAATCAGCTAACTACACTGCCT p	cT
10a_5ptoαP	TGCAGTCCAGAA-GTTTGACTCA-CACAAATTCGGATCTACAGGGTA p	cT
10a_5pto*alpha* T7 biot	TGCAGTCCAGAA-GTTTGACTCA-CACAAATTCGGATCTACAGGGTA TTTTTTT Biot	On-bead cT
10b_5ptoαP	TGCAGTCCAGAA-GTTTGACTCA-CACAAATTCGGTTCTACAGGGTA p	cT
212_3ptoαP	TGCAGTCCAGAA-GTTTGACTCA-TGGCCGTGACTGGAGACTGTTA p	cT
132_3ptoαP	TGCAGTCCAGAA-GTTTGACTCA-CGACCATGGCTGTAGACTGTTA p	cT
495_3ptoαP	TGCAGTCCAGAA-GTTTGACTCA-AAGAAGTGCACCATGTTTGTTT p	cT
17_5ptoαP	TGCAGTCCAGAA-GTTTGACTCA-CTACCTGCACTGTAAGCACTTTG p	cT
130a_3ptoαP	TGCAGTCCAGAA-GTTTGACTCA-AUGCCCTTTTAACATTGCACTG p	cT
134_5ptoαP	TGCAGTCCAGAA-GTTTGACTCA-CCCCTCTGGTCAACCAGTCACA p	cT
136_5ptoαP	TGCAGTCCAGAA-GTTTGACTCA-CCATCATCAAAACAAATGGAGT p	cT
301a_3ptoαP	TGCAGTCCAGAA-GTTTGACTCA-GCTTTGACAATACTATTGCACTG p	cT
140_5ptoαP	TGCAGTCCAGAA-GTTTGACTCA-CTACCATAGGGTAAAACCACTG p	cT
1983toαP	TGCAGTCCAGAA-GTTTGACTCA-AGAAAACATGCTCCAGGTGAG p	cT
cel_248toαP	TGCAGTCCAGAA-GTTTGACTCA-TGAGCGTTATCCGTGCACGTGTAT p	cT
39-cetoα T7 biot	TG-CAGTCCAGAA-GTTTGACTC-A-CAAGCTGATTTACACCC TTTTTTT Biot	On-bead cT
Let7a	UGAGGUAGUAGGUUGUAUAGUU	miRNA

DLet7a	TGAGGTAGTAGGTTGTATAGTT	DNA target
mir133b	UUUGGUCCCCUUCAACCAGCUA	miRNA
miR-7-5p	UGGAAGACUAGUGAUUUUGUUGUU	miRNA
miR-153-3p	UUGCAUAGUCACAAAAGUGAUC	miRNA
mmu-miR-153-5p	GUCAUUUUUGUGACGUUGCAGCU	miRNA
hsa-miR-34b-5p	UAGGCAGUGUCAUUAGCUGAUUG	miRNA
mmu-miR-34b-5p	AGGCAGUGUAAUUAGCUGAUUGU	miRNA
mmu-miR-34b-3p	AAUCACUAACUCCACUGCCAUC	miRNA
miR-34c-5p	AGGCAGUGUAGUUAGCUGAUUGC	miRNA
miR-10a-5p	UACCCUGUAGAUCCGAAUUUGUG	miRNA
miR-10b-5p	UACCCUGUAGAACCGAAUUUGUG	miRNA
miR-212-3p	UAACAGUCUCCAGUCACGGCCA	miRNA
miR-132-3p	UAACAGUCUACAGCCAUGGUCG	miRNA
miR-495-3p	AAACAAACAUGGUGCACUUCUU	miRNA
mmu-mir-17-5p	CAAAGUGCUUACAGUGCAGGUAG	miRNA
mmu-miR-130a-3p	CAGUGCAAUGUUAAAAGGGCAU	miRNA
mmu-miR-134-5p	UGUGACUGGUUGACCAGAGGGG	miRNA
mmu-miR-136-5p	ACUCCAUUUGUUUUGAUGAUGG	miRNA
mmu-miR-301a-3p	CAGUGCAAUAGUAUUGUCAAAGC	miRNA
mmu-miR-140-5p	CAGUGGUUUUACCCUAUGGUAG	miRNA
mmu-miR-1983	CUCACCUGGAGCAUGUUUUCU	miRNA
cel-miR-248	AUACACGUGCACGGAUAACGCUCA	miRNA
mir-39-ce	UCACCGGGUGUAAAUCAGCUUG	miRNA
Let7atoα_ lig1_T5_B	p CTACTACCTCA TTTTT Biot	Lig1 oligonu-cleotide
Let7atoα lig2	TG-CAGTCCAGAA-GAGA GACTC AC -AACTATACAAC	Lig2 oligonu-cleotide
301a_3p_toα_ lig1T5B	p ACTATTGCACTG TTTTT Biot	Lig1 oligonu-cleotide

301a_3p_toα lig2	TG-CAGTCCAGAA-GAGA GACTC AC - GCTTTGACAAT	Lig2 oligonu-cleotide
mir31*toα ligout_B	TG-CAGTCCAGAA-GAGA GACTC AC TTTTT - GATGGCAATAT GTTGGCATAGCA TTTTT Biot	Lig-out oligonu-cleotide
mir31*toα_ lig1_T5_B	GTTGGCATAGCA TTTTT Biot	Lig1 oligonu-cleotide
mir31*toα lig2	TG-CAGTCCAGAA-GAGA GACTC AC TTTTT - GATGGCAATAT	Lig2 oligonu-cleotide
301a_3ptoα ligout(2)_B	TG-CAGTCCAGAA-GAGA GACTC AC -TTTTT GCTTTGACAATACTATTGCACTG TTTTT	Lig-out oligonu-cleotide
301a_3p_toα lig2 (2)	TG-CAGTCCAGAA-GAGA GACTC AC TTTTT - GCTTTGACAAT	Lig2 oligonu-cleotide
136_5ptoα ligout_Biot	TGCAGTCCAGAA-GTTTGACTCA TTTTT -CCATCATCAAA ACAAATGGAGT TTTTT	Lig-out oligonu-cleotide
136_5pToα lig1_T5_B	ACAAATGGAGT TTTTT Biot	Lig1 oligonu-cleotide
136_5pToα lig2	TGCAGTCCAGAA-GTTTGACTCA TTTTT -CCATCATCAAA	Lig2 oligonu-cleotide
Let7atoα lig2(2)	TG-CAGTCCAGAA-GAGA GACTC AC TTTTT -AACTATACAAC	Lig2 oligonu-cleotide
Let7atoα_ ligout(2)B	TG-CAGTCCAGAA-GAGA GACTC AC TTTTT -AACTATACAACCTACTACCTCA TTTTT	Lig-out oligonu-cleotide
cel_248toα ligout_B	TG-CAGTCCAGAA-GAGA GACTC AC-TTTTT - TGAGCGTTATCC GTGCACGTGTAT TTTTT	Lig-out oligonu-cleotide
cel_248toα lig2	TG-CAGTCCAGAA-GAGA GACTC AC-TTTTT - TGAGCGTTATCC	Lig2 oligonu-cleotide
cel_248toα lig1_T5_B	GTGCACGTGTAT TTTTT Biot	Lig1 oligonu-cleotide
β	CATTCATCCCAG	Trigger

βtoβ	C*T*G*GGATGAATGCTGGGATGAA p	aT
pT β	T*T*T*TT CTGGGATGAATG p	pT
rTβ	Atto633 *A*T*TCATAATGCTGGGATGAAT BHQ2	rT
Let7a++	UGA GGU AGU AGG UUG UAU AGUU GCTAA	modified miRNA
Let7atoβ	TGCTGGGATGAA-GTTTG ACT C-AACT ATA CAA CCT ACT ACC TCA p	cT
ms2t1toβ	TGCTGGGATGAAGTTTGACTCAAAAAACGAGAG AAAGATCGCGAGGAAGATCAATACATAAA-GAGT	cT
mst4toβ	TGCTGGGATGAAGTTTGACTCAAAAAA GAATATAGCTCTGGTGGTT p	cT
mst5toβ	TGCTGGGATGAAGTTTGACTCAAAAAA GAGCGGATACGATCGAGATATT p	cT
mst6toβ	TGCTGGGATGAAGTTTGACTCAAAAAA GGAAAATAGTTCCCATCGTATT p	cT
mst7toβ	TGCTGGGATGAAGTTTGACTCAAAAAA GAACCCATTTCCCATTT p	cT
MS2- HS1	GGGGGAGGCGCTGCATCCTGCAACTTGTGCC CCATAGGAGCACCGTTGGAGAACGTGCATTGC-CCGGGGG	HS
MS2- HS2	ATAAAGACCGCGTGTCTGATCCACGGCGC ACATTGGTCTCGGACCAATAGAGCCGCTCTCA-GAGCAAAAA	HS
MS2- HS3	TTTTTAACTCCACACCAGGCGATCGGAGA TGGAATCGGATGCAGACGATAAGTC-TATCGTCGCAATTTTT	HS
MS2- HS4	ATATTAAAATAGTTCCCATCGTATCGTCTC GCCATCTACGATTCCGTAGTGTGAGCGGATAC-GATTTATA	HS
MS2- HS5	TTTTTTTACCAAAATGGATTTGGGTCGCT TTGACTATTGCCCAGAATATCATGGACTC-TAGCTCATTATA	HS
mGFP 3WJ2_left P	TGCTGGGATGAA GAGA GACTC CTACTTGAAT T CGCCGTAGGTCAGGG p	3WJ template
mGFP 3WJ2_right_6	CGGCTGAAGCACTGC T ATTCAA	3WJ primer
mGFP 3WJ2_right_8	CGGCTGAAGCACTGC T ATTCAAGT	3WJ primer
mGFP_3WJ2 DNA_target	CCGGCAAGCTGCCCGTGCCCTGGCCCACCCTCG TGACCACCCTGACCTACGGCGTGCAGTGCTT CAGCCGCTACCCCGACCACATGAAGCAGCAC-GACTTCTTCAAGT	DNA target

mGFP_capture _3 biot_3	AGAAGTCGTGCTGCTTCATG TTTTTTTTTT Biot	capture strand
mGFP_capture _1 biot_3	GGCCAGGGCACGGGCAGCTTAA TTTTTTTTTT Biot	capture strand
15 mer (Thrombin)	GGTTGGTGTGGTTGG	aptamer
29 mer (Thrombin)	AGTCCGTGGTAGGGCAGGTTGGGGTGACT	aptamer
Veap121 (VEGF165)	TGTGGGGGTGGACGGGCCGGGTAGA	aptamer
SL2-B (VEGF165)	CAATTGGGCCCGTCCGTATGGTGGGT	aptamer
Scrambled 15-mer	GTGGTTGGTGGTTGG	scrambled aptamer
Scrambled Veap121	GGGGGTGTGAGCGGTCGCGGGTAGA	scrambled aptamer
Scrambled SL2B	CCCTGCCCAGGGATTGTATGGTGGGT	scrambled aptamer
SL2-Btoα NBI (10)	TGCAGTCCAGAAGTTTGACTCAACCCACCATATT	cT
SL2-Btoα NBI (8)	TGCAGTCCAGAAGTTTGACTCAACCCACCAAT	cT
mT_29mertoα BssSI (8)	TTCTGGACTGCTCGTGAGTCACCCTT	caged trigger
mT_29mertoα BssSI (6)	TTCTGGACTGCTCGTGAGTCACTT	caged trigger
mT_29mertoα BssSI (4)	TTCTGGACTGCTCGTGAGTCTT	caged trigger
15mer_T12B act	GGTTGGTGTGGTTGGTTTTTTTTTTTTTT CAAGTAG	PEA aptamer
29mer_T12_cT	CTAACTGAATGCTACTTGAATGTTTTTTTTTTTT AGTCCGTGGTAGGGCAGGTTGGGGTGACT	PEA aptamer
29mer_T12B act	AGTCCGTGGTAGGGCAGGTTGGGGTGAC TTTTTTTTTTTTTTTCAAGTAG	PEA aptamer
15mer_T12_cT	CTAACTGAATGCTACTTGAATGTTTTTTTTTTTT GGTTGGTGTGGTTGG	PEA aptamer
S_T_29mer _T12 act	GAGTCGGGAGCGCTAGAGGTGTGGTTCG TTTTTTTTTTTTT TTCAAGTAG	PEA Scrambled aptamer
S_T_15mer _T12_cT	CTAACTGAATGCTACTTGAATGTTTTTTTTTTTT GGTGTTGGTTTGGGG	PEA Scrambled aptamer

VEAP121 _T12 act	TGTGGGGGTGGACGGGCCGGGTAGA TTTTTTTTTTTTT TTCAAGTAG	PEA aptamer
VEAP121 _T12_cT	CTAACTGAATGCTACTTGAATGTTTTTTTTTTTTT TGTGGGGGTGGACGGGCCGGGTAGA	PEA aptamer
SL2B_T12B act	CAATTGGGCCCGTCCGTATGGTGGGT TTTTTTTTTTTTT TTCAAGTAG	PEA aptamer
SL2B_T12 _cT	CTAACTGAATGCTACTTGAATGTTTTTTTTTTTTT CAATTGGGCCCGTCCGTATGGTGGGT	PEA aptamer
IG_25mer _T12B act	TGTTAGGGGGTTGGTTTTGGGTTGG TTTTTTTTTTTTT TTCAAGTAG	PEA aptamer
IG_25mer _T12_cT	CTAACTGAATGCTACTTGAATGTTTTTTTTTTTTT TGTTAGGGGGTTGGTTTTGGGTTGG	PEA aptamer
IG_34mer _T12B act	GGGGTTGGTTGTGTTGGGTGTTGTGTCCAACC CC TTTTTTTTTTTTT TTCAAGTAG	PEA aptamer
INFG_34mer _T12_cT	CTAACTGAATGCTACTTGAATGTTTTTTTTTTTTT GGGGTTGGTTGTGTTGGGTGTTGTGTCCAAC-CCC p	PEA aptamer
T_29mer _T12 act -1_V2	AGTCCGTGGTAGGGCAGGTTGGGGTGAC TTTTTTTTTTTTTATCAAGTAG	PEA aptamer
T_15merT12cT _NBI	CTAACTGAATG GAGA GACTC CTACTTGAAT-GTTTTTTTTTTTTGGTTGGTGTGGTTGG	PEA aptamer
TNF_25mer _T12B act	TGGTGGATGGCGCAGTCGGCGACAA TTTTTTTTTTTTT TTCAAGTAG	PEA aptamer
TNF_25mer _T12_cT	CTAACTGAATGCTACTTGAATGTTTTTTTTTTTTT TGGTGGATGGCGCAGTCGGCGACAA	PEA aptamer
VEGF_25mer _T12B act	CCGTCTTCCAGACAAGAGTGCAGGG TTTTTTTTTTTTT TTCAAGTAG	PEA aptamer
VEGF_25mer _T12_cT	CTAACTGAATGCTACTTGAATGTTTTTTTTTTTTT CCGTCTTCCAGACAAGAGTGCAGGG	PEA aptamer
29mer_T12B act(2)	AGTCCGTGGTAGGGCAGGTTGGGGTGAC TTTTTTTTTTTTTTTTCAATTAG	PEA aptamer
15mer_T12 _cT(2)	CTAATTGAATGCTACTTGAATG TTTTTTTTTTTTGGTTGGTGTGGTTGG	PEA aptamer
15merT12_cT _V2	CTAACTGAATG CTAATTGAATG TTTTTTTTTTTTGGTTGGTGTGGTTGG	PEA aptamer
T_15merT12 _NBItoγ _GAGA	CTAACTGAATG GAGA GACTC TTTTTTTTTTTTGGTTGGTGTGGTTGG	PEA aptamer
T_29mer_T12 _rNBI_GAGA	AGTCCGTGGTAGGGCAGGTTGGGGTGAC TTTTTTTTTTTTTTT GAGTCTCTC	PEA aptamer
T_15merT12 _NBItoγ _GATT	CTAACTGAATG GATT GACTC TTTTTTTTTTTTGGTTGGTGTGGTTGG	PEA aptamer

T_29mer_T1 2_rNBI_GATT	AGTCCGTGGTAGGGCAGGTTGGGGTGAC TTTTTTTTTTTTTTT GAGTCAATC	PEA aptamer
NBItoαP Sp18T5Biot	Biot TTTTT/intsp18/ TGCAGTCCAGAAGTTTGACTCA- CATTGCTTCATTTTGAAGCAATGT GAGT	sT
NBItoαP int Biot	Biot TGCAGTCCAGAAGTTTGACTCA- CATTGCTTCATTT/biot/TTTGAAGCAATGT GAGT	sT
NBItoα _GAAT_AC	TG-CAGTCCAGAA-GAAT GACTC - ACATTGCTTCA TTT TGAAGCAAT	sT
NBItoα _AAAT_AC	TG-CAGTCCAGAA-AAAT GACTC - ACATTGCTTCA TTT TGAAGCAAT	sT
NBItoα _ATAT_AC	TG-CAGTCCAGAA-ATAT GACTC - ACATTGCTTCA TTT TGAAGCAAT	sT
NBItoα _AGAT_AC	TG-CAGTCCAGAA-AGAT GACTC - ACATTGCTTCA TTT TGAAGCAAT	sT
NBItoα _ACAT_AC	TG-CAGTCCAGAA-ACAT GACTC - ACATTGCTTCA TTT TGAAGCAAT	sT
NBItoα _TAAT_AC	TG-CAGTCCAGAA-TAAT GACTC - ACATTGCTTCA TTT TGAAGCAAT	sT
NBItoα _TTAT_AC	TG-CAGTCCAGAA-TTAT GACTC - ACATTGCTTCA TTT TGAAGCAAT	sT
NBItoα _TGAT_AC	TG-CAGTCCAGAA-TGAT GACTC - ACATTGCTTCA TTT TGAAGCAAT	sT
NBItoα _TCAT_AC	TG-CAGTCCAGAA-TCAT GACTC - ACATTGCTTCA TTT TGAAGCAAT	sT
NBItoα _GTAT_AC	TG-CAGTCCAGAA-GTAT GACTC - ACATTGCTTCA TTT TGAAGCAAT	sT
NBItoα _GGAT_AC	TG-CAGTCCAGAA-GGAT GACTC - ACATTGCTTCA TTT TGAAGCAAT	sT
NBItoα _GCAT_AC	TG-CAGTCCAGAA-GCAT GACTC - ACATTGCTTCA TTT TGAAGCAAT	sT
NBItoα _CAAT_AC	TG-CAGTCCAGAA-CAAT GACTC - ACATTGCTTCA TTT TGAAGCAAT	sT
NBItoα _CTAT_AC	TG-CAGTCCAGAA-CTAT GACTC - ACATTGCTTCA TTT TGAAGCAAT	sT
NBItoα _CGAT_AC	TG-CAGTCCAGAA-CGAT GACTC - ACATTGCTTCA TTT TGAAGCAAT	sT
NBItoα _CCAT_AC	TG-CAGTCCAGAA-CCAT GACTC - ACATTGCTTCA TTT TGAAGCAAT	sT
NBItoα _GAAA_AC	TG-CAGTCCAGAA-GAAA GACTC - ACATTGCTTCA TTT TGAAGCAAT	sT

NBItoα _GAAG_AC	TG-CAGTCCAGAA-GAAG GACTC - ACATTGCTTCA TTT TGAAGCAAT	sT
NBItoα _GAAC_AC	TG-CAGTCCAGAA-GAAC GACTC - ACATTGCTTCA TTT TGAAGCAAT	sT
NBItoα _GATA_AC	TG-CAGTCCAGAA-GATA GACTC - ACATTGCTTCA TTT TGAAGCAAT	sT
NBItoα _GATT_AC	TG-CAGTCCAGAA-GATT GACTC - ACATTGCTTCA TTT TGAAGCAAT	sT
NBItoα _GATG_AC	TG-CAGTCCAGAA-GATG GACTC - ACATTGCTTCA TTT TGAAGCAAT	sT
NBItoα _GATC_AC	TG-CAGTCCAGAA-GATC GACTC - ACATTGCTTCA TTT TGAAGCAAT	sT
NBItoα _GAGA_AC	TG-CAGTCCAGAA-GAGA GACTC - ACATTGCTTCA TTT TGAAGCAAT	sT
NBItoα _GAGT_AC	TG-CAGTCCAGAA-GAGT GACTC - ACATTGCTTCA TTT TGAAGCAAT	sT
NBItoα _GAGG_AC	TG-CAGTCCAGAA-GAGG GACTC - ACATTGCTTCA TTT TGAAGCAAT	sT
NBItoα _GAGC_AC	TG-CAGTCCAGAA-GAGC GACTC - ACATTGCTTCA TTT TGAAGCAAT	sT
NBItoα _GACA_AC	TG-CAGTCCAGAA-GACA GACTC - ACATTGCTTCA TTT TGAAGCAAT	sT
NBItoα _GACT_AC	TG-CAGTCCAGAA-GACT GACTC - ACATTGCTTCA TTT TGAAGCAAT	sT
NBItoα _GACG_AC	TG-CAGTCCAGAA-GACG GACTC - ACATTGCTTCA TTT TGAAGCAAT	sT
NBItoα _GACC_AC	TG-CAGTCCAGAA-GACC GACTC - ACATTGCTTCA TTT TGAAGCAAT	sT
NBItoα _GAAT_AA	TG-CAGTCCAGAA-GAAT GACTC - AAATTGCTTCA TTT TGAAGCAAT	sT
NBItoα _GAAT_AT	TG-CAGTCCAGAA-GAAT GACTC - ATATTGCTTCA TTT TGAAGCAAT	sT
NBItoα _GAAT_AG	TG-CAGTCCAGAA-GAAT GACTC - AGATTGCTTCA TTT TGAAGCAAT	sT
NBItoα _GAAT_TA	TG-CAGTCCAGAA-GAAT GACTC - TAATTGCTTCA TTT TGAAGCAAT	sT
NBItoα _GAAT_TT	TG-CAGTCCAGAA-GAAT GACTC - TTATTGCTTCA TTT TGAAGCAAT	sT
NBItoα _GAAT_TG	TG-CAGTCCAGAA-GAAT GACTC - TGATTGCTTCA TTT TGAAGCAAT	sT
NBItoα _GAAT_TC	TG-CAGTCCAGAA-GAAT GACTC - TCATTGCTTCA TTT TGAAGCAAT	sT

NBItoα _GAAT_GA	TG-CAGTCCAGAA-GAAT GACTC - GAATTGCTTCA TTT TGAAGCAAT	sT
NBItoα _GAAT_GT	TG-CAGTCCAGAA-GAAT GACTC - GTATTGCTTCA TTT TGAAGCAAT	sT
NBItoα _GAAT_GG	TG-CAGTCCAGAA-GAAT GACTC - GGATTGCTTCA TTT TGAAGCAAT	sT
NBItoα _GAAT_GC	TG-CAGTCCAGAA-GAAT GACTC - GCATTGCTTCA TTT TGAAGCAAT	sT
NBItoα _GAAT_CA	TG-CAGTCCAGAA-GAAT GACTC - CAATTGCTTCA TTT TGAAGCAAT	sT
NBItoα _GAAT_CT	TG-CAGTCCAGAA-GAAT GACTC - CTATTGCTTCA TTT TGAAGCAAT	sT
NBItoα _GAAT_CG	TG-CAGTCCAGAA-GAAT GACTC - CGATTGCTTCA TTT TGAAGCAAT	sT
NBItoα _GAAT_CC	TG-CAGTCCAGAA-GAAT GACTC - CCATTGCTTCA TTT TGAAGCAAT	sT
NBItoα _GGTT_AC	TG-CAGTCCAGAA-GGTT GACTC - ACATTGCTTCA TTT TGAAGCAAT	sT
NBItoα _GGAA_AC	TG-CAGTCCAGAA-GGAA GACTC - ACATTGCTTCA TTT TGAAGCAAT	sT
NBItoα _GAAT_AC_S1	T*G-CAGTCCAGAA-GAAT GACTC - ACATTGCTTCA TTT TGAAGCAAT	sT
NBItoα _GAAT_AC_S2	T*G*-CAGTCCAGAA-GAAT GACTC - ACATTGCTTCA TTT TGAAGCAAT	sT
NBItoα _GAAT_AC_S3	T*G*-C*AGTCCAGAA-GAAT GACTC - ACATTGCTTCA TTT TGAAGCAAT	sT
NBItoα _GAAT_AC_S4	T*G*-C*A*GTCCAGAA-GAAT GACTC - ACATTGCTTCA TTT TGAAGCAAT	sT
NBItoα _GAAT_AC_S5	T*G*-C*A*G*TCCAGAA-GAAT GACTC - ACATTGCTTCA TTT TGAAGCAAT	sT
NBItoα _GAAT_AC_S6	T*G*-C*A*G*T*CCAGAA-GAAT GACTC - ACATTGCTTCA TTT TGAAGCAAT	sT
NBItoα _GGGA_TC	TGCAGTCCAGAAGGGA-GACTC- TCATTGCTTCATTTTGAAGCAAT	sT
NBItoα _CGGA_TC	TGCAGTCCAGAACGGA-GACTC- TCATTGCTTCATTTTGAAGCAAT	sT
NBItoα _GGGA_TT	TGCAGTCCAGAAGGGA-GACTC- TTATTGCTTCATTTTGAAGCAAT	sT
NBItoα _GCGA_TC	TGCAGTCCAGAAGCGA-GACTC- TCATTGCTTCATTTTGAAGCAAT	sT
NBItoα _GGGA_TG	TGCAGTCCAGAAGGGA-GACTC- TGATTGCTTCATTTTGAAGCAAT	sT

NBItoγ _GAGT_AC	TGCTAACTGAAGAGT-GACTC-ACATTGCTTCATTTTGAAGCAAT	sT
NBItoγ _GAGA_AC	TGCTAACTGAAGAGA-GACTC-ACATTGCTTCATTTTGAAGCAAT	sT
NBItoγ _GAGC_AC	TGCTAACTGAAGAGC-GACTC-ACATTGCTTCATTTTGAAGCAAT	sT
NBItoγ _GATT_AC	TGCTAACTGAAGATT-GACTC-ACATTGCTTCATTTTGAAGCAAT	sT
NBItoγ _TCAT_AC	TGCTAACTGAATCAT-GACTC-ACATTGCTTCATTTTGAAGCAAT	sT
NBItoγ _GAGA_AC _Sp18T5Biot	Biot TTTTT/intsp18/TGCTAACTGAAGAGA-GACTC-ACATTGCTTCATTTTGAAGCAAT	sT
NBItoα _GAGA_AC _Sp18T5Biot	Biot TTTTT/intsp18/-TG-CAGTCCAGAA-GAGA GACTC - ACATTGCTTCA TTT TGAAGCAAT	sT
NBItoα _GACA_AC _Sp18T5Biot	Biot TTTTT/intsp18/-TG-CAGTCCAGA-GACA GACTC - ACATTGCTTCA TTT TGAAGCAAT	sT
NBItopTαC1 _GACA_AC _Sp18T5Biot	Biot TTTTT/intsp18/-CATTCTGGACTGG-GACA GACTC - ACATTGCTTCA TTT TGAAGCAAT	sT
NBItoβ	TG-CTGGGATGAA-GTTT GACTC ACATTGCTTCATTTTGAAGCAATGTGAGT-CAAACTTCTGGACTGTT	sT
TSBtopTγ	CATTCAGTTAGTTGTTT GACTC ATTGCTAGGACCGGCTT	kT
TSBtopTαT5	CATTCTGGACTGAAAAAGTTT GACTC ATTGCTAGGACCGGCTT	kT
polyAtopTαT5	CATTCTGGACTGAAAAAGTTT GACTC ATTTTTTTTTTTTTTTTTTTTTTTTAA	kT
TSBtopTγP(3)	C*A*T*TCAGTTAGTTGTTT GACTC ATTGCTAGGACCGGCTT p	kT
TSBtopTα T5P(2)	C*A*T*TCTGGACTGAAAAAGTTT GACT CATTGCTAGGACCGGCTT p	kT
polyAtopTα T5P(2)	C*A*T*TCTGGACTGAAAAAGTTT GACTC ATTTTTTTTTTTTTTTTTTTTTTTTTGG p	kT
TSBtopTαA4 P	C*A*T*TCTGGACTGTTTT-GTTT GACTC ATTGCTAGGACCGGCTT p	kT
TSBtopTαA3 P	C*A*T*TCTGGACTGTTT-GTTT GACTC ATTGCTAGGACCGGCTT p	kT
TSBtopTαA2 P	C*A*T*TCTGGACTGTT-GTTT GACTC ATTGCTAGGACCGGCTT p	kT

TSBtopTαA1 P	C*A*T*TCTGGACTGT-GTTT GACTCA TTGCTAGGACCGGCTT p	kT
TSBtopTαT1 P	C*A*T*TCTGGACTGA-GTTT GACTC ATTGCTAGGACCGGCTT p	kT
TSBtopTαG1 P	C*A*T*TCTGGACTGC-GTTT GACTC ATTGCTAGGACCGGCTT p	kT
TSBtopTαC1 P	C*A*T*TCTGGACTGG-GTTT GACTC ATTGCTAGGACCGGCTT p	kT
NBItoγ _DS _source_Biot5	Biot TTTTTTTTTT TGAGGTAGTAGGTTGTATAGCCCAC GAGTCGAGA	sT
NBItoγ _DS _source_Biot3	TGCTAACTGAA TCTCGACTC GTGGGCTATACAACCTACTACCTCA TTTTTTTTTT Biot	sT
NBItopTγA1 _DS_Biot5	Biot TTTTTTTTTT TACCCTGTAGAACCGAATTTGCC AC GAGTCGAGA	skT
NBItopTγA1 _DS_Biot3	CATTCAGTTAGTTCTC GACTC GTGGCAAATTCGGTTCTACAGGGTA TTTTTTTTTT Biot	skT
TSBtoβP _NBI_(14)	TGCTGGGATGAAGTTT GACTC ATTGCTAGGACCGGCTT p	cT
polyAtoβP _NBI_(24)	TGCTGGGATGAAGTTT GACTC ATTTTTTTTTTTTTTTTTTTTTTTTAA p	cT
TSBtoγP _NBI_(14)	TGCTAACTGAAGTTT GACTC ATTGCTAGGACCGGCTT p	cT
polyAtoγP _NBI_(24)	TGCTAACTGAAGTTT GACTC ATTTTTTTTTTTTTTTTTTTTTTTTAA p	cT
PolyA_Tail(30) Biot	Biot AAAAAAAAAAAAAAAAAAAAAAAAAAAAAA	DNA target
TotalSeqB Biot	Biot GCTTTAAGGCCGGTCCTAGCAA	DNA target
DLet7a T10 Cholesterol_Pro	ChoPro TTTTTTTTTTTGAGGTAGTAGGTTGTATAGTT	Cholesterol oligonu-cleotide
γ	CATTCAGTTAG	Trigger
Cγ-2PS3	C*T*A*ACTGAATGCTAACTGAA p	aT
pTγ PS3	A*A*C*TAACTGAATG p	pT
MBγBsmI Atto633	Atto663- C*A*T*CGATATACTAACTGAATGCGATG-BHQ2	rT
TSBtoγP	TGCTAACTGAAGTTT GACTC ATTGCTAGGACCGGCTT p	cT
TotalSeqB	GCTTTAAGGCCGGTCCTAGCAA	Target

Let7atoγP	TGCTAACTGAAGTTT GACTC AAACTATACAACCTACTACCTCA p	cT
TD05_TSB	AAGGAGCAGCGTGGAGGATAAACACCGTGGAG GATAGTTCGGTGGCTGTTCAGGGTCT CCTCCCGGTGTTAGGGTGTGTCGTCGTGGT AAGCCGGTCCTAGCAA	Modified aptamer
TE02_TSB	AAGGAGCAGCGTGGAGGATATAGGCAGT GGTTTGACGTCCGCATGTTGGGAATA GCCACGCCTTTAGGGTGTGTCG TCGTGGTAAGCCGGTCCTAGCAA	Modified Aptamer
TSBtoαP	TGCAGTCCAGAAGTTT GACTC ATTGCTAGGACCGGCTT p	cT
TD05	AAGGAGCAGCGTGGAGGATAAACACCG TGGAGGATAGTTCGGTGGCTGTT CAGGGTCTCCTCCCGGTGTTAGGGTGT-GTCGTCGTGGTAA	aptamer
TE02	AAGGAGCAGCGTGGAGGATATAGGCAG TGGTTTGACGTCCGCATGTTGGG AATAGC-CACGCCTTTAGGGTGTGTCGTCGTGGTAA	aptamer
NBItoγ Sp18T5Biot	Biot TTTTT /intsp18/ TGCTAACTGAAGTTT GACTC ACATTGCTTCATTTTGAAGCAATGTGAGT	sT
Let7atoαT7Mal	TGCAGTCCAGAAGTTTGACTCAAACTATA-CAACCTACTACCTCA TTTTTTT Mal	cT
17_5ptoαT7Mal	TGCAGTCCAGAAGTTT GACTC ACTACCTGCACTGTAAGCACTTTGTTTTTTT Maleimide	cT
132_3ptoαT7Mal	TGCAGTCCAGAAGTTT GACTC ACGACCATGGCTGTAGACTGTTATTTTTTT Maleimide	cT

Table 6.1: Sequences of the oligonucleotides used in this study.

"*" denotes phosphorothioate backbone modification. "p" denotes 3'-phosphate modification. /intsp18/ denotes an internal Spacer18 modification (Biomers). "ChoPro" denotes a Cholesterol Prolinol modification. "Biot" denotes a biotin modification.

6.3 Buffer compositions

Component	Concentration
Tris HCl pH 7.9	20 mM
$(NH4)_2SO_4$	10 mM
KCl	40 mM
$MgSO_4$	10 mM
dNTP	25 μM each
Synperonic F 104	0.1% (w/v)
Netropsin	2 μM

Table 6.2: 1x miRBuffer composition.

Component	Concentration
Tris-HCl pH 7.5	20 mM
NaCl	1 M
EDTA	1 mM
Tween 20	0.2% (v/v)

Table 6.3: 1x binding and washing buffer composition.

Component	Concentration
Tris-HCl pH 7.5	5 mM
NaCl	50 mM
EDTA	500 μM
$MgSO_4$	5 mM

Table 6.4: 1x storage buffer composition.

6.4 MiRNA detection

6.4.1 In tubes

All reaction mixtures were assembled at 4°C in 200 μl PCR tubes. miRBuffer 4x (see table 6.2) was diluted in mQ water to reach a 1x final concentration. The templates were then added to reach final concentrations of 0.5 nM of cT, 50 nM of aT, 12 nM of pT and 50 nM of rT, unless specified otherwise. After homogenization, BSA (200 mg/mL) and the enzymes were added [Nb.BsmI (300 U/mL), Nt.BstNBI (10 U/mL), Vent(exo-) (80 U/mL), ttRecJ (23 nM)]. The targeted miRNA was serially diluted on parafilm in 1X Tris-EDTA buffer (Sigma Aldrich) using low-binding DNA tips (Eppendorf). Typically, 10 fold dilutions were realized but it can be adapted according to the desired final concentration. miRNA was first added to the thermocyler tube (Bio-rad) and the mixture containing the buffer, templates and enzymes was added, reaching a final volume of 10 μL.

Unless specified otherwise, in presence of Klenow Fragment (exo–) (5 U/mL), the pT concentration was lowered to 8 nM.

Samples were incubated at 50°C in a thermocycler (CFX96 Touch, Bio-Rad) and the fluorescence was recorded in real-time every two minutes. Fluorescence time traces were normalized and the amplification time (At) determined as 20 % of the maximum fluorescence signal.

6.4.2 In droplets

6.4.2.1 Microfluidic devices preparation

Soft lithography

The mold was prepared by spin-coating a thin layer of SU-8 photosensitive resist (MicroChem Corp., USA) on a 4-inch silicon wafer. By choosing the viscosity of the resin and the spin-coating speed of the SU-8 resin according to the manufacturer instructions, it is possible to adjust the thickness of the SU-8 layer. The photoresist was then polymerized by an exposition to UV light through a photolithography mask. The unpolymerized resin was washed by introducing the wafer in a developer solvent (PDMEA).The obtained mold is finally washed with isopropanol and dried.

PDMS chip preparation

44 g of a mixture of Sylgard 184 PDMS resin and the curing agent (Dow Corning, MI, USA) (10:1 (w/w)) was mixed until it became cloudy and poured on the mold. It was then degazed (10 min) in a vacuum chamber and baked for 2 hours at 70°C in an oven for PDMS cross-linking. The PDMS was then peeled from the mold and cut around the chip design. Inlets and outlets were punched using a biopsy hole puncher of 1.5 mm diameter (Integra Miltex, PA, USA).

Plasma cleaning

To remove dust or debris, a 1 mm thick glass slide and the PMDS chip were cleaned with isopropanol and dried with an air gun. The glass surface and the PDMS were activated by plasma treatment in a plasma oven. To do so, three vacuum/O2 cycles were realized and the O_2 pressure fixed around 300 mTorr. A plasma was created for 60 seconds in the chamber, vaccum broken and the activated surfaces brought together for bonding.

Hydrophobic treatment

The chip is then baked at 200°C for 5 hours to make its walls hydrophobic.

6.4.2.2 Droplets generation

An aqueous phase was emulsified using a microfluidic chip, a pressure pump controller MFCS-EZ (Fluigent, France) and 200 μm diameter PTFE tubing (C.I.L., France). The aqueous sample phase is composed of the mixture described in section 6.4.1 with optionally fluorescent dextrans used to barcode different aqueous phases. The oil phase is composed of fluorinated oil (Novec-7500, 3M) containing 1% (w/w) fluorosurfactant (FluoSurf, Emulseo). The emulsion composed of 10 μm diameter droplet was collected in a tip.

6.4.2.3 Droplets incubation

The collected emulsion was incubated at 50°C in a thermocycler (CFX96 Touch, Bio-Rad) and the fluorescence was recorded in real-time.

6.4.2.4 Droplets analysis

After incubation, droplets are sandwiched in a microscopy chamber composed of two glass slides sealed with an epoxy glue (Sader). The two glass slides (a bottom slide (76x52x1 mm) and a 0.17 mm thick coverslip) were treated with fluorosilane solution (Novec-1720, 3M) to become hydrophobic. 10 μm diameter polystyrene particles in an aqueous solution (Polysciences, Inc., PA, USA) were deposited on the bottom slide and dried on a heating plate at 100°C for 30 s. These particles act as spacer to avoid droplet compression and control the chamber thickness. Fluorescence images were then taken using an epifluorescence microscope Nikon Eclipse Ti equipped with a motorized XY stage (Nikon), a camera Nikon DSQi2, an apochromatic 10X (N.A. 0.45) (Nikon) and a CoolLed pE-4000 illumination source. Images were then analyzed using a Mathematica software (Wolfram) according to a previously described procedure [178].

6.4.3 Capture on particles

Particles functionalization

20 μL of sepharose beads at 10^4 beads.μL^{-1} (GE Healthcare) were washed 3 times with 1x binding and washing buffer (BW) (+ 40 μL 1x BW, vortex 10 s, centrifuge, discard supernatant) and resuspended in 40 μL of 1x BW. 30 μL of this solution was mixed with 75 μL of 20 nM of biotinylated cT (in 1x BW) and quickly vortexed 20 s. The resulting mixture was incubated 15 min at room temperature, with a 20 s vortex every 5 min. The solution was centrifuged, the supernatant discarded and the beads washed 2 times with 1x BW (+ 40 μL 1x BW, vortex 10 s, centrifuge, discard supernatant) and 1 time with 1x storage buffer (SB) (+ 40 μL 1x SB, vortex 10 s, centrifuge, discard supernatant). Finally, the beads were resuspended in 150 μL of 1x SB (500 beads.μL^{-1}, $1.2.10^7$ cTs per bead) and stored at 4°C. Beads were vortexed 20 s prior to utilization.

Capture

Unless specified otherwise, the capture took place as follow. A mixture containing 1 nM of pT (used as a carrier DNA), 1x miRBuffer, the target miRNA (diluted on parafilm as described in section 6.4.1) and optionally Klenow Fragment (exo–) (5 U/mL). This mixture was assembled on ice. 19 μL of this solution was mixed with 1 µL of sepharose beads at 80 beads.μL^{-1} (diluted in 1x SB from the stock previously prepared). The tube was incubated at 40°C for 40 min and shaked at 2000 rpm. If applicable, the tube were then incubated 30 min at 55°C to deactivate Klenow. Supernatant was discarded and, if applicable, the beads were washed 2 times with 1x miRBuffer (+ 20μL 1x miRBuffer, vortex 10 s, centrifuge, discard supernatant).

The beads were then added to an amplification mixture similar to the one described in section 6.4.1 without cT (as cT is now on the beads) and with 10 nM of pT. As the beads were in 1x miRBuffer, the 4x miRBuffer proportion in the amplification mixture has to be adapted so that the final concentration of miRBuffer reaches 1x.

Amplification

The samples were incubated at 50°C in a thermocycler (CFX96 Touch, Bio-Rad) and the fluorescence was recorded in real-time. The time traces were normalized and the At determined as 20 % of the maximum fluorescence signal.

6.4.4 Ligation in tubes

All reaction mixtures were assembled at 4°C in 200 μl PCR tubes. miRBuffer 4x (see table 6.2) was diluted in mQ water to reach a 1x final concentration and supplemented with 1 mM of ATP. The templates were then added to reach final concentrations of 10 nM of lig1 oligonucleotide, 2 nM of lig2 oligonucleotide, 50 nM of aT, 5 nM of pT and 50 nM of rT, unless specified otherwise. After homogenization, BSA (200 mg/mL) and the enzymes were added [Nb.BsmI (300 U/mL), Nt.BstNBI (10 U/mL), Vent(exo-) (80 U/mL), ttRecJ (23 nM), SplintR Ligase (250 U/mL)]. The targeted miRNA was serially diluted on parafilm in 1X Tris-EDTA buffer (Sigma Aldrich) using low-binding DNA tips (Eppendorf). Typically, 10 fold dilutions were realized but it can be adapted according to the desired final concentration. miRNA was first added to the thermocyler tube (Bio-rad) and the mixture containing the buffer, templates and enzymes was added, reaching a final volume of 10 μL.

Samples were incubated 1 hour at 25 or 37°C then followed by an incubation at 50°C in a thermocycler (CFX96 Touch, Bio-Rad) and the fluorescence was recorded in real-time. The time traces were normalized and the At determined as 20 % of the maximum fluorescence signal.

6.4.5 Ligation based capture on particles

Particles functionalization

10 μL of Dynabeads MyOne Streptavidin at 10^7 beads.μL^{-1} (ThermoFisher Scientific) were washed 3 times with 1x BW (+ 20 μL 1x BW, vortex 10 s, particles gathering with a magnet, discard supernatant) and resuspended in 20 μL of 1x BW. This solution was then mixed with 20 μL of 100 nM of biotinylated lig1 oligonucleotide (in 1x BW) and quickly vortexed 20 s. The resulting mixture was incubated 15 min at room temperature, with a 20 s vortex every 5 min. Particles were gathered with a magnet, supernatant discarded and the beads were washed 2 times with 1x BW (+ 80 μL 1x BW, vortex 10 s, particles gathering with a magnet, discard supernatant) and 1 time with 1x SB buffer (+ 80 μL 1x SB, vortex 10 s, particles gathering with a magnet, discard supernatant). Finally, the beads were resuspended in 10 μL of 1x SB (10^7 bead per μL) and stored at 4°C. Beads were vortexed 20 s prior to utilization.

Capture

Unless specified otherwise, the capture took place as follow. A mixture containing 20 nM lig2 oligonucleotide, 25 μM of each DNTP, SplintR Ligase (250 U/mL), Klenow Fragment (exo–) (5 U/mL) and the target miRNA (diluted on parafilm as described in section 6.4.1) in 1x SplintR ligase buffer (NEB) was assembled on ice. 18 μL of this solution was mixed with 2 µL of dynabeads at 10^7 bead per μL. The tube was incubated at 37°C for 60 min and shaked at 2000 rpm. If applicable, the tube were then incubated 30 min at 55°C to deactivate Klenow. Supernatant was discarded and, if applicable, the beads were washed 2 times with

1x BW (+ 40μL 1x BW, vortex 10 s, sonification 10 s, particles gathering with a magnet, discard supernatant), washed 1 time with 1x SB buffer (+ 40μL 1x SB Buffer, vortex 10 s, sonification 10 s, particles gathering with a magnet, discard supernatant) and resuspended in 4 μL of 1x SB buffer.

The beads were then added to an amplification mixture similar to the one described in section 6.4.4 without lig1 oligonucleotide (as lig1 is now on the beads).

Amplification

The samples were incubated at 50°C in a thermocycler (CFX96 Touch, Bio-Rad) and the fluorescence was recorded in real-time. The time traces were normalized and the At determined as 20 % of the maximum fluorescence signal.

6.5 Long RNA and DNA detection

6.5.1 RNaseH approach

6.5.2 Detection assay

All reaction mixtures were assembled at 4°C in 200 μl PCR tubes. miRBuffer 4x (see table 6.2) was diluted in mQ water to reach a 1x final concentration. The templates were then added to reach final concentrations of 50 nM of aT, 8 nM of pT and 50 nM of rT, unless specified otherwise. Optionally, 1 nM of different HSs can be added for MS2 detection. After homogenization, BSA (200 mg/mL) and the enzymes were added [Nb.BsmI (300 U/mL), Nt.BstNBI (10 U/mL), Vent(exo-) (80 U/mL), ttRecJ (23 nM), Klenow Fragment (exo–) (5 U/mL), RNAse H (3.2 U/L) or Thermostable RNase H (80 U/L)]. 10 fold dilutions of the target RNA or miRNA, were realized on parafilm in 1X Tris-EDTA buffer (Sigma Aldrich) using low-binding DNA tips (Eppendorf). The target was first added to the thermocyler tubes in equimolar concentrations and the target DNA was added at the same concentration. Finally, the mixture containing the buffer, templates and enzymes was added, reaching a final volume of 10 μL.

The samples were incubated at 48°C in a thermocycler (CFX96 Touch, Bio-Rad) and the fluorescence was recorded in real-time. The time traces were normalized and the At determined as 20 % of the maximum fluorescence signal.

6.5.3 3WJ

6.5.3.1 In solution

All reaction mixtures were assembled at 4°C in 200 μl PCR tubes. miRBuffer 4x (see table 6.2) was diluted in mQ water to reach a 1x final concentration. The templates were then added to reach final concentrations of 50 nM of aT, 8 nM of pT and 50 nM of rT, unless specified otherwise. After homogenization, BSA (200 mg/mL) and the enzymes were added [Nb.BsmI (300 U/mL), Nt.BstNBI (10 U/mL), Vent(exo-) (80 U/mL), ttRecJ (23 nM), Klenow Fragment (exo–) (5 U/mL)]. 10 fold dilutions of the target DNA, the 3WJ Template and the 3WJ Primer were realized on parafilm in 1X Tris-EDTA buffer (Sigma Aldrich) using low-binding DNA tips (Eppendorf). The 3WJ template and primer were first added to the

thermocyler tubes in equimolar concentrations and the target DNA was added at the same concentration. Finally, the mixture containing the buffer, templates and enzymes was added, reaching a final volume of 10 μL.

The samples were incubated at 48°C in a thermocycler (CFX96 Touch, Bio-Rad) and the fluorescence was recorded in real-time. The time traces were normalized and the At determined as 20 % of the maximum fluorescence signal.

6.5.3.2 On beads

Particles functionalization

20 μL of Dynabeads MyOne Streptavidin at 10^7 beads.μL^{-1} (ThermoFisher Scientific) were washed 3 times with 1x BW (+ 40 μL 1x BW, vortex 10 s, particles gathering with a magnet, discard supernatant) and resuspended in 20 μL of 1x BW. This solution was then mixed with 20 μL of 100 nM of each biotinylated capture strand (in 1x BW) and quickly vortexed 20 s. The resulting mixture was incubated 15 min at room temperature, with a 20 s vortex every 5 min. Particles were gathered with a magnet, supernatant discarded and the beads were washed 2 times with 1x BW (+ 80 μL 1x BW, vortex 10 s, particles gathering with a magnet, discard supernatant) and 1 time with 1x SB buffer (+ 80 μL 1x SB, vortex 10 s, particles gathering with a magnet, discard supernatant). Finally, the beads were resuspended in 20 μL of 1x SB (10^7 bead per μL) and stored at 4°C. Beads were vortexed 20 s prior to utilization.

Capture

Unless specified otherwise, the capture took place as follow. A mixture containing 10 nM of 3WJ primer and template, and the target DNA (diluted on parafilm as described in section 6.4.1) in 1x miRBuffer was assembled on ice. 18 μL of this solution was mixed with 2 µL of dynabeads at 10^7 bead per μL. The tube was incubated at 25°C for 60 min and shaked at 2000 rpm. Supernatant was discarded and the beads were washed 4 times with [1x PBS + 0.05% Tween20] (+ 40μL [1x PBS + 0.05% Tween20], vortex 10 s, sonification 10 s, particles gathering with a magnet, discard supernatant), washed 1 time with 1x miRBuffer (+ 40μL 1x miRBuffer, vortex 10 s, sonification 10 s, particles gathering with a magnet, discard supernatant) and resuspended in 4 μL of 1x miRBuffer.

The beads were then added to an amplification mixture similar to the one described in section 6.5.3.1 without 3WJ primer and template.

Amplification

The samples were incubated at 48°C in a thermocycler (CFX96 Touch, Bio-Rad) and the fluorescence was recorded in real-time. The time traces were normalized and the At determined as 20 % of the maximum fluorescence signal.

6.6 Protein detection

6.6.1 Aptamer and cT mediated detection

All reaction mixtures were assembled at 4°C in 200 μl PCR tubes. miRBuffer 4x (see table 6.2) was diluted in mQ water to reach a 1x final concentration. The templates were then added to reach final concentrations of 500 pM of aptamer, 0.5 nM of cT, 50 nM of aT, 8 nM

of pT and 50 nM of rT, unless specified otherwise. After homogenization, BSA (200 mg/mL) and the enzymes were added [Nb.BsmI (300 U/mL), Nt.BstNBI (10 U/mL), Vent(exo-) (80 U/mL), ttRecJ (23 nM)]. VEGF165 was serially diluted on parafilm in [10mM HEPES, 10 mM NaCl, 200 mg/mL BSA] using low-binding tips (Eppendorf). Typically, 10 fold dilutions were realized but it can be adapted according to the desired final concentration. VEGF165 was first added to the thermocyler tube (Bio-rad) and the mixture containing the buffer, templates and enzymes was added, reaching a final volume of 10 μL.

The samples were incubated at 48°C or 50°C in a thermocycler (CFX96 Touch, Bio-Rad) and the fluorescence was recorded in real-time. The time traces were normalized and the At determined as 20 % of the maximum fluorescence signal.

6.6.2 Aptamer and caged trigger mediated detection

All reaction mixtures were assembled at 4°C in 200 μl PCR tubes. miRBuffer 4x (see table 6.2) was diluted in mQ water to reach a 1x final concentration. The templates were then added to reach final concentrations of 400 pM of aptamer, 0.5 nM of caged trigger, 50 nM of aT, 8 nM of pT and 50 nM of rT, unless specified otherwise. After homogenization, BSA (200 mg/mL) and the enzymes were added [Nb.BsmI (300 U/mL), Nt.BstNBI (10 U/mL), Vent(exo-) (80 U/mL), ttRecJ (23 nM)]. The human alpha-Thrombin was first diluted 10 times in mQ water and serially diluted on parafilm in 5 % glycerol using low-binding tips (Eppendorf). Typically, 10 fold dilutions were realized but it can be adapted according to the desired final concentration. Human alpha-Thrombin was first added to the thermocyler tube (Bio-rad) and the mixture containing the buffer, templates and enzymes was added, reaching a final volume of 10 μL.

The samples were incubated at 50°C in a thermocycler (CFX96 Touch, Bio-Rad) and the fluorescence was recorded in real-time. The time traces were normalized and the At determined as 20 % of the maximum fluorescence signal.

6.6.3 PEA and aptamer mediated detection

All reaction mixtures were assembled at 4°C in 200 μl PCR tubes. FS Buffer 5x (NEB) was diluted in mQ water to reach a 1x final concentration and supplented with 25 μM of dNTPS and 3 mM of $MgSO_4$. The templates were then added to reach final concentrations of 10 nM of aptamer1-cT, 10 nM of aptamer2-act 100 nM of aT, 30 nM of pT and 50 nM of rT, unless specified otherwise. After homogenization, BSA (200 mg/mL) and the enzymes were added [Nb.BsmI (300 U/mL), Nt.BstNBI (10 U/mL), Bst large fragment (36 U/mL), ttRecJ (23 nM)]. The target protein was serially diluted on parafilm (see below for details on the dilution) using low-binding tips (Eppendorf). Typically, 10 fold dilutions were realized but it can be adapted according to the desired final concentration. The target protein was first added to the thermocyler tube (Bio-rad) and the mixture containing the buffer, templates and enzymes was added, reaching a final volume of 10 μL.

The samples were incubated at 37°C in a thermocycler (CFX96 Touch, Bio-Rad) and the fluorescence was recorded in real-time. The time traces were normalized and the At determined as 20 % of the maximum fluorescence signal.

Thrombin dilution: The human alpha-Thrombin was first diluted 10 times in mQ water and serially diluted on parafilm in 5 % glycerol using low-binding tips (Eppendorf).

VEGF165 dilution: Lyophylised VEGF165 was resuspended in [10mM HEPES, 10 mM NaCl, 200 mg/mL BSA] and serially diluted on parafilm in [10mM HEPES, 10 mM NaCl, 200 mg/mL BSA] using low-binding tips (Eppendorf).

INFg dilution Lyophylised INFg was resuspended in mQ and serially diluted on parafilm in mQ using low-binding tips (Eppendorf).

6.6.4 Heterogeneous assays

ELISA MAX™ Deluxe Set Human IFN- , ELISA MAX™ Deluxe Set Mouse IL-12 (p70), ELISA MAX™ Deluxe Set Mouse IL-4 (BioLegend, USA) were used.

ELISA:

The protocol for ELISA test was as follow:

1. Prepare a 1X solution of capture antibody from the stock (200X) in 1X Coating Buffer A. Add 100 μL of this solution to the wells of a high binding polystyrene plate (Microplate, 96 well, PS, Half area, high binding, white, Greiner). Seal the plate with PCR seal (4titude) and incubate overnight at 4°C.

2. Wash the plate 4 times by adding 200 μL of [PBS 1X + 0.05 % Tween 20] per well and blot the plate by firmly tapping the plate upside down on absorbent paper.

3. Add 200 μL of 1X Assay Diluent A per well and seal the plate. Incubate 1 hour at room temperature at 500 rpm in a thermomixeur. This is step is realized to block further nonspecific binding.

4. Wash the plate 4 times by adding 200 μL of [PBS 1X + 0.05 % Tween 20] per well and blot the plate by firmly tapping the plate upside down on absorbent paper.

5. Reconstitute the target protein lyophilized standard in 1X Assay Diluent A, according to the supplier's instruction. Dilute the protein in 1X Assay Diluent A to the desired concentration. Add 100 μL of the appropriate sample dilutions per well and seal the plate. Incubate 2 hours at room temperature at 500 rpm.

6. Wash the plate 4 times by adding 200 μL of [PBS 1X + 0.05 % Tween 20] per well and blot the plate by firmly tapping the plate upside down on absorbent paper.

7. Prepare a 1X solution of detection antibody from the stock (200X) in 1X Assay Diluent A. Add 100 μL of this solution per well. Seal the plate and incubate 1 hour at room temperature at 500 rpm.

8. Wash the plate 4 times by adding 200 μL of [PBS 1X + 0.05 % Tween 20] per well and blot the plate by firmly tapping the plate upside down on absorbent paper.

9. Add 100 μL of 1x Avidin-HRP (diluted in 1X Assay Diluent A) per well. Seal the plate and incubate 30 minutes at room temperature at 500 rpm.

10. Wash the plate 5 times by adding 200 μL of [PBS 1X + 0.05 % Tween 20] per well and wait at least 30 seconds between each wash. Finally, blot the plate by firmly tapping the plate upside down on absorbent paper.

11. Add 100 μL of Substrate D solution per well and seal the plate. Incubate 15 minutes at room temperature at 500 rpm in the dark.

12. Add 100 μL of 0.16 M H_2SO_4 to each well. This stops the enzymatic reaction.

13. Transfer the contents of each well to a plate suited for absorbance measurement. Measure the absorbance at 450 and 570 nm. Subtract the absorbance at 570 nm from the absorbance at 450 nm.

All dilutions and solution preparations were realized in protein LoBind® tubes (Eppendorf) using epT.IPS LoRetention (Eppendorf).

cT-based immuno-PUMA:

The protocol for cT-based immuno-PUMA test was as follow:

1-8: similar to the ELISA test steps described previously.

9. Wash the plate 4 times by adding 200 μL of [PBS 1X + 0.05 % Tween 20] per well and blot the plate by firmly tapping the plate upside down on absorbent paper.

10. Add 100 μL of 590 pM TotalSeqA0951-PE-Streptavidin (Biolegend) (diluted in 1X Assay Diluent A) per well. Seal the plate and incubate 30 minutes at room temperature at 500 rpm.

11. Wash the plate 4 times by adding 200 μL of [PBS 1X + 0.05 % Tween 20] per well and wait at least 30 seconds between each wash.

12. Wash the plate 1 time by adding 200 μL of 1x miRBuffer salts (miRBuffer 1x without dNTPs, netropsin and synperonic). Blot the plate by firmly tapping the plate upside down on absorbent paper.

13. Prepare the PUMA amplification mixture at 4°C in 200 μl PCR tubes. Dilute miRBuffer 4x (see table 6.2) in mQ water to reach a 1x final concentration. Add the templates to reach final concentrations of 0.5 nM of cT, 50 nM of aT, 6 nM of pT and 50 nM of rT. After homogenization, add BSA (200 mg/mL) and the enzymes [Nb.BsmI (300 U/mL), Nt.BstNBI (10 U/mL), Vent(exo-) (80 U/mL), ttRecJ (23 nM), Klenow Fragment (exo–) (5 U/mL) if applicable]. Finally, add 25 μL of the mixture containing the buffer, templates and enzymes.

14. Add 25 μL of mineral oil per well and seal the plate. Pre-heat the plate reader at 50°C before adding the plate.

sT-based immuno-PUMA:

The protocol for the sT-based immuno-PUMA test was as follow:

1-8: similar to the ELISA test steps described previously.

9. Add 100 μL of 1.8 nM streptavidin (diluted in 1X Assay Diluent A) per well. Seal the plate and incubate 30 minutes at room temperature at 500 rpm.

10. Wash the plate 4 times by adding 200 μL of [PBS 1X + 0.05 % Tween 20] per well and blot the plate by firmly tapping the plate upside down on absorbent paper.

11. Add 100 μL of 1.8 nM biotinylated sT (diluted in 1X Assay Diluent A) per well. Seal the plate and incubate 30 minutes at room temperature at 500 rpm.

12. Wash the plate 4 times by adding 200 μL of [PBS 1X + 0.05 % Tween 20] per well and wait at least 30 seconds between each wash.

13. Wash the plate 1 time by adding 200 μL of 1x miRBuffer salts (miRBuffer 1x without dNTPs, netropsin and synperonic). Blot the plate by firmly tapping the plate upside down on absorbent paper.

14. Prepare the PUMA amplification mixture at 4°C in 200 μl PCR tubes. Dilute miRBuffer 4x (see table 6.2) in mQ water to reach a 1x final concentration. Add the templates to reach final concentrations of 50 nM of aT, 6 nM of pT and 50 nM of rT. After homogenization, add BSA (200 mg/mL) and the enzymes [Nb.BsmI (300 U/mL), Nt.BstNBI

(10 U/mL), Vent(exo-) (80 U/mL), ttRecJ (23 nM)]. Finally, add 25 μL of the mixture containing the buffer, templates and enzymes.

15. Add 25 μL of mineral oil per well and seal the plate. Pre-heat the plate reader at 50°C before adding the plate.

Classifier:

The protocol for the immuno-PUMA classifier test was as follow:

1. Prepare a solution containing 0.5X of each of the two capture antibodies from their stocks (200X) in 1X Coating Buffer A. Add 100 μL of this solution to the wells of a high binding polystyrene plate (Microplate, 96 well, PS, Half area, high binding, white, Greiner). Seal the plate with PCR seal (4titude) and incubate overnight at 4°C.

2. Wash the plate 4 times by adding 200 μL of [PBS 1X + 0.05 % Tween 20] per well and blot the plate by firmly tapping the plate upside down on absorbent paper.

3. Add 200 μL of 1X Assay Diluent A per well and seal the plate. Incubate 1 hour at room temperature at 500 rpm in a thermomixeur. This is step is realized to block further nonspecific binding.

4. Wash the plate 4 times by adding 200 μL of [PBS 1X + 0.05 % Tween 20] per well and blot the plate by firmly tapping the plate upside down on absorbent paper.

5. Reconstitute the target proteins lyophilized standard in 1X Assay Diluent A, according to the supplier's instruction. Dilute the proteins in 1X Assay Diluent A to the desired concentrations. Add 100 μL of the appropriate sample dilutions per well and seal the plate. Incubate 2 hours at room temperature at 500 rpm.

6. Wash the plate 4 times by adding 200 μL of [PBS 1X + 0.05 % Tween 20] per well and blot the plate by firmly tapping the plate upside down on absorbent paper.

7. Prepare 1.4 μM solutions of detection antibodies : streptavidin (one per detection antibody). Mix each of those solutions with 1.4 μM solutions of the desired biotinylated oligonucleotide. Finally, mix the two oligonucleotide : streptavidin : detection antibody solutions at the last moment and add 100 μL of it to each well. Seal the plate and incubate 1 hour at room temperature at 500 rpm.

8. Wash the plate 4 times by adding 200 μL of [PBS 1X + 0.05 % Tween 20] per well and blot the plate by firmly tapping the plate upside down on absorbent paper.

9. Wash the plate 1 time by adding 200 μL of 1x miRBuffer salts (miRBuffer 1x without dNTPs, netropsin and synperonic). Blot the plate by firmly tapping the plate upside down on absorbent paper.

10. Prepare the PUMA amplification mixture at 4°C in 200 μl PCR tubes. Dilute miRBuffer 4x (see table 6.2) in mQ water to reach a 1x final concentration. Add the templates to reach final concentrations of 0.5 nM of each cT if applicable, 50 nM of aT, 6 nM of pT and 50 nM of rT. After homogenization, add BSA (200 mg/mL) and the enzymes [Nb.BsmI (300 U/mL), Nt.BstNBI (10 U/mL), Vent(exo-) (80 U/mL) or Bst large fragment (36 U.mL^{-1}) and ttRecJ (23 nM)]. Finally, add 25 μL of the mixture containing the buffer, templates and enzymes.

11. Add 25 μL of mineral oil per well and seal the plate. Pre-heat the plate reader at 50°C before adding the plate.

6.6.5 Production rate experiments

All reaction mixtures were assembled at 4°C in 200 μl PCR tubes. miRBuffer 4x (see table 6.2) was diluted in mQ water to reach a 1x final concentration. 50 nM of rT was then added. After homogenization, BSA (200 mg/mL) and the enzymes were added [Nt.BstNBI (10 U/mL), Vent(exo-) (80 U/mL) or Klenow Fragment (exo–) (5 U/mL) or Bst large fragment (36 U.mL^{-1}) or Bst 2.0 WS (40 U/mL)]. The targeted sT was serially diluted on parafilm in 1X Tris-EDTA buffer (Sigma Aldrich) using low-binding DNA tips (Eppendorf). Typically, 10 fold dilutions were realized but it can be adapted according to the desired final concentration. sT was first added to the thermocyler tube (Bio-rad) and the mixture containing the buffer, templates and enzymes was added, reaching a final volume of 10 μL.

The samples were incubated at 50°C in a thermocycler (CFX96 Touch, Bio-Rad) and the fluorescence was recorded in real-time. The time traces were normalized, derived and the production rates extracted.

6.6.6 Bradford assays

A solution of 1x Dye reagent (Bio-rad protein assay) was prepared and filtered with 5 μm diameter filters. Standard dilution of Pierce Bovine Gamma Globulin (Thermo Scientific) was realized in 1x PBS. 10 μL of sample and standard were mixed with 200 μL of 1x Dye reagent. The solutions were incubated 5 minutes at room temperature and absorbance was measured at 595 nm.

6.7 Cells phenotyping

6.7.1 Cell culture

The base medium for Ramos and Jurkat cell lines is ATCC-formulated RPMI-1640 Medium (ATCC 30-2001). The complete medium consists RPMI-1640 supplemented with 10% fetal bovine serum (ATCC 30-2020). The cells are suspended in the complete medium and seeded on 25 cm^2 or 75 cm^2 culture flask. The culture is maintained in an incubator at 37°C with 5% CO2. On reaching 75-80% confluency the cells are passaged. After retrieving from cell culture, the cells were finally re-suspended in TBS 1x at the concentration of 2.10^6 cells.mL^{-1}.

6.7.2 Aptamer folding

Aptamers were diluted to 500 nM in aptamer folding buffer (1× Tris Borate Saline (TBS), 5 mM $MgCl_2$, 4.5 g.L^{-1} glucose) and heated to 95°C for five minutes (Thermomixer, Eppendorf) then cooled on ice for 10 min. This protocol was adapted from the literature [231].

6.7.3 Cells staining

All staining steps were performed at 4°C in 0.5 mL DNA LoBind tubes (Eppendorf). 2.10^5 cells were resuspended in 500 µL of staining buffer (1× TBS, 5 mM$MgCl_2$, 4.5 g.L^{-1} glucose, 1 mg.mL^{-1} BSA (SigmaAldrich) and 0.1 mg.mL^{-1} salmon sperm DNA) with a concentration

of 21 nM of aptamer and let 30 minutes on ice. Cells were then washed three times with the staining buffer (centrifugation 300 rpm, 5 min, 4°C, resuspension in Staining Buffer) and two more times with TBS 1X. The cells were finally diluted in tubes at the desired concentration in TBS 1X.

6.7.4 Reaction mixture assembly

All reaction mixtures were assembled at 4°C in 200 µL PCR tubes (Bio-Rad). The templates (cT, aT, pT and rT) and the cells were mixed with the reaction buffer (FS Buffer 1X (NEB), TBS 0.2X (coming from the cell suspension) or 12.5% of cellular media (RPMI + 10% Fetal Bovine Serum + 1% Penicillin / Streptomycin), 25 μM each dNTP (NEB), 3 mM $MgS0_4$ and 200 U.μL^{-1} BSA (NEB)), together with 1% Evagreen 20X (Biotium) and the enzymes (200 U.mL^{-1} Nb.BsmI (NEB), 10 U.mL^{-1} Nt.BstNBI (NEB), 80 U.mL^{-1} Vent(exo-) (NEB) or 36 U.mL^{-1} Bst large fragment (NEB) and 23 nM ttRecJ (in-house brewed)). The mixtures were then incubated in a thermocycler (CFX 96 wells, Biorad) at 37°C and Atto633 as well as Evagreen fluorescence were monitored.

6.8 Microfluidic chambers

6.8.1 Chamber fabrication

Homemade Parafilm chambers or commercial PMMA straight channel chips (ChipShop) were used. Homemade Parafilm chambers were realized as follow. The desired channel shapes were cut in a single Parafilm layer with a cutter plotter. The layer was then placed between a cover glass (50 x 75 mm, Thermo Scientific) and another cover glass (22 x 22 mm, VWR) and heat-sealed. Chambers were passivated with BSA or novec 1720 if needed, washed with isopropanol and mQ water, filled with the reaction mixtures and finally sealed with either epoxy glue (Sader) or vacuum grease (Borer).

6.8.2 Reaction mixture assembly

Reaction mixture assembly and particles grafting were realized as already described in section 6.4.3.

6.8.3 THA grafting and THA beads preparation

THA preparation, THA grafting and THA beads preparation were realized as already reported by our team [211].

Briefly, 250mg sodium hyaluronate (ref. HA40K-1, Lifecore biomedical) were dissolved in 25mL of MES buffer (0.1M MES, pH 4.75). 50mg of PDPH (ref. 22301, Thermofisher) were added, dissolved and 300mg of EDC-HCl (ref. 8510070025, Merck Millipore) were finally added. The mixture was then stirred at room temperature for 6 hours and dialysed against milliQ water overnight at 4°C using a dialysis cassette MWCO 3.5 kDa (ref. 66130 Thermofisher). The solution was retrieved , 100mg of TCEP (ref. C4706-2G, Sigma-Aldrich) added and the mixture stirred for 3 hours at room temperature. The reaction mechanism

is given in figure 6.1. The solution was then dialysed three successive times during three hours at room temperature against NaCl (0.1M, pH 3.5) using a new cassette MWCO 3.5 kDa. Finally, the mixture was dialysed three more times during 3 hours at room temperature against milliQ and freeze-dried overnight. A white solid was obtained. Its thiol concentration was assessed using the Ellman's test.

Two distinct solutions were prepared, they are to be mixed at a 1:1 ratio (v/v) at the last moment. The first one contained THA (36 mg/mL) and 500 μM of TCEP in 1x miRBuffer. The other one contained PEGDVS (20mg/mL), 5 pM of Dylight405-Maleimide and 500 nM of the desired maleimide oligonucleotide in 1x miRBuffer. The Michael addition mechanism used to crosslink the hydrogel and add maleimide oligonucleotide in it is given in figure 6.2. After polymerization, the hydrogel spot was washed 2 times with 1x miRBuffer.

THA beads were generously given by Dr.Sieskind. The beads were at a concentration of 0.25 mg/mL. A 250 μL solution containing 6.3 μg of THA beads, TCEP (500 μM) and 3.3 μM of the cT-maleimide was prepared in 1x miRBuffer. The mixture was incubated 1 hour at 37°C under agitation (2000 rpm). The beads were then washed two times with 1x miRBuffer and resuspended in 1 mL of 1x miRBuffer.

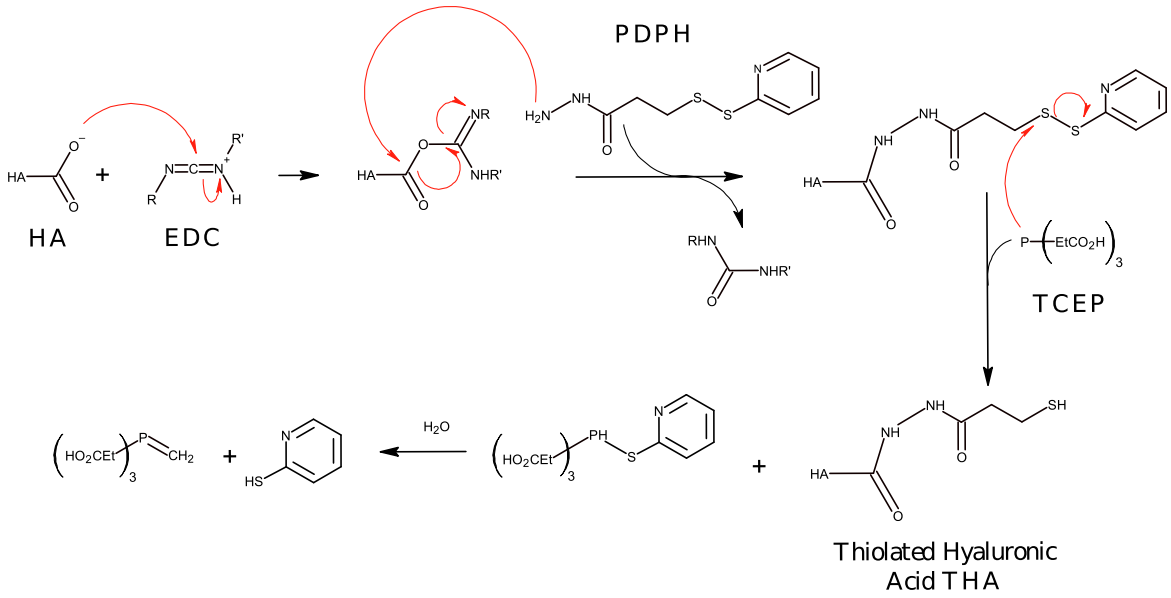

Figure 6.1: **Hyaluronic acid thiolation mechanism.** The deprotonated hyaluronic acid reacts on EDC. PDPH then attacks the resulting intermediate. The disulfid bond is reduced by TCEP to produce the thiolated hyaluronic acid. Image and information extracted from [211].

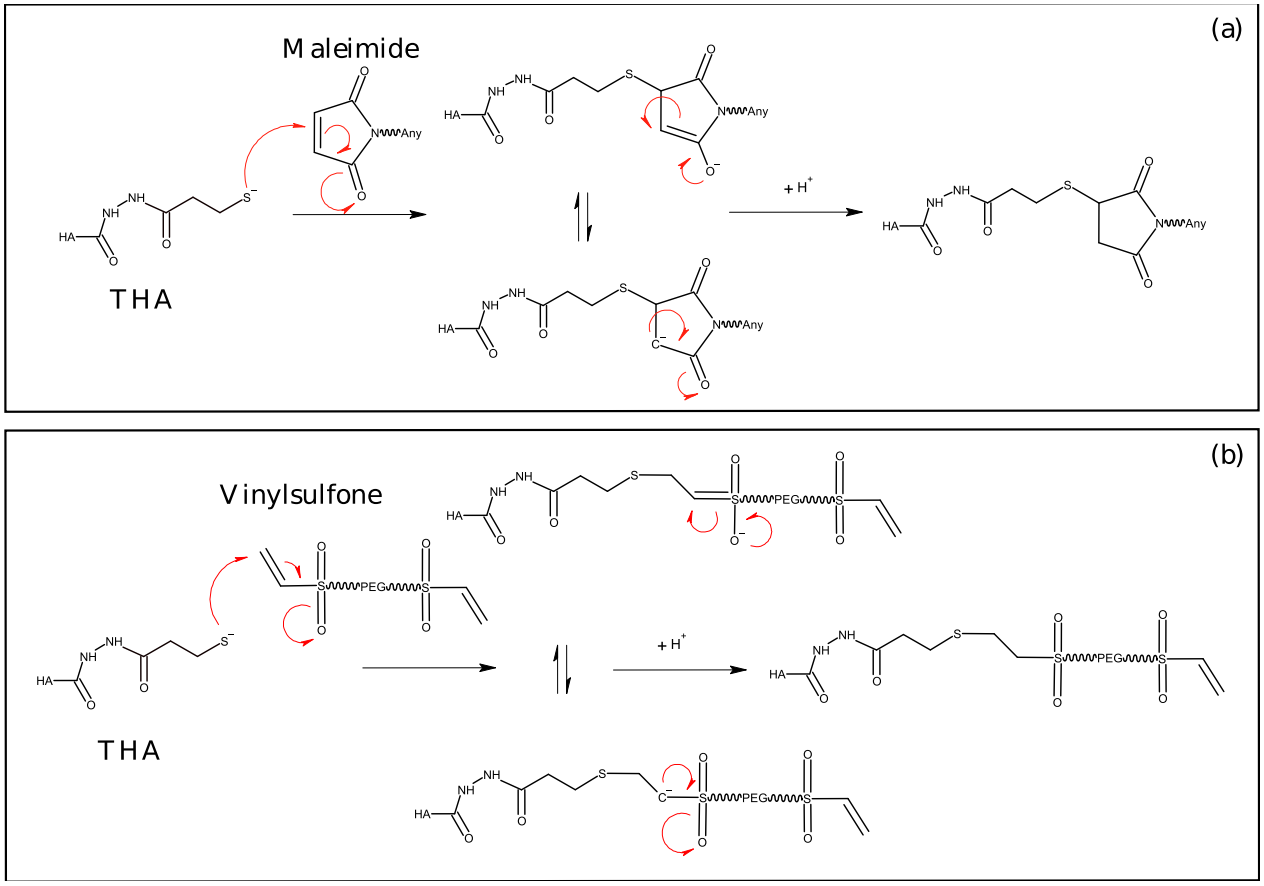

Figure 6.2: **Michael Addition of maleimide and vinylsulfone groups on THA mechanism. a.** Michael Addition of the THA thiol group on the maleimide. "Any" represents a compound which can be linked there. **b.** Michael Addition of the THA thiol group on the vinylslufone. This reaction is used for hydrogel crosslinking. Image and information extracted from [211].

Appendix A

Appendix Kd

.

Oligonucleotide 1	**Sequence 1**	**Oligonucleotide 2**	**Sequence 2**	**T (°C)**	**ΔG (kcal/mol)**	K_d
301a-3ptoα lig2 (2)	TG-CAGTCCAGAA-GAGA GACTC AC TTTTT - GCTTTGACAAT	mmu-miR301a-3p	CAGUGCAAUA GUAUUGUCAAAGC	50	-10,44	$8{,}70.10^{-8}$
301a-3ptoα ligout(2)	TG-CAGTCCAGAA-GAGA GACTC AC -TTTTT GCTTTGACAATAC-TATTGCACTG TTTTT	mmu-miR301a-3p	CAGUGCAAUA GUAUUGUCAAAGC	50	-20,49	$1{,}39.10^{-14}$
Let7atoα lig2(2)	TG-CAGTCCAGAA-GAGA GACTC AC TTTTT -AACTATACAAC	Let7a	UGA GGU AGU AGG UUG UAU AGU U	50	-8,53	$1{,}70.10^{-6}$
Let7atoα ligout(2)	TG-CAGTCCAGAA-GAGA GACTC AC TTTTT -AACTATACAACC TACTACCTCA TTTTT	Let7a	UGA GGU AGU AGG UUG UAU AGU U	50	-18,19	$4{,}99.10^{-13}$
15mer-cT	CTAACTGAATGCTA CTTGAATGTTTTTT TTTTTTGGTTGGTG TGGTTGG	29mer-act-V2	AGTCCGTGGTAGGGC AGGTTGGGGTGAC TTTTTTTTTTTTTA TCAAGTAG	37	-9.66	$1.56.10^{-7}$
15mer-cT	CTAACTGAATGCTAC TTGAATGTTTTTTT TTTTTGGTTGGTGT GGTTGG	29mer-act	AGTCCGTGGTAGG GCAGGTTGGGGTG ACTTTTTTTTTTT TTTTCAAGTAG	37	-9.91	$1.04.10^{-7}$

15mer-act	GGTTGGTGTGGTT GGTTTTTTTTTT TTTTCAAGTAG	29mer-cT	CTAACTGAATGCT ACTTGAATGTT TTTTTTTTTTA GTCCGTGGTAGG GCAGGTTGGGGT GACT	37	-9.91	$1.04.10^{-7}$
15mer-cT-GAGA	CTAACTGAATGG AGAGACTCTTT TTTTTTTTTGGTT GGTGTGGTTGG	29mer-act-GAGA	AGTCCGTGGTAG GGCAGGTTGGGG TGACTTTTTTT TTTTTTTGAGTCT CTC	37	-12.11	$2.93.10^{-9}$
15mer-cT-GATT	CTAACTGAATGGATT GACTCTTTTTTTT TTTGGTTGGTGTG GTTGG	29mer-act-GATT	AGTCCGTGGTAG GGCAGGTTGGGGTGA CTTTTTTTTTTT TTTGAGTCAATC	37	-11.58	$6.92.10^{-9}$
15 mer (Thrombin)	GGTTGGTGTGGTTGG	15mertoα 8 bases	TTCTGGACTGCTC GTGCCAACCACTT	48	-10.48	$7.38.10^{-8}$
15 mer (Thrombin)	GGTTGGTGTGGTTGG	15mertoα 6 bases	TTCTGGACTGC TCGTGCCAACCTT	48	-8.38	$1.98.10^{-6}$
15 mer (Thrombin)	GGTTGGTGTGGTTGG	15mertoα 4 bases	TTCTGGACTGCTCG TGCCAATT	48	-4.40	$1.01.10^{-3}$

TSBtopTαA4	CATTCTGGA CTGTTTTGTTTGA CTCATTGCTAGGA CCGGCTT	pTαA4	AAAACAGTCCAGA ATG	50	-14.17	$2.61.10^{-10}$
TSBtopTαA3	CATTCTGGACT GTTTGTTTGACTC ATTGCTAGGACCGG CTT	pTαA3	AAACAGTCCAGAATG	50	-13.54	$6.96.10^{-10}$
TSBtopTαA2	CATTCTGGAC TGTTGTTTGACT-CAT TGCTAGGACCG-GCTT	pTαA2	AACAGTCCAGAATG	50	-12.93	$1.80.10^{-9}$
TSBtopTαA1	CATTCTGGACTG TGTTTGACT-CATTGC TAGGACCGGCTT	pTαA1	ACAGTCCAGAATG	50	-12.36	$4.37.10^{-9}$
TSBtopTαT1	CATTCTGGACT GAGTTTGACTCATT GCTAGGACCGGCTT	pTαT1	TCAGTCCAGAATG	50	-12.13	$6.26.10^{-9}$
TSBtopTαC1	CATTCTGGACTGG GTTTGACT-CATTGCT AGGACCGGCTT	pTαC1P	CCAGTCCAGAATG	50	-11.41	$1.92.10^{-8}$

Table A.0: K_d for two different oligonucleotides at a given temperature. The data were obtained via Nupack. The concentration of Na^+ was set to 0.08 M and the concentration of Mg^{++} at 0.01M. The concentrations of the different oligonucleotides were set up to 1 μM.

Bibliography

[1] Ron Brookmeyer, Elizabeth Johnson, Kathryn Ziegler-Graham, and H. Michael Arrighi. Forecasting the global burden of Alzheimer's disease. *Alzheimer's & Dementia: The Journal of the Alzheimer's Association*, 3(3):186–191, July 2007.

[p. 1]

[2] Clifford R. Jack and David M. Holtzman. Biomarker Modeling of Alzheimer's Disease. *Neuron*, 80(6):1347–1358, December 2013.

[p. 1]

[3] Subodh Kumar and P. Hemachandra Reddy. Are circulating microRNAs peripheral biomarkers for Alzheimer's disease? *Biochimica et Biophysica Acta (BBA) - Molecular Basis of Disease*, 1862(9):1617–1627, September 2016.

[p. 1]

[4] C. G. Carter and D. F. Houlihan. Protein synthesis. In *Fish Physiology*, volume 20 of *Nitrogen Excretion*, pages 31–75. Academic Press, January 2001.

[p. 1]

[5] Bruce Alberts, Alexander Johnson, Julian Lewis, Martin Raff, Keith Roberts, and Peter Walter. The Generation of Antibody Diversity. *Molecular Biology of the Cell. 4th edition*, 2002.

[p. 1, 2, 5]

[6] Yu-Chieh Wang, Suzanne E Peterson, and Jeanne F Loring. Protein post-translational modifications and regulation of pluripotency in human stem cells. *Cell Research*, 24(2):143–160, February 2014.

[p. 2]

[7] Limor Cohen and David R. Walt. Highly Sensitive and Multiplexed Protein Measurements. *Chemical Reviews*, 119(1):293–321, January 2019.

[p. 3, 5, 7, 12, 14]

[8] Hye-Jin Park, Kang-Woo Lee, Eun S. Park, Stephanie Oh, Run Yan, Jie Zhang, Thomas G. Beach, Charles H. Adler, Michael Voronkov, Steven P. Braithwaite, Jeffry B. Stock, and M. Maral Mouradian. Dysregulation of protein phosphatase 2A in

parkinson disease and dementia with lewy bodies. *Annals of Clinical and Translational Neurology*, 3(10):769–780, 2016.

[p. 3]

[9] James E. Bradner, Denes Hnisz, and Richard A. Young. Transcriptional Addiction in Cancer. *Cell*, 168(4):629–643, February 2017.

[p. 3]

[10] Xuecheng Jiang, Shuyan Cheng, Weiqing Chen, Luming Wang, Feng Shi, and Chenggang Zhu. Comparison of oligonucleotide-labeled antibody probe assays for prostate-specific antigen detection. *Analytical Biochemistry*, 424(1):1–7, May 2012.

[p. 3]

[11] Claudio Soto and Sandra Pritzkow. Protein misfolding, aggregation, and conformational strains in neurodegenerative diseases. *Nature Neuroscience*, 21(10):1332–1340, October 2018.

[p. 3]

[12] Qing Wang, Raghothama Chaerkady, Jian Wu, Hee Jung Hwang, Nick Papadopoulos, Levy Kopelovich, Anirban Maitra, Hanno Matthaei, James R. Eshleman, Ralph H. Hruban, Kenneth W. Kinzler, Akhilesh Pandey, and Bert Vogelstein. Mutant proteins as cancer-specific biomarkers. *Proceedings of the National Academy of Sciences of the United States of America*, 108(6):2444–2449, February 2011.

[p. 3]

[13] Elena A. Ponomarenko, Ekaterina V. Poverennaya, Ekaterina V. Ilgisonis, Mikhail A. Pyatnitskiy, Arthur T. Kopylov, Victor G. Zgoda, Andrey V. Lisitsa, and Alexander I. Archakov. The Size of the Human Proteome: The Width and Depth. *International Journal of Analytical Chemistry*, 2016:7436849, 2016.

[p. 3]

[14] Mathias Uhlén, Linn Fagerberg, Björn M. Hallström, Cecilia Lindskog, Per Oksvold, Adil Mardinoglu, Asa Sivertsson, Caroline Kampf, Evelina Sjöstedt, Anna Asplund, IngMarie Olsson, Karolina Edlund, Emma Lundberg, Sanjay Navani, Cristina Al-Khalili Szigyarto, Jacob Odeberg, Dijana Djureinovic, Jenny Ottosson Takanen, Sophia Hober, Tove Alm, Per-Henrik Edqvist, Holger Berling, Hanna Tegel, Jan Mulder, Johan Rockberg, Peter Nilsson, Jochen M. Schwenk, Marica Hamsten, Kalle von Feilitzen, Mattias Forsberg, Lukas Persson, Fredric Johansson, Martin Zwahlen, Gunnar von Heijne, Jens Nielsen, and Fredrik Pontén. Proteomics. Tissue-based map of the human proteome. *Science (New York, N.Y.)*, 347(6220):1260419, January 2015.

[p. 3]

[15] William C. S. Cho. Proteomics Technologies and Challenges. *Genomics, Proteomics & Bioinformatics*, 5(2):77–85, January 2007.

[p. 3]

[16] Kondethimmanahalli Chandramouli and Pei-Yuan Qian. Proteomics: Challenges, Techniques and Possibilities to Overcome Biological Sample Complexity. *Human Genomics and Proteomics*, 2009:239204, December 2009.

[p. 3]

[17] Philip Cohen. The origins of protein phosphorylation. *Nature Cell Biology*, 4(5):E127–E130, May 2002.

[p. 3]

[18] Liat Ashkenazi-Hoffnung, Kfir Oved, Roy Navon, Tom Friedman, Olga Boico, Meital Paz, Gali Kronenfeld, Liat Etshtein, Asi Cohen, Tanya M. Gottlieb, Eran Eden, Irina Chistyakov, Isaac Srugo, Adi Klein, Shai Ashkenazi, and Oded Scheuerman. A host-protein signature is superior to other biomarkers for differentiating between bacterial and viral disease in patients with respiratory infection and fever without source: a prospective observational study. *European Journal of Clinical Microbiology & Infectious Diseases*, 37(7):1361–1371, July 2018.

[p. 3]

[19] Minju Ha and V. Narry Kim. Regulation of microRNA biogenesis. *Nature Reviews Molecular Cell Biology*, 15(8):509–524, August 2014.

[p. 3]

[20] R. C. Lee, R. L. Feinbaum, and V. Ambros. The C. elegans heterochronic gene lin-4 encodes small RNAs with antisense complementarity to lin-14. *Cell*, 75(5):843–854, December 1993.

[p. 3]

[21] Andrew Fire, SiQun Xu, Mary K Montgomery, Steven A Kostas, Samuel E Driver, and Craig C Mello. Potent and specific genetic interference by double-stranded RNA in Caenorhabditis elegans. *Nature*, 391:6, 1998.

[p. 3]

[22] Eugene Berezikov, Victor Guryev, José van de Belt, Erno Wienholds, Ronald H. A. Plasterk, and Edwin Cuppen. Phylogenetic Shadowing and Computational Identification of Human microRNA Genes. *Cell*, 120(1):21–24, January 2005.

[p. 3]

[23] Jacob O'Brien, Heyam Hayder, Yara Zayed, and Chun Peng. Overview of MicroRNA Biogenesis, Mechanisms of Actions, and Circulation. *Frontiers in Endocrinology*, 9:402, August 2018.

[p. 3]

[24] Kioomars Saliminejad, Hamid Reza Khorram Khorshid, Shahrzad Soleymani Fard, and Seyed Hamidollah Ghaffari. An overview of microRNAs: Biology, functions, therapeutics, and analysis methods. *Journal of Cellular Physiology*, 234(5):5451–5465, May 2019.

[p. 3]

[25] Richard I. Gregory, Kai-ping Yan, Govindasamy Amuthan, Thimmaiah Chendrimada, Behzad Doratotaj, Neil Cooch, and Ramin Shiekhattar. The Microprocessor complex mediates the genesis of microRNAs. *Nature*, 432(7014):235–240, November 2004.

[p. 3]

[26] Julia Höck and Gunter Meister. The Argonaute protein family. *Genome Biology*, 9(2):210, 2008.

[p. 3]

[27] Thomas Jet, Guillaume Gines, Yannick Rondelez, and Valérie Taly. Advances in multiplexed techniques for the detection and quantification of microRNAs. *Chemical Society Reviews*, 50(6):4141–4161, 2021.

[p. 4, 18, 21]

[28] Runcheng He, Xinxiang Yan, Jifeng Guo, Qian Xu, Beisha Tang, and Qiying Sun. Recent Advances in Biomarkers for Parkinson's Disease. *Frontiers in Aging Neuroscience*, 10, October 2018.

[p. 4]

[29] Ali Khodadadian, Mohsen Hemmati-Dinarvand, Ashkan Kalantary-Charvadeh, Amin Ghobadi, and Mahta Mazaheri. Candidate biomarkers for Parkinson's disease. *Biomedicine & Pharmacotherapy*, 104:699–704, August 2018.

[p. 4]

[30] YaXing Gui, Hai Liu, LiShan Zhang, Wen Lv, and XingYue Hu. Altered microRNA profiles in cerebrospinal fluid exosome in Parkinson disease and Alzheimer disease. *Oncotarget*, 6(35), November 2015.

[p. 4]

[31] Madalena Martins, Alexandra Rosa, Leonor C. Guedes, Benedita V. Fonseca, Kristina Gotovac, Sara Violante, Tiago Mestre, Miguel Coelho, Mário M. Rosa, Eden R. Martin, Jeffery M. Vance, Tiago F. Outeiro, Liyong Wang, Fran Borovecki, Joaquim J. Ferreira, and Sofia A. Oliveira. Convergence of miRNA Expression Profiling, -Synuclein Interacton and GWAS in Parkinson's Disease. *PLoS ONE*, 6(10):e25443, October 2011.

[p. 4]

[32] Yong Peng and Carlo M Croce. The role of MicroRNAs in human cancer. *Signal Transduction and Targeted Therapy*, 1(1):15004, December 2016.

[p. 4]

[33] Eiichiro Satake, Marcus G. Pezzolesi, Zaipul I. Md Dom, Adam M. Smiles, Monika A. Niewczas, and Andrzej S. Krolewski. Circulating miRNA Profiles Associated With

Hyperglycemia in Patients With Type 1 Diabetes. *Diabetes*, 67(5):1013–1023, May 2018.

[p. 4]

[34] Carlo M. Croce. Causes and consequences of microRNA dysregulation in cancer. *Nature Reviews Genetics*, 10(10):704–714, October 2009.

[p. 4]

[35] Yoko Karube, Hisaaki Tanaka, Hirotaka Osada, Shuta Tomida, Yoshio Tatematsu, Kiyoshi Yanagisawa, Yasushi Yatabe, Junichi Takamizawa, Shinichiro Miyoshi, Tetsuya Mitsudomi, and Takashi Takahashi. Reduced expression of Dicer associated with poor prognosis in lung cancer patients. *Cancer Science*, 96(2):111–115, February 2005.

[p. 4]

[36] Sarah Roush and Frank J. Slack. The let-7 family of microRNAs. *Trends in Cell Biology*, 18(10):505–516, October 2008.

[p. 4]

[37] Haifeng Dong, Jianping Lei, Lin Ding, Yongqiang Wen, Huangxian Ju, and Xueji Zhang. MicroRNA: Function, Detection, and Bioanalysis. *Chemical Reviews*, 113(8):6207–6233, August 2013.

[p. 5]

[38] Patrick S. Mitchell, Rachael K. Parkin, Evan M. Kroh, Brian R. Fritz, Stacia K. Wyman, Era L. Pogosova-Agadjanyan, Amelia Peterson, Jennifer Noteboom, Kathy C. O'Briant, April Allen, Daniel W. Lin, Nicole Urban, Charles W. Drescher, Beatrice S. Knudsen, Derek L. Stirewalt, Robert Gentleman, Robert L. Vessella, Peter S. Nelson, Daniel B. Martin, and Muneesh Tewari. Circulating microRNAs as stable blood-based markers for cancer detection. *Proceedings of the National Academy of Sciences of the United States of America*, 105(30):10513–10518, July 2008.

[p. 5]

[39] David P Bartel. MicroRNAs: Genomics, Biogenesis, Mechanism, and Function. *Cell*, 116(2):281–297, January 2004.

[p. 5]

[40] Chao Zhang, Yumeng Zhao, Xuemei Xu, Rui Xu, Haowen Li, Xiaoyan Teng, Yuzhen Du, Yanyan Miao, Hsiao-chu Lin, and Da Han. Cancer diagnosis with DNA molecular computation. *Nature Nanotechnology*, 15(8):709–715, August 2020.

[p. 5, 108, 145]

[41] A. Hulanicki, S. Glab, and F. Ingman. Chemical sensors: definitions and classification. *Pure and Applied Chemistry*, 63(9):1247–1250, January 1991.

[p. 5]

[42] Lu Zhang, Yacine Mazouzi, Michèle Salmain, Bo Liedberg, and Souhir Boujday. Antibody-Gold Nanoparticle Bioconjugates for Biosensors: Synthesis, Characterization and Selected Applications. *Biosensors and Bioelectronics*, 165:112370, October 2020.

[p. 5]

[43] Peter J. Delves and Ivan M. Roitt. The Immune System. *New England Journal of Medicine*, 343(1):37–49, July 2000.

[p. 5]

[44] Xiaowen Yu, Yu-Ping Yang, Emre Dikici, Sapna K. Deo, and Sylvia Daunert. Beyond Antibodies as Binding Partners: The Role of Antibody Mimetics in Bioanalysis. *Annual Review of Analytical Chemistry*, 10(1):293–320, June 2017.

[p. 6, 7]

[45] Nicole A Doria-Rose and M Gordon Joyce. Strategies to guide the antibody affinity maturation process. *Current Opinion in Virology*, 11:137–147, April 2015.

[p. 5]

[46] Neil S. Lipman, Lynn R. Jackson, Laura J. Trudel, and Frances Weis-Garcia. Monoclonal Versus Polyclonal Antibodies: Distinguishing Characteristics, Applications, and Information Resources. *ILAR Journal*, 46(3):258–268, January 2005.

[p. 5]

[47] G. Köhler and C. Milstein. Continuous cultures of fused cells secreting antibody of predefined specificity. *Nature*, 256(5517):495–497, August 1975.

[p. 6]

[48] Olive Leavy. The birth of monoclonal antibodies. *Nature Immunology*, 17(S1):S13–S13, December 2016.

[p. 6]

[49] Bebee Pathare, Vrushali Tambe, and Vandana Patil. A review on various analytical methods used in determination of dissociation constant. *International Journal of Pharmacy and Pharmaceutical Sciences*, 6(8):10, 2014.

[p. 6]

[50] Victor Vivcharuk, Jason Baardsnes, Christophe Deprez, Traian Sulea, Maria Jaramillo, Christopher R. Corbeil, Alaka Mullick, Joanne Magoon, Anne Marcil, Yves Durocher, Maureen D. O'Connor-McCourt, and Enrico O. Purisima. Assisted Design of Antibody and Protein Therapeutics (ADAPT). *PLOS ONE*, 12(7):e0181490, July 2017.

[p. 6]

[51] Karen L. Mansfield, Daniel L. Horton, Nicholas Johnson, Li Li, Alan D. T. Barrett, Derek J. Smith, Sareen E. Galbraith, Tom Solomon, and Anthony R. Fooks. Flavivirus-induced antibody cross-reactivity. *The Journal of General Virology*, 92(Pt 12):2821–2829, December 2011.

[p. 6]

[52] Adam MacNeil, Zachary Reed, and Pierre E. Rollin. Serologic Cross-Reactivity of Human IgM and IgG Antibodies to Five Species of Ebola Virus. *PLOS Neglected Tropical Diseases*, 5(6):e1175, June 2011.

[p. 6]

[53] Alix Bouvier-Müller and Frédéric Ducongé. Application of aptamers for in vivo molecular imaging and theranostics. *Advanced Drug Delivery Reviews*, 134:94–106, September 2018.

[p. 6, 77]

[54] A. D. Ellington and J. W. Szostak. In vitro selection of RNA molecules that bind specific ligands. *Nature*, 346(6287):818–822, August 1990.

[p. 6]

[55] C. Tuerk and L. Gold. Systematic evolution of ligands by exponential enrichment: RNA ligands to bacteriophage T4 DNA polymerase. *Science*, 249(4968):505–510, August 1990.

[p. 6]

[56] Yi Xi Wu and Young Jik Kwon. Aptamers: The "evolution" of SELEX. *Methods*, 106:21, August 2016.

[p. 6]

[57] Saw Yi Toh, Marimuthu Citartan, Subash C. B. Gopinath, and Thean-Hock Tang. Aptamers as a replacement for antibodies in enzyme-linked immunosorbent assay. *Biosensors & Bioelectronics*, 64:392–403, February 2015.

[p. 6, 10]

[58] John Goodchild. Conjugates of oligonucleotides and modified oligonucleotides: a review of their synthesis and properties. *Bioconjugate Chemistry*, 1(3):165–187, May 1990.

[p. 6]

[59] A.V. Lakhin, V.Z. Tarantul, and L.V. Gening. Aptamers: Problems, Solutions and Prospects. *Acta Naturae*, 5(4):34–43, 2013.

[p. 6]

[60] C. Hamers-Casterman, T. Atarhouch, S. Muyldermans, G. Robinson, C. Hammers, E. Bajyana Songa, N. Bendahman, and R. Hammers. Naturally occurring antibodies devoid of light chains. *Nature*, 363(6428):446–448, June 1993.

[p. 7]

[61] Andrew S. Greenberg, David Avila, Marianne Hughes, Austin Hughes, E. Churchill McKinney, and Martin F. Flajnik. A new antigen receptor gene family that undergoes rearrangement and extensive somatic diversification in sharks. *Nature*, 374(6518):168–173, March 1995.

[p. 7]

[62] Hamed Zare, Hossein Aghamollaei, Maryam Hosseindokht, Mohammad Heiat, Ali Razei, and Hamid Bakherad. Nanobodies, the potent agents to detect and treat the Coronavirus infections: A systematic review. *Molecular and Cellular Probes*, 55:101692, February 2021.

[p. 7]

[63] Aaron L Nelson. Antibody fragments. *mAbs*, 2(1):77–83, 2010.

[p. 7]

[64] Samuel H Barondes. Bifunctional properties of lectins: lectins redefined. *Trends in Biochemical Sciences*, 13(12):480–482, December 1988.

[p. 7]

[65] Fang Mi, Ming Guan, Cunming Hu, Fei Peng, Shijiao Sun, and Xiaomei Wang. Application of lectin-based biosensor technology in the detection of foodborne pathogenic bacteria: a review. *Analyst*, 146(2):429–443, 2021.

[p. 7]

[66] Marketa Lastovickova, Dana Strouhalova, and Janette Bobalova. Use of Lectin-based Affinity Techniques in Breast Cancer Glycoproteomics: A Review. *Journal of Proteome Research*, 19(5):1885–1899, May 2020.

[p. 7]

[67] Abdul Rasheed Baloch, Abdul Wahid Baloch, Brian J. Sutton, and Xiaoying Zhang. Antibody mimetics: promising complementary agents to animal-sourced antibodies. *Critical Reviews in Biotechnology*, 36(2):268–275, March 2016.

[p. 7]

[68] Stephan Kraemer, Jonathan D. Vaught, Christopher Bock, Larry Gold, Evaldas Katilius, Tracy R. Keeney, Nancy Kim, Nicholas A. Saccomano, Sheri K. Wilcox, Dom Zichi, and Glenn M. Sanders. From SOMAmer-Based Biomarker Discovery to Diagnostic and Clinical Applications: A SOMAmer-Based, Streamlined Multiplex Proteomic Assay. *PLOS ONE*, 6(10):e26332, October 2011.

[p. 7]

[69] Preston Hensley. SOMAmers and SOMAscan – A Protein Biomarker Discovery Platform for Rapid Analysis of Sample Collections From Bench Top to the Clinic. *Journal of Biomolecular Techniques : JBT*, 24(Suppl):S5, May 2013.

[p. 7]

[70] Derek Jones, Hyojin Kim, Xiaohua Zhang, Adam Zemla, Garrett Stevenson, W. F. Drew Bennett, Daniel Kirshner, Sergio E. Wong, Felice C. Lightstone, and Jonathan E. Allen. Improved Protein–Ligand Binding Affinity Prediction with Structure-Based Deep Fusion Inference. *Journal of Chemical Information and Modeling*, 61(4):1583–1592, April 2021.

[p. 7]

[71] Joseph J. BelBruno. Molecularly Imprinted Polymers. *Chemical Reviews*, 119(1):94–119, January 2019.

[p. 7]

[72] Rosalyn S. Yalow and Solomon A. Berson. Immunoassay of endogenous plasma insulin in man. *Journal of Clinical Investigation*, 39(7):1157–1175, July 1960.

[p. 7]

[73] L. E. Miles and C. N. Hales. Labelled antibodies and immunological assay systems. *Nature*, 219(5150):186–189, July 1968.

[p. 7]

[74] Rudolf M Lequin. Enzyme Immunoassay (EIA)/Enzyme-Linked Immunosorbent Assay (ELISA). *Clinical Chemistry*, 51(12):2415–2418, December 2005.

[p. 7]

[75] Eva Engvall and Peter Perlmann. Enzyme-linked immunosorbent assay (ELISA) quantitative assay of immunoglobulin G. *Immunochemistry*, 8(9):871–874, September 1971.

[p. 7]

[76] B. K. Van Weemen and A. H. W. M. Schuurs. Immunoassay using antigen—enzyme conjugates. *FEBS Letters*, 15(3):232–236, 1971.

[p. 7]

[77] Karolina Boguszewska, Michał Szewczuk, Sandra Urbaniak, and Bolesław T. Karwowski. Review: immunoassays in DNA damage and instability detection. *Cellular and molecular life sciences*, 76(23):4689–4704, December 2019.

[p. 7, 9]

[78] DrKarishma Shah and DrPanagiotis Maghsoudlou. Enzyme-linked immunosorbent assay (ELISA): the basics. *British Journal of Hospital Medicine*, 77(7):4, 2016.

[p. 8]

[79] Nathaniel L. Rosi and Chad A. Mirkin. Nanostructures in Biodiagnostics. *Chemical Reviews*, 105(4):1547–1562, April 2005.

[p. 8]

[80] Hongquan Zhang, Qiang Zhao, Xing-Fang Li, and X. Chris Le. Ultrasensitive assays for proteins. *The Analyst*, 132(8):724, 2007.

[p. 8, 23, 24]

[81] Błażej Kudłak and Monika Wieczerzak. Aptamer based tools for environmental and therapeutic monitoring: A review of developments, applications, future perspectives. *Critical Reviews in Environmental Science and Technology*, 50(8):816–867, April 2020.

[p. 10]

[82] Jeevalatha Vivekananda and Johnathan L. Kiel. Anti-Francisella tularensis DNA aptamers detect tularemia antigen from different subspecies by Aptamer-Linked Immobilized Sorbent Assay. *Laboratory Investigation*, 86(6):610–618, June 2006.

[p. 10]

[83] Regina Stoltenburg, Petra Krafčiková, Viktor Víglaský, and Beate Strehlitz. G-quadruplex aptamer targeting Protein A and its capability to detect Staphylococcus aureus demonstrated by ELONA. *Scientific Reports*, 6(1):33812, December 2016.

[p. 10]

[84] Monali Mukherjee, C. Nandhini, and Praveena Bhatt. Colorimetric and chemiluminescence based enzyme linked apta-sorbent assay (ELASA) for ochratoxin A detection. *Spectrochimica Acta Part A: Molecular and Biomolecular Spectroscopy*, 244:118875, January 2021.

[p. 10]

[85] Cecil C. Czerkinsky, Lars-Åke Nilsson, Håkan Nygren, Örjan Ouchterlony, and Andrej Tarkowski. A solid-phase enzyme-linked immunospot (ELISPOT) assay for enumeration of specific antibody-secreting cells. *Journal of Immunological Methods*, 65(1-2):109–121, December 1983.

[p. 10]

[86] Takashi Taguchi, Jerry R. McGhee, Robert L. Coffman, Kenneth W. Beagley, John H. Eldridge, Kiyoshi Takatsu, and Hiroshi Kiyono. Detection of individual mouse splenic T cells producing IFN- and IL-5 using the enzyme-linked immunospot (ELISPOT) assay. *Journal of Immunological Methods*, 128(1):65–73, January 1990.

[p. 11]

[87] Meredith Slota, Jong-Baeck Lim, Yushe Dang, and Mary L Disis. ELISpot for measuring human immune responses to vaccines. *Expert Review of Vaccines*, 10(3):299–306, March 2011.

[p. 11]

[88] H. Towbin, T. Staehelin, and J. Gordon. Electrophoretic transfer of proteins from polyacrylamide gels to nitrocellulose sheets: procedure and some applications. *Proceedings*

of the National Academy of Sciences of the United States of America, 76(9):4350–4354, September 1979.

[p. 11]

[89] J. Renart, J. Reiser, and G. R. Stark. Transfer of proteins from gels to diazobenzyloxymethyl-paper and detection with antisera: a method for studying antibody specificity and antigen structure. *Proceedings of the National Academy of Sciences of the United States of America*, 76(7):3116–3120, July 1979.

[p. 11]

[90] W. N. Burnette. "Western blotting": electrophoretic transfer of proteins from sodium dodecyl sulfate–polyacrylamide gels to unmodified nitrocellulose and radiographic detection with antibody and radioiodinated protein A. *Analytical Biochemistry*, 112(2):195–203, April 1981.

[p. 11]

[91] Biji T. Kurien and R. Hal Scofield. Western blotting. *Methods*, 38(4):283–293, April 2006.

[p. 11]

[92] Gholam Hossein Meftahi, Zahra Bahari, Ali Zarei Mahmoudabadi, Maryam Iman, and Zohreh Jangravi. Applications of western blot technique: From bench to bedside. *Biochemistry and Molecular Biology Education*, 49(4):509–517, 2021.

[p. 11]

[93] Jessica G. Duarte and Jonathan M. Blackburn. Advances in the development of human protein microarrays. *Expert Review of Proteomics*, 14(7):627–641, July 2017.

[p. 11]

[94] Oliver Poetz, Jochen M. Schwenk, Stefan Kramer, Dieter Stoll, Markus F. Templin, and Thomas O. Joos. Protein microarrays: catching the proteome. *Mechanisms of Ageing and Development*, 126(1):161–170, January 2005.

[p. 12]

[95] Nicolai Grebenchtchikov, Arend Brinkman, Simone P J van Broekhoven, Danielle de Jong, Anneke Geurts-Moespot, Paul N Span, Harry A Peters, Henk Portengen, John A Foekens, C G J (Fred) Sweep, and Lambert C J Dorssers. Development of an ELISA for Measurement of BCAR1 Protein in Human Breast Cancer Tissue. *Clinical Chemistry*, 50(8):1356–1363, August 2004.

[p. 12]

[96] Adriana Aguilar-Mahecha, Christiane Cantin, Maureen O'Connor-McCourt, Andre Nantel, and Mark Basik. Development of reverse phase protein microarrays for the validation of clusterin, a mid-abundant blood biomarker. *Proteome Science*, 7(1):15, April 2009.

[p. 12]

[97] Chang-Gong Liu, George Adrian Calin, Stefano Volinia, and Carlo M Croce. MicroRNA expression profiling using microarrays. *Nature Protocols*, 3(4):563–578, April 2008.

[p. 12]

[98] Stefanie Boellner and Karl-Friedrich Becker. Reverse Phase Protein Arrays—Quantitative Assessment of Multiple Biomarkers in Biopsies for Clinical Use. *Microarrays*, 4(2):98–114, March 2015.

[p. 12]

[99] David M. Rissin, David R. Fournier, Tomasz Piech, Cheuk W. Kan, Todd G. Campbell, Linan Song, Lei Chang, Andrew J. Rivnak, Purvish P. Patel, Gail K. Provuncher, Evan P. Ferrell, Stuart C. Howes, Brian A. Pink, Kaitlin A. Minnehan, David H. Wilson, and David C. Duffy. Simultaneous Detection of Single Molecules and Singulated Ensembles of Molecules Enables Immunoassays with Broad Dynamic Range. *Analytical Chemistry*, 83(6):2279–2285, March 2011.

[p. 13]

[100] Andrew J. Rivnak, David M. Rissin, Cheuk W. Kan, Linan Song, Matthew W. Fishburn, Tomasz Piech, Todd G. Campbell, Derek R. DuPont, Melissa Gardel, Sean Sullivan, Brian A. Pink, Carlos G. Cabrera, David R. Fournier, and David C. Duffy. A fully-automated, six-plex single molecule immunoassay for measuring cytokines in blood. *Journal of Immunological Methods*, 424:20–27, September 2015.

[p. 13]

[101] David M. Rissin, Cheuk W. Kan, Todd G. Campbell, Stuart C. Howes, David R. Fournier, Linan Song, Tomasz Piech, Purvish P. Patel, Lei Chang, Andrew J. Rivnak, Evan P. Ferrell, Jeffrey D. Randall, Gail K. Provuncher, David R. Walt, and David C. Duffy. Single-Molecule enzyme-linked immunosorbent assay detects serum proteins at subfemtomolar concentrations. *Nature biotechnology*, 28(6):595–599, June 2010.

[p. 13]

[102] Elif Burcu Bahadır and Mustafa Kemal Sezgintürk. Lateral flow assays: Principles, designs and labels. *TrAC Trends in Analytical Chemistry*, 82:286–306, September 2016.

[p. 13, 14]

[103] Peter Berger and Catharine Sturgeon. Pregnancy testing with hCG – future prospects. *Trends in Endocrinology & Metabolism*, 25(12):637–648, December 2014.

[p. 14]

[104] Yuao Wu, Karla X. Vazquez-Prada, Yajun Liu, Andrew K. Whittaker, Run Zhang, and Hang T. Ta. Recent Advances in the Development of Theranostic Nanoparticles for Cardiovascular Diseases. *Nanotheranostics*, 5(4):499–514, 2021.

[p. 14]

[105] Guillaume Gines, Roberta Menezes, Wenjin Xiao, Yannick Rondelez, and Valerie Taly. Emerging isothermal amplification technologies for microRNA biosensing: Applications to liquid biopsies. *Molecular Aspects of Medicine*, November 2019.

[p. 14, 17, 19]

[106] R. K. Saiki, S. Scharf, F. Faloona, K. B. Mullis, G. T. Horn, H. A. Erlich, and N. Arnheim. Enzymatic amplification of beta-globin genomic sequences and restriction site analysis for diagnosis of sickle cell anemia. *Science*, 230(4732):1350–1354, December 1985.

[p. 15]

[107] Heather D. VanGuilder, Kent E. Vrana, and Willard M. Freeman. Twenty-five years of quantitative PCR for gene expression analysis. *BioTechniques*, 44(5):619–626, April 2008.

[p. 15]

[108] Lewis Z. Hong, Lihan Zhou, Ruiyang Zou, Chin Meng Khoo, Adeline Lai San Chew, Chih-Liang Chin, and Shian-Jiun Shih. Systematic evaluation of multiple qPCR platforms, NanoString and miRNA-Seq for microRNA biomarker discovery in human biofluids. *Scientific Reports*, 11(1):4435, December 2021.

[p. 15]

[109] C. Chen. Real-time quantification of microRNAs by stem-loop RT-PCR. *Nucleic Acids Research*, 33(20):e179–e179, November 2005.

[p. 15]

[110] Eric A. Hunt, David Broyles, Trajen Head, and Sapna K. Deo. MicroRNA Detection: Current Technology and Research Strategies. *Annual Review of Analytical Chemistry*, 8(1):217–237, July 2015.

[p. 15, 16]

[111] Peter Androvic, Lukas Valihrach, Julie Elling, Robert Sjoback, and Mikael Kubista. Two-tailed RT-qPCR: a novel method for highly accurate miRNA quantification. *Nucleic Acids Research*, 45(15):e144, September 2017.

[p. 16]

[112] Tsugunori Notomi, Hiroto Okayama, Harumi Masubuchi, Toshihiro Yonekawa, Keiko Watanabe, Nobuyuki Amino, and Tetsu Hase. Loop-mediated isothermal amplification of DNA. *Nucleic Acids Research*, 28(12):e63, June 2000.

[p. 16]

[113] Cuiping Li, Zhengping Li, Hongxia Jia, and Jingli Yan. One-step ultrasensitive detection of microRNAs with loop-mediated isothermal amplification (LAMP). *Chemical Communications*, 47(9):2595–2597, February 2011.

[p. 16, 17]

[114] Yuanyuan Sun, Hui Tian, Chenghui Liu, Yueying Sun, and Zhengping Li. One-step detection of microRNA with high sensitivity and specificity via target-triggered loop-mediated isothermal amplification (TT-LAMP). *Chemical Communications*, 53(80):11040–11043, October 2017.

[p. 16]

[115] Weimin Tian, Pengjie Li, Wenli He, Chenghui Liu, and Zhengping Li. Rolling circle extension-actuated loop-mediated isothermal amplification (RCA-LAMP) for ultrasensitive detection of microRNAs. *Biosensors and Bioelectronics*, 128:17–22, March 2019.

[p. 16]

[116] Abdu Ahmed Abdullah AL-maskri, Jiawei Ye, Jadera Talap, Haihong Hu, Lianli Sun, Lushan Yu, Sheng Cai, and Su Zeng. Reverse transcription-based loop-mediated isothermal amplification strategy for real-time miRNA detection with phosphorothioated probes. *Analytica Chimica Acta*, 1126:1–6, August 2020.

[p. 16]

[117] Sarah L. Daubendiek and Eric T. Kool. Generation of catalytic RNAs by rolling transcription of synthetic DNA nanocircles. *Nature Biotechnology*, 15(3):273–277, March 1997.

[p. 17]

[118] M. Monsur Ali, Feng Li, Zhiqing Zhang, Kaixiang Zhang, Dong-Ku Kang, James A. Ankrum, X. Chris Le, and Weian Zhao. Rolling circle amplification: a versatile tool for chemical biology, materials science and medicine. *Chemical Society Reviews*, 43(10):3324–3341, April 2014.

[p. 17, 18]

[119] Søren Peter Jonstrup, Jørn Koch, and Jørgen Kjems. A microRNA detection system based on padlock probes and rolling circle amplification. *RNA*, 12(9):1747–1752, January 2006.

[p. 17]

[120] Hirokazu Takahashi, Masahiko Ohkawachi, Kyohei Horio, Toshiro Kobori, Tsunehiro Aki, Yukihiko Matsumura, Yutaka Nakashimada, and Yoshiko Okamura. RNase H-assisted RNA-primed rolling circle amplification for targeted RNA sequence detection. *Scientific Reports*, 8(1):7770, December 2018.

[p. 17]

[121] Yuntao Zhou, Qing Huang, Jimin Gao, Jianxin Lu, Xizhong Shen, and Chunhai Fan. A dumbbell probe-mediated rolling circle amplification strategy for highly sensitive microRNA detection. *Nucleic Acids Research*, 38(15):e156, August 2010.

[p. 17]

[122] Paul M. Lizardi, Xiaohua Huang, Zhengrong Zhu, Patricia Bray-Ward, David C. Thomas, and David C. Ward. Mutation detection and single-molecule counting using isothermal rolling-circle amplification. *Nature Genetics*, 19(3):225–232, July 1998.

[p. 17]

[123] Fredrik Dahl, Johan Banér, Mats Gullberg, Maritha Mendel-Hartvig, Ulf Landegren, and Mats Nilsson. Circle-to-circle amplification for precise and sensitive DNA analysis. *Proceedings of the National Academy of Sciences*, 101(13):4548–4553, March 2004.

[p. 17]

[124] Taku Murakami, Jun Sumaoka, and Makoto Komiyama. Sensitive isothermal detection of nucleic-acid sequence by primer generation-rolling circle amplification. *Nucleic Acids Research*, 37(3):e19, February 2009.

[p. 17]

[125] J. Van Ness, L. K. Van Ness, and D. J. Galas. Isothermal reactions for the amplification of oligonucleotides. *Proceedings of the National Academy of Sciences*, 100(8):4504–4509, April 2003.

[p. 18]

[126] Eric Tan, Jennifer Wong, Doris Nguyen, Yolanda Zhang, Barbara Erwin, Lori K. Van Ness, Shenda M. Baker, David J. Galas, and Angelika Niemz. Isothermal DNA Amplification Coupled with DNA Nanosphere-Based Colorimetric Detection. *Analytical Chemistry*, 77(24):7984–7992, December 2005.

[p. 18]

[127] Eric Tan, Barbara Erwin, Shale Dames, Tanya Ferguson, Megan Buechel, Bruce Irvine, Karl Voelkerding, and Angelika Niemz. Specific versus Nonspecific Isothermal DNA Amplification through Thermophilic Polymerase and Nicking Enzyme Activities. *Biochemistry*, 47(38):9987–9999, September 2008.

[p. 18]

[128] Jifeng Qian, Tanya M. Ferguson, Deepali N. Shinde, Alissa J. Ramírez-Borrero, Arend Hintze, Christoph Adami, and Angelika Niemz. Sequence dependence of isothermal DNA amplification via EXPAR. *Nucleic Acids Research*, 40(11):e87–e87, June 2012.

[p. 18]

[129] Hongxia Jia, Zhengping Li, Chenghui Liu, and Yongqiang Cheng. Ultrasensitive Detection of microRNAs by Exponential Isothermal Amplification. *Angewandte Chemie International Edition*, 49(32):5498–5501, July 2010.

[p. 18, 19]

[130] Yongjie Xu, Dandan Li, Wei Cheng, Rong Hu, Ye Sang, Yibing Yin, Shijia Ding, and Huangxian Ju. Chemiluminescence imaging for microRNA detection based on cascade

exponential isothermal amplification machinery. *Analytica Chimica Acta*, 936:229–235, September 2016.

[p. 18]

[131] Jun Chen, Xueqing Zhou, Yingjun Ma, Xiulian Lin, Zong Dai, and Xiaoyong Zou. Asymmetric exponential amplification reaction on a toehold/biotin featured template: an ultrasensitive and specific strategy for isothermal microRNAs analysis. *Nucleic Acids Research*, page gkw504, June 2016.

[p. 18]

[132] Yongxi Zhao, Feng Chen, Qian Li, Lihua Wang, and Chunhai Fan. Isothermal Amplification of Nucleic Acids. *Chemical Reviews*, 115(22):12491–12545, November 2015.

[p. 19, 20]

[133] J. Compton. Nucleic acid sequence-based amplification. *Nature*, 350(6313):91–92, March 1991.

[p. 19]

[134] J. C. Guatelli, K. M. Whitfield, D. Y. Kwoh, K. J. Barringer, D. D. Richman, and T. R. Gingeras. Isothermal, in vitro amplification of nucleic acids by a multienzyme reaction modeled after retroviral replication. *Proceedings of the National Academy of Sciences*, 87(5):1874–1878, March 1990.

[p. 19, 20]

[135] S A Burchill, L Perebolte, C Johnston, B Top, and P Selby. Comparison of the RNA-amplification based methods RT–PCR and NASBA for the detection of circulating tumour cells. *British Journal of Cancer*, 86(1):102–109, January 2002.

[p. 19]

[136] Andreas Mader, Ulrike Riehle, Thomas Brandstetter, Elmar Stickeler, and Juergen Ruehe. Universal nucleic acid sequence-based amplification for simultaneous amplification of messengerRNAs and microRNAs. *Analytica Chimica Acta*, 754:1–7, November 2012.

[p. 19]

[137] Valérie Taly, Deniz Pekin, Abdel El Abed, and Pierre Laurent-Puig. Detecting biomarkers with microdroplet technology. *Trends in Molecular Medicine*, 18(7):405–416, July 2012.

[p. 20]

[138] Yannick Rondelez, Guillaume Tresset, Kazuhito V Tabata, Hideyuki Arata, Hiroyuki Fujita, Shoji Takeuchi, and Hiroyuki Noji. Microfabricated arrays of femtoliter chambers allow single molecule enzymology. *Nature Biotechnology*, 23(3):361–365, March 2005.

[p. 20]

[139] Paola Campomenosi, Elisabetta Gini, Douglas M. Noonan, Albino Poli, Paola D'Antona, Nicola Rotolo, Lorenzo Dominioni, and Andrea Imperatori. A comparison between quantitative PCR and droplet digital PCR technologies for circulating microRNA quantification in human lung cancer. *BMC Biotechnology*, 16(1):60, December 2016.

[p. 20]

[140] Erica V. Stein, David L. Duewer, Natalia Farkas, Erica L. Romsos, Lili Wang, and Kenneth D. Cole. Steps to achieve quantitative measurements of microRNA using two step droplet digital PCR. *PLOS ONE*, 12(11):e0188085, November 2017.

[p. 20]

[141] Kaixiang Zhang, Dong-Ku Kang, M. Monsur Ali, Linan Liu, Louai Labanieh, Mengrou Lu, Hamidreza Riazifar, Thi N. Nguyen, Jason A. Zell, Michelle A. Digman, Enrico Gratton, Jinghong Li, and Weian Zhao. Digital quantification of miRNA directly in plasma using integrated comprehensive droplet digital detection. *Lab on a Chip*, 15(21):4217–4226, 2015.

[p. 20]

[142] Zhian Hu, Fujian Xu, Gongwei Sun, Sichun Zhang, and Xinrong Zhang. Homogeneous multiplexed digital detection of microRNA with ligation-rolling circle amplification. *Chemical Communications*, 56(40):5409–5412, 2020.

[p. 21]

[143] Alexander Johnson-Buck, Jieming Li, Muneesh Tewari, and Nils G. Walter. A guide to nucleic acid detection by single-molecule kinetic fingerprinting. *Methods*, 153:3–12, January 2019.

[p. 21]

[144] Catherine Foye, Irene K. Yan, Waseem David, Neha Shukla, Yacob Habboush, Lori Chase, Kristen Ryland, Vivek Kesari, and Tushar Patel. Comparison of miRNA quantitation by Nanostring in serum and plasma samples. *PLOS ONE*, 12(12):e0189165, December 2017.

[p. 21]

[145] T Sano, C. Smith, and C. Cantor. Immuno-PCR: very sensitive antigen detection by means of specific antibody-DNA conjugates. *Science*, 258(5079):120–122, October 1992.

[p. 21]

[146] Kris Janssen, Karel Knez, Dragana Spasic, and Jeroen Lammertyn. Nucleic Acids for Ultra-Sensitive Protein Detection. *Sensors*, 13(1):1353–1384, January 2013.

[p. 21]

[147] H Zhou, R J Fisher, and T S Papas. Universal immuno-PCR for ultra-sensitive target protein detection. *Nucleic Acids Research*, 21(25):6038–6039, December 1993.

[p. 21]

[148] E R Hendrickson, T M Truby, R D Joerger, W R Majarian, and R C Ebersole. High sensitivity multianalyte immunoassay using covalent DNA-labeled antibodies and polymerase chain reaction. *Nucleic Acids Research*, 23(3):522–529, February 1995.

[p. 21]

[149] C M Niemeyer, M Adler, B Pignataro, S Lenhert, S Gao, L Chi, H Fuchs, and D Blohm. Self-assembly of DNA-streptavidin nanostructures and their use as reagents in immuno-PCR. *Nucleic Acids Research*, 27(23):4553–4561, December 1999.

[p. 22]

[150] Christof M Niemeyer, Michael Adler, and Ron Wacker. Detecting antigens by quantitative immuno-PCR. *Nature Protocols*, 2(8):1918–1930, August 2007.

[p. 22]

[151] Mohammad Pourhassan-Moghaddam, Mohammad Rahmati-Yamchi, Abolfazl Akbarzadeh, Hadis Daraee, Kazem Nejati-Koshki, Younes Hanifehpour, and Sang Joo. Protein detection through different platforms of immuno-loop-mediated isothermal amplification. *Nanoscale Research Letters*, 8(1):485, 2013.

[p. 22, 23]

[152] Xiude Hua, Wei Yin, Haiyan Shi, Ming Li, Yanru Wang, Hong Wang, Yonghao Ye, Hee Joo Kim, Shirley J. Gee, Minghua Wang, Fengquan Liu, and Bruce D. Hammock. Development of Phage Immuno-Loop-Mediated Isothermal Amplification Assays for Organophosphorus Pesticides in Agro-products. *Analytical Chemistry*, 86(16):8441–8447, August 2014.

[p. 22]

[153] Hongmei Cao, Xueen Fang, Haipeng Li, Hua Li, and Jilie Kong. Ultrasensitive detection of mucin 1 biomarker by immuno-loop-mediated isothermal amplification. *Talanta*, 164:588–592, March 2017.

[p. 22]

[154] Hongmei Cao, Xueen Fang, Peng Liu, Hua Li, Weiwei Chen, Baohong Liu, and Jilie Kong. Magnetic-Immuno-Loop-Mediated Isothermal Amplification Based on DNA Encapsulating Liposome for the Ultrasensitive Detection of P-glycoprotein. *Scientific Reports*, 7(1):9312, December 2017.

[p. 22]

[155] Peng Liu, Xueen Fang, Hongmei Cao, Mingli Gu, Jilie Kong, and Anmei Deng. Nano-biotinylated liposome-based immunoassay for the ultrasensitive detection of protein biomarker in urine. *Talanta*, 179:472–477, March 2018.

[p. 22]

[156] B. Schweitzer, S. Wiltshire, J. Lambert, S. O'Malley, K. Kukanskis, Z. Zhu, S. F. Kingsmore, P. M. Lizardi, and D. C. Ward. Immunoassays with rolling circle DNA amplification: a versatile platform for ultrasensitive antigen detection. *Proceedings of the National Academy of Sciences of the United States of America*, 97(18):10113–10119, August 2000.

[p. 23]

[157] Barry Schweitzer, Scott Roberts, Brian Grimwade, Weiping Shao, Minjuan Wang, Qin Fu, Quiping Shu, Isabelle Laroche, Zhimin Zhou, Velizar T. Tchernev, Jason Christiansen, Mark Velleca, and Stephen F. Kingsmore. Multiplexed protein profiling on microarrays by rolling-circle amplification. *Nature Biotechnology*, 20(4):359–365, April 2002.

[p. 23]

[158] Steve Wiltshire, Shawn O'Malley, Jeremy Lambert, Kari Kukanskis, David Edgar, Stephen F Kingsmore, and Barry Schweitzer. Detection of Multiple Allergen-specific IgEs on Microarrays by Immunoassay with Rolling Circle Amplification. *Clinical Chemistry*, 46(12):1990–1993, December 2000.

[p. 23]

[159] Haiyan Liu, Li Zhang, Yuzhi Xu, Jun Chen, Yang Wang, Qixing Huang, Xingyu Chen, Yi Liu, Zong Dai, Xiaoyong Zou, and Zhanchao Li. Sandwich immunoassay coupled with isothermal exponential amplification reaction: An ultrasensitive approach for determination of tumor marker MUC1. *Talanta*, 204:248–254, November 2019.

[p. 23]

[160] Xinyan Zhao, Tao Dong, Zhaochu Yang, Nuno Pires, and Nils Høivik. Compatible immuno-NASBA LOC device for quantitative detection of waterborne pathogens: design and validation. *Lab on a Chip*, 12(3):602–612, February 2012.

[p. 23]

[161] Simon Fredriksson, Mats Gullberg, Jonas Jarvius, Charlotta Olsson, Kristian Pietras, Sigrún Margrét Gústafsdóttir, Arne Östman, and Ulf Landegren. Protein detection using proximity-dependent DNA ligation assays. *Nature Biotechnology*, 20(5):473–477, May 2002.

[p. 24]

[162] Pengzhi Wang, Yi Yang, Tianqi Hong, and Guoqiang Zhu. Proximity ligation assay: an ultrasensitive method for protein quantification and its applications in pathogen detection. *Applied Microbiology and Biotechnology*, 105(3):923–935, February 2021.

[p. 24, 25]

[163] Bin Deng, Yanwen Lin, Chuan Wang, Feng Li, Zhixin Wang, Hongquan Zhang, Xing-Fang Li, and X. Chris Le. Aptamer binding assays for proteins: The thrombin example—A review. *Analytica Chimica Acta*, 837:1–15, July 2014.

[p. 24, 81, 84]

[164] Rongqin Ke, Rachel Yuan Nong, Simon Fredriksson, Ulf Landegren, and Mats Nilsson. Improving Precision of Proximity Ligation Assay by Amplified Single Molecule Detection. *PLOS ONE*, 8(7):e69813, July 2013.

[p. 24]

[165] Martin Lundberg, Stine Buch Thorsen, Erika Assarsson, Andrea Villablanca, Bonnie Tran, Nick Gee, Mick Knowles, Birgitte Sander Nielsen, Eduardo González Couto, Roberto Martin, Olle Nilsson, Christian Fermer, Jörg Schlingemann, Ib Jarle Christensen, Hans-Jorgen Nielsen, Björn Ekström, Claes Andersson, Mats Gustafsson, Nils Brunner, Jan Stenvang, and Simon Fredriksson. Multiplexed homogeneous proximity ligation assays for high-throughput protein biomarker research in serological material. *Molecular & cellular proteomics*, 10(4), April 2011.

[p. 25]

[166] Erika Assarsson, Martin Lundberg, Göran Holmquist, Johan Björkesten, Stine Bucht Thorsen, Daniel Ekman, Anna Eriksson, Emma Rennel Dickens, Sandra Ohlsson, Gabriella Edfeldt, Ann-Catrin Andersson, Patrik Lindstedt, Jan Stenvang, Mats Gullberg, and Simon Fredriksson. Homogenous 96-Plex PEA Immunoassay Exhibiting High Sensitivity, Specificity, and Excellent Scalability. *PLoS ONE*, 9(4):e95192, April 2014.

[p. 25]

[167] Martin Lundberg, Anna Eriksson, Bonnie Tran, Erika Assarsson, and Simon Fredriksson. Homogeneous antibody-based proximity extension assays provide sensitive and specific detection of low-abundant proteins in human blood. *Nucleic Acids Research*, 39(15):e102–e102, August 2011.

[p. 25]

[168] D. A. Di Giusto. Proximity extension of circular DNA aptamers with real-time protein detection. *Nucleic Acids Research*, 33(6):e64–e64, March 2005.

[p. 25]

[169] Megha Bhardwaj, Korbinian Weigl, Kaja Tikk, Axel Benner, Petra Schrotz-King, and Hermann Brenner. Multiplex screening of 275 plasma protein biomarkers to identify a signature for early detection of colorectal cancer. *Molecular Oncology*, 14(1):8–21, 2020.

[p. 25]

[170] Heping Zhou, Kerri Bouwman, Mark Schotanus, Cornelius Verweij, Jorge A Marrero, Deborah Dillon, Jose Costa, Paul Lizardi, and Brian B Haab. Two-color, rolling-circle amplification on antibody microarrays for sensitive, multiplexed serum-protein measurements. *Genome Biology*, page 12, 2004.

[p. 26]

[171] Jiyoon Bu, Jae-Eul Shim, Tae Hee Lee, and Young-Ho Cho. Multi-modal liquid biopsy platform for cancer screening: screening both cancer-associated rare cells and cancer cell-derived vesicles on the fabric filters for a reliable liquid biopsy analysis. *Nano Convergence*, 6(1):39, November 2019.

[p. 26]

[172] Raffaele Palmirotta, Domenica Lovero, Paola Cafforio, Claudia Felici, Francesco Mannavola, Eleonora Pellè, Davide Quaresmini, Marco Tucci, and Franco Silvestris. Liquid biopsy of cancer: a multimodal diagnostic tool in clinical oncology. *Therapeutic Advances in Medical Oncology*, 10:1758835918794630, January 2018.

[p. 26]

[173] Qiao Yang, Zihan Xu, Linpeng Zheng, Luping Zhang, Qiai You, and Jianguo Sun. Multimodal detection of PD-L1: reasonable biomarkers for immune checkpoint inhibitor. *American Journal of Cancer Research*, 8(9):1689–1696, September 2018.

[p. 26]

[174] Yong Hui Nies, Nor Haliza Mohamad Najib, Wei Ling Lim, Mohd Amir Kamaruzzaman, Mohamad Fairuz Yahaya, and Seong Lin Teoh. MicroRNA Dysregulation in Parkinson's Disease: A Narrative Review. *Frontiers in Neuroscience*, 15:509, 2021.

[p. 26]

[175] K. Montagne, R. Plasson, Y. Sakai, T. Fujii, and Y. Rondelez. Programming an in vitro DNA oscillator using a molecular networking strategy. *Molecular Systems Biology*, 7(1):466–466, February 2011.

[p. 31, 120]

[176] Alexandre Baccouche, Kevin Montagne, Adrien Padirac, Teruo Fujii, and Yannick Rondelez. Dynamic DNA-toolbox reaction circuits: A walkthrough. *Methods*, 67(2):234–249, May 2014.

[p. 31, 120]

[177] Kevin Montagne, Guillaume Gines, Teruo Fujii, and Yannick Rondelez. Boosting functionality of synthetic DNA circuits with tailored deactivation. *Nature Communications*, 7:13474, November 2016.

[p. 31, 32, 122]

[178] Guillaume Gines, Roberta Menezes, Kaori Nara, Anne-Sophie Kirstetter, Valerie Taly, and Yannick Rondelez. Isothermal digital detection of microRNAs using background-free molecular circuit. *Science Advances*, 6(4):eaay5952, January 2020.

[p. 33, 37, 38, 120, 162]

[179] Linas Mazutis, John Gilbert, W Lloyd Ung, David A Weitz, Andrew D Griffiths, and John A Heyman. Single-cell analysis and sorting using droplet-based microfluidics. *Nature Protocols*, 8(5):870–891, May 2013.

[p. 38]

[180] Subhash Kulkarni, Julia Ganz, James Bayrer, Laren Becker, Milena Bogunovic, and Meenakshi Rao. Advances in Enteric Neurobiology: The "Brain" in the Gut in Health and Disease. *The Journal of Neuroscience*, 38(44):9346–9354, October 2018.

[p. 39]

[181] Francisco Pan-Montojo, Mathias Schwarz, Clemens Winkler, Mike Arnhold, Gregory A. O'Sullivan, Arun Pal, Jonas Said, Giovanni Marsico, Jean-Marc Verbavatz, Margarita Rodrigo-Angulo, Gabriele Gille, Richard H. W. Funk, and Heinz Reichmann. Environmental toxins trigger PD-like progression via increased alpha-synuclein release from enteric neurons in mice. *Scientific Reports*, 2(1):898, December 2012.

[p. 39]

[182] Morten Gersel Stokholm, Erik Hvid Danielsen, Stephen Jacques Hamilton-Dutoit, and Per Borghammer. Pathological -synuclein in gastrointestinal tissues from prodromal Parkinson disease patients: -Synuclein in Prodromal PD. *Annals of Neurology*, 79(6):940–949, June 2016.

[p. 39]

[183] Frank Gillardon, Matthias Mack, Wolfgang Rist, Cathrin Schnack, Martin Lenter, Tobias Hildebrandt, and Bastian Hengerer. MicroRNA and proteome expression profiling in early-symptomatic -synuclein(A30P)-transgenic mice. *Proteomics Clin Applications*, 2(5):697–705, May 2008.

[p. 39]

[184] Loredana Leggio, Silvia Vivarelli, Francesca L'Episcopo, Cataldo Tirolo, Salvo Caniglia, Nunzio Testa, Bianca Marchetti, and Nunzio Iraci. microRNAs in Parkinson's Disease: From Pathogenesis to Novel Diagnostic and Therapeutic Approaches. *International Journal of Molecular Sciences*, 18(12):2698, December 2017.

[p. 39]

[185] Roberta Menezes, Adèle Dramé-Maigné, Valérie Taly, Yannick Rondelez, and Guillaume Gines. Streamlined digital bioassays with a 3D printed sample changer. *The Analyst*, 145(2):572–581, 2020.

[p. 42]

[186] Thomas Jet. *Détection digitale et multiplexe de microARN pour le diagnostic moléculaire*. These de doctorat, Université de Paris (2017-2021), 2017.

[p. 46, 51, 56, 59]

[187] Stefan Lutzmayer, Balaji Enugutti, and Michael D. Nodine. Novel small RNA spike-in oligonucleotides enable absolute normalization of small RNA-Seq data. *Scientific Reports*, 7(1):5913, December 2017.

[p. 52]

[188] Gary K Geiss, Roger E Bumgarner, Brian Birditt, Timothy Dahl, Naeem Dowidar, Dwayne L Dunaway, H Perry Fell, Sean Ferree, Renee D George, Tammy Grogan, Jeffrey J James, Malini Maysuria, Jeffrey D Mitton, Paola Oliveri, Jennifer L Osborn, Tao Peng, Amber L Ratcliffe, Philippa J Webster, Eric H Davidson, Leroy Hood, and Krassen Dimitrov. Direct multiplexed measurement of gene expression with color-coded probe pairs. *Nature Biotechnology*, 26(3):10, 2008.

[p. 54]

[189] Victor M Corman, Olfert Landt, Marco Kaiser, Richard Molenkamp, Adam Meijer, Daniel KW Chu, Tobias Bleicker, Sebastian Brünink, Julia Schneider, Marie Luisa Schmidt, Daphne GJC Mulders, Bart L Haagmans, Bas van der Veer, Sharon van den Brink, Lisa Wijsman, Gabriel Goderski, Jean-Louis Romette, Joanna Ellis, Maria Zambon, Malik Peiris, Herman Goossens, Chantal Reusken, Marion PG Koopmans, and Christian Drosten. Detection of 2019 novel coronavirus (2019-nCoV) by real-time RT-PCR. *Eurosurveillance*, 25(3), January 2020.

[p. 64]

[190] Rebeca Miranda-Castro, Noemí de-los Santos-Álvarez, and María Jesús Lobo-Castañón. Long noncoding RNAs: from genomic junk to rising stars in the early detection of cancer. *Analytical and Bioanalytical Chemistry*, 411(19):4265–4275, July 2019.

[p. 64]

[191] Dominique Cheneval, Tania Kastelic, Peter Fuerst, and Christian N. Parker. A Review of Methods to Monitor the Modulation of mRNA Stability: A Novel Approach to Drug Discovery and Therapeutic Intervention. *Journal of Biomolecular Screening*, 15(6):609–622, July 2010.

[p. 64]

[192] Lukasz J. Kiełpiński, Peter H. Hagedorn, Morten Lindow, and Jeppe Vinther. RNase H sequence preferences influence antisense oligonucleotide efficiency. *Nucleic Acids Research*, 45(22):12932–12944, December 2017.

[p. 64]

[193] Randolph Lopez, Ruofan Wang, and Georg Seelig. A molecular multi-gene classifier for disease diagnostics. *Nature Chemistry*, 10(7):746–754, July 2018.

[p. 65, 145]

[194] Dominic Lambert and David E. Draper. Denaturation of RNA secondary and tertiary structure by urea: simple unfolded state models and free energy parameters account for measured m-values. *Biochemistry*, 51(44):9014–9026, November 2012.

[p. 69]

[195] S. D. Wharam. Specific detection of DNA and RNA targets using a novel isothermal nucleic acid amplification assay based on the formation of a three-way junction structure. *Nucleic Acids Research*, 29(11):54e–54, June 2001.

[p. 70]

[196] Taku Murakami, Jun Sumaoka, and Makoto Komiyama. Sensitive RNA detection by combining three-way junction formation and primer generation-rolling circle amplification. *Nucleic Acids Research*, 40(3):e22–e22, February 2012.

[p. 70]

[197] Seoyoung Lee, Hyowon Jang, Hyo Yong Kim, and Hyun Gyu Park. Three-way junction-induced isothermal amplification for nucleic acid detection. *Biosensors and Bioelectronics*, 147:111762, January 2020.

[p. 70]

[198] Yongya Li, Hayam Mansour, Colton J. F. Watson, Yanan Tang, Adam J. MacNeil, and Feng Li. Amplified detection of nucleic acids and proteins using an isothermal proximity CRISPR Cas12a assay. *Chemical Science*, 2021.

[p. 70]

[199] Shu-Rong Yan, Mohammad Mehdi Foroughi, Mohadeseh Safaei, Shohreh Jahani, Nasser Ebrahimpour, Fariba Borhani, Nadia Rezaei Zade Baravati, Zahra Aramesh-Boroujeni, and Loke Kok Foong. A review: Recent advances in ultrasensitive and highly specific recognition aptasensors with various detection strategies. *International Journal of Biological Macromolecules*, 155:184–207, July 2020.

[p. 78]

[200] Hongxia Chen, Yafei Hou, Fangjie Qi, Jiangjiang Zhang, Kwangnak Koh, Zhongming Shen, and Genxi Li. Detection of vascular endothelial growth factor based on rolling circle amplification as a means of signal enhancement in surface plasmon resonance. *Biosensors and Bioelectronics*, 61:83–87, November 2014.

[p. 78]

[201] Harleen Kaur and Lin-Yue Lanry Yung. Probing High Affinity Sequences of DNA Aptamer against VEGF165. *PLoS ONE*, 7(2):e31196, February 2012.

[p. 78]

[202] Ishak Afsin Kariper, Zafer Üstündağ, and Mustafa Oguzhan Caglayan. A Sensitive Spectrophotometric Ellipsometry based Aptasensor for the Vascular Endothelial Growth Factor Detection. *Talanta*, page 121982, December 2020.

[p. 87]

[203] Akira Tsuchiya, Siti N. Hashim, Shoko Ise, Takafumi Furuhata, Kiyohiko Kawai, Rie Wakabayashi, Masahiro Goto, Noriho Kamiya, and Shinsuke Sando. BODIPY-labeled Fluorescent Aptamer Sensors for Turn-on Sensing of Interferon-gamma and Adenine Compounds on Cells. *Analytical Sciences*, 32(5):543–547, 2016.

[p. 88]

[204] Ying Liu, Nazgul Tuleouva, Erlan Ramanculov, and Alexander Revzin. Aptamer-Based Electrochemical Biosensor for Interferon Gamma Detection. *Analytical Chemistry*, 82(19):8131–8136, October 2010.

[p. 88]

[205] Hatem Tallima, Mohamed Salah, Fatem R. Guirguis, and Rashika El Ridi. Transforming growth factor- and Th17 responses in resistance to primary murine schistosomiasis mansoni. *Cytokine*, 48(3):239–245, December 2009.

[p. 91]

[206] Yuan Meng, Katrina High, Joseph Antonello, Michael W Washabaugh, and Qinjian Zhao. Enhanced sensitivity and precision in an enzyme-linked immunosorbent assay with fluorogenic substrates compared with commonly used chromogenic substrates. *Anal. Biochem.*, page 10, 2005.

[p. 92]

[207] J. W. Jaroszewski, V. Clausen, J. S. Cohen, and O. Dahl. NMR investigations of duplex stability of phosphorothioate and phosphorodithioate DNA analogues modified in both strands. *Nucleic Acids Research*, 24(5):829–834, March 1996.

[p. 100]

[208] G. Gines, A. S. Zadorin, J.-C. Galas, T. Fujii, A. Estevez-Torres, and Y. Rondelez. Microscopic agents programmed by DNA circuits. *Nature Nanotechnology*, 12(4):351–359, May 2017.

[p. 100]

[209] Kevin M. Cherry and Lulu Qian. Scaling up molecular pattern recognition with DNA-based winner-take-all neural networks. *Nature*, 559(7714):370–376, July 2018.

[p. 108, 145]

[210] Yannick Rondelez and Guillaume Gines. Multiplex Digital MicroRNA Detection Using Cross-Inhibitory DNA Circuits. *ACS Sensors*, 5(8):2430–2437, August 2020.

[p. 108, 109, 142]

[211] Remi Sieskind. *Evolution dirigée d'enzymes in vitro, auto-sélection par programmation moléculaire*. These de doctorat, Université de Paris (2015-2019), 2015.

[p. 108, 137, 171, 172, 173]

[212] Marion M. Bradford. A rapid and sensitive method for the quantitation of microgram quantities of protein utilizing the principle of protein-dye binding. *Analytical Biochemistry*, 72(1):248–254, May 1976.

[p. 108]

[213] Mariia Darmostuk, Silvie Rimpelova, Helena Gbelcova, and Tomas Ruml. Current approaches in SELEX: An update to aptamer selection technology. *Biotechnology Advances*, 33(6):1141–1161, November 2015.

[p. 118]

[214] Tianqi Song, Shalin Shah, Hieu Bui, Sudhanshu Garg, Abeer Eshra, Daniel Fu, Ming Yang, Reem Mokhtar, and John Reif. Programming DNA-Based Biomolecular Reaction Networks on Cancer Cell Membranes. *Journal of the American Chemical Society*, 141(42):16539–16543, October 2019.

[p. 120]

[215] Mingxu You, Guizhi Zhu, Tao Chen, Michael J. Donovan, and Weihong Tan. Programmable and Multiparameter DNA-Based Logic Platform For Cancer Recognition and Targeted Therapy. *Journal of the American Chemical Society*, 137(2):667–674, January 2015.

[p. 120]

[216] Long Li, Xigao Chen, Cheng Cui, Xiaoshu Pan, Xiaowei Li, Hoda Safari Yazd, Qiong Wu, Liping Qiu, Juan Li, and Weihong Tan. Aptamer Displacement Reaction from Live-Cell Surfaces and Its Applications. *Journal of the American Chemical Society*, 141(43):17174–17179, October 2019.

[p. 120]

[217] Shreyas N. Dahotre, Yun Min Chang, Andreas Wieland, Samantha R. Stammen, and Gabriel A. Kwong. Individually addressable and dynamic DNA gates for multiplexed cell sorting. *Proceedings of the National Academy of Sciences*, 115(17):4357–4362, April 2018.

[p. 120]

[218] A. Padirac, T. Fujii, and Y. Rondelez. Bottom-up construction of in vitro switchable memories. *Proceedings of the National Academy of Sciences*, 109(47):E3212–E3220, November 2012.

[p. 120]

[219] Vasily A Shenshin, Camille Lescanne, Guillaume Gines, and Yannick Rondelez. A small-molecule chemical interface for molecular programs. *Nucleic Acids Research*, 49(13):7765–7774, July 2021.

[p. 121]

[220] Zhiwen Tang, Dihua Shangguan, Kemin Wang, Hui Shi, Kwame Sefah, Prabodhika Mallikratchy, Hui William Chen, Ying Li, and Weihong Tan. Selection of Aptamers for Molecular Recognition and Characterization of Cancer Cells. *Analytical Chemistry*, 79(13):4900–4907, July 2007.

[p. 123]

[221] Georg Urtel, Marc Van Der Hofstadt, Jean-Christophe Galas, and André Estevez-Torres. rEXPAR: An Isothermal Amplification Scheme That Is Robust to Autocatalytic Parasites. *Biochemistry*, 58(23):2675–2681, June 2019.

[p. 123]

[222] Mingxu You, Yifan Lyu, Da Han, Liping Qiu, Qiaoling Liu, Tao Chen, Cuichen Sam Wu, Lu Peng, Liqin Zhang, Gang Bao, and Weihong Tan. DNA probes for monitoring dynamic and transient molecular encounters on live cell membranes. *Nature Nanotechnology*, 12(5):453–459, May 2017.

[p. 125]

[223] Anton S. Zadorin, Yannick Rondelez, Jean-Christophe Galas, and André Estevez-Torres. Synthesis of Programmable Reaction-Diffusion Fronts Using DNA Catalyzers. *Physical Review Letters*, 114(6):068301, February 2015.

[p. 129]

[224] Anis Senoussi, Shunnichi Kashida, Raphael Voituriez, Jean-Christophe Galas, Ananyo Maitra, and André Estevez-Torres. Tunable corrugated patterns in an active nematic sheet. *Proceedings of the National Academy of Sciences*, 116(45):22464–22470, November 2019.

[p. 130]

[225] J. Thiele, Y. Ma, D. Foschepoth, M. M. K. Hansen, C. Steffen, H. A. Heus, and W. T. S. Huck. DNA-functionalized hydrogels for confined membrane-free in vitro transcription/translation. *Lab on a Chip*, 14(15):2651, 2014.

[p. 137]

[226] Larysa Baraban, Bergoi Ibarlucea, Eunhye Baek, and Gianaurelio Cuniberti. Hybrid Silicon Nanowire Devices and Their Functional Diversity. *Advanced Science*, page 1900522, June 2019.

[p. 139]

[227] Eric Stern, Robin Wagner, Fred J. Sigworth, Ronald Breaker, Tarek M. Fahmy, and Mark A. Reed. Importance of the Debye Screening Length on Nanowire Field Effect Transistor Sensors. *Nano Letters*, 7(11):3405–3409, November 2007.

[p. 139]

[228] Zibo Chen, Ryan D. Kibler, Andrew Hunt, Florian Busch, Jocelynn Pearl, Mengxuan Jia, Zachary L. VanAernum, Basile I. M. Wicky, Galen Dods, Hanna Liao, Matthew S. Wilken, Christie Ciarlo, Shon Green, Hana El-Samad, John Stamatoyannopoulos, Vicki H. Wysocki, Michael C. Jewett, Scott E. Boyken, and David Baker. De novo design of protein logic gates. *Science*, 368(6486):78–84, April 2020.

[p. 145]

[229] Yongqi Yu, Qunqun Guo, Wenli Jiang, Hui Zhang, and Chenxin Cai. Dual-Aptamer-Assisted AND Logic Gate for Cyclic Enzymatic Signal Amplification Electrochemical Detection of Tumor-Derived Small Extracellular Vesicles. *Analytical Chemistry*, August 2021.

[p. 145]

[230] Xiaoyi Ma, Xifeng Chen, Yuguo Tang, Ruhong Yan, and Peng Miao. Triple-Input Molecular AND Logic Gates for Sensitive Detection of Multiple miRNAs. *ACS Applied Materials & Interfaces*, 11(44):41157–41164, November 2019.

[p. 145]

[231] Cyrille L. Delley, Leqian Liu, Maen F. Sarhan, and Adam R. Abate. Combined aptamer and transcriptome sequencing of single cells. *Scientific Reports*, 8(1):2919, December 2018.

[p. 170]

RÉSUMÉ

Les récentes avancées en matière de diagnostic moléculaire donnent une idée des avantages qu'il y a à quantifier simultanément plusieurs biomarqueurs pour obtenir un diagnostic robuste d'une maladie. Parmi ces biomarqueurs, nous pouvons distinguer les microARNs (miARNs) et les protéines. Les miARNs sont une classe d'ARN courts (21-25 nucléotides) impliqués dans la régulation post-transcriptionnelle d'environ 60% des gènes humains. De l'autre côté, les protéines résultent de la transcription-traduction des gènes et reflètent ainsi le phénotype cellulaire. Tous deux sont dérégulés dans un certain nombre de maladies, comme les cancers, les maladies neurodégénératives ou les infections, et peuvent servir de biomarqueurs apportant des informations complémentaires. Les outils utilisés pour les mesurer doivent être sensibles, spécifiques et quantitatifs. De plus, la détection des niveaux de traces est un défi en raison de la toxicité et des effets de fond provenant d'échantillons biologiques.
Dans cette thèse de doctorat, nous avons développé une méthode de détection sensible applicable à plusieurs classes de biomarqueurs. Nous rapportons le développement d'une plateforme générique, appelée Amplificateur Moléculaire Ultrasensible Programmable (PUMA) pour la détection des miARNs et des protéines.
Nous nous sommes concentrés sur la détection de miARNs dérégulés dans la maladie de Parkinson, tel que mir7-5p. Nous avons travaillé sur une étape de capture utilisant des particules fonctionnalisées avec de l'ADN et montré qu'elle permettait d'éliminer la toxicité des matrices biologiques. Une étape de capture par ligation a ensuite été introduite pour tenter d'augmenter la sensibilité et la spécificité de l'approche.
Concernant la détection de protéines, une preuve de principe a été obtenue pour la détection de l'alpha-thrombine humaine grâce à des aptamères dans une approche d'extension de proximité. Une méthode immuno-PUMA (inspirée de l'immuno-PCR) a été développée pour la quantification d'interleukines, atteignant des limites de détection dans la gamme du femtomolaire. Notre travail démontre la détection de deux classes importantes de biomarqueurs, les miARNs et les protéines, en raison de la polyvalence de l'approche PUMA . En outre, des résultats préliminaires ont montré la possibilité de détecter des cellules vivantes en combinant l'amplificateur moléculaire avec des aptamères spécifiques aux cellules. Couplé à un dispositif microfluidique, ce test permettra la détection multiplexée et multimodale de différentes classes de biomarqueurs pour l'identification de signatures intégrées de maladies.

MOTS CLÉS

Biomarqueur; Diagnostic; Maladie neurodégénérative; Programmation moléculaire.

ABSTRACT

Recent molecular diagnosis advances give an idea of what are the benefits of quantifying several biomarkers simultaneously to get a robust diagnostic of a disease. Among those biomarkers, we can distinguish microRNAs (miRNAs) and proteins. MiRNAs are a class of short RNAs (21-25 nucleotides) involved in the post-transcriptional regulation of approximately 60% of human genes. On the other side, proteins result from gene transcription-translation and thus reflect cell phenotype. Both of these are dysregulated in a number of diseases, such as cancers, neurodegenerative and infectious diseases, and can serve as biomarkers, bringing complementary information. The tools used to profile them need to be sensitive, specific and quantitative. Additionally, the detection of trace levels is challenging because of toxicity and background effects arising from the biological samples.
In this PhD thesis, we developed a sensitive detection method applicable to multiple classes of biomarkers. We report the development of a generic platform, called Programmable Ultrasensitive Molecular Amplifier (PUMA) that can be used for the detection of both miRNAs and proteins.
We focused on the detection of miRNAs dysregulated in Parkinson's disease, such as mir7-5p. We worked on a capture step using DNA-functionalized particles and showed that it eliminates the toxicity of biological matrices. A ligation-based capture step was also introduced in an attempt to increase the sensitivity and specificity of the approach.
Concerning protein biomarkers, a proof of principle was obtained for the detection of human alpha-thrombin thanks to aptamers in a homogeneous proximity extension assay. An immuno-PUMA method (inspired from immuno-PCR) was developed for the quantification of interleukins, reaching limits of detection in the femtomolar range.
Our work demonstrates the detection of two important classes of biomarkers, miRNA and protein, owing to the versatility of the PUMA approach. Moreover, preliminary results have shown the possibility to detect live cells combining the molecular amplifier with cell-specific aptamers. Coupled to a microfluidic setup, this assay will allow the multiplexed and multimodal detection of different classes of biomarkers for the identification of integrated disease signatures.

KEYWORDS

Biomarker; Diagnosis; Neurodegenerative disease; Molecular programming.